



Nouvelle approche pour l'obtention de modèles asymptotiques en océanographie

Stevan Bellec

► To cite this version:

Stevan Bellec. Nouvelle approche pour l'obtention de modèles asymptotiques en océanographie. Mathématiques générales [math.GM]. Université de Bordeaux, 2016. Français. NNT : 2016BORD0182 . tel-01393300

HAL Id: tel-01393300

<https://theses.hal.science/tel-01393300>

Submitted on 7 Nov 2016

HAL is a multi-disciplinary open access archive for the deposit and dissemination of scientific research documents, whether they are published or not. The documents may come from teaching and research institutions in France or abroad, or from public or private research centers.

L'archive ouverte pluridisciplinaire **HAL**, est destinée au dépôt et à la diffusion de documents scientifiques de niveau recherche, publiés ou non, émanant des établissements d'enseignement et de recherche français ou étrangers, des laboratoires publics ou privés.

ÉCOLE DOCTORALE DE MATHÉMATIQUES ET INFORMATIQUE DE BORDEAUX

SPÉCIALITÉ : MATHÉMATIQUES APPLIQUÉES

PRÉSENTÉE PAR

Stevan Bellec

POUR OBTENIR LE GRADE DE

DOCTEUR DE L'UNIVERSITÉ DE BORDEAUX

SUJET :

Nouvelle approche pour l'obtention de modèles asymptotiques en océanographie.

Soutenue publiquement le 5 Octobre 2016

Directeur de thèse : M. Colin Mathieu MdC (Université de Bordeaux)
M. Ricchiuto Mario DR (INRIA)
Rapporteurs : M. Coulombel Jean-François DR CNRS (Université de Nantes)
M Goubet Olivier Professeur (Université de Picardie)

Composition du jury :

Directeur de thèse :	M. Colin Mathieu	MdC (Université de Bordeaux)
	M. Ricchiuto Mario	DR (INRIA)
Rapporteurs :	M. Coulombel Jean-François	DR CNRS (Université de Nantes)
	M Goubet Olivier	Professeur (Université de Picardie)
Examinateurs :	M. Besse Christophe	Professeur (Université de Toulouse)
	M. Duchêne Vincent	CR CNRS (Université de Rennes)
	M. Lannes David	DR CNRS (Université de Bordeaux)

Remerciements

Au moment de conclure la rédaction de ce manuscrit, mes premières pensées vont vers mes deux directeurs Mathieu Colin et Mario Ricchiuto. Je tiens à les remercier pour leur disponibilité, leur gentillesse, leur patience (surtout lorsqu'ils ont dû relire mon anglais) et leur aide. Ce fut un réel plaisir de travailler avec eux pendant ces trois années.

J'aimerais également remercier grandement Jean-François Coulombel et Olivier Goubet qui me font l'honneur d'être rapporteurs de cette thèse et, par conséquent, d'avoir accepter de relire ce manuscrit.

Je remercie ensuite Christophe Besse, Vincent Duchêne et David Lannes d'avoir accepté de faire partie de mon jury de thèse.

Je remercie les personnes de l'IMB et de l'INRIA que j'ai eu la chance de côtoyer tout au long de ces trois années. Je pense notamment à Andrea avec qui j'ai beaucoup aimé travailler, mais aussi à Quentin, Xi, Simon, Bin-Bin et Sébastien qui m'ont aidé à survivre aux repas du haut-carré, et plus généralement à l'ensemble de l'équipe CARDAMOM sans qui le travail n'aurait pas été le même.

Je remercie également Erik, Thomas, Benoit, Benjamin, Geoffrey, qui m'ont aidé à me vider la tête dans les moments difficiles. Je tiens tout particulièrement à remercier Benjamin qui a su me faire voyager régulièrement entre l'IMB et l'INRIA. Merci pour ta gentillesse, tes connaissances, ta curiosité et ta motivation pour le jogging. Merci aussi à Geoffrey qui a su, quant à lui, me changer les idées quotidiennement malgré la distance.

J'aimerais ensuite remercier ma mère et mes sœurs pour leur soutient constant depuis toutes ces années. Elles ont toujours cru en moi, malgré les difficultés et les moments de doute. Si j'en suis là aujourd'hui, c'est aussi et surtout grâce à elles.

Enfin, je terminerai cette page en remerciant Sophie. Tu as toujours été là pour me soutenir, me réconforter et me motiver. Je ne trouve pas de mots pour te dire à quel point je suis heureux de t'avoir à mes côtés. Merci.

Résumé

Dans ce manuscrit, nous nous intéressons à l'étude du mouvement des vagues soumises uniquement à leur poids par le biais d'équations asymptotiques. Nous commençons par rappeler la dérivation des principaux modèles généralement utilisés (Boussinesq, Green-Naghdi,...). Nous introduisons également un nouveau modèle exprimé en amplitude-flux qui correspond à une variante des équations de Nwogu. Dans le second chapitre, nous démontrons un résultat d'existence en temps long pour ces nouvelles équations et nous étudions l'existence d'ondes solitaires pour les équations de Boussinesq. Ce travail permet notamment de calculer avec une grande précision ces solutions exactes. Le troisième chapitre détail les différences non linéaires que l'on retrouve entre les différentes équations de Boussinesq (modèles en flux-amplitude comparés aux modèles en vitesse-amplitude). Enfin, les deux derniers chapitres introduisent un nouveau paradigme pour trouver des schémas numériques adaptés aux modèles asymptotiques. L'idée est d'appliquer une analyse asymptotique aux équations d'Euler discrétisées. Ce nouveau paradigme est appliqué aux équations de Peregrine, de Nwogu et de Green-Naghdi. Plusieurs cas test sont proposés dans ces deux chapitres.

Mots clés : Modèles asymptotiques, Equations de Boussinesq, Onde Solitaire, Méthode de Galerkin, Vitesse de phase, Shoaling non linéaire.

Abstract

In this work, we are interested in the evolution of water waves under the gravity force using asymptotics models. We start by recalling the derivation of most used models (Boussinesq, Green-Naghdi,...) and we introduce a new model expressed amplitude-flux, which is an alternative version of the Nwogu equations. In the second chapter, we prove a long time existence result for the new model and we investigate the existence of solitary waves for the Boussinesq models. This work allow us to compute these solutions with a good precision. The third chapter highlights the nonlinear differences between the Boussinesq equations (amplitude-flux models versus amplitude-velocity models). Finally, the two last chapter introduce a new paradigm in order to find numerical schemes adapted to asymptotics models. The idea is to apply an asymptotic analysis to a discretized Euler system. This new paradigm is applied to Peregrine equations, Nwogu equations and Green-Naghdi equations. Test cases are presented in these two chapters.

Key words : Asymptotics models, Boussinesq equations, Solitary waves, Galerkin method, Phase velocity, Nonlinear shoaling.

Table des matières

1	Introduction	11
1.1	Introduction générale et plan de la thèse	12
1.2	Modélisation mathématique	13
1.2.1	Les équations d'Euler à surface libre	13
1.3	Les différents modèles asymptotiques	15
1.3.1	Présentation des équations	16
1.3.2	Caractéristiques de dispersion	18
1.4	Résultats d'existence de solutions pour les équations de type Boussinesq	19
1.4.1	Existence en temps long	19
1.4.2	Existence d'ondes solitaires	20
1.5	Schémas numériques adaptés aux équations asymptotiques	23
1.5.1	Explication du nouveau paradigme	24
1.5.2	Résultats de la nouvelle approche	24
1.6	Perspectives de recherche	25
2	Modélisation et mise en équations du problème	29
2.1	Introduction	30
2.2	Notations et modélisation mathématique	30
2.3	Développement asymptotique	34
2.4	Equations de Saint-Venant (ou shallow water)	37
2.5	Equations de Boussinesq	38
2.5.1	Equations de Peregrine	39
2.5.2	Equations d'Abbott	40
2.6	Equations de Boussinesq étendues (ou améliorées)	41
2.6.1	Modèle de Beji-Nadaoka	41
2.6.2	Modèle de Madsen et Sørensen	43
2.6.3	Modèle de Nwogu	45
2.6.4	Modèles <i>abcd</i>	49
2.7	Equations de Green-Naghdi	51

3 On the existence of solution for Boussinesq type equations	55
3.1 Introduction	56
3.2 Context and notations	57
3.3 Long time existence theory for Nwogu-Abbott equations.	58
3.4 Solitary waves solutions for Boussinesq systems	64
3.4.1 Solitary waves solutions for the Beji-Nadaoka equations	67
3.4.2 Solitary waves solutions for Madsen-Sørensen equations	74
3.4.3 Solitary waves solutions for Nwogu equations	76
3.4.4 Discussion on solitary waves for Nwogu-Abbott equations	80
4 On the nonlinear behavior of Boussinesq type models : wave amplitude-velocity vs wave amplitude-flux forms	85
4.1 Introduction	86
4.2 Weakly nonlinear Boussinesq type models	87
4.2.1 Models of Peregrine and Abbott	88
4.2.2 Beji-Nadaoka and BNA models	89
4.2.3 Madsen-Sørensen and MSP models	90
4.2.4 Nwogu and NA models	91
4.2.5 Summary	92
4.3 Theoretical analysis of the models	93
4.3.1 Properties of Airy model	93
4.3.2 Dispersion properties	96
4.3.3 Shoaling properties	100
4.4 Numerical experiments	106
4.4.1 Numerical discretization and implementation	106
4.4.2 Initial validation	107
4.4.3 Physical experiments	110
4.5 Conclusions	117
5 Discrete asymptotic equations for long wave propagation	119
5.1 Introduction	120
5.2 Context and notations	120
5.3 Galerkin discretization of the Peregrine equations	122
5.4 A new setting to derive discrete asymptotic models	124
5.4.1 Semi-discretization of the 2D-Euler equations in non-dimensional form .	124
5.4.2 Asymptotic expansions on the velocity U and the pressure P	127
5.4.3 Depth-averaged equations	130
5.5 Study of the linear dispersion characteristics.	133
5.5.1 Linear characteristics of the new numerical model.	133
5.5.2 Linear characteristics of the classical Peregrine model.	138
5.5.3 Analysis of the computations	139
5.6 Numerical experiments	142

5.6.1	Soliton propagation	142
5.6.2	Linear dispersion and linear shoaling test	143
5.7	Conclusions and perspectives	145
6	Discrete asymptotic equations for Nwogu model	147
6.1	Introduction	148
6.2	Setting and Notation	149
6.3	A new setting for deriving discrete Green-Naghdi and Nwogu equations	151
6.3.1	Extension of the procedure to obtain the Green-Naghdi equations.	151
6.3.2	Discrete Nwogu equations	155
6.3.3	Study of the linear dispersion characteristics.	157
6.4	Numerical experiments	160
6.4.1	Soliton propagation.	160
6.4.2	Periodic wave propagation	161
6.4.3	Periodic wave propagation over a shelf.	162
6.5	Conclusion and future works	164

Chapitre 1

Introduction

Contents

1.1	Introduction générale et plan de la thèse	12
1.2	Modélisation mathématique	13
1.2.1	Les équations d'Euler à surface libre	13
1.3	Les différents modèles asymptotiques	15
1.3.1	Présentation des équations	16
1.3.2	Caractéristiques de dispersion	18
1.4	Résultats d'existence de solutions pour les équations de type Boussinesq	19
1.4.1	Existence en temps long	19
1.4.2	Existence d'ondes solitaires	20
1.5	Schémas numériques adaptés aux équations asymptotiques	23
1.5.1	Explication du nouveau paradigme	24
1.5.2	Résultats de la nouvelle approche	24
1.6	Perspectives de recherche	25

1.1 Introduction générale et plan de la thèse

La modélisation des écoulements littoraux à surface libre en eau peu profonde représente aujourd’hui un enjeu scientifique de taille. La prise en compte des effets hydrodynamiques tels que les effets dispersifs et non-linéaires est un des objectifs importants de cette modélisation. Leur étude s’avère cruciale si l’on veut être capable de prédire l’impact de phénomènes à grande échelle tels que la propagation d’un tsunami. L’analyse et la simulation des équations de la physique associées à ces écoulements se révèlent être très complexes au vu des échelles considérées. En effet, pour modéliser des écoulements dans une situation réelle, la résolution numérique de ces équations est très coûteuse en temps de calcul (notamment en 3 dimensions). Il est alors impératif de réduire la complexité du système d’équations en négligeant des termes qui, selon les situations, ont une influence négligeable devant les autres. C’est ce qui a amené les physiciens et mathématiciens à pratiquer des analyses asymptotiques sur des petits paramètres introduits *via* un principe d’adimensionnement des différentes variables. Ce procédé leur a permis de dériver des équations simplifiées à partir de régimes physiques particuliers. Le premier modèle qui a vu le jour remonte à la fin du XIXème siècle et fut dérivé par Joseph Boussinesq [22] pour décrire la propagation d’une vague de faible amplitude en eau peu profonde sur un fond plat. Depuis, ce modèle a été largement étudié et amélioré au cours des dernières décennies incluant de plus en plus de phénomènes, on pense notamment aux effets non-linéaires (le modèle de Green-Naghdi en est le parfait exemple), aux effets liés à la variation du fond [63], ou en cherchant à améliorer les caractéristiques de dispersion des équations [60, 11, 57]. Du fait de la présence de termes dispersifs ou du caractère hyperbolique de certains modèles, le traitement numérique de ces équations n’est pas trivial. Plusieurs approches existent dans la littérature, chacune possédant ses avantages et ses inconvénients [17, 21, 38, 45, 59, 64].

L’objectif de cette thèse est de proposer un nouveau paradigme pour obtenir des schémas numériques plus adaptés aux modèles asymptotiques reproduisant plus fidèlement les effets de dispersions des différents modèles. Pour atteindre cet objectif, nous développons plusieurs outils qui seront présentés sur 6 chapitres auto-contenus. Le premier présente la dérivation détaillée de la plupart des modèles d’équations utilisés en pratique. Nous montrerons, notamment, que les modèles de type Boussinesq peuvent être répartis en deux familles. La première, la plus commune, regroupe les équations ayant pour inconnues une variable représentant l’élévation de la surface des vagues et une vitesse moyennée sur la dimension verticale. La seconde famille, quant à elle, est constituée de modèles formulés en fonction d’une variable représentant l’élévation de la surface et d’une variable qui s’apparente à un flux. Cette vision des modèles nous permettra d’en introduire un nouveau de type Boussinesq aux propriétés très prometteuses. Le deuxième chapitre permettra de justifier l’existence de solutions en temps long de ce nouveau modèle. On y proposera également une preuve d’existence d’ondes solitaires pour les modèles de Boussinesq et une méthode pour les calculer, lorsqu’elles existent, avec une forte précision (ce chapitre est largement inspiré de l’article [12] publié dans *Advances in Differential Equations*). Dans le troisième chapitre, on compare les propriétés de dispersion linéaires et non-linéaires des deux familles de modèles de Boussinesq. Ces différences s’avèrent très importantes notamment lorsque l’on souhaite modéliser des situations physiques où les effets non-linéaires sont prépondérants,

comme le déferlement des vagues par exemple (ce chapitre s'inspire de l'article [39] publié dans *Coastal Engineering*). Dans le quatrième chapitre nous présentons le nouveau paradigme sur un cas simple pour mettre en évidence ses avantages. Enfin, dans le dernier chapitre nous étendons cette méthode à d'autres modèles asymptotiques plus utilisés dans la pratique (ces deux chapitres s'inspirent de deux articles, dont l'un est en cours de révision et l'autre en cours de soumission). Dans la suite de cette introduction nous allons présenter en détails chacun des travaux de cette thèse.

1.2 Modélisation mathématique

1.2.1 Les équations d'Euler à surface libre

Commençons par rappeler le cadre physique utilisé pour modéliser une vague. Dans ce manuscrit, nous nous intéressons à l'évolution d'un fluide soumis uniquement à son propre poids. Nous négligeons donc toutes autres effets extérieurs comme la force de Coriolis par exemple. Nous supposons qu'il n'y a aucun échange entre l'extérieur et le fluide qui se retrouve délimité par deux frontières : le fond (supposé fixe au cours du temps) et la surface du fluide (qui varie au cours du temps). Nous supposons de plus que ces deux frontières sont paramétrées par des graphes ce qui exclut tout déferlement des vagues. Le fluide est supposé parfait, incompressible, irrotationnel et homogène. Sa viscosité et sa conductivité thermique ne sont donc pas prises en compte. Enfin, nous négligeons les tensions de surface et nous supposons qu'il n'y a que la pression atmosphérique qui agit sur le fluide. La modélisation mathématique d'un tel écoulement nécessite l'utilisation des équations d'Euler à surface libre. Avant d'énoncer ce système d'équations, nous allons introduire les notations qui seront utilisées dans tout ce manuscrit.

Nous nous intéressons essentiellement à des situations en 2 dimensions pour alléger les notations. On note z la variable de la dimension verticale et x celle de la dimension horizontale (lorsque l'on écrira les équations en 3 dimensions, on notera y la seconde dimension horizontale). On note $(u, w)^T$ le vecteur vitesse où $u = u(t, x, z)$ et $w = w(t, x, z)$ représentent respectivement ses composantes horizontale et verticale (on notera v la seconde composante horizontale), ρ la masse volumique du fluide (qui est constante) et $p = p(t, x, z)$ la pression.

La position du fluide au repos sera paramétrée par $z = 0$ et la surface du fluide par l'équation suivante

$$z = \eta(t, x),$$

où η est une inconnue du problème qui représente la forme des vagues. De plus, on paramètre le fond par

$$z = -d(x),$$

où $d(x)$ est la bathymétrie et est une donnée du problème. Enfin, on note $h = h(t, x)$ la profondeur totale de l'eau. On a alors la relation suivante

$$h(t, x) = d(x) + \eta(t, x).$$

Les inconnues du problème sont les vitesses u , w , l'élévation de la surface η et la pression p . Toutes ces notations sont résumées sur la figure 1.1.

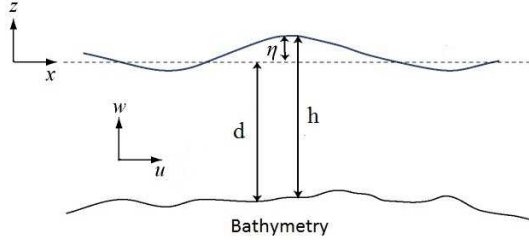


Figure 1.1 – Présentation du problème étudié

Dans ce contexte, le mouvement du fluide est décrit par les équations d'Euler

$$\left\{ \begin{array}{l} u_t + uu_x + wu_z + \frac{p_x}{\rho} = 0, \\ w_t + uw_x + ww_z + \frac{p_z}{\rho} + g = 0, \\ u_x + w_z = 0, \\ u_z - w_x = 0, \end{array} \right. \quad (1.2.1)$$

auxquelles nous ajoutons les conditions aux bords suivantes :

- en $z = \eta$,

$$w = \eta_t + u\eta_x, \quad (1.2.2)$$

$$p = 0. \quad (1.2.3)$$

- en $z = -d(x)$,

$$w = -d_x u. \quad (1.2.4)$$

Les deux premières équations du système (1.2.1) sont les équations de bilan de la quantité de mouvement et découlent directement du principe fondamental de la dynamique. La troisième équation correspond à la conservation de la masse associée à l'incompressibilité du fluide et la quatrième à l'irrotationnalité du fluide. Enfin, les conditions aux bords (1.2.2) et (1.2.4) sont des conditions cinématiques classiques qui traduisent deux hypothèses différentes. La première suppose qu'une particule située à la surface y reste pendant la totalité de l'écoulement. La deuxième suppose que le fond est imperméable. L'équation (1.2.3) traduit la continuité entre la pression du fluide et la pression extérieure qui est supposée constante. La pression p n'intervenant dans les équations que par son gradient, on peut définir cette pression extérieure à une constante près.

On la suppose donc nulle dans la suite.

D'un point de vue physique, la dynamique du fluide dépend de plusieurs grandeurs caractéristiques qui sont utilisées par les physiciens et les mathématiciens pour adimensionner le système en vue de faire apparaître les petits paramètres utiles pour simplifier les équations d'Euler au travers d'une analyse asymptotique. On note d_0 la profondeur caractéristique du milieu, λ la longueur d'onde de la vague qui servira de longueur horizontale caractéristique et a l'amplitude des vagues. On introduit alors les variables adimensionnées suivantes :

$$\begin{aligned}\tilde{x} &= \frac{x}{\lambda}, \quad \tilde{z} = \frac{z}{d_0}, \quad \tilde{t} = \frac{\sqrt{gd_0}}{\lambda} t, \quad \tilde{\eta} = \frac{\eta}{a}, \\ \tilde{u} &= \frac{d_0}{a\sqrt{gd_0}} u, \quad \tilde{w} = \frac{\lambda}{a} \frac{1}{\sqrt{gd_0}} w, \quad \tilde{p} = \frac{p}{gd_0\rho}.\end{aligned}$$

Ce choix d'adimensionnement n'est pas dû au hasard. Il repose notamment sur la théorie linéaire qui est décrite dans [49] qui met notamment en évidence la vitesse caractéristique de propagation d'une vague $c_0 = \sqrt{gd_0}$ (sans effet dispersif) que nous retrouverons régulièrement dans ce manuscrit. Une substitution dans les équations d'Euler permet de faire apparaître les deux paramètres suivant :

$$\varepsilon = \frac{a}{d_0}, \quad \sigma = \frac{d_0}{\lambda}.$$

ε est appelé paramètre de "non-linéarité" car on le retrouve devant tous les termes non-linéaires du système d'Euler. σ est appelé paramètre de "dispersion" ou de "faible profondeur" et intervient dans les équations *via* son carré. Dans la plupart des situations qui nous intéressent, les paramètres ε et σ seront petits (océanographie côtière, propagation d'un tsunami,...). Par exemple, en océanographie côtière, pour une houle de longueur d'onde $\lambda \approx 100$ m, contenant des vagues d'amplitude $a \approx 1$ m qui se propagent sur le plateau continental qui a pour profondeur $d_0 \approx 10$ m, les paramètres σ^2 et ε sont environ égaux à

$$\sigma^2 \approx 10^{-2}, \quad \varepsilon \approx 10^{-1}.$$

1.3 Les différents modèles asymptotiques

Pour écrire des modèles asymptotiques qui approchent les équations d'Euler, on se place dans des régimes asymptotiques spécifiques. Dans ce manuscrit, on considère surtout le régime de faible profondeur d'eau qui correspond à considérer σ très petit. Sous cette hypothèse, on peut considérer différents régimes concernant le paramètre ε . On présentera le régime faiblement non-linéaire (ε petit mais du même ordre que σ^2) et le régime fortement non-linéaire (ε quelconque). Historiquement, pour ces régimes asymptotiques, les équations les plus connues et utilisées pour les applications physiques sont celles de Saint-Venant, Boussinesq ou Green-Naghdi. Pour hiérarchiser les différents modèles, la littérature regorge d'approches différentes. La plus courante consiste à étudier les caractéristiques de dispersion des équations et de les comparer à celles des équations d'Euler. Dans les deux prochaines parties, nous présentons les

différents modèles asymptotiques qui nous intéressent dans ce manuscrit, puis nous discuterons des caractéristiques de dispersion de ces modèles.

1.3.1 Présentation des équations

Comme présenté précédemment, pour les problèmes physiques que l'on souhaite modéliser, une hypothèse qui ressort lorsqu'on observe les valeurs de ε et σ est de supposer σ^2 très petit et ε quelconque. Une analyse asymptotique au premier ordre (i.e. que l'on néglige les termes d'ordre σ^2) mène au modèle de Saint-Venant. Ces équations, très connues et utilisées pour modéliser la propagation des vagues en eaux très peu profondes (lorsque celles-ci atteignent la plage par exemple) ont l'avantage de simplifier grandement les équations d'Euler. Malheureusement, tous les effets dispersifs sont négligés. Dans le cadre de la modélisation de la propagation des vagues pour des eaux plus profondes, ces effets sont primordiaux. L'idée naturelle qui en résulte est d'étendre l'analyse asymptotique à l'ordre suivant puisque le petit paramètre σ est situé devant les termes responsables des effets dispersifs. C'est exactement comme cela que l'on obtient le modèle de Green-Naghdi. Ces équations prennent en compte plus d'effets dispersifs. D'un point de vue mathématique, c'est, aujourd'hui, le modèle le plus proche des équations d'Euler dans ce régime asymptotique. Au delà de cet état de fait, ces équations contiennent de nombreux termes non-linéaires (on parle d'équations fortement non-linéaires). Du point de vue de la résolution numérique, elles restent trop compliquées même dans le cadre de la modélisation en 2 dimensions. On doit notamment inverser un opérateur non local en temps. Récemment, D. Lannes et F. Marche ont cherché à simplifier ce système pour rendre la résolution numérique plus simple tout en conservant l'ordre de l'analyse asymptotique [52]. Mais, la solution la plus efficace (en terme de temps de calcul notamment) reste d'avoir recours à l'hypothèse de Boussinesq lorsque le problème physique que l'on souhaite modéliser le permet. Celle-ci fut énoncée par Boussinesq lui-même pour dériver son modèle asymptotique. L'idée est de négliger non seulement les effets dispersifs des équations d'Euler mais aussi ceux non-linéaires dans la mesure du raisonnable. Pour cette famille de modèles appelés aussi modèles faiblement non-linéaires, on suppose que σ^2 et ε sont très petits devant 1, mais on rajoute l'hypothèse supplémentaire $\varepsilon = \mathcal{O}(\sigma^2)$. Si on reproduit l'analyse asymptotique jusqu'à l'ordre σ^4 , on peut également négliger les termes de l'ordre de $\varepsilon\sigma^2$. Les premières équations de ce régime asymptotique datent de la fin du XIXème siècle. Elles sont composées de deux équations vérifiées par l'élévation de la surface des vagues η et par la vitesse horizontale moyennée sur la profondeur \bar{u} . Ce système ne prenait pas en compte l'effet de la variation du fond. En 1967, D. H. Peregrine a dérivé un système d'équations généralisant celles de Boussinesq en ajoutant ces effets [63],

$$\begin{cases} \eta_t + [h\bar{u}]_x = 0, \\ \bar{u}_t + \bar{u}\bar{u}_x + g\eta_x + \frac{d^2}{6}\bar{u}_{txx} - \frac{d}{2}[d\bar{u}]_{txx} = 0, \end{cases} \quad (1.3.1)$$

Notons que la première équation de ce système est exacte alors que dans la seconde des termes d'ordre $\varepsilon\sigma^2$ et σ^4 ont été négligés.

De nombreux chercheurs ont voulu améliorer ce résultat qui reste physiquement applicable uni-

quement pour des petites valeurs de σ et qui, par conséquent, néglige encore trop d'effets dispersifs. Ils ont de fait eu recours à des astuces consistant à ajouter des termes d'ordre σ^4 ou $\varepsilon\sigma^2$ (donc négligeables) pour améliorer les caractéristiques de dispersion linéaires à leur gré. Une autre approche consiste à écrire un système asymptotique où la vitesse moyennée sur la verticale est remplacée par une vitesse évaluée à une profondeur que l'on peut choisir. Elle fut introduite pour la première fois en 1994 par O. Nwogu. Cette dérivation permet d'obtenir des équations qui décrivent les effets dispersifs de la propagation d'une vague en eau plus profonde ($\sigma \approx 0.7$ voir [72] pour les détails) sans augmenter de manière importante la complexité des équations. Aucun terme non-linéaire n'est ajouté par rapport aux équations de Peregrine. Elles s'écrivent

$$\begin{cases} \eta_t + (hu^\alpha)_x + \left(B_1 d^3 u_{xx}^\alpha + B_2 d^2 (du^\alpha)_{xx} \right)_x = 0, \\ u_t^\alpha + u^\alpha u_x^\alpha + g\eta_x + A_1 d^2 u_{txx}^\alpha + A_2 d(du^\alpha)_{txx} = 0, \end{cases} \quad (1.3.2)$$

où u^α est la vitesse horizontale évaluée en $z = -\theta d$, $\theta \in (0, 1)$ et

$$A_1 = \frac{\theta^2}{2}, \quad A_2 = \theta, \quad B_1 = \frac{\theta^2}{2} - \frac{1}{6}, \quad B_2 = \theta + \frac{1}{2}.$$

Notons que pour ce système la première équation n'est pas exacte contrairement aux équations de Peregrine.

D'un point de vue numérique, les équations de type Boussinesq ont été largement étudiées, ce qui a même permis l'élaboration de nouveaux modèles. En effet, lorsque l'on observe le système (1.3.1), il apparaît plus judicieux de choisir comme inconnues η et $h\bar{u}$. La réécriture du système en fonction de ces nouvelles variables transforme la première équation en une équation linéaire, mais la seconde ne s'y adapte pas aussi facilement. En effet, elle conserve des dérivées de \bar{u} qui deviennent alors des dérivées de $\frac{\bar{q}}{h}$, ce qui inclut donc des termes non-linéaires et complique alors les équations. C'est en faisant ce constat que M. B. Abbott a eu l'idée d'exprimer asymptotiquement les équations de Peregrine en fonction de η et $q = h\bar{u}$. Pour cela, il a négligé (ou rajouté selon le point de vue) des termes non-linéaires d'ordre $\varepsilon\sigma^2$ pour transformer les dérivées de \bar{u} en dérivées de \bar{q} . Le modèle de type Boussinesq que l'on obtient s'écrit

$$\begin{cases} \eta_t + \bar{q}_x = 0, \\ \bar{q}_t + \left(\frac{\bar{q}^2}{h} \right)_x + gh\eta_x + \frac{d^3}{6} \left(\frac{\bar{q}}{d} \right)_{txx} - \frac{d^2}{2} \bar{q}_{txx} = 0. \end{cases} \quad (1.3.3)$$

Les deux modèles diffèrent donc uniquement par des termes non-linéaires. Il en résulte que les caractéristiques de dispersion linéaire que l'on a évoqué précédemment sont exactement les mêmes. D'un point de vue numérique, la formulation conservative des équations d'Abbot apporte plus de souplesse dans leur résolution. Naturellement, de nombreux auteurs ont donc amélioré ces équations en ayant recours à certaines astuces énoncées précédemment [57].

On peut donc conclure que pour une équation de type Boussinesq formulée en fonction de la vitesse et de l'amplitude, il existe une formulation en fonction d'un flux et de l'amplitude (et vice-versa). On se retrouve donc avec deux familles de modèles de type Boussinesq. Naturellement le

système de Nwogu appartient à la première famille. Il est donc possible de dériver son équivalent en fonction de l’élévation de la surface et d’une quantité qui s’apparenterait à un flux, ce qui permet d’obtenir les équations suivantes

$$\begin{cases} \eta_t + Q_x + \left[B_1 d^3 \left(\frac{Q}{d} \right)_{xx} + B_2 d^2 Q_{xx} \right]_x = 0, \\ Q_t + \left(\frac{Q^2}{d + \eta} \right)_x + g(d + \eta) \eta_x + \left(A_1 d^3 \left(\frac{Q}{d} \right)_{txx} + A_2 d^2 Q_{txx} \right) = 0, \end{cases} \quad (1.3.4)$$

où $Q = hu^\alpha$ et A_1, A_2, B_1 et B_2 sont les mêmes constantes que dans le modèle de Nwogu.

Ce modèle dérivé des équations de Nwogu est, à notre connaissance, nouveau et s’avère très prometteur notamment du point de vue de la résolution numérique. En effet, sa première équation est linéaire (ce qui n’est pas le cas des équations de Nwogu) et sa seconde est très proche de celle du système d’Abbot, ce qui nous a amené à le nommer : modèle de Nwogu-Abbott.

Le chapitre 2 de cette thèse regroupe toutes les dérivations rigoureuses des modèles cités ci-dessus. L’objectif est de regrouper de manière exhaustive tous les modèles asymptotiques utilisés en pratique pour modéliser le problème physique présenté précédemment. On détaille également la dérivation du nouveau modèle faiblement non-linéaire : le modèle de Nwogu-Abbott.

1.3.2 Caractéristiques de dispersion

Dans la partie précédente, nous avons régulièrement fait référence aux caractéristiques de dispersion des modèles et à leur importance justifiant même certaines dérivations uniquement sur le fait que ces caractéristiques s’en retrouvent améliorées. Cette vision des choses vient du caractère dispersif des équations d’Euler et du fait que l’analyse asymptotique à l’origine des différents modèles de type Boussinesq négligent des termes responsables de ces effets. Il est donc naturel de chercher à optimiser l’erreur de dispersion qui est commise tout en conservant le même régime asymptotique. De ce fait, cela nous permet de justifier l’utilisation de certains modèles en dehors de leur domaine de validité.

Plusieurs chercheurs se sont attelés à cette tâche dans un cadre linéaire (voir [36]) qui permet, comme souvent, d’utiliser des solutions analytiques. Ces études ont notamment permis d’optimiser les valeurs des paramètres présents dans les modèles ($\theta = \sqrt{0.22} - 1$ par exemple pour le modèle de Nwogu). Néanmoins, ces études ne prennent pas en compte les effets non-linéaires des différents modèles alors que certains d’entre eux sont également négligés dans l’analyse asymptotique à l’origine des modèles de Boussinesq. La théorie de Stokes du premier et second ordre permet de quantifier l’erreur que l’on commet en négligeant ces termes, mais cette étude n’est valable que pour un fond plat. Les tests numériques restent donc nécessaires pour comparer les modèles dans un régime non-linéaire avec une bathymétrie variable.

Le chapitre 4 de ce manuscrit a pour but de hiérarchiser les modèles de type Boussinesq introduits dans le chapitre 2. En effet, les modèles de Boussinesq peuvent être répartis en deux familles : les modèles formulés en fonction de la surface et d’une vitesse horizontale, appelés modèles en vitesse-amplitude ; et ceux exprimés en fonction de la surface et d’un flux, appelés

modèles en flux-amplitude. Comme dit précédemment, un modèle d'une famille a son équivalent dans l'autre en ajoutant quelques termes non-linéaires négligeables dans le régime asymptotique des modèles de Boussinesq. Dans ce chapitre, on compare donc les caractéristiques de dispersion non-linéaire d'un point de vue théorique et numérique. Cette étude met en évidence deux comportements propres à chaque famille d'équations de Boussinesq : les modèles formulés en vitesse-amplitude surévaluent de manière importante l'amplitude de la vague ; alors que les modèles formulés en flux-amplitude sous-évaluent celle-ci. Ce résultat peut paraître anodin mais il s'avère crucial pour déterminer, par exemple, un critère de déferlement d'une vague. En effet, ce dernier doit être adapté au modèle choisi et à la formulation de celui-ci.

1.4 Résultats d'existence de solutions pour les équations de type Boussinesq

Dans cette partie, nous présentons d'une part une théorie de Cauchy pour les équations de Nwogu-Abbott introduites précédemment et, d'autre part, l'existence d'ondes solitaires pour les équations de type Boussinesq.

1.4.1 Existence en temps long

En complément de la dérivation des équations asymptotiques, une analyse rigoureuse de ces modèles est requise en tant que modèles approximatifs des équations d'Euler à surface libre. Une multitude de travaux vont dans ce sens depuis quelques décennies par l'intermédiaire de Ovsjannikov [62] ou Craig [32] par exemple. Pour justifier un modèle, il est courant de répondre aux deux questions suivantes :

- *Le modèle asymptotique est-il bien posé dans un intervalle de temps pertinent ?*
- *Est-ce que ce modèle approche convenablement la solution des équations d'Euler à surface libre ?*

Pour répondre à ces questions, deux types de résultats peuvent être envisagés : l'*existence* des solutions et leur *consistance* avec les équations d'Euler.

La consistance des différents modèles asymptotiques avec les équations d'Euler a été largement étudié dans les dernières décennies (voir [49] pour la définition et les résultats principaux). Elle a notamment été démontrée pour les équations de type Boussinesq (pour les équations de Peregrine, Nwogu, systèmes abcd,...) avec un fond plat dans une formulation vitesse-amplitude (voir le travail de J. L. Bona, T. Colin et D. Lannes [20]). A notre connaissance, un tel résultat n'existe pas pour les modèles de Boussinesq formulés en flux-amplitude. Mais, nous pensons qu'il s'adapte bien en démontrant la consistance du modèle exprimé en flux-amplitude avec son "*alter-ego*" formulé en vitesse-amplitude (par exemple le système d'Abbot est consistant avec celui de Peregrine qui l'est lui-même avec celui de Euler, on en déduirait alors le résultat par transitivité).

L’existence de solution en temps long a aussi été largement étudiée pour les modèles de Boussinesq formulés en vitesse-amplitude. Généralement, l’intervalle de temps d’existence dépend des petits paramètres σ et ε . Le caractère hyperbolique des équations de Boussinesq avec fond plat nécessite de chercher un temps d’existence de l’ordre de $\frac{1}{\varepsilon}$ qui correspond au temps optimal appelé “temps hyperbolique” (voir [49] ou [58] pour les détails). Cette propriété n’est vérifiée que par un nombre limité de modèle de Boussinesq [24, 67, 68]. Là encore, il n’y a pas, à notre connaissance, de résultats sur les modèles de Boussinesq exprimés en flux-amplitude.

C’est pour cette raison que dans la première partie du chapitre 3, nous démontrons un théorème d’existence sur le nouveau modèle de Boussinesq que nous avons introduit : le modèle de Nwogu-Abbott (1.3.4). Le résultat suivant est démontré

Théorème 1. *Soit $(\eta_0, q_0) \in H^2(\mathbb{R}) \times H^4(\mathbb{R})$ tel que*

$$d + \varepsilon \eta_0(x) \geq a \quad \forall x \in \mathbb{R}, \quad (1.4.1)$$

$$g(d + \varepsilon \eta_0) - \varepsilon^2 \frac{q_0^2}{(d + \varepsilon \eta_0)^2} \geq b \quad \forall x \in \mathbb{R}, \quad (1.4.2)$$

où $a > 0$, $b > 0$, $(\alpha, \beta) \in \mathbb{R}_+^2$ et la bathymétrie d est constante. Alors, il existe un temps $T > 0$ indépendant de ε et une unique solution locale au problème de Cauchy associé aux équations de Nwogu-Abbott à fond plat telle que

$$\eta \in C([0, \frac{T}{\varepsilon}]; L^2(\mathbb{R})),$$

$$q \in C([0, \frac{T}{\varepsilon}]; L^2(\mathbb{R})),$$

avec les conditions initiales

$$\eta(0, x) = \eta_0(x), \quad q(0, x) = q_0(x).$$

Le système de Nwogu-Abbott est donc bien posé sur un intervalle de temps $[0, \frac{T}{\varepsilon}]$. Ce résultat justifie encore plus l’intérêt de ce nouveau modèle qui, rappelons le, est plus adapté à la résolution numérique que certains modèles de Boussinesq tout en conservant des caractéristiques de dispersion linéaire au même niveau que celles des équations de Nwogu. Notons que nous n’étudions pas ici la consistance de ce modèle avec les équations d’Euler à surface libre. Mais, nous sommes convaincus que ce résultat est vrai et le réservons pour un travail ultérieur.

1.4.2 Existence d’ondes solitaires

Lorsque l’on résout numériquement un système d’équations aux dérivées partielles, il est important de vérifier la pertinence des schémas et leur implémentation. Un moyen efficace de faire cela est d’avoir recours à une grille de convergence qui permet notamment de mettre en évidence les différences d’ordre de convergence entre les schémas. Pour réaliser ces études, il est nécessaire de considérer des solutions particulières dont on connaît la forme générale à chaque temps et qui, dans le cadre des équations dispersives, sont indépendantes des caractéristiques de dispersion

pour éviter toute influence de celles-ci. Les solutions classiquement utilisées sont les ondes solitaires (ou solitons). Ce sont des solutions positives, globales en temps et suffisamment régulières (au moins C^2) qui se propagent sans aucune déformation au cours du temps sur un fond plat à une vitesse de propagation constante notée c . On suppose également qu'une telle solution et ses dérivées première et seconde tendent vers zéro à l'infini. Ces solutions très particulières permettent notamment de comparer les caractéristiques des différents modèles dans des cadres très spécifiques (dans le cas non-linéaire par exemple). Il est donc très important d'étudier l'existence d'ondes solitaires pour un modèle asymptotique donné et d'être capable de calculer ces solutions avec une grande précision.

La littérature regorge de telles études pour des modèles variés. On peut notamment citer le soliton du modèle de Green-Naghdi utilisé dans de nombreux travaux ([52] notamment) et qui s'écrit sous la forme analytique suivante

$$\begin{cases} \eta(\xi) = A \operatorname{sech}^2 \left(\frac{\sqrt{3A}}{2d\sqrt{d+A}} \xi \right), \\ \bar{u}(\xi) = c \frac{\eta(\xi)}{d + \eta(\xi)}, \end{cases} \quad (1.4.3)$$

où A est un réel qui correspond à l'amplitude du soliton, d est la bathymétrie constante et c est la vitesse de propagation définie par la relation suivante

$$c = \sqrt{g(d+A)}.$$

Malgré cet exemple pratique, tous les systèmes asymptotiques considérés ne disposent pas de solutions analytiques connues. Par exemple, il n'existe pas encore d'expression analytique d'une onde solitaire solution des équations d'Euler, bien qu'il soit possible d'en calculer numériquement [29]. De la même manière, aucun soliton n'a été trouvé pour la majorité des équations de type Boussinesq présentés dans ce manuscrit ce qui restreint les possibilités de cas test. Des alternatives ont notamment été proposées par G. Wei et J. T. Kirby [74]. Ces derniers ont décidé d'utiliser une onde solitaire approchée pour étudier leur schéma numérique appliqué aux équations de Nwogu. Ce soliton s'écrit

$$\begin{cases} \eta(\xi) = a_1 \operatorname{sech}^2(b\xi) + a_2 \operatorname{sech}^4(b\xi), \\ \bar{u}(\xi) = a \operatorname{sech}^2(b\xi). \end{cases} \quad (1.4.4)$$

avec

$$\begin{aligned} b &= \frac{\sqrt{c^2 - gd}}{2d\sqrt{\beta gd - \alpha c^2}}, \\ a &= \frac{c^2 - gd}{c}, \\ a_1 &= \frac{d}{3} \frac{c^2 - gd}{\beta gd - \alpha c^2}, \\ a_2 &= -\frac{d}{2} \left(\frac{c^2 - gd}{c^2} \right)^2 \frac{\beta gd + 2\alpha c^2}{\beta gd - \alpha c^2}. \end{aligned}$$

Il a été maintes et maintes fois réutilisé dans la littérature comme solution particulière des équations de Nwogu [40, 72]. Néanmoins, ce n'est pas une solution exacte du système de Nwogu mais d'un autre système qui diffère de ce dernier uniquement par des termes d'ordre $\varepsilon\sigma^2$ et σ^4 . Elle permet donc de pratiquer certains tests numériques avec les équations de Nwogu dans des régimes asymptotiques très particuliers (il faut vraiment se placer dans le régime $\sigma^2 \ll 1$ et $\varepsilon \ll 1$) [72, 74]. Cette solution analytique peut avoir du sens lorsque l'on modélise un problème physique. Mais, d'un point de vue mathématique, elle n'est pas viable et ne permet pas d'étudier les propriétés des équations en toute généralité. Cette approche peut, bien entendu, se généraliser à la majorité des équations de type Boussinesq (Madsen-Sørensen, Beji-Nadaoka pour ne citer qu'eux).

La deuxième partie du chapitre 3 est dédiée à l'étude de l'existence d'ondes solitaires pour les équations de type Boussinesq. L'idée ici est de déterminer pour quelles vitesses de propagation une onde solitaire existe et de la calculer numériquement avec une grande précision. Un des points cruciaux de ce travail concerne la relation très importante qui existe entre la vitesse de propagation et l'amplitude initiale du soliton. C'est pour cela, qu'en cas d'existence, nous donnons cette relation centrale pour le calcul pratique du soliton. Nous étudions également le comportement des solitons à l'infini et montrons qu'ils y décroissent exponentiellement.

Le cas du modèle de Nwogu-Abbott est traité à part car, pour le moment, nous n'avons pas encore démontré l'existence d'onde solitaire même si certains résultats numériques, détaillés dans le chapitre 3, tendent à conjecturer leurs existences pour une vitesse de propagation supérieure à \sqrt{gd} . Les résultats obtenus sont résumés brièvement dans le théorème-bilan suivant

Théorème 2. *On note $c_0 = \sqrt{gd}$ et on considère les modèles de Boussinesq suivants.*

1) Equations de Beji-Nadaoka.

Soit $\gamma = \alpha_B + 1/3$. On suppose que l'une des hypothèses suivantes est vérifiée :

- i) $\gamma = 0$, $c > c_0$,
- ii) $\alpha_B < 0$, $\gamma > 0$, $c > c_0$,
- iii) $\alpha_B > 0$, $\gamma > 0$, $c \in (c_0, c_0 \frac{2 - \frac{\alpha_B}{\gamma}}{\sqrt{\frac{\alpha_B}{\gamma}}})$.

Alors il existe une unique onde solitaire solution des équations de Beji-Nadaoka de la forme $(\eta_c(x - ct), u_c(x - ct))$. De plus, l'amplitude A de η_c et la vitesse de propagation c vérifient la relation suivante :

$$c^4 \gamma \left[\frac{A^3}{6(d+A)^3} - \frac{A^2}{2(d+A)^2} \right] + c^2 c_0^2 \left[\gamma \log\left(\frac{A+d}{d}\right) - \gamma \frac{A}{d+A} + \frac{\alpha_B}{2} \frac{A^2}{d(d+A)} \right] - c_0^4 \frac{\alpha_B A^2}{2d^2} = 0. \quad (1.4.5)$$

Inversement, si $\gamma < 0$, $\alpha_B < 0$ et $c \geq 0$, alors les équations de Beji-Nadaoka n'ont pas de solutions de la forme précédente.

2) Equations de Madsen-Sørensen.

Pour tout $c > c_0$, il existe une unique onde solitaire de la forme $(\eta_c(x - ct), q_c(x - ct))$ solution des équations de Madsen-Sørensen.

De plus, la relation entre la vitesse de propagation c et de l'amplitude A de η_c est donnée par

$$c^2 = c_0^2 \frac{\frac{A^2}{2} + \frac{A^3}{6d}}{dA - d^2 \log(\frac{d+A}{d})}. \quad (1.4.6)$$

Inversement, si $c \leq c_0$, alors les équations de Madsen-Sørensen n'ont pas de solution de la forme précédente.

3) Equations de Nwogu.

On suppose que l'une des hypothèses suivantes est vérifiée :

i) $\alpha \in (-\frac{1}{2}, -\frac{1}{9})$ et $c > c_0$,

ii) $\alpha \in (-\frac{1}{9}, 0)$ et $c > c_0 \sqrt{\frac{\frac{\beta^2}{\alpha^2}}{2 - \frac{\beta}{\alpha}}}$.

Alors, il existe une unique onde solitaire de la forme $(\eta_c(x-ct), u_c(x-ct))$ solution des équations de Nwogu. L'amplitude U de u_c et la vitesse de propagation du soliton c satisfont

$$\begin{aligned} \frac{1}{6}U^3 - \left(\frac{c}{2} + \frac{\beta c_0^2}{4c\alpha} \right) U^2 + c_0^2 \left(\frac{c}{3} + \frac{\beta}{2c\alpha} (\beta c_0^2 - \alpha c^2) \right) \frac{U}{c\alpha}, \\ - \frac{c_0^2(\beta c_0^2 - \alpha c^2)}{c^2 \alpha^2} \left(\frac{c}{3} + \frac{\beta}{2c\alpha} (\beta c_0^2 - \alpha c^2) \right) \log(1 + \frac{c\alpha}{\beta c_0^2 - \alpha c^2} U) = 0. \end{aligned} \quad (1.4.7)$$

Inversement, si $c \leq c_0$, alors les équations de Nwogu n'ont pas de solution de la forme précédente.

4) Equations de Nwogu-Abbott.

Pour tout $c \leq c_0$, les équations de Nwogu-Abbott n'admettent pas d'ondes solitaires comme solution.

Les résultats de ce chapitre 3 sont très largement réutilisés dans la suite de la thèse pour valider l'implémentation des schémas numériques considérés. Ils sont également réutilisés dans le chapitre 4 dans un cas test qui étudie des effets non-linéaires des modèles de Boussinesq.

1.5 Schémas numériques adaptés aux équations asymptotiques

Comme nous l'avons rappelé précédemment, pour modéliser un écoulement à surface libre, on a généralement recours à des modèles asymptotiques dérivés à partir des équations d'Euler. Les modèles obtenus sont souvent complexes (bien qu'ils soient plus simples que les équations d'Euler) et peuvent avoir un fort caractère hyperbolique ou contenir des termes dispersifs via des dérivées du troisième ordre. En conséquence, les schémas numériques à mettre en œuvre pour résoudre ces équations sont extrêmement complexes (voir [25]). Notons également que le modèle numérique obtenu ne peut contenir plus de physique que le modèle asymptotique. Dans le meilleur des cas, il reproduit seulement les effets dispersifs ou non-linéaires du modèle étudié, bien que généralement la troncature du schéma numérique utilisé filtre plusieurs effets dispersifs ou non-linéaires. Cela représente une limitation évidente de la méthodologie. Ajoutons que de nombreux modèles de nature et de forme différentes existent dans la littérature et qu'une solution

universelle pour palier à ce problème ne semble pas possible. C'est dans ce contexte que nous proposons de mettre en œuvre une approche nouvelle et innovante qui sera expliquée dans la prochaine partie.

1.5.1 Explication du nouveau paradigme

Nous souhaitons présenter un nouveau paradigme qui pourrait améliorer la relation (équations asymptotiques)-(schéma numérique) qui semble avoir montré plusieurs limites. L'idée est d'inverser le paradigme usuel décrit ci-dessous :

$$\text{modèle physique} \longmapsto \text{modèle asymptotique} \longmapsto \text{modèle numérique.}$$

Plus précisément, au lieu de discrétiser des équations relativement complexes, nous proposons d'introduire la démarche suivante :

- *Ecrire directement des schémas numériques sur les équations d'Euler qui sont dans un certain sens les bonnes équations à étudier,*
- *Effectuer l'analyse asymptotique sur ces équations discrètes ou semi-discrètes pour obtenir de nouveaux modèles asymptotiques discrets.*

Dans le chapitre 5, nous appliquons ce nouveau paradigme aux équations de Peregrine dans le but de mettre en évidence les différences qui apparaissent. Pour cela, nous commençons par discrétiser les équations d'Euler à surface libre par rapport à la variable horizontale x en utilisant une méthode de Galerkin avec les fonctions \mathbb{P}_1 . On choisit de ne pas discrétiser la variable verticale z car l'analyse asymptotique que nous allons utiliser repose sur un procédé de moyennisation par rapport à celle-ci qui permet l'obtention d'équations asymptotiques indépendantes de z . On adapte ensuite la dérivation des équations de Peregrine aux équations d'Euler semi-discrètes. Les calculs mènent à un nouveau schéma numérique consistant avec les équations de Peregrine. Pour évaluer l'impact qu'a le nouveau paradigme sur ce nouveau schéma, nous présentons dans le chapitre 5 un schéma numérique "classique". Pour cela, on applique la *même* méthode de Galerkin avec les fonctions \mathbb{P}_1 directement sur les équations de Peregrine. La fin de ce chapitre 5 est consacrée à la comparaison entre les deux schémas d'un point de vue théorique et numérique à l'aide de cas test.

Le chapitre 6 a pour vocation, quant à lui, d'étendre cette méthode à des modèles asymptotiques plus pertinents physiquement, comme les modèles de Nwogu et Green-Naghdi. Nous détaillons la dérivation de ces nouveaux modèles asymptotiques discrets dans ce dernier chapitre ainsi qu'une comparaison numérique entre le nouveau schéma obtenu pour les équations de Nwogu avec un schéma obtenu de manière "classique".

1.5.2 Résultats de la nouvelle approche

Comme nous l'avons précisé précédemment, dans le but de calibrer l'effet de la nouvelle méthode sur le schéma numérique qui en résulte, on applique la même méthode de Galerkin sur les

équations d’Euler et sur les équations de Peregrine. De fait, on finit par comparer les schémas que l’on obtient et qui sont tout deux consistants avec le système de Peregrine.

Lorsque l’on étudie les deux schémas de plus près, on se rend compte que d’importantes différences existent. La première qui peut être relevée concerne la discrétisation du terme “ $(h\bar{u})_x$ ” dans la première équation du système (1.3.1). En effet, lorsque l’on applique directement une méthode de Galerkin à ce terme on obtient une discrétisation symétrique en h et \bar{u} , alors que celle obtenue *via* le nouveau paradigme ne l’est pas. Cette première différence a notamment un impact sur les propriétés de shoaling⁽¹⁾ du schéma numérique. La seconde variante notable entre les deux schémas se trouve dans la discrétisation des termes $\frac{d^2}{6}\bar{u}_{txx} - \frac{d}{2}[d\bar{u}]_{txx}$ de la seconde équation du système (1.3.1), responsables des effets dispersifs du modèle de Peregrine. Une étude des opérateurs discrets permet de démontrer, dans le chapitre 5, que le schéma numérique obtenu avec le nouveau paradigme conserve des caractéristiques de dispersion proches de celles des équations continues. Pour confirmer cette étude, nous procédons à des tests numériques. Nous commençons par pratiquer un test de convergence (à l’aide de la propagation d’une onde solitaire) qui nous permet de mettre en évidence que le nouveau paradigme n’a aucune influence sur l’ordre de convergence. Néanmoins, la propagation d’une onde monochromatique solution des équations de Peregrine linéaires avec chaque schéma fait apparaître deux comportements différents : avec le nouveau schéma, l’onde conserve une vitesse proche de celle calculée avec la théorie de Stokes, même pour un pas en espace grossier ; alors qu’avec le schéma “classique”, cette vitesse est sous-évaluée. Le chapitre 6 présente des résultats similaires pour des schémas consistants avec les équations de Nwogu. Il se termine avec un cas test issu d’une situation physique, mettant en jeu plusieurs caractéristiques de dispersion (vitesse de phase d’une onde et gradient de shoaling). Encore une fois, il apparaît que le schéma issu du nouveau paradigme reproduit mieux le comportement global de la vague (pour un pas en espace relativement élevé) que celui obtenu de manière classique en appliquant directement une méthode de Galerkin aux équations de Nwogu.

1.6 Perspectives de recherche

Dans cette partie nous proposons différentes perspectives de recherche qui pourraient prolonger ce manuscrit.

- En continuité du résultat en temps long présenté dans la partie 3.3 pour les équations de Nwogu-Abbott, nous envisageons d’étendre cette étude à tous les modèles de Boussinesq formulés en flux-amplitude. La suite logique sera d’étudier la consistance de ces modèles avec les équations d’Euler à surface libre en se basant sur les résultats de J. L. Bona, T. Colin et D. Lannes [20].
- La partie 3.4.4 de ce manuscrit propose une méthode pour approcher numériquement une onde solitaire pour les équations de Nwogu-Abbott. Nous espérons pouvoir fournir un résultat

¹Propriétés qui mettent en évidence la relation entre l’amplitude d’une vague et la variation du fond

d'existence pour ces équations, ce qui permettra d'étudier ce nouveau modèle de manière plus précise.

Le nouveau paradigme introduit dans le chapitre 5 pour trouver des nouveaux schémas numériques consistants avec les équations asymptotiques est nouveau et de nombreuses choses restent à être étudiées. Nous exposons ici plusieurs des ces perspectives :

- L'une des questions assez importante qui intervient naturellement est de savoir ce qu'il se passe lorsque l'on change le schéma numérique de base appliqué aux équations d'Euler. Le choix de ce schéma initial représente un nouveau degré de liberté pour la modélisation de la propagation des vagues. De fait, un changement aussi simple que de discréteriser uniquement les équations d'Euler par rapport à la variable verticale pourrait permettre de dériver de nouveaux modèles de type Boussinesq. Cette approche ressemble beaucoup aux modèles multi-couches que l'on peut retrouver dans la littérature pour résoudre numériquement les équations d'Euler. On espère, par le biais de cette étude, relier ces méthodes multi-couches avec les modèles de types Boussinesq.

- Une autre piste d'amélioration consisterait à étudier la conservation des propriétés d'un schéma initialement choisi pour discréteriser les équations d'Euler à surface libre après l'application de l'analyse asymptotique. On souhaite en déduire des conditions de stabilité et/ou de convergence que doit vérifier le schéma initial.

- Le cas des conditions aux bords du domaine constitue un réel défi pour l'avenir. Dans ce manuscrit nous ne considérons que le cas des conditions périodiques pour éviter tout problème. Quand celles-ci ne convenaient pas pour certaines simulations numériques (étude de shoaling par exemple), nous avons utilisé des zones de relaxation pour atténuer la vague jusque zéro sans provoquer de réflexion qui aurait pu invalider les résultats. Nous espérons donc appliquer cette méthode à d'autres conditons aux bords. Notons tout de même que l'étude des équations de Boussinesq avec des conditions de Dirichlet, par exemple, est encore un problème ouvert ne serait-ce que pour démontrer l'existence de solutions [3].

- Dans ce manuscrit, nous nous sommes concentrés sur les équations de Boussinesq qui sont des modèles faiblement non-linéaires. La nouvelle méthode a donc logiquement eu peu d'influence sur les effets non-linéaires du modèle. Dans la partie 6.3.1, nous présentons un nouveau schéma numérique pour les équations de Green-Naghdi obtenu avec ce nouveau paradigme. Par la suite, nous étudierons, à partir de ce schéma numérique, l'impact que peut avoir le nouveau paradigme sur les effets non-linéaires en utilisant différents tests numériques.

- Enfin, il sera nécessaire d'étendre ce nouveau paradigme au cas des équations asymptotiques en deux dimensions. Même si la procédure ne changera pas beaucoup, la plupart des simplifications que l'on fait dans les chapitres 5 et 6 se basent sur des études de consistance qui ne sont pas applicables en dimension 2. Nous espérons néanmoins valider le nouveau schéma

numériquement *via* des cas tests que nous effectuerons d'abord sur les équations de Peregrine $2D$, puis que nous étendrons sur d'autres modèles.

Chapitre 2

Modélisation et mise en équations du problème

Contents

2.1	Introduction	30
2.2	Notations et modélisation mathématique	30
2.3	Développement asymptotique	34
2.4	Equations de Saint-Venant (ou shallow water)	37
2.5	Equations de Boussinesq	38
2.5.1	Equations de Peregrine	39
2.5.2	Equations d'Abbott	40
2.6	Equations de Boussinesq étendues (ou améliorées)	41
2.6.1	Modèle de Beji-Nadaoka	41
2.6.2	Modèle de Madsen et Sørensen	43
2.6.3	Modèle de Nwogu	45
2.6.4	Modèles <i>abcd</i>	49
2.7	Equations de Green-Naghdi	51

2.1 Introduction

Lorsque l'on souhaite modéliser l'évolution d'un écoulement littoral à surface libre, les équations d'Euler s'imposent naturellement. La complexité et le fort caractère non-linéaire de ces équations limitent leur utilisation pour effectuer des calculs numériques. En effet, les temps de calcul qui en résultent sont souvent trop longs. On a alors généralement recourt à des modèles simplifiés *via* une analyse asymptotique. Pour cela, on néglige certains effets dispersifs ou non-linéaires en considérant des régimes asymptotiques adéquats. Ce premier chapitre a pour but de référencer des modèles asymptotiques qui représentent des alternatives intéressantes aux équations d'Euler. On souhaite proposer le détail des différentes dérivations pour les modèles asymptotiques les plus utilisés dans la pratique. L'idée récurrente des dérivations est de remplacer les équations d'Euler par des équations réduites faisant intervenir une vitesse indépendante de la dimension verticale (via une intégration sur la profondeur ou en évaluant les vitesses en une profondeur arbitraire). Un des aspects importants de ces modèles est de conserver au maximum les propriétés de dispersion des équations d'Euler. Ces propriétés sont cruciales pour modéliser différentes situations physiques comme le déferlement des vagues sur la côte (voir [66]). C'est pour cela que l'on fonde les développements asymptotiques sur des petits paramètres qui apparaissent lors de l'adimensionnement des équations d'Euler et qui s'apparentent à ces effets. En pratique, il existe une multitude de modèles qui permettent cela. Mais, dans le contexte de ce document, on se propose de passer en revue les plus connus et les plus utilisés. On commencera par le plus simple : le modèle de Saint-Venant. Puis, on détaillera plusieurs modèles de type Boussinesq (dérivés par Peregrine, Nwogu, Beji et Nadaoka, Madsen et Sørensen). En plus de rappeler les dérivations rigoureuses de ces modèles, l'un des objectifs de ce chapitre est de mettre en évidence deux familles de modèles de Boussinesq. La première, la plus commune, regroupe les équations ayant pour inconnues l'élévation de la surface des vagues et une vitesse horizontale. On l'appellera famille des modèles en "vitesse-amplitude" (ou en " (η, u) "). La seconde famille, quant à elle, est constituée de modèles formulés en fonction de l'élévation de la surface et d'une variable qui s'apparente à un flux. On l'appellera famille des modèles en "flux-amplitude" (ou en " (η, q) "). Cette manière de voir les choses nous permettra d'introduire un nouveau modèle de Boussinesq aux propriétés très prometteuses. On terminera par présenter la dérivation du modèle de Green-Naghdi qui est composé d'équations fortement non-linéaires. Pour commencer, on va rappeler le problème que l'on souhaite modéliser et introduire les notations utilisées. Ensuite, on mettra en œuvre la méthode d'analyse asymptotique qui est à la base de tous les modèles.

2.2 Notations et modélisation mathématique

Pour simplifier les calculs et les notations, nous allons nous placer dans une configuration en 2 dimensions d'espace (les calculs s'adaptent parfaitement aux problèmes en 3 dimensions). Commençons par rappeler le problème physique. On souhaite modéliser l'écoulement d'un fluide irrotationnel et incompressible se mouvant à surface libre et soumis à la gravité (g désignera la constante gravitationnelle). On notera z la variable de la dimension verticale et x celle de la dimension horizontale (y la seconde dimension horizontale pour les équations en 3D), $(u, w)^T$ le

vecteur vitesse (v la seconde composante horizontale), ρ la densité et p la pression. Le vecteur vitesse dérive d'un potentiel que l'on notera Φ .

La position de la mer au repos sera paramétrée par $z = 0$ (on suppose que c'est une droite) et l'élévation de la surface de la mer par l'équation suivante

$$z = \eta(t, x),$$

où η est une inconnue du problème. On note a l'amplitude maximale des vagues (donc la valeur maximale que prend la fonction η). $d(x)$ représente la bathymétrie qui est supposée indépendante du temps et qui est supposée connue. Le fond est alors paramétré par

$$z = -d(x),$$

où d est une fonction suffisamment régulière. On note d_0 la profondeur moyenne. Enfin, h est la profondeur totale de l'eau. Ainsi

$$h(t, x) = d(x) + \eta(t, x).$$

Enfin, λ représente la longueur d'onde de la vague modélisée. Les notations sont résumées sur la figure 2.1.

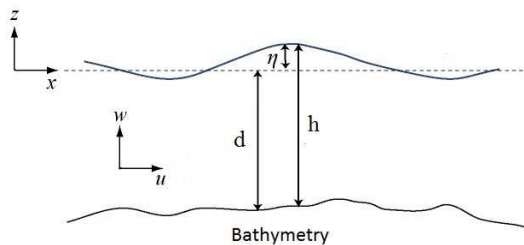


Figure 2.1 – Présentation du problème étudié

On introduit les deux paramètres qui vont permettre d'obtenir les différents modèles asymptotiques, ε et σ

$$\varepsilon = \frac{a}{d_0}, \quad \sigma = \frac{d_0}{\lambda}.$$

ε est appelé paramètre de non-linéarité car on le retrouve devant tous les termes non-linéaires du système d'Euler. Pour une raison similaire, σ est appelé paramètre de dispersion (ou de "faible profondeur"). Pour alléger les notations, nous n'écrirons plus les dépendances en t et x des fonctions. Dans ce contexte, le mouvement du fluide est décrit par les équations d'Euler que l'on rappelle ici

$$u_t + uu_x + wu_z + \frac{p_x}{\rho} = 0, \quad (2.2.1)$$

$$w_t + uw_x + ww_z + \frac{p_z}{\rho} + g = 0, \quad (2.2.2)$$

$$u_x + w_z = 0, \quad (2.2.3)$$

$$u_z - w_x = 0. \quad (2.2.4)$$

On rajoute trois hypothèses supplémentaires pour définir les conditions aux bords.

Conditions aux bords

- Dans un premier temps, on suppose qu'une particule à la surface reste toujours à la surface. Soit $M(t) = \begin{pmatrix} x(t) \\ z(t) \end{pmatrix}$ un point de la surface d'abscisse $x(t)$ et d'ordonnée $z(t)$. La vitesse de ce point est

$$\vec{V} = \begin{pmatrix} \frac{dx}{dt} \\ \frac{dz}{dt} \end{pmatrix} = \begin{pmatrix} u \\ w \end{pmatrix}.$$

Etant donné que le point M reste sur la surface, on en déduit que $\forall t \in \mathbb{R}^+$, $z(t) = \eta(t, x(t))$. En dérivant cette relation par rapport à la variable t , on obtient la première condition aux bords, dite condition cinématique,

$$w(t, x, \eta(t, x)) = \eta_t(t, x) + u(t, x, \eta(t, x))\eta_x(t, x). \quad (2.2.5)$$

- L'écoulement se faisant à surface libre, la pression sur la surface est égale à la pression atmosphérique qui est une constante. La pression n'intervenant dans les équations d'Euler que via son gradient, on peut la redéfinir à une constante près. On peut alors considérer que la pression est nulle en $z = \eta$

$$p(t, x, \eta) = 0. \quad (2.2.6)$$

- Enfin, on suppose que le fond est imperméable. Soit $M(t) = \begin{pmatrix} x(t) \\ z(t) \end{pmatrix}$ un point situé sur le fond d'équation $z = -d(x)$. Sa vitesse est

$$\vec{V} = \begin{pmatrix} u \\ w \end{pmatrix}.$$

On note \vec{n} un vecteur normal à la courbe représentant le fond. Ce vecteur peut s'écrire

$$\vec{n} = \begin{pmatrix} d_x \\ 1 \end{pmatrix}.$$

L'imperméabilité du fond se traduit alors par la relation suivante :

$$\vec{V} \cdot \vec{n} = 0.$$

Ce qui se traduit là encore par une condition cinématique en $z = -d$,

$$w(t, x, -d(x)) = -d_x(x)u(t, x, -d(x)). \quad (2.2.7)$$

Le système d'équations (2.2.1)-(2.2.7) est le point de départ de tous les modèles que nous allons présenter dans la suite.

En vue de simplifier les prochaines dérivations de modèles, on va reformuler le problème présenté ci-dessus en éliminant définitivement la pression des équations d'Euler. Pour cela, on utilise la condition d'irrotationalité (2.2.4) (qui donne $w_x = u_z$) pour réécrire les deux équations (2.2.1) et (2.2.2) de la manière suivante

$$u_t + uu_x + ww_x + \frac{p_x}{\rho} = 0, \quad (2.2.8)$$

$$w_t + uu_z + ww_z + \frac{p_z}{\rho} + g = 0. \quad (2.2.9)$$

On rappelle que la vitesse dérive d'un potentiel Φ

$$u = \Phi_x, \quad w = \Phi_z,$$

et on intègre l'équation (2.2.9) par rapport à z entre η et une hauteur z arbitraire.,

$$\Phi_t(z) - \Phi_t(\eta) + \frac{u(z)^2}{2} - \frac{u(\eta)^2}{2} + \frac{w(z)^2}{2} - \frac{w(\eta)^2}{2} + \frac{p(z)}{\rho} - \frac{p(\eta)}{\rho} + gz - g\eta = 0. \quad (2.2.10)$$

On en déduit une expression de la dérivée par rapport à x de la pression

$$\frac{p_x}{\rho} = - \left(u_t + \frac{[u^2]_x}{2} + \frac{[w^2]_x}{2} \right) + [\Phi_t(\eta)]_x + \frac{[u(\eta)^2]_x}{2} + \frac{[w(\eta)^2]_x}{2} + g\eta_x. \quad (2.2.11)$$

On substitue l'équation (2.2.11) dans l'équation (2.2.8). Après simplifications, on obtient

$$[\Phi_t(\eta)]_x + g\eta_x + \left[\frac{u^2(\eta)}{2} \right]_x + \left[\frac{w^2(\eta)}{2} \right]_x = 0.$$

On développe alors la dérivée de $\Phi_t(\eta)$ par rapport à x pour faire apparaître uniquement u , w et η comme inconnues.

$$\begin{aligned} [\Phi(\eta)]_x &= \Phi_x(\eta) + \eta_x \Phi_z(\eta), \\ &= u(\eta) + \eta_x w(\eta). \end{aligned}$$

Les équations d'Euler reformulées s'écrivent alors

$$u_t(\eta) + \eta_x w_t(\eta) + g\eta_x + \left[\frac{u^2(\eta)}{2} \right]_x + \left[\frac{w^2(\eta)}{2} \right]_x = 0, \quad (2.2.12)$$

$$u_x + w_z = 0, \quad (2.2.13)$$

$$u_z - w_x = 0. \quad (2.2.14)$$

Avec les conditions aux bords :

en $z = \eta$,

$$w = \eta_t + u\eta_x, \quad (2.2.15)$$

en $z = -d$,

$$w = -d_x u. \quad (2.2.16)$$

L'équation (2.2.12) est une simplification des équations (2.2.1)-(2.2.2) avec la condition (2.2.6). Elle s'apparente à l'équation de Bernoulli évaluée à la surface. On peut maintenant commencer l'analyse asymptotique du problème.

2.3 Développement asymptotique

Dans cette partie, nous allons exprimer les vitesses verticale w et horizontale u en fonction d'une nouvelle variable indépendante de z au travers d'un développement asymptotique. Ce dernier est obtenu grâce à des manipulations sur les équations (2.2.12)-(2.2.16). Pour cela, nous introduisons de nouvelles variables non-dimensionnées qui vont permettre de faire apparaître les petits paramètres σ^2 et ε qui auront un rôle central dans cette analyse. On pose

$$\tilde{x} = \frac{x}{\lambda}, \quad \tilde{z} = \frac{z}{d_0}, \quad \tilde{t} = \frac{\sqrt{gd_0}}{\lambda} t, \quad \tilde{\eta} = \frac{\eta}{a},$$

$$\tilde{u} = \frac{d_0}{a\sqrt{gd_0}} u, \quad \tilde{w} = \frac{\lambda}{a} \frac{1}{\sqrt{gd_0}} w.$$

Le système d'Euler adimensionné devient

$$\tilde{u}_{\tilde{t}}(\tilde{\eta}) + \varepsilon\sigma^2 \tilde{\eta}_{\tilde{x}} \tilde{w}_{\tilde{t}}(\tilde{\eta}) + \tilde{\eta}_{\tilde{x}} + \varepsilon \left[\frac{\tilde{u}^2(\tilde{\eta})}{2} \right]_{\tilde{x}} + \varepsilon\sigma^2 \left[\frac{\tilde{w}^2(\tilde{\eta})}{2} \right]_{\tilde{x}} = 0 \quad (2.3.1)$$

$$\tilde{u}_{\tilde{x}} + \tilde{w}_{\tilde{z}} = 0, \quad (2.3.2)$$

$$\tilde{u}_{\tilde{z}} - \sigma^2 \tilde{w}_{\tilde{x}} = 0. \quad (2.3.3)$$

Les conditions aux bords s'écrivent :

en $\tilde{z} = \varepsilon\tilde{\eta}$,

$$\tilde{w} = \tilde{\eta}_{\tilde{t}} + \varepsilon\tilde{u}\tilde{\eta}_{\tilde{x}}. \quad (2.3.4)$$

en $\tilde{z} = -\tilde{d}$,

$$\tilde{w} = -\tilde{d}_{\tilde{x}}\tilde{u}. \quad (2.3.5)$$

Pour plus de généralité, on va supposer dans cette partie que σ^2 est très petit devant 1 et ε est quelconque. Notre objectif est d'exprimer les vitesses non-dimensionnées \tilde{u} et \tilde{w} en fonction de la vitesse horizontale moyennée sur la profondeur. On la note $\tilde{\tilde{u}}$ et elle est définie par

$$\tilde{\tilde{u}} = \frac{1}{\tilde{d} + \varepsilon \tilde{\eta}} \int_{-\tilde{d}}^{\varepsilon \tilde{\eta}} \tilde{u} dz. \quad (2.3.6)$$

On va uniquement travailler avec les deux équations (2.3.2) et (2.3.3) en utilisant les conditions aux bords (2.3.4) et (2.3.5).

On commence par intégrer l'équation (2.3.3) entre 0 et une hauteur \tilde{z} quelconque en négligeant les termes d'ordre σ^2 . On note \tilde{u}^0 la vitesse horizontale non-dimensionnée en $z = 0$ qui joue ici le rôle de constante d'intégration. Cette fonction ne va servir que d'intermédiaire, on va chercher à s'en affranchir par la suite.

$$\tilde{u} = \tilde{u}^0 + \mathcal{O}(\sigma^2). \quad (2.3.7)$$

On substitue cette expression dans l'équation (2.3.2), puis on intègre l'équation qui en résulte entre $-\tilde{d}$ et \tilde{z}

$$\tilde{w} - \tilde{w}(-\tilde{d}) = -(\tilde{z} + \tilde{d})\tilde{u}_{\tilde{x}}^0 + \mathcal{O}(\sigma^2).$$

On utilise les conditions aux bords (2.3.5) pour obtenir un développement asymptotique de \tilde{w} en fonction de \tilde{u} à l'ordre 2

$$\tilde{w} = -(\tilde{z}\tilde{u}_{\tilde{x}}^0 + (\tilde{d}\tilde{u}^0)_{\tilde{x}}) + \mathcal{O}(\sigma^2). \quad (2.3.8)$$

Remarque 1. *Dans cette thèse, on va considérer principalement des modèles asymptotiques de types Boussinesq ou Green-Naghdi dans lesquels on néglige les termes d'ordre σ^4 . Pour dériver ces modèles nous avons seulement besoin d'un développement asymptotique d'ordre σ^2 pour la vitesse verticale w , au vu de la présence des termes σ^2 dans l'équation (2.3.1). Il est néanmoins possible d'obtenir des modèles asymptotiques plus précis en poussant plus loin les développements asymptotiques, mais nous ne le ferons pas ici (voir [36, 56] pour plus de détails).*

On remet alors l'expression (2.3.8) dans l'équation (2.2.14) et on intègre entre 0 et \tilde{z} pour obtenir un développement asymptotique à l'ordre 4 en σ de \tilde{u} en fonction de \tilde{u}^0

$$\tilde{u} = \tilde{u}^0 - \sigma^2 \left(\frac{\tilde{z}^2}{2} \tilde{u}_{\tilde{x}\tilde{x}}^0 + \tilde{z}(\tilde{d}\tilde{u}^0)_{\tilde{x}\tilde{x}} \right) + \mathcal{O}(\sigma^4). \quad (2.3.9)$$

On va maintenant exprimer \tilde{u}^0 en fonction de $\tilde{\tilde{u}}$. Pour cela, on commence par intégrer l'équation (2.3.9) entre $-\tilde{d}$ et $\varepsilon \tilde{\eta}$ par rapport à \tilde{z} et on divise par \tilde{h} pour obtenir une expression de $\tilde{\tilde{u}}$

$$\tilde{\tilde{u}} = \tilde{u}^0 - \sigma^2 \left(\frac{1}{6} (\varepsilon^2 \tilde{\eta}^2 - \varepsilon \tilde{\eta} \tilde{d} + \tilde{d}^2) \tilde{u}_{\tilde{x}\tilde{x}}^0 + \frac{\varepsilon \tilde{\eta} - \tilde{d}}{2} (\tilde{d}\tilde{u}^0)_{\tilde{x}\tilde{x}} \right) + \mathcal{O}(\sigma^4). \quad (2.3.10)$$

Comme on néglige les termes d'ordre σ^4 , on a la possibilité de faire plusieurs simplifications qui nous permettent notamment d'inverser la relation précédente. Pour faire cela, on commence par isoler \tilde{u}^0

$$\tilde{u}^0 = \tilde{\tilde{u}} + \sigma^2 \left(\frac{1}{6} (\varepsilon^2 \tilde{\eta}^2 - \varepsilon \tilde{\eta} \tilde{d} + \tilde{d}^2) \tilde{u}_{\tilde{x}\tilde{x}}^0 + \frac{\varepsilon \tilde{\eta} - \tilde{d}}{2} (\tilde{d}\tilde{u}^0)_{\tilde{x}\tilde{x}} \right) + \mathcal{O}(\sigma^4). \quad (2.3.11)$$

Lorsqu'on néglige les termes d'ordre σ^2 , cette relation est équivalente à

$$\tilde{u}^0 = \tilde{u} + \mathcal{O}(\sigma^2). \quad (2.3.12)$$

On substitue alors l'équation (2.3.12) dans l'équation (2.3.11) pour inverser définitivement l'équation (2.3.10), ce qui permet d'exprimer \tilde{u}^0 en fonction de \tilde{u}

$$\tilde{u}^0 = \tilde{u} + \sigma^2 \left(\left(\frac{\tilde{h}^2}{6} - \frac{\tilde{d}}{2}(\tilde{h} - \tilde{d}) \right) \tilde{u}_{\tilde{x}\tilde{x}} + \left(\frac{\tilde{h}}{2} - \tilde{d} \right) (\tilde{d}\tilde{u})_{\tilde{x}\tilde{x}} \right) + \mathcal{O}(\sigma^4). \quad (2.3.13)$$

Pour finir, on remplace l'expression de \tilde{u}^0 obtenue dans (2.3.9).

$$\tilde{u} = \tilde{u} - \sigma^2 \left(\left(\frac{\tilde{z}^2}{2} - \left(\frac{\tilde{h}^2}{6} - \frac{\tilde{d}(\tilde{h} - \tilde{d})}{2} \right) \right) \tilde{u}_{\tilde{x}\tilde{x}} + \left(\tilde{z} - \left(\frac{\tilde{h}}{2} - \tilde{d} \right) \right) (\tilde{d}\tilde{u})_{\tilde{x}\tilde{x}} \right) + \mathcal{O}(\sigma^4). \quad (2.3.14)$$

On a alors exprimé \tilde{u} en fonction de \tilde{u} en ne négligeant uniquement des termes de l'ordre de σ^4 . Cette expression va nous permettre de dériver les différents modèles asymptotiques. On en déduit également un développement asymptotique de la vitesse verticale \tilde{w} en substituant l'équation (2.3.13) dans l'équation (2.3.8)

$$\tilde{w} = - \left(\tilde{z}\tilde{u}_{\tilde{x}} + (\tilde{d}\tilde{u})_{\tilde{x}} \right) + \mathcal{O}(\sigma^2). \quad (2.3.15)$$

Avant d'aller plus loin, il est important de préciser que les modèles asymptotiques que nous allons présenter se composent de deux équations. On appellera la première l'équation de *continuité* et la seconde l'équation du *moment*. Il est possible d'obtenir l'équation de continuité sans négliger le moindre terme pour tous les modèles dont les inconnues sont η et \bar{u} lorsque l'on choisit des conditions aux bords cinématiques pour les équations d'Euler. Pour cela, on intègre la condition d'incompressibilité (2.2.3) sur toute la profondeur. On applique la formule de Leibnitz⁽¹⁾ à l'équation (2.2.3) intégrée

$$\int_{-d}^{\eta} w_z dz + \int_{-d}^{\eta} u_x dz = 0.$$

On utilise les conditions aux bords (2.2.15)-(2.2.16) pour obtenir l'équation classique :

$$\eta_t + (h\bar{u})_x = 0. \quad (2.3.16)$$

Dans la suite, nous allons montrer comment obtenir les modèles asymptotiques en partant des expressions et des équations présentées auparavant. Commençons par le modèle le plus simple : les équations de Saint-Venant.

¹Soient trois fonctions $f(x, y)$, $a(x)$, $b(x)$ telles que f et f_x sont continues en x et en y , et telles que a et b sont C^1 , alors

$$\frac{\partial}{\partial x} \left(\int_{a(x)}^{b(x)} f(x, y) dy \right) = \int_{a(x)}^{b(x)} f_x(x, y) dy + f(x, b(x))b'(x) - f(x, a(x))a'(x).$$

2.4 Equations de Saint-Venant (ou shallow water)

Pour ce modèle, on se place dans le régime asymptotique particulier $\sigma^2 \ll 1$ et ε est quelconque. On négligera donc tous les termes d'ordre σ^2 .

Formulation en vitesse-amplitude

On va chercher à exprimer le système d'Euler en fonction des deux variables η et \bar{u} , où η représente encore l'élévation de la surface et \bar{u} la vitesse moyennée sur la profondeur.

Notons que l'équation (2.3.16) est vérifiée pour ces deux variables et sera donc l'équation de continuité du système de Saint-Venant. Pour trouver l'équation du moment, on reprend le développement asymptotique (2.3.14). Dans ce régime asymptotique, il se réduit à

$$\tilde{u} = \tilde{\bar{u}} + \mathcal{O}(\sigma^2). \quad (2.4.1)$$

D'où, en évaluant cette relation en $\tilde{z} = \varepsilon\tilde{\eta}$

$$\tilde{u}(\varepsilon\tilde{\eta}) = \tilde{\bar{u}} + \mathcal{O}(\sigma^2). \quad (2.4.2)$$

On substitue alors cette équation dans (2.3.1) pour obtenir l'équation du moment

$$\tilde{\bar{u}}_t + \varepsilon\tilde{\bar{u}}\tilde{\bar{u}}_x + \tilde{\eta}_x = \mathcal{O}(\sigma^2). \quad (2.4.3)$$

Pour finir, on néglige tous les termes d'ordre σ^2 dans l'équation (2.4.3) et on revient aux variables physiques pour obtenir le modèle de Saint-Venant 1D qui s'écrit :

$$\eta_t + (h\bar{u})_x = 0, \quad (2.4.4)$$

$$\bar{u}_t + \bar{u}\bar{u}_x + g\eta_x = 0. \quad (2.4.5)$$

Les mêmes calculs sur le modèle d'Euler en 3 dimensions fournissent les équations de Saint-Venant 2D

$$\eta_t + \nabla \cdot (h\bar{\mathbf{u}}) = 0, \quad (2.4.6)$$

$$\bar{\mathbf{u}}_t + (\bar{\mathbf{u}} \cdot \nabla)\bar{\mathbf{u}} + g\nabla\eta = 0, \quad (2.4.7)$$

où $\bar{\mathbf{u}} = (\bar{u}, \bar{v})^T$ est le vecteur vitesse selon x et y (pas selon la dimension verticale toujours notée z) et ∇ est l'opérateur gradient par rapport aux dimensions horizontales x et y .

Pour ce système, il est possible d'écrire ces équations dans une formulation plus adaptée aux calculs numériques. Nous allons montrer comment obtenir cette formulation dans le prochain paragraphe.

Formulation en flux-amplitude

Pour obtenir la seconde formulation des équations de Saint-Venant, il suffit de changer d'inconnues. On choisit de garder la variable η qui représente l'élévation de la surface et de remplacer la vitesse moyenne \bar{u} par le flux \bar{q} défini par

$$\bar{q} = h\bar{u}. \quad (2.4.8)$$

En prenant en compte ces nouvelles variables, l'équation de continuité reste inchangée car la variable \bar{q} y apparaît naturellement. En ce qui concerne l'équation du moment, on multiplie l'équation de continuité (2.4.4) par \bar{u} et on l'additionne à l'équation du moment (2.4.5) multipliée par h . En remarquant que $\eta_t = h_t$, on obtient alors les équations de Saint-Venant dans une formulation en flux-amplitude

$$\eta_t + \bar{q}_x = 0, \quad (2.4.9)$$

$$\bar{q}_t + \left(\frac{\bar{q}^2}{h} \right)_x + gh\eta_x = 0. \quad (2.4.10)$$

La version 2D s'écrit de même

$$\eta_t + \nabla \cdot \bar{\mathbf{q}} = 0, \quad (2.4.11)$$

$$\bar{\mathbf{q}}_t + \nabla \left(\frac{\bar{\mathbf{q}} \cdot \bar{\mathbf{q}}}{h} \right) + gh\nabla\eta = 0, \quad (2.4.12)$$

où $\bar{\mathbf{q}} = h\bar{\mathbf{u}}$.

2.5 Equations de Boussinesq

Cette partie est dédiée à la présentation d'une famille de modèles asymptotiques très vaste et très utilisée dans la modélisation mathématique des vagues : la famille des modèles de type Boussinesq. Le premier de ces modèles fut dérivé à la fin du XIXème siècle par Joseph Boussinesq [22] pour décrire la propagation d'une vague de faible amplitude en eau peu profonde sur un fond plat en prenant en compte des effets dispersifs complètement négligés dans les équations de Saint-Venant (ce qui revient à prendre en compte les termes d'ordre σ^2). Sa dérivation repose sur une hypothèse concernant les paramètres ε et σ introduits précédemment dans la partie 2.2. On suppose que

$$\varepsilon \ll 1, \sigma^2 \ll 1, \text{ et } \varepsilon = \mathcal{O}(\sigma^2).$$

Notons que supposer ε de l'ordre de σ^2 revient à traiter un problème avec un nombre d'Ursell Ur de l'ordre de 1 ($Ur = a\lambda^2/d_0^3 = \varepsilon/\sigma^2$). De plus, l'hypothèse de considérer de petites valeurs de ε fournit un caractère faiblement non-linéaire aux équations que l'on va obtenir. Cette hypothèse caractérise la famille des modèles de type Boussinesq que nous allons présenter dans la suite. De fait, ils seront obtenus en négligeant les termes d'ordre σ^4 et $\varepsilon\sigma^2$ dans les équations d'Euler adimensionnées. Le premier système d'équations à avoir amélioré celui de Boussinesq (il prend

en compte la variation de la bathymétrie en plus), qui peut être considéré comme le plus simple, est le modèle dérivé pour la première fois par Peregrine en 1967 (voir [63]). Nous allons en détailler sa dérivation dans la prochaine partie et proposer une méthode pour en obtenir une formulation en flux-amplitude obtenue initialement par Abbott [1] en 1978.

2.5.1 Equations de Peregrine

Ce modèle se compose d'un système de deux équations aux dérivées partielles couplées sur les variables η et \bar{u} . Il conserve l'équation (2.3.16) de continuité qui est donc, pour mémoire, une équation exacte.

La seconde équation va, quant à elle, être obtenue en substituant le développement asymptotique (2.3.14) de \tilde{u} dans l'équation (2.3.1).

Sous l'hypothèse de Boussinesq, en négligeant les termes d'ordre $\varepsilon\sigma^2$ et σ^4 , l'équation (2.3.1) devient

$$\tilde{u}_{\tilde{t}}(\tilde{\eta}) + \tilde{\eta}_{\tilde{x}} + \varepsilon \left[\frac{\tilde{u}^2(\tilde{\eta})}{2} \right]_{\tilde{x}} = \mathcal{O}(\varepsilon\sigma^2, \sigma^4). \quad (2.5.1)$$

De la même manière, le développement (2.3.14) devient

$$\tilde{u} = \tilde{\bar{u}} - \sigma^2 \left(\left(\frac{\tilde{z}^2}{2} - \frac{\tilde{d}^2}{6} \right) \tilde{\bar{u}}_{\tilde{x}\tilde{x}} + \left(\tilde{z} + \frac{\tilde{d}}{2} \right) (\tilde{d}\tilde{\bar{u}})_{\tilde{x}\tilde{x}} \right) + \mathcal{O}(\varepsilon\sigma^2, \sigma^4). \quad (2.5.2)$$

Dans le but de substituer les différentes expressions inconnues $\tilde{u}_{\tilde{t}}(\tilde{\eta})$ et $\tilde{u}(\tilde{\eta})$ dans (2.5.1), on dérive la relation (2.5.2) par rapport à \tilde{t} puis on l'évalue en $\varepsilon\eta$:

$$\begin{aligned} \tilde{u}(\varepsilon\tilde{\eta}) &= \tilde{\bar{u}} + \sigma^2 \left(\frac{\tilde{d}^2}{6} \tilde{\bar{u}}_{\tilde{x}\tilde{x}} - \frac{\tilde{d}}{2} (\tilde{d}\tilde{\bar{u}})_{\tilde{x}\tilde{x}} \right) + \mathcal{O}(\varepsilon\sigma^2, \sigma^4), \\ \tilde{u}_{\tilde{t}}(\varepsilon\tilde{\eta}) &= \tilde{\bar{u}} + \sigma^2 \left(\frac{\tilde{d}^2}{6} \tilde{\bar{u}}_{\tilde{x}\tilde{x}} - \frac{\tilde{d}}{2} (\tilde{d}\tilde{\bar{u}})_{\tilde{x}\tilde{x}} \right) + \mathcal{O}(\varepsilon\sigma^2, \sigma^4), \end{aligned}$$

On substitue ces expressions dans l'équation (2.5.1) pour obtenir

$$\tilde{u}_{\tilde{t}} + \varepsilon \tilde{\bar{u}} \tilde{u}_{\tilde{x}} + \tilde{\eta}_{\tilde{x}} + \sigma^2 \left(\frac{\tilde{d}^2}{6} \tilde{\bar{u}}_{\tilde{t}\tilde{x}\tilde{x}} - \frac{\tilde{d}}{2} (\tilde{d}\tilde{\bar{u}})_{\tilde{t}\tilde{x}\tilde{x}} \right) + \mathcal{O}(\sigma^4, \varepsilon\sigma^2) = 0. \quad (2.5.3)$$

Le système d'équations du modèle de Peregrine s'écrit alors en négligeant les termes d'ordre σ^4 et d'ordre $\varepsilon\sigma^2$ dans l'équation (2.5.3) et en revenant aux variables dimensionnées,

$$\eta_t + (h\bar{u})_x = 0, \quad (2.5.4)$$

$$\bar{u}_t + \bar{u}\bar{u}_x + g\eta_x + \left(\frac{d^2}{6} \bar{u}_{txx} - \frac{d}{2} (d\bar{u})_{txx} \right) = 0. \quad (2.5.5)$$

Remarque 2. On remarque que les équations de Peregrine correspondent aux équations de Saint-Venant auxquelles on a rajouté des termes qui changent les caractéristiques de dispersion du modèle. Nous verrons, par la suite dans quelle mesure ces termes influencent le domaine de validité du modèle.

En reproduisant ces calculs sur les équations d'Euler en 3 dimensions, il est possible d'obtenir la version 2D des équations de Peregrine

$$\eta_t + \nabla \cdot (h\bar{\mathbf{u}}) = 0, \quad (2.5.6)$$

$$\bar{\mathbf{u}}_t + (\bar{\mathbf{u}} \cdot \nabla) \bar{\mathbf{u}} + g \nabla \eta + \frac{d^2}{6} \nabla \left(\nabla \cdot \bar{\mathbf{u}}_t \right) - \frac{d}{2} \nabla \left(\nabla \cdot (d\bar{\mathbf{u}}_t) \right) = 0, \quad (2.5.7)$$

où $\bar{\mathbf{u}}$ est le vecteur à deux dimensions composé des vitesses moyennes selon x et y . De plus, ∇ désigne l'opérateur gradient par rapport à x et y .

Comme pour les équations de Saint-Venant, il est possible de dériver une formulation flux-amplitude de ce système d'équations. Il est néanmoins important de noter que, dans ce cas, les équations ne sont pas équivalentes. C'est donc un modèle de type Boussinesq différent de celui de Peregrine. Nous détaillons la dérivation de cet autre modèle, appelé communément système d'Abbott, dans la prochaine partie.

2.5.2 Equations d'Abbott

Pour dériver les équations d'Abbott, nous allons appliquer une méthode qui est utilisable pour toutes les équations de type Boussinesq puisqu'elle repose sur une asymptotique d'ordre $\varepsilon\sigma^2$. Cette fois-ci, on travaille sur les équations de Peregrine dans leur forme non-dimensionnelle, que l'on rappelle maintenant

$$\tilde{\eta}_t + (\tilde{h}\tilde{u})_{\tilde{x}} = 0, \quad (2.5.8)$$

$$\tilde{u}_{\tilde{t}} + \varepsilon \tilde{u} \tilde{u}_{\tilde{x}} + \tilde{\eta}_{\tilde{x}} + \sigma^2 \left(\frac{\tilde{d}^2}{6} \tilde{u}_{\tilde{t}\tilde{x}\tilde{x}} - \frac{\tilde{d}}{2} (\tilde{d}\tilde{u})_{\tilde{t}\tilde{x}\tilde{x}} \right) = 0. \quad (2.5.9)$$

On va leur appliquer la manipulation suivante : on multiplie l'équation (2.5.8) par $\varepsilon\tilde{u}$ (le ε est important ici car on veut faire apparaître la dérivée temporelle de $\tilde{h} = \tilde{d} + \varepsilon\tilde{\eta}$), la seconde équation par \tilde{h} et on additionne les deux. On obtient alors

$$\tilde{q}_{\tilde{t}} + \varepsilon \left(\frac{\tilde{q}^2}{\tilde{h}} \right)_{\tilde{x}} + \tilde{h}\tilde{\eta}_{\tilde{x}} + \sigma^2 \tilde{h} \left(\frac{\tilde{d}^2}{6} \tilde{u}_{\tilde{t}\tilde{x}\tilde{x}} - \frac{\tilde{d}}{2} (\tilde{d}\tilde{u})_{\tilde{t}\tilde{x}\tilde{x}} \right) = \mathcal{O}(\sigma^4, \varepsilon\sigma^2). \quad (2.5.10)$$

En rappelant que

$$\tilde{q} = \tilde{d}\tilde{u} + \mathcal{O}(\varepsilon), \quad (2.5.11)$$

on peut faire apparaître le flux non-dimensionné \tilde{q} dans les termes d'ordre σ^2 de l'équation du moment (2.5.10) en négligeant des termes non-linéaires d'ordre $\varepsilon\sigma^2$. On obtient alors

$$\tilde{q}_{\tilde{t}} + \varepsilon \left(\frac{\tilde{q}^2}{\tilde{h}} \right)_{\tilde{x}} + \tilde{h}\tilde{\eta}_{\tilde{x}} + \sigma^2 \left(\frac{\tilde{d}^3}{6} \left(\frac{\tilde{q}}{\tilde{d}} \right)_{\tilde{t}\tilde{x}\tilde{x}} - \frac{\tilde{d}^2}{2} \tilde{q}_{\tilde{t}\tilde{x}\tilde{x}} \right) = \mathcal{O}(\sigma^4, \varepsilon\sigma^2). \quad (2.5.12)$$

On revient aux équations dimensionnées pour obtenir les équation d'Abbott

$$\eta_t + \bar{q}_x = 0, \quad (2.5.13)$$

$$\bar{q}_t + \left(\frac{\bar{q}^2}{h} \right)_x + gh\eta_x + \left(\frac{d^3}{6} \left(\frac{\bar{q}}{d} \right)_{txx} - \frac{d^2}{2} \bar{q}_{txx} \right) = 0. \quad (2.5.14)$$

Remarque 3. Le terme $\frac{d^3}{6} \left(\frac{\bar{q}}{d}\right)_{txx}$ n'introduit jamais de singularité dans l'équation. Pour s'en convaincre, il suffit de développer la dérivée et de remarquer que la présence du d^3 devant évite tout problème.

Il est important de noter que les équations d'Abbott ne sont pas équivalentes à celles de Peregrine. En effet, contrairement aux cas des équations de Saint-Venant, on a rajouté des termes négligeables pour obtenir les équations d'Abbott à partir des équations de Peregrine. Néanmoins, les termes ajoutés sont tous non-linéaires, ce qui implique que les caractéristiques de dispersion linéaire sont les mêmes pour les deux modèles.

Encore une fois, on peut adapter ce modèle à un problème en $2D$,

$$\eta_t + \nabla \cdot \bar{\mathbf{q}} = 0, \quad (2.5.15)$$

$$\bar{\mathbf{q}}_t + \nabla \left(\frac{\bar{\mathbf{q}} \cdot \bar{\mathbf{q}}}{h} \right) + gh \nabla \eta + \frac{d^3}{6} \nabla \left(\nabla \cdot \left(\frac{\bar{\mathbf{q}}_t}{d} \right) \right) - \frac{d^2}{2} \nabla \left(\nabla \cdot \bar{\mathbf{q}}_t \right) = 0, \quad (2.5.16)$$

où $\bar{\mathbf{q}} = h \bar{\mathbf{u}}$.

Les modèles de Peregrine et d'Abbott permettent de prendre en compte des effets qui sont entièrement négligés par le modèle de Saint-Venant. Ce sont les effets dispersifs (Voir le chapitre 4 pour plus de détails). Ces effets sont directement liés au petit paramètre σ introduit précédemment. Ils s'avèrent cruciaux lorsque l'on souhaite modéliser des phénomènes physiques. Par contre, les effets dispersifs provenant des équations de Peregrine et Abbott s'avèrent limités pour les écoulements ayant un σ supérieur à 0.3 (voir [72]). Plusieurs auteurs ont alors cherché à améliorer ces effets sans changer l'ordre de l'analyse asymptotique. L'idée étant d'optimiser les effets dispersifs pour une asymptotique donnée. En général, cette amélioration intervient au travers d'un paramètre réel que l'on peut ajuster. Dans la prochaine partie, nous présentons la dérivation de plusieurs de ces modèles de Boussinesq dit "améliorés".

2.6 Equations de Boussinesq étendues (ou améliorées)

Comme on l'a dit précédemment, les modèles de Peregrine et d'Abbott ne suffisent pas pour modéliser des problèmes physiques où la dispersion joue un rôle prépondérant (le déferlement des vagues par exemple). C'est pourquoi, dans plusieurs travaux, les auteurs ont cherché à étendre le domaine de validité en utilisant le caractère asymptotique des équations. Pour cela, ils ont eu recours à deux méthodes différentes : la première est d'ajouter des termes négligeables, la seconde est de changer une des inconnues. Cette partie est dédiée à la dérivation de plusieurs de ces modèles.

2.6.1 Modèle de Beji-Nadaoka

On va commencer par le modèle présenté initialement par S. Beji et K. Nadaoka [11] en 1996. C'est pourquoi, dans la suite, nous y ferons référence comme le modèle de Beji-Nadaoka. Il se base sur une idée très simple : modifier les termes dispersifs dans l'équation du moment

de Peregrine pour optimiser leurs effets. Après avoir rappelé la dérivation de ce modèle, nous introduirons une formulation en amplitude-flux qui s'apparente aux équations de Abbott.

Formulation en vitesse-amplitude

L'équation de continuité de Peregrine (2.4.4) (qui est exacte) reste inchangée ici. Reprenons l'équation du moment (2.5.3) sous forme non-dimensionnée,

$$\tilde{u}_{\tilde{t}} + \varepsilon \tilde{u} \tilde{u}_{\tilde{x}} + \tilde{\eta}_{\tilde{x}} + \sigma^2 \left(\frac{\tilde{d}^2}{6} \tilde{u}_{\tilde{t}\tilde{x}\tilde{x}} - \frac{\tilde{d}}{2} (\tilde{d}\tilde{u})_{\tilde{t}\tilde{x}\tilde{x}} \right) = \mathcal{O}(\sigma^4, \varepsilon\sigma^2).$$

On ajoute et soustrait $\alpha_B \sigma^2 \left(\frac{\tilde{d}^2}{6} \tilde{u}_{\tilde{t}\tilde{x}\tilde{x}} - \frac{\tilde{d}}{2} (\tilde{d}\tilde{u})_{\tilde{t}\tilde{x}\tilde{x}} \right)$, où α_B est un réel quelconque.

$$\tilde{u}_{\tilde{t}} + \varepsilon \tilde{u} \tilde{u}_{\tilde{x}} + \tilde{\eta}_{\tilde{x}} + (1 + \alpha_B) \sigma^2 \left(\frac{\tilde{d}^2}{6} \tilde{u}_{\tilde{t}\tilde{x}\tilde{x}} - \frac{\tilde{d}}{2} (\tilde{d}\tilde{u})_{\tilde{t}\tilde{x}\tilde{x}} \right) - \alpha_B \sigma^2 \left(\frac{\tilde{d}^2}{6} \tilde{u}_{\tilde{t}\tilde{x}\tilde{x}} - \frac{\tilde{d}}{2} (\tilde{d}\tilde{u})_{\tilde{t}\tilde{x}\tilde{x}} \right) = \mathcal{O}(\sigma^4, \varepsilon\sigma^2).$$

De cette même équation, on déduit la relation suivante en négligeant les termes d'ordre σ^2 et ε ,

$$\tilde{u}_{\tilde{t}} = -\tilde{\eta}_{\tilde{x}} + \mathcal{O}(\varepsilon, \sigma^2).$$

On utilise alors cette expression pour modifier les termes qui sont uniquement en facteur de α_B . On obtient alors le système de Beji-Nadaoka en revenant aux variables dimensionnées

$$\eta_t + (h\bar{u})_x = 0, \quad (2.6.1)$$

$$\bar{u}_t + \bar{u}\bar{u}_x + g\eta_x + (1 + \alpha_B) \left(\frac{d^2}{6} \bar{u}_{txx} - \frac{d}{2} (d\bar{u})_{txx} \right) + \alpha_B g \left(\frac{d^2}{6} \eta_{xxx} - \frac{d}{2} (d\eta_x)_{xx} \right) = 0. \quad (2.6.2)$$

Encore une fois, ces calculs s'adaptent aux équations d'Euler à surface libre en 3 dimensions pour obtenir le système d'équations de Beji-Nadaoka 2D

$$\eta_t + \nabla \cdot [(d + \eta)\bar{\mathbf{u}}] = 0, \quad (2.6.3)$$

$$\begin{aligned} \bar{\mathbf{u}}_t + (\bar{\mathbf{u}} \cdot \nabla) \bar{\mathbf{u}} + g\nabla\eta + (1 + \alpha_B) & \left(\frac{d^2}{6} \nabla \left(\nabla \cdot \bar{\mathbf{u}}_t \right) - \frac{d}{2} \nabla \left(\nabla \cdot (d\bar{\mathbf{u}}_t) \right) \right) \\ & + g\alpha_B \left(\frac{d^3}{6} \nabla \left(\nabla \cdot \nabla\eta \right) - \frac{d^2}{2} \nabla \left(\nabla \cdot (d\nabla\eta) \right) \right) = 0, \end{aligned} \quad (2.6.4)$$

C'est la présence du réel α_B qui nous permet de modifier les caractéristiques de dispersion linéaire. Nous verrons dans le chapitre 4 quelle est la valeur optimale de ce paramètre. Nous remarquons également que pour le choix très particulier de $\alpha_B = 0$, on retrouve les équations de Peregrine.

Formulation en flux-amplitude

Comme pour les équations de Peregrine qui permettent de dériver les équations d'Abbott, il est possible d'obtenir une formulation des équations de Beji-Nadaoka en utilisant les variables (η, \bar{q}) . Pour cela, on applique exactement la même méthode que celle décrite dans la partie 2.5.2. On obtient alors les équations suivantes

$$\eta_t + \bar{q}_x = 0, \quad (2.6.5)$$

$$\bar{q}_t + \left(\frac{\bar{q}^2}{h} \right)_x + gh\eta_x + (1 + \alpha_B) \left(\frac{d^3}{6} \left(\frac{\bar{q}}{d} \right)_{txx} - \frac{d^2}{2} \bar{q}_{txx} \right) + \alpha_B gd \left(\frac{d^3}{6} \eta_{xxx} - \frac{d^2}{2} (d\eta)_{xxx} \right) = 0. \quad (2.6.6)$$

La version 2D de ce système peut s'écrire

$$\eta_t + \nabla \cdot \bar{\mathbf{q}} = 0, \quad (2.6.7)$$

$$\begin{aligned} \bar{\mathbf{q}}_t + \nabla \cdot \left(\frac{\bar{\mathbf{q}} \cdot \bar{\mathbf{q}}}{h} \right) + gh\nabla\eta + (1 + \alpha_B) \left(\frac{d^3}{6} \nabla \left(\nabla \cdot \left(\frac{\bar{\mathbf{q}}_t}{d} \right) \right) - \frac{d}{2} \nabla \left(\nabla \cdot \bar{\mathbf{q}}_t \right) \right) \\ + gd\alpha_B \left(\frac{d^3}{6} \nabla \left(\nabla \cdot \nabla\eta \right) - \frac{d^2}{2} \nabla \left(\nabla \cdot (d\nabla\eta) \right) \right) = 0. \end{aligned} \quad (2.6.8)$$

Il est important de noter que pour $\alpha_B = 0$, on retrouve les équations d'Abbott. C'est pour cela que dans la suite, nous l'appellerons : modèle de Beji-Nadaoka-Abbott.

2.6.2 Modèle de Madsen et Sørensen

Ce modèle a été dérivé initialement par P.A. Madsen et O.R. Sørensen [55] en 1992, c'est pour cela qu'on le nommera modèle de Madsen-Sørensen. Il se base sur un principe assez similaire à celui de Beji-Nadaoka avec comme point de départ les équations d'Abbott.

Nous rappelons encore une fois comment dériver ce modèle et nous présenterons une formulation amplitude-vitesse qui se rapproche des équations de Peregrine et de Beji-Nadaoka.

Formulation en flux-amplitude

Pour obtenir ce modèle, on modifie uniquement l'équation du moment. Mais, en plus de manipuler des termes d'ordre σ^4 et $\varepsilon\sigma^2$, on fait une hypothèse de pente douce. En effet, on suppose que la bathymétrie d varie très peu. On admet que, dans cette situation, on peut négliger d_x^2 et d_{xx} devant 1. Reprenons les équations d'Abbott (2.5.13)-(2.5.14) en leur appliquant cette hypothèse. On obtient alors, en utilisant les variables non-dimensionnées et en ayant négligé les dérivées de la bathymétrie,

$$\tilde{\eta}_{\tilde{t}} + \tilde{\bar{q}}_{\tilde{x}} = 0, \quad (2.6.9)$$

$$\tilde{\bar{q}}_{\tilde{t}} + \varepsilon \left(\frac{\tilde{\bar{q}}^2}{\tilde{h}} \right)_{\tilde{x}} + \tilde{h}\tilde{\eta}_{\tilde{x}} - \sigma^2 \left(\frac{\tilde{d}^2}{3} \tilde{\bar{q}}_{\tilde{t}\tilde{x}\tilde{x}} + \frac{\tilde{d}_{\tilde{x}}\tilde{d}}{3} \tilde{\bar{q}}_{\tilde{t}\tilde{x}} \right) = \mathcal{O}(\sigma^4, \varepsilon\sigma^2). \quad (2.6.10)$$

On reproduit alors un procédé similaire à celui présenté dans la partie 2.6.1. On ajoute et on soustrait " $B\tilde{d}^2\tilde{\tilde{q}}_{\tilde{t}\tilde{x}\tilde{x}}$ " à la seconde équation, où B est un réel quelconque. En négligeant les termes d'ordre ε et σ^2 dans l'équation (2.6.10) on obtient la relation suivante

$$\tilde{q}_{\tilde{t}} + \tilde{d}\tilde{\eta} = \mathcal{O}(\varepsilon, \sigma^2). \quad (2.6.11)$$

Il suffit alors d'utiliser cette relation pour modifier le terme "+ $B\tilde{d}^2\tilde{\tilde{q}}_{\tilde{t}\tilde{x}\tilde{x}}$ ". La seconde équation devient, en appliquant toujours l'hypothèse de pente douce pour simplifier,

$$\tilde{q}_{\tilde{t}} + \varepsilon \left(\frac{\tilde{q}^2}{\tilde{h}} \right)_{\tilde{x}} + \tilde{h}\tilde{\eta}_{\tilde{x}} - \sigma^2 \left((B + \frac{1}{3})\tilde{d}^2\tilde{\tilde{q}}_{\tilde{t}\tilde{x}\tilde{x}} + \frac{\tilde{d}_{\tilde{x}}\tilde{d}}{3}\tilde{\tilde{q}}_{\tilde{t}\tilde{x}} + B\tilde{d}^3\tilde{\eta}_{\tilde{x}\tilde{x}\tilde{x}} + 2B\tilde{d}^2\tilde{d}_{\tilde{x}}\tilde{\eta}_{\tilde{x}\tilde{x}} \right) = \mathcal{O}(\sigma^4, \varepsilon\sigma^2). \quad (2.6.12)$$

Enfin, la première équation d'Abbott reste inchangée et on revient aux variables physiques pour obtenir les équations de Madsen-Sørensen

$$\eta_t + \bar{q}_x = 0, \quad (2.6.13)$$

$$\bar{q}_t + \left(\frac{\bar{q}^2}{h} \right)_x + gh\eta_x - (B + \frac{1}{3})d^2\bar{q}_{txx} - \frac{d}{3}d_x\bar{q}_{tx} - Bgd^3\eta_{xxx} - 2Bgd^2d_x\eta_{xx} = 0, \quad (2.6.14)$$

où B est un réel quelconque qui a exactement le même rôle que α_B pour le modèle de Beji-Nadaoka, à savoir optimiser la relation de dispersion linéaire du modèle (voir le chapitre 4 pour plus de détails).

La version 2D des équations de Madsen-Sørensen est

$$\eta_t + \nabla \cdot \bar{\mathbf{q}} = 0, \quad (2.6.15)$$

$$\begin{aligned} \bar{\mathbf{q}}_t + \nabla \left(\frac{\bar{\mathbf{q}} \cdot \bar{\mathbf{q}}}{h} \right) + gh\nabla\eta - \beta d^2\nabla(\nabla \cdot \bar{\mathbf{q}}_t) - \frac{d}{6}\mathcal{D}(\bar{\mathbf{q}}_t, d) - \frac{d(\nabla d)}{6}\nabla \cdot \bar{\mathbf{q}}_t \\ - Bgd^3\nabla(\Delta\eta) - Bgd^2\left(\mathcal{D}(\nabla\eta, d) + (\nabla d)\Delta\eta\right) = 0, \end{aligned} \quad (2.6.16)$$

où $\bar{\mathbf{q}} = \begin{pmatrix} q^1 \\ q^2 \end{pmatrix} = \begin{pmatrix} h\bar{u} \\ h\bar{v} \end{pmatrix}$ et \mathcal{D} est l'opérateur défini par

$$\mathcal{D}(\bar{\mathbf{q}}, d) = \begin{pmatrix} d_x q_x^1 + d_y q_x^2 \\ d_x q_y^1 + d_y q_y^2 \end{pmatrix}.$$

De plus, $\beta = B + 1/3$ et ∇ désigne toujours l'opérateur gradient en x et y .

Ce modèle n'est pas équivalent au modèle de Beji-Nadaoka-Abbott précédemment introduit. En effet, en plus de l'hypothèse faite sur la bathymétrie, ils diffèrent par les termes qu'on a choisi de modifier. Pour le modèle de Madsen-Sørensen, on change uniquement des termes en \bar{q}_{txx} alors

que pour les équations de Beji-Nadaoka on modifie tous ceux d'ordre σ^2 . Néanmoins, pour un fond plat (lorsque d est constante), les deux modèles sont exactement les mêmes. Il faut faire attention ici, lorsque $B = 0$, on n'obtient pas exactement les équations d'Abbott à cause de l'hypothèse de pente douce.

Formulation en vitesse-amplitude

Comme expliqué précédemment, les équations de Madsen-Sørensen ne sont pas la version (η, q) des équations de Beji-Nadaoka. Il est donc possible de dériver une version des équations de Madsen-Sørensen en (η, u) en inversant la méthode utilisée pour obtenir les équations d'Abbott (voir la partie 2.5.2) et en conservant l'hypothèse de pente douce pour simplifier les équations. On obtient de nouvelles équations que l'on appellera équations de Madsen-Sørensen-Peregrine dans la suite (car à bathymétrie constante et pour $B = 0$, on retrouve les équations de Peregrine)

$$\eta_t + (h\bar{u})_x = 0, \quad (2.6.17)$$

$$\bar{u}_t + \bar{u}\bar{u}_x + g\eta_x - (B + \frac{1}{3})d^2\bar{u}_{txx} - (1 + 2B)dd_x\bar{u}_{tx} - Bgd(d\eta_{xxx} + 2d_x\eta_{xx}) = 0, \quad (2.6.18)$$

où B est toujours un réel quelconque. La version 2D s'écrit en notant encore $\beta = B + 1/3$

$$\eta_t + \nabla \cdot h\bar{\mathbf{u}} = 0, \quad (2.6.19)$$

$$\begin{aligned} \bar{\mathbf{u}}_t + (\bar{\mathbf{u}} \cdot \nabla)\bar{\mathbf{u}} + g\nabla\eta - \beta d^2\nabla(\nabla \cdot \bar{\mathbf{u}}_t) - (\beta + \frac{1}{6})d\mathcal{D}(\bar{\mathbf{u}}_t, d) - \frac{d(\nabla d)}{6}\nabla \cdot \bar{\mathbf{u}}_t \\ - \beta\mathcal{D}_2(\bar{\mathbf{u}}, d) - Bgd^3\nabla(\Delta\eta) - Bgd^2\left(\mathcal{D}(\nabla\eta, d) + (\nabla d)\Delta\eta\right) = 0, \end{aligned} \quad (2.6.20)$$

où \mathcal{D}_2 est l'opérateur défini par

$$\mathcal{D}(\bar{\mathbf{u}}, d) = \begin{pmatrix} d_x u_x + d_x v_y \\ d_y u_x + d_y v_y \end{pmatrix}.$$

Comme toujours, les équations de Madsen-Sørensen et Madsen-Sørensen-Peregrine ne diffèrent que par des termes non-linéaires. Ainsi, les caractéristiques de dispersion linéaire que nous étudierons plus tard sont les mêmes pour ces deux modèles. De plus, à bathymétrie constante, les équations de Beji-Nadaoka et de Madsen-Sørensen-Peregrine sont identiques.

2.6.3 Modèle de Nwogu

Cette partie est consacrée à la dérivation d'équations de Boussinesq améliorées dans leur formulation amplitude-vitesse et amplitude-flux. Ces modèles permettent d'obtenir de nouvelles équations de type Boussinesq qui améliorent les caractéristiques de dispersion linéaire (voir le chapitre 4).

Formulation en amplitude-vitesse

Commençons par présenter la dérivation des équations de Nwogu introduite pour la première fois par O. Nwogu [60] en 1994. Là où les autres modèles de types Boussinesq modifiaient directement les équations de Peregrine ou d'Abbott, l'idée de Nwogu est de changer l'une des inconnues. En effet, on ne considère plus les équations en fonction de la vitesse moyenne mais en fonction de la vitesse horizontale évaluée à une profondeur choisie arbitrairement ce qui permet d'avoir un degré de liberté pour améliorer l'effet de la dispersion. Dans la suite, on notera cette profondeur arbitraire z_α et la vitesse horizontale évaluée en cette profondeur u^α .

Pour obtenir ce modèle, on va partir des deux équations de Peregrine que l'on rappelle ici sous forme non-dimensionnée,

$$\tilde{\eta}_{\tilde{t}} + (\tilde{h}\tilde{u})_{\tilde{x}} = 0, \quad (2.6.21)$$

$$\tilde{u}_{\tilde{t}} + \varepsilon \tilde{u} \tilde{u}_{\tilde{x}} + \tilde{\eta}_{\tilde{x}} + \sigma^2 \left(\frac{\tilde{d}^2}{6} \tilde{u}_{\tilde{t}\tilde{x}\tilde{x}} - \frac{\tilde{d}}{2} (\tilde{d}\tilde{u})_{\tilde{t}\tilde{x}\tilde{x}} \right) = \mathcal{O}(\sigma^4, \varepsilon\sigma^2). \quad (2.6.22)$$

On utilise ensuite l'équation (2.3.14) qui donne le développement asymptotique de la vitesse horizontale \tilde{u} . On évalue cette expression en \tilde{z}_α pour exprimer \tilde{u}^α en fonction de \tilde{u} ,

$$\tilde{u}(\tilde{z}_\alpha) = \tilde{u} - \sigma^2 \left(\left(\frac{\tilde{z}_\alpha^2}{2} - \frac{\tilde{d}^2}{6} \right) \tilde{u}_{\tilde{x}\tilde{x}} + \left(\tilde{z}_\alpha + \frac{\tilde{d}}{2} \right) (\tilde{d}\tilde{u})_{\tilde{x}\tilde{x}} \right) + \mathcal{O}(\varepsilon\sigma^2, \sigma^4). \quad (2.6.23)$$

On inverse ensuite cette relation pour exprimer la vitesse moyenne en fonction de la vitesse horizontale en \tilde{z}_α en négligeant des termes d'ordre $\varepsilon\sigma^2$ et σ^4

$$\tilde{u} = \tilde{u}^\alpha + \sigma^2 \left(\left(\frac{\tilde{z}_\alpha^2}{2} - \frac{\tilde{d}^2}{6} \right) \tilde{u}_{\tilde{x}\tilde{x}}^\alpha + \left(\tilde{z}_\alpha + \frac{\tilde{d}}{2} \right) (\tilde{d}\tilde{u}^\alpha)_{\tilde{x}\tilde{x}} \right) + \mathcal{O}(\varepsilon\sigma^2, \sigma^4). \quad (2.6.24)$$

Enfin, on substitue cette expression dans les équations de Peregrine non-dimensionnées,

$$\tilde{\eta}_{\tilde{t}} + [(\tilde{d} + \varepsilon\tilde{\eta})\tilde{u}^\alpha]_{\tilde{x}} + \sigma^2 \left[\left(\frac{\tilde{z}_\alpha^2}{2} - \frac{\tilde{d}^2}{6} \right) \tilde{d}\tilde{u}_{\tilde{x}\tilde{x}}^\alpha + \left(\tilde{z}_\alpha + \frac{\tilde{d}}{2} \right) \tilde{d}(\tilde{d}\tilde{u}^\alpha)_{\tilde{x}\tilde{x}} \right]_{\tilde{x}} = \mathcal{O}(\varepsilon\sigma^2, \sigma^4), \quad (2.6.25)$$

$$\tilde{u}_{\tilde{t}}^\alpha + \varepsilon \tilde{u}^\alpha \tilde{u}_{\tilde{x}}^\alpha + \tilde{\eta}_{\tilde{x}} + \sigma^2 \left(\left(\frac{\tilde{z}_\alpha^2}{2} - \frac{\tilde{d}^2}{6} \right) \tilde{u}_{\tilde{t}\tilde{x}\tilde{x}}^\alpha + \left(\tilde{z}_\alpha + \frac{\tilde{d}}{2} \right) (\tilde{d}\tilde{u}^\alpha)_{\tilde{t}\tilde{x}\tilde{x}} \right) = \mathcal{O}(\varepsilon\sigma^2, \sigma^4). \quad (2.6.26)$$

On revient alors aux variables dimensionnelles pour obtenir les équations de Nwogu

$$\eta_t + (hu^\alpha)_x + \left(\left(\frac{dz_\alpha^2}{2} - \frac{d^3}{6} \right) u_{xx}^\alpha + \left(dz_\alpha + \frac{d^2}{2} \right) (du^\alpha)_{xx} \right)_x = 0, \quad (2.6.27)$$

$$u_t^\alpha + u^\alpha u_x^\alpha + g\eta_x + \left(\frac{z_\alpha^2}{2} - \frac{d^2}{6} \right) u_{txx}^\alpha + \left(z_\alpha + \frac{d}{2} \right) (du^\alpha)_{txx} = 0. \quad (2.6.28)$$

Remarque 4. *Dans ce modèle, la première équation n'est pas exacte contrairement aux équations que nous avons présentées auparavant. Néanmoins, nous verrons dans le chapitre 4 que ce modèle peut avoir, selon le choix du z_α , des meilleures caractéristiques de dispersion linéaire.*

Pour simplifier les notations et faire apparaître le degré de liberté au travers d'une constante réelle, on pose $z_\alpha = (-1 + \sqrt{1 + 2\alpha})d$, où $\alpha \in (-1/2, 0)$. Dans la suite, nous préférerons noter $z_\alpha = \theta d$, avec $\theta \in (-1, 0)$. On obtient alors les équations de Nwogu sous sa forme la plus classique

$$\eta_t + (hu^\alpha)_x + \left(B_1 d^3 u_{xx}^\alpha + B_2 d^2 (du^\alpha)_{xx} \right)_x = 0, \quad (2.6.29)$$

$$u_t^\alpha + u^\alpha u_x^\alpha + g\eta_x + A_1 d^2 u_{txx}^\alpha + A_2 d (du^\alpha)_{txx} = 0, \quad (2.6.30)$$

où

$$A_1 = \frac{\theta^2}{2}, \quad A_2 = \theta, \quad B_1 = \frac{\theta^2}{2} - \frac{1}{6}, \quad B_2 = \theta + \frac{1}{2}.$$

Notons que $A_1 + A_2 = \alpha$ et $B_1 + B_2 = \alpha + \frac{1}{3}$.

Une procédure tout à fait similaire permet d'obtenir une version 2D des équations de Nwogu

$$\eta_t + \nabla \cdot (h\mathbf{u}^\alpha) + \nabla \cdot \left(B_1 d^3 \nabla \left(\nabla \cdot \mathbf{u}^\alpha \right) + B_2 d^2 \nabla \left(\nabla \cdot (d\mathbf{u}^\alpha) \right) \right) = 0, \quad (2.6.31)$$

$$\mathbf{u}_t^\alpha + (\mathbf{u}^\alpha \cdot \nabla) \mathbf{u}^\alpha + g\nabla\eta + A_1 d^2 \nabla \left(\nabla \cdot \mathbf{u}_t^\alpha \right) + A_2 d \nabla \left(\nabla \cdot (d\mathbf{u}_t^\alpha) \right) = 0, \quad (2.6.32)$$

où \mathbf{u}^α désigne le vecteur vitesse $(u, v)^T$ évalué en $z = \theta d$ et ∇ l'opérateur gradient en deux dimensions (par rapport à x et y).

Ce modèle semble là encore être une extension des équations de Saint-Venant mais cette fois-ci on retrouve des termes d'ordre σ^2 dans les deux équations. Dans le cas général, il n'existe pas de valeurs du paramètre θ qui permette de retrouver les équations de Peregrine. Néanmoins, si la bathymétrie est constante, en choisissant $\theta = \sqrt{1/3} - 1$, on retrouve les équations de Peregrine à fond plat. Les équations de Nwogu et de Peregrine font donc partie de la même famille. On en déduit qu'il semble possible de trouver une formulation qui étendrait les équations d'Abbott de la même manière que les équations de Nwogu étendent celles de Peregrine. C'est l'objet de la prochaine partie.

Formulation flux-amplitude

Nous allons maintenant présenter un nouveau modèle qui a été dérivé en détails pour la première fois dans [12]. On va reproduire la même procédure que dans la partie 2.5.2 mais sur les équations de Nwogu. L'idée ici est d'exprimer les équations de Nwogu en fonction de la surface η et d'une nouvelle variable $q^\alpha = hu^\alpha$ qui s'apparente à un flux. A notre connaissance ces équations n'ont jamais été dérivées dans la littérature.

On reprend comme point de départ les équations de Nwogu non-dimensionnées (2.6.25)-(2.6.26). On garde la première équation inchangée et on remplace la seconde par la somme de la première multipliée par $\varepsilon \tilde{u}^\alpha$ et de la seconde par $\tilde{d} + \varepsilon \tilde{\eta}$. On obtient le système suivant en négligeant les termes d'ordre $\varepsilon \sigma^2$ et σ^4

$$\tilde{\eta}_{\tilde{t}} + \tilde{q}_{\tilde{x}}^{\alpha} + \sigma^2 \left[\left(\frac{\tilde{z}_{\alpha}^2}{2} - \frac{\tilde{d}^2}{6} \right) \tilde{d} \tilde{u}_{\tilde{x}\tilde{x}}^{\alpha} + \left(\tilde{z}_{\alpha} + \frac{\tilde{d}}{2} \right) \tilde{d} (\tilde{d} \tilde{u}^{\alpha})_{\tilde{x}\tilde{x}} \right]_{\tilde{x}} = \mathcal{O}(\varepsilon \sigma^2, \sigma^4), \quad (2.6.33)$$

$$\begin{aligned} & \tilde{q}_{\tilde{t}}^{\alpha} + \varepsilon \left(\frac{(\tilde{q}^{\alpha})^2}{\tilde{h}} \right)_{\tilde{x}} + \tilde{h} \tilde{\eta}_{\tilde{x}} + \sigma^2 \tilde{h} \left(\left(\frac{\tilde{z}_{\alpha}^2}{2} - \frac{\tilde{d}^2}{6} \right) \tilde{u}_{\tilde{t}\tilde{x}\tilde{x}}^{\alpha} + \left(\tilde{z}_{\alpha} + \frac{\tilde{d}}{2} \right) (\tilde{d} \tilde{u}^{\alpha})_{\tilde{t}\tilde{x}\tilde{x}} \right) \\ & + \varepsilon \sigma^2 \tilde{u}^{\alpha} \left[\left(\frac{\tilde{z}_{\alpha}^2}{2} - \frac{\tilde{d}^2}{6} \right) \tilde{d} \tilde{u}_{\tilde{x}\tilde{x}}^{\alpha} + \left(\tilde{z}_{\alpha} + \frac{\tilde{d}}{2} \right) \tilde{d} (\tilde{d} \tilde{u}^{\alpha})_{\tilde{x}\tilde{x}} \right]_{\tilde{x}} = \mathcal{O}(\varepsilon \sigma^2, \sigma^4). \end{aligned} \quad (2.6.34)$$

On exprime maintenant \tilde{u}^{α} en fonction de \tilde{q}^{α}

$$\tilde{u}^{\alpha} = \frac{\tilde{q}^{\alpha}}{\tilde{d}} + \mathcal{O}(\varepsilon).$$

On substitue l'expression de u^{α} dans les équations (2.6.33) et (2.6.34) et on néglige les termes d'ordre $\varepsilon \sigma^2$ et d'ordre σ^4 ,

$$\tilde{\eta}_{\tilde{t}} + \tilde{q}_{\tilde{x}}^{\alpha} + \sigma^2 \left[\left(\frac{\tilde{z}_{\alpha}^2 \tilde{d}}{2} - \frac{\tilde{d}^3}{6} \right) \left(\frac{\tilde{q}^{\alpha}}{\tilde{d}} \right)_{\tilde{x}\tilde{x}} + \left(\tilde{z}_{\alpha} \tilde{d} + \frac{\tilde{d}^2}{2} \right) \tilde{q}_{\tilde{x}\tilde{x}}^{\alpha} \right]_{\tilde{x}} = \mathcal{O}(\varepsilon \sigma^2, \sigma^4), \quad (2.6.35)$$

$$\tilde{q}_{\tilde{t}}^{\alpha} + \varepsilon \left(\frac{(\tilde{q}^{\alpha})^2}{\tilde{h}} \right)_{\tilde{x}} + \tilde{h} \tilde{\eta}_{\tilde{x}} + \sigma^2 \left(\left(\frac{\tilde{z}_{\alpha}^2 \tilde{d}}{2} - \frac{\tilde{d}^3}{6} \right) \left(\frac{\tilde{q}^{\alpha}}{\tilde{d}} \right)_{\tilde{t}\tilde{x}\tilde{x}} + \left(\tilde{d} \tilde{z}_{\alpha} + \frac{\tilde{d}^2}{2} \right) \tilde{q}_{\tilde{t}\tilde{x}\tilde{x}}^{\alpha} \right) = \mathcal{O}(\varepsilon \sigma^2, \sigma^4). \quad (2.6.36)$$

Enfin, on revient aux variables dimensionnées après avoir négligé les termes d'ordre σ^4 et $\varepsilon \sigma^2$ pour obtenir de nouvelles équations

$$\eta_t + q_x^{\alpha} + \left[\left(\frac{z_{\alpha}^2 d}{2} - \frac{d^3}{6} \right) \left(\frac{q^{\alpha}}{d} \right)_{xx} + \left(z_{\alpha} d + \frac{d^2}{2} \right) q_{xx}^{\alpha} \right]_x = 0, \quad (2.6.37)$$

$$q_t^{\alpha} + \left(\frac{(q^{\alpha})^2}{h} \right)_x + g h \eta_x + \left(\left(\frac{z_{\alpha}^2 d}{2} - \frac{d^3}{6} \right) \left(\frac{q^{\alpha}}{d} \right)_{txx} + \left(d z_{\alpha} + \frac{d^2}{2} \right) q_{txx}^{\alpha} \right) = 0. \quad (2.6.38)$$

On finit par poser $z_{\alpha} = \theta d$ avec $\theta \in (-1, 0)$ pour obtenir une formulation similaire à celle des équations de Nwogu (2.6.29)-(2.6.30).

$$\eta_t + q_x^{\alpha} + \left[B_1 d^3 \left(\frac{q^{\alpha}}{d} \right)_{xx} + B_2 d^2 q_{xx}^{\alpha} \right]_x = 0, \quad (2.6.39)$$

$$q_t^{\alpha} + \left(\frac{(q^{\alpha})^2}{d + \eta} \right)_x + g(d + \eta) \eta_x + \left(A_1 d^3 \left(\frac{q^{\alpha}}{d} \right)_{txx} + A_2 d^2 q_{txx}^{\alpha} \right) = 0, \quad (2.6.40)$$

où

$$A_1 = \frac{\theta^2}{2}, \quad A_2 = \theta, \quad B_1 = \frac{\theta^2}{2} - \frac{1}{6}, \quad B_2 = \theta + \frac{1}{2}.$$

On peut encore une fois obtenir une version 2D de ce système en appliquant la même méthode aux équations de Nwogu (2.6.31)-(2.6.32),

$$\eta_t + \nabla \cdot \mathbf{q}^{\alpha} + \nabla \cdot \left[B_1 d^2 \nabla \left(\nabla \cdot \left(\frac{\mathbf{q}^{\alpha}}{d} \right) \right) + B_2 d^2 \nabla \left(\nabla \cdot \mathbf{q}^{\alpha} \right) \right] = 0, \quad (2.6.41)$$

$$\mathbf{q}_t^\alpha + \nabla(\mathbf{q}^\alpha \cdot \mathbf{u}^\alpha) + g(d + \eta)\nabla\eta + A_1 d^2 \nabla \left(\nabla \cdot \left(\frac{\mathbf{q}_t^\alpha}{d} \right) \right) + A_2 d \nabla \left(\nabla \cdot \mathbf{q}_t^\alpha \right) = 0, \quad (2.6.42)$$

où $\mathbf{q}^\alpha = (d + \eta)\mathbf{u}^\alpha$.

Lorsque l'on considère ces équations à bathymétrie constante et en prenant $\theta = \sqrt{1/3} - 1$, on retrouve les équations d'Abbott. C'est pourquoi, nous ferons référence à ces équations comme les équations de Nwogu-Abbott. Ces équations sont très prometteuses de par leur formulation conservative similaire à celles des équations d'Abbott qui simplifient grandement la résolution numérique. De plus, elles diffèrent des équations de Nwogu uniquement par des termes non-linéaires. On en déduit donc que les caractéristiques de dispersion linéaire de ce modèle sont les mêmes que celles des équations de Nwogu.

2.6.4 Modèles *abcd*

Dans cette partie, nous allons dériver une généralisation des équations de Nwogu à fond plat présentée et étudiée notamment par J. L. Bona, M. Chen et J-C. Saut dans [18]. Dans la suite, la bathymétrie sera désignée par la constante d_0 et non plus par d . L'idée est d'appliquer la méthode de dérivation des équations de Beji-Nadaoka aux équations de Nwogu.

Encore une fois, nous proposerons une formulation amplitude-flux de ce modèle.

Formulation amplitude-vitesse

Le point de départ de cette dérivation est donc les équations de Nwogu à fond plat non dimensionnées que l'on rappelle ici (on note la vitesse \tilde{u} pour simplifier les notations). Remarquons que dans ce cas particulier $\tilde{d}_0 = 1$.

$$\tilde{\eta}_{\tilde{t}} + ((1 + \varepsilon \tilde{\eta})\tilde{u})_{\tilde{x}} + \sigma^2 \beta \tilde{u}_{\tilde{x}\tilde{x}\tilde{x}} = \mathcal{O}(\varepsilon \sigma^2, \sigma^4), \quad (2.6.43)$$

$$\tilde{u}_{\tilde{t}} + \varepsilon \tilde{u} \tilde{u}_{\tilde{x}} + \tilde{\eta}_{\tilde{x}} + \sigma^2 \alpha \tilde{u}_{\tilde{t}\tilde{x}\tilde{x}} = \mathcal{O}(\varepsilon \sigma^2, \sigma^4), \quad (2.6.44)$$

où $\alpha = \theta^2/2 + \theta$ et $\beta = \theta^2/2 + \theta + 1/3$. Lorsque l'on néglige les termes d'ordre ε et σ^2 dans le système (2.6.43)-(2.6.44), on obtient

$$\tilde{\eta}_{\tilde{t}} + \tilde{u}_{\tilde{x}} = \mathcal{O}(\varepsilon, \sigma^2), \quad (2.6.45)$$

$$\tilde{u}_{\tilde{t}} + \tilde{\eta}_{\tilde{x}} = \mathcal{O}(\varepsilon, \sigma^2). \quad (2.6.46)$$

On applique le procédé utilisé dans la partie 2.6.1 : on ajoute et on soustrait $\lambda \beta \tilde{u}_{\tilde{x}\tilde{x}\tilde{x}}$ à l'équation (2.6.43) et $\mu \alpha \tilde{u}_{\tilde{t}\tilde{x}\tilde{x}}$ à l'équation (2.6.44), où λ et μ sont des réels quelconques. On utilise l'équation (2.6.45) pour modifier le terme en facteur de “+ $\lambda \beta$ ” dans la première équation et l'équation (2.6.46) pour modifier le terme en facteur de “+ $\mu \alpha$ ” dans la seconde. On revient aux variables dimensionnées en posant

$$\mathbf{a} = (1 - \lambda)\beta, \mathbf{b} = \lambda\beta, \mathbf{c} = \mu\alpha, \mathbf{d} = (1 - \mu)\alpha.$$

On obtient alors les modèles de Boussinesq *abcd* qui s'écrivent sous la forme

$$\eta_t + (hu)_x + \mathbf{a}d_0^3 u_{xxx} - \mathbf{b}d^2 \eta_{txx} = 0, \quad (2.6.47)$$

$$u_t + uu_x + g\eta_x + \mathbf{c}gd_0^2 \eta_{xxx} - \mathbf{d}d_0^2 u_{txx} = 0. \quad (2.6.48)$$

Cette écriture généralise les modèles précédent à bathymétrie constante formulés en vitesse-amplitude. En effet, en choisissant judicieusement la valeur des constantes μ , λ et θ , on peut retrouver des modèles présentés précédemment ou obtenir d'autres modèles de type Boussinesq que nous ne détaillerons pas ici. Par exemple :

- si on prend $\lambda = 0$, $\mu = 0$ et θ quelconque dans $(0, 1)$, on retrouve les équations de Nwogu.
- si on prend λ et μ quelconques et $\theta = \sqrt{1/3} - 1$, on retrouve les équations de Beji-Nadaoka à fond plat.
- si on prend $\lambda = 1$, $\mu = 0$ et $\theta = \sqrt{2/3} - 1$, on retrouve les équations de Benjamin-Bona-Mahony (BBM, voir [14]).

On peut aussi remarquer que pour tout choix de λ , μ et θ

$$\mathbf{a} + \mathbf{b} + \mathbf{c} + \mathbf{d} = \frac{1}{3}.$$

Formulation amplitude-flux

De la même manière que pour tous les autres modèles de Boussinesq, il est possible d'obtenir une version des équations de type *abcd* en flux-amplitude. Pour cela, il suffit de négliger quelques termes d'ordre $\varepsilon\sigma^2$ ou bien de reproduire la méthode précédente sur les équations de Nwogu-Abbott. On obtient alors le système suivant

$$\eta_t + q_x + \mathbf{a}d_0^2 q_{xxx} - \mathbf{b}d^2 \eta_{txx} = 0, \quad (2.6.49)$$

$$q_t + \left(\frac{q^2}{h} \right)_x + gh\eta_x + \mathbf{c}gd_0^3 \eta_{xxx} - \mathbf{d}d_0^2 q_{txx} = 0, \quad (2.6.50)$$

où **a**, **b**, **c** et **d** sont définis comme précédemment. Encore une fois, un choix particulier des constantes qui régissent ces systèmes nous permet d'obtenir des modèles connus. Par exemple :

- si on prend $\lambda = 0$, $\mu = 0$ et θ quelconque dans $(0, 1)$, on retrouve les équations de Nwogu-Abbott à fond plat.
- si on prend λ et μ quelconques et $\theta = \sqrt{1/3} - 1$, on retrouve les équations de Madsen-Sørensen à fond plat.
- si on prend $\lambda = 1$, $\mu = 0$ et $\theta = \sqrt{2/3} - 1$, on retrouve une version des équations de Benjamin-Bona-Mahony en flux-amplitude.

Nous venons de présenter la majorité des modèles de type Boussinesq qui sont utilisés dans la modélisation des écoulements à surface libre. Nous aurons l'occasion d'étudier plus en détail cette famille de modèle par la suite. Mais, pour être le plus exhaustif possible, il nous faut présenter un autre modèle plus non-linéaire que ceux que nous avons présenté auparavant. C'est l'objectif de la prochaine partie qui est dédiée à la dérivation des équations de Green-Naghdi.

2.7 Equations de Green-Naghdi

Nous allons proposer une dérivation pour les équations de Green-Naghdi qui s'inspire de ce que l'on a proposé précédemment pour insister sur le fait que ces équations généralisent les équations de Peregrine. On suppose ici que σ^2 est petit devant 1 et que ε est quelconque. Autrement dit, on va pousser le développement asymptotique qui permet d'obtenir les équations de Saint-Venant jusqu'à l'ordre σ^4 comme pour les équations de Peregrine, mais en gardant tous les termes d'ordre $\varepsilon\sigma^2$. Pour ce modèle, on va considérer la surface d'élévation η et la vitesse moyenne \bar{u} comme inconnues. L'équation de continuité est donc identique à celle du modèle de Peregrine et de Saint-Venant. On la rappelle ici sous forme non-dimensionnée

$$\tilde{\eta}_{\tilde{t}} + (\tilde{h}\tilde{u})_{\tilde{x}} = 0. \quad (2.7.1)$$

Pour dériver l'équation du moment du modèle de Green-Naghdi, on reprend le développement asymptotique de \tilde{u} (2.3.14) et de \tilde{w} (2.3.15). Pour substituer dans l'équation (2.3.1), on a besoin d'avoir les expressions de $\tilde{u}(\varepsilon\tilde{\eta})$, $\tilde{w}(\varepsilon\tilde{\eta})$, $\tilde{u}_{\tilde{t}}(\varepsilon\tilde{\eta})$ et $\tilde{w}_{\tilde{t}}(\varepsilon\tilde{\eta})$ en fonction de \tilde{u} et $\tilde{\eta}$. On commence par évaluer les relations (2.3.14) et (2.3.15) en $\varepsilon\tilde{\eta}$ au niveau de la surface libre

$$\tilde{u}(\varepsilon\tilde{\eta}) = \tilde{u} - \sigma^2 \left(\left(\frac{\tilde{h}^2}{3} - \frac{\tilde{h}\tilde{d}}{2} \right) \tilde{u}_{\tilde{x}\tilde{x}} + \frac{\tilde{h}}{2} (\tilde{d}\tilde{u})_{\tilde{x}\tilde{x}} \right) + \mathcal{O}(\sigma^4), \quad (2.7.2)$$

et

$$\tilde{w}(\varepsilon\tilde{\eta}) = - \left((\tilde{h} - \tilde{d}) \tilde{u}_{\tilde{x}} + (\tilde{d}\tilde{u})_{\tilde{x}} \right) + \mathcal{O}(\sigma^2). \quad (2.7.3)$$

On dérive ensuite l'équation (2.3.14) par rapport à \tilde{t} pour trouver l'expression de $\tilde{u}_{\tilde{t}}(\varepsilon\tilde{\eta})$

$$\begin{aligned} \tilde{u}_{\tilde{t}} &= \tilde{u}_{\tilde{t}} - \sigma^2 \left(\left(\frac{\tilde{z}^2}{2} - \left(\frac{\tilde{h}^2}{6} - \frac{\tilde{d}(\tilde{h} - \tilde{d})}{2} \right) \right) \tilde{u}_{\tilde{t}\tilde{x}\tilde{x}} + \left(\tilde{z} - \left(\frac{\tilde{h}}{2} - \tilde{d} \right) \right) (\tilde{d}\tilde{u})_{\tilde{t}\tilde{x}\tilde{x}} \right) \\ &\quad + \sigma^2 \left(\left(\frac{\tilde{h}}{3} - \frac{\tilde{d}}{2} \right) \tilde{h}_{\tilde{t}} \tilde{u}_{\tilde{x}\tilde{x}} + \frac{\tilde{h}_{\tilde{t}}}{2} (\tilde{d}\tilde{u})_{\tilde{x}\tilde{x}} \right) + \mathcal{O}(\sigma^4). \end{aligned} \quad (2.7.4)$$

On évalue cette relation en $\varepsilon\tilde{\eta}$ et on utilise l'équation (2.7.1) pour exprimer $\tilde{h}_{\tilde{t}}$ en fonction de \tilde{u} (il faut au préalable multiplier l'équation par ε pour bien faire apparaître la dérivée temporelle de \tilde{h}). On obtient l'expression de $\tilde{u}_{\tilde{t}}(\varepsilon\tilde{\eta})$

$$\begin{aligned} \tilde{u}_{\tilde{t}}(\varepsilon\tilde{\eta}) &= \tilde{u}_{\tilde{t}} - \sigma^2 \left(\left(\frac{\tilde{h}^2}{3} - \frac{\tilde{h}\tilde{d}}{2} \right) \tilde{u}_{\tilde{t}\tilde{x}\tilde{x}} + \frac{\tilde{h}}{2} (\tilde{d}\tilde{u})_{\tilde{t}\tilde{x}\tilde{x}} \right) \\ &\quad - \sigma^2 \left(\left(\frac{\tilde{h}}{3} - \frac{\tilde{d}}{2} \right) (\tilde{h}\tilde{u})_{\tilde{x}} \tilde{u}_{\tilde{x}\tilde{x}} + \frac{(\tilde{h}\tilde{u})_{\tilde{x}}}{2} (\tilde{d}\tilde{u})_{\tilde{x}\tilde{x}} \right) + \mathcal{O}(\sigma^4). \end{aligned} \quad (2.7.5)$$

De la même manière, on peut trouver l'expression de $\tilde{w}_{\tilde{t}}(\varepsilon\tilde{\eta})$ à partir de l'équation (2.3.15)

$$\tilde{w}_{\tilde{t}}(\varepsilon\tilde{\eta}) = -((\tilde{h} - \tilde{d}) \tilde{u}_{\tilde{t}\tilde{x}} + (\tilde{d}\tilde{u})_{\tilde{t}\tilde{x}}) + \mathcal{O}(\sigma^2). \quad (2.7.6)$$

Il ne reste plus qu'à substituer les différentes expressions (2.7.2), (2.7.3), (2.7.5) et (2.7.6) dans l'équation (2.3.1) que l'on rappelle ici

$$\tilde{u}_{\tilde{t}}(\tilde{\eta}) + \varepsilon\sigma^2\tilde{\eta}_{\tilde{x}}\tilde{w}_{\tilde{t}}(\tilde{\eta}) + \tilde{\eta}_{\tilde{x}} + \varepsilon\left[\frac{\tilde{u}^2(\tilde{\eta})}{2}\right]_{\tilde{x}} + \varepsilon\sigma^2\left[\frac{\tilde{w}^2(\tilde{\eta})}{2}\right]_{\tilde{x}} = 0.$$

On néglige alors tous les termes d'ordre σ^4 . En réarrangeant l'équation qui en résulte et en factorisant comme il faut, on obtient l'équation suivante

$$\tilde{\bar{u}}_{\tilde{t}} + \varepsilon\tilde{\bar{u}}\tilde{\bar{u}}_{\tilde{x}} + \tilde{\eta}_{\tilde{x}} - \frac{\sigma^2}{\tilde{h}}\left[\left(\frac{\tilde{h}^3}{3} - \frac{\tilde{h}^2\tilde{d}}{2}\right)\tilde{\mathcal{P}} + \frac{\tilde{h}^2}{2}\tilde{\mathcal{Q}}\right]_{\tilde{x}} + \sigma^2\tilde{d}_{\tilde{x}}\left((\tilde{h} - \tilde{d})\tilde{\mathcal{P}} + \tilde{\mathcal{Q}}\right) = \mathcal{O}(\sigma^4), \quad (2.7.7)$$

avec

$$\tilde{\mathcal{P}} = \tilde{\bar{u}}_{\tilde{t}\tilde{x}} + \varepsilon\tilde{\bar{u}}\tilde{\bar{u}}_{\tilde{x}\tilde{x}} - \varepsilon\tilde{\bar{u}}_{\tilde{x}}^2 \text{ et } \tilde{\mathcal{Q}} = (\tilde{\bar{u}}_{\tilde{t}\tilde{x}} + \varepsilon\tilde{\bar{u}}(\tilde{\bar{u}}_{\tilde{x}\tilde{x}} - \varepsilon\tilde{\bar{u}}_{\tilde{x}}\tilde{\bar{u}}_{\tilde{x}})).$$

Pour finir, on néglige les termes d'ordre σ^4 et on revient aux variables dimensionnées. On obtient alors les équations de Green-Naghdi rappelées ici

$$\eta_t + (h\bar{u})_x = 0, \quad (2.7.8)$$

$$\bar{u}_t + \bar{u}\bar{u}_x + g\eta_x - \frac{1}{h}\left[\left(\frac{h^3}{3} - \frac{h^2d}{2}\right)\mathcal{P} + \frac{h^2}{2}\mathcal{Q}\right]_x + d_x\left((h-d)\mathcal{P} + \mathcal{Q}\right) = 0, \quad (2.7.9)$$

où

$$\mathcal{P} = \bar{u}_{tx} + \bar{u}\bar{u}_{xx} - \bar{u}_x^2 \text{ et } \mathcal{Q} = (d\bar{u})_{tx} + \bar{u}(d\bar{u})_{xx} - \bar{u}_x(d\bar{u})_x.$$

En appliquant une procédure similaire aux équations d'Euler 3D, on obtient la version 2D des équations de Green-Naghdi

$$\eta_t + \nabla \cdot (h\bar{\mathbf{u}}) = 0, \quad (2.7.10)$$

$$\begin{aligned} & \left(1 + \frac{1}{h}\tau[h, d]\right)\bar{\mathbf{u}}_t + (\bar{\mathbf{u}} \cdot \nabla)\bar{\mathbf{u}} + g\nabla\eta \\ & - \frac{1}{3h}\nabla\left[h^3((\bar{\mathbf{u}} \cdot \nabla)(\nabla \cdot \bar{\mathbf{u}}) - (\nabla \cdot \bar{\mathbf{u}})^2)\right] + \mathcal{Q}[h, d]\bar{\mathbf{u}} = 0, \end{aligned} \quad (2.7.11)$$

où

$$\tau[h, d]W = -\frac{1}{3}\nabla(h^3\nabla \cdot W) - \frac{1}{2}\left[\nabla(h^2(\nabla d) \cdot W) - h^2(\nabla d)\nabla \cdot W\right] + h(\nabla d)[(\nabla d) \cdot W],$$

et

$$\begin{aligned} \mathcal{Q}[h, d]W = & -\frac{1}{2h}\left[\nabla(h^2(W \cdot \nabla)^2(d)) - h^2((W \cdot \nabla)(\nabla \cdot W) - (\nabla \cdot W)^2)(\nabla d)\right] \\ & + [(W \cdot \nabla)^2 d]\nabla d. \end{aligned}$$

Ce système d'équations diffère de celui de Peregrine uniquement via les termes non-linéaires qui n'ont pas été négligés. Il s'avère donc globalement plus proche des équations d'Euler. Néanmoins, ce que l'on gagne en précision est perdu d'un point de vue résolution numérique.

En effet, on doit gérer beaucoup plus de termes non-linéaires et on doit inverser un opérateur différentiel qui se redéfinit à chaque pas de temps (c'est l'opérateur τ dans les équations $2D$ qui dépend de η). Il est néanmoins possible de s'affranchir de ce problème. D. Lannes et F. Marche ont en effet développé un nouveau modèle dérivé directement des équations de Green-Naghdi en négligeant certains termes d'ordre σ^4 pour remplacer l'opérateur $\frac{1}{h}\tau[h, d]$ par un opérateur diagonal qui ne dépend plus de h . Ce procédé permet d'obtenir des équations ne contenant qu'un opérateur à inverser indépendant de la variable t et qui conservent les mêmes caractéristiques de dispersion linéaire que celles des équations de Green-Naghdi. Le lecteur intéressé pourra se référer à [52] pour les détails de la dérivation de ces équations.

Chapter 3

On the existence of solution for Boussinesq type equations

Contents

3.1	Introduction	56
3.2	Context and notations	57
3.3	Long time existence theory for Nwogu-Abbott equations.	58
3.4	Solitary waves solutions for Boussinesq systems	64
3.4.1	Solitary waves solutions for the Beji-Nadaoka equations	67
3.4.2	Solitary waves solutions for Madsen-Sørensen equations	74
3.4.3	Solitary waves solutions for Nwogu equations	76
3.4.4	Discussion on solitary waves for Nwogu-Abbott equations	80

3.1 Introduction

The description of the motion of the free surface and the evolution of the velocity field of an ideal, incompressible and irrotational fluid under the gravity is well-described by the Euler equations, especially when surface tension and dissipative effects are neglected. However, in many physical situations, the Euler equations appear too complex compared to the complexity of the flow one wants to describe. Consequently, many asymptotic models have been introduced, fitting restricted physical regimes. Starting from the Boussinesq equations of Peregrine [63], several Boussinesq systems have been developed such that, for example, the enhanced equations of Madsen-Sørensen [55], the equations of Beji-Nadaoka [11], the equations of Nwogu [60], the nonlinear Serre-Green-Naghdi equations [51] and shallow water type models [43] (see Chapter 2 for details). Even though all the systems have similar linear dispersion characteristics and formulations, they are not nonlinearly equivalent and their behaviors differ when one deals with practical applications (see chapter 4 for details).

In view of justifying the derivation of Boussinesq system, it is very important to show that they are well-posed. We pay attention to the dependence of the existence time and the size of the solution with respect to parameter ε which represents the nonlinear effects. Under some technical conditions on the initial data we expect an existence result on a time interval $[0, \frac{T}{\varepsilon}]$ (where T is independant of ε) which corresponds to the optimal existence time for Boussinesq systems with flat bottom (see [49, 58] for details). As mentionned in [67] (see also [24, 68]), this property is known for only a limited number of Boussinesq systems setting in 1D or 2D. Note also that initial value problem for the water waves problems has been widely studied for decades. We refer to the work of D. Lannes [6, 50] (see also [49] and the references therein). The question of local well-posedness for asymptotic models is also of interest [19] and widely studied for the systems using the (η, u) -formulation. To our knowledge, no existence results are known for the (η, q) -formulation, this is the reason why we present a long time existence theory for the new Boussinesq model, called Nwogu-Abbott system, introduced for the first time in [39] and in Section 2.6.3. This study is the aim of Section 3.3 of this chapter. Another interesting issue is the question of the consistency of the asymptotic equations with Euler system (2.2.1)-(2.2.4). This question is treated in [20] for general Boussinesq systems written in (η, u) -formulation. This problem appears more delicate with the (η, q) -version since one has to deal with different variables between Euler system and Nwogu-Abbott equations for example.

After proving the well-posedness of the different asymptotic models, it is natural to solve them numerically. The literature concerning numerical treatment of the previous systems is abundant and contains very promising approach involving finite differences, finite volumes or finite elements approaches. Due to the presence of higher order partial derivatives in the different models cited above, the finite difference scheme is widely used despite its poor local mesh adaptivity potential (see [11, 41, 47, 60]). To check the accuracy of numerical schemes as well as for practical applications in coastal engineering and to estimate the validity of models, it is very useful to study the existence of particular global solutions: the solitary waves. A solitary wave is a global positive and regular solution (of class C^2 for instance), which propagates at a constant speed c with a constant shape. In addition, a solitary wave and its first and second

derivatives tends to zero at infinity. In Section 3.4, we present some result on the existence of solitary waves for part of the Boussinesq models presented in Chapter 2 (namely, Beji-Nadaoka, Madsen-Sørensen, Nwogu and Nwogu-Abbott equations). We also give a relation between the amplitude A of one of the component of the solitary wave and the speed of propagation c , that enables to make some effective computations and proves the link between the two quantities. Note that there is a large class of results concerning the existence of solitary waves for Boussinesq systems (see [9, 26, 27]).

3.2 Context and notations

Before going further, let us recall some notation. We only deal with 2-D and 1-D problems. We denote by (x, z) respectively the horizontal and the vertical spatial dimension and by d the depth at still water. In this chapter, we assume that $d = d_0$ is a constant. $\eta(t, x)$ is the surface elevation from its rest position. The total depth is then $h(t, x) = d + \eta(t, x)$. u denotes the horizontal velocity and g the acceleration due to gravity. Let a be a typical wave amplitude and λ a typical wavelength. In view of performing an asymptotic analysis, we introduce the nonlinearity parameter ε and the dispersion parameter σ defined by

$$\varepsilon = \frac{a}{d}, \quad \sigma = \frac{d}{\lambda}.$$

Starting from Euler equations, one can distinguish two family-type of asymptotic models (see Chapter 2). The first one uses the velocity u and the surface elevation η as unknowns. This is the case for the Beji-Nadaoka equations (see Section 2.6.1 for details)

$$\begin{aligned} \eta_t + [(d + \eta)\bar{u}]_x &= 0, \\ \bar{u}_t + \bar{u}\bar{u}_x + g\eta_x - (\frac{1}{3} + \alpha_B)d^2\bar{u}_{txx} - g\alpha_B d^2\eta_{xxx} &= 0, \end{aligned} \tag{3.2.1}$$

where \bar{u} denotes the depth averaged horizontal velocity, and for the Nwogu formulation (see Section 2.6.3)

$$\begin{aligned} \eta_t + [(d + \eta)u^\alpha]_x + \beta d^3 u_{xxx}^\alpha &= 0, \\ u_t^\alpha + u^\alpha u_x^\alpha + g\eta_x + \alpha d^2 u_{txx}^\alpha &= 0, \end{aligned} \tag{3.2.2}$$

with $\theta \in (-1, 0)$, where u^α denotes the horizontal velocity at depth θd , and

$$\alpha = \theta + \frac{\theta^2}{2}, \quad \beta = \frac{\theta^2}{2} + \theta - \frac{1}{3}.$$

Another different point of view consists in writing the asymptotic models with a different variable $q(t, x) = h(t, x)u(t, x)$, where q is homogeneous to a flux. This formulation was used, for example, by Madsen and Sørensen to derive the following set of equations (see Section 2.6.2)

$$\begin{aligned} \eta_t + \bar{q}_x &= 0, \\ \bar{q}_t + \left(\frac{\bar{q}^2}{h}\right)_x + gh\eta_x - (\beta + \frac{1}{3})d^2\bar{q}_{txx} - g\beta d^3\eta_{xxx} &= 0, \end{aligned} \tag{3.2.3}$$

with $\beta \in \mathbb{R}$, and for the Nwogu-Abbott formulation (see Section 2.6.3)

$$\begin{aligned}\eta_t + q_x^\alpha + \beta d^2 q_{xxx}^\alpha &= 0, \\ q_t^\alpha + \left(\frac{(q^\alpha)^2}{h} \right)_x + gh\eta_x + \alpha d^2 q_{txx}^\alpha &= 0,\end{aligned}\tag{3.2.4}$$

where

$$\alpha = \theta + \frac{\theta^2}{2}, \quad \beta = \frac{\theta^2}{2} + \theta - \frac{1}{3}.$$

3.3 Long time existence theory for Nwogu-Abbott equations.

In this section, we only focus on the Nwogu-Abbott equations. Our aim here is to provide a local Cauchy theory for this set of equations. For that purpose, we introduce the following problem written in a dimensionless form with a constant flat bathymetry d for $(t, x) \in \mathbb{R}_+^* \times \mathbb{R}$, denoting by Q the flux in order to simplify the notations:

$$\begin{cases} \eta_t + Q_x + \beta \sigma^2 d^2 Q_{xxx} = 0, \end{cases}\tag{3.3.1}$$

$$\begin{cases} Q_t + \varepsilon \left(\frac{Q^2}{d + \varepsilon \eta} \right)_x + g(d + \varepsilon \eta) \eta_x + \alpha \sigma^2 d^2 Q_{txx} = 0. \end{cases}\tag{3.3.2}$$

The existence results concerning Equations (3.3.1)-(3.3.2) is as follows

Theorem 1. *Assume that $(\eta_0, Q_0) \in H^2(\mathbb{R}) \times H^4(\mathbb{R})$ satisfy*

$$d + \varepsilon \eta_0(x) \geq a \text{ on } \mathbb{R},\tag{3.3.3}$$

$$g(d + \varepsilon \eta_0) - \varepsilon^2 \frac{Q_0^2}{(d + \varepsilon \eta_0)^2} \geq b \text{ on } \mathbb{R},\tag{3.3.4}$$

with $a > 0$, $b > 0$ and that the bathymetry d is constant. Then there exists a time $T > 0$ independant of the parameter ε and a unique local solution to the initial value problem (3.3.1)-(3.3.2) such that

$$\eta \in C([0, \frac{T}{\varepsilon}]; L^2(\mathbb{R})),$$

$$Q \in C([0, \frac{T}{\varepsilon}]; L^2(\mathbb{R})),$$

with

$$\eta(0, x) = \eta_0(x), \quad Q(0, x) = Q_0(x).$$

Conditions (3.3.3)-(3.3.4) are important in the sequel. Actually, we need this condition in the energy estimates used in the proof.

We believe that Theorem 1 can be adapted to 2D version of Nwogu-Abbott system. However, for the sake of clarity, we decide to present the long time existence theory in dimension 1.

We introduce the following problem written in a dimensionless form with a constant flat bathymetry d for $(t, x) \in \mathbb{R}_+^* \times \mathbb{R}$

$$\begin{cases} \partial_t \eta + Q_x + \beta \sigma^2 d^2 Q_{xxx} = 0, \\ Q_t + \varepsilon \left(\frac{Q^2}{d + \varepsilon \eta} \right)_x + g(d + \varepsilon \eta) \eta_x + \alpha \sigma^2 d^2 Q_{txx} = 0, \end{cases} \quad (3.3.5)$$

with the initial condition

$$\begin{cases} \eta(0, x) = \eta_0(x), & x \in \mathbb{R}, \\ Q(0, x) = Q_0(x), & x \in \mathbb{R}, \end{cases} \quad (3.3.7)$$

$$\begin{cases} \eta(0, x) = \eta_0(x), \\ Q(0, x) = Q_0(x), \end{cases} \quad (3.3.8)$$

and where $(\alpha, \beta) \in \mathbb{R}_-^2$ are fixed negative real. We recall that the small parameters ε and σ^2 are of the same order. For convenience, we first introduce a constant C such that $\sigma^2 = C\varepsilon$ and rewrite System (3.3.5)-(3.3.6) into, by denoting $\tilde{\alpha} = -Cd^2\alpha$ and $\tilde{\beta} = -Cd^2\beta$ and dropping the tilde

$$\begin{cases} \partial_t \eta + Q_x - \beta \varepsilon Q_{xxx} = 0, \\ \partial_t (1 - \alpha \varepsilon \partial_x^2) Q + \varepsilon \left(\frac{Q^2}{d + \varepsilon \eta} \right)_x + g(d + \varepsilon \eta) \eta_x = 0. \end{cases} \quad (3.3.9)$$

$$(3.3.10)$$

Note now that coefficients α and β are positive. In order to apply the usual energy estimates one has to deal with the presence of the third order derivative in space in Equation (3.3.9) and the conservative terms of (3.3.10). Moreover, one has to prove that the quantity $d + \varepsilon \eta$ stay bounded away from 0. We recall the standard notations that we will use in the sequel. For $1 \leq p \leq \infty$, the $L^p(\mathbb{R})$ -norm is denoted by $|\cdot|_p$ and the $H^s(\mathbb{R})$ -norm by $\|\cdot\|_s$ for $s \in \mathbb{R}_+$. Moreover, for $s > 0$ and $T > 0$, we denote

$$\|\cdot\|_{T,s} = \sup_{t \in [0, T]} \|\cdot\|_s$$

the norm of the space $L^\infty(0, T; H^s(\mathbb{R}))$. First note that we only give a sketch of the proof, pointing out the difficulties and omitting the classical details. As usual, the proof is based on a fixed point theorem (see [5]). Due to the quasilinear-like behavior of the equations, we introduce the following function space

$$X_T = \left\{ \begin{array}{l} U = (\eta, Q) : \eta \in C([0, T]; L^2(\mathbb{R})), \\ Q \in C([0, T]; L^2(\mathbb{R})), \|U(t)\|_{X_t} < +\infty \end{array} \right\}.$$

where

$$\|(\eta, Q)\|_{X_t} = \|\eta\|_{T,2} + \|Q\|_{T,4} + \|\eta_t\|_{T,1} + \|Q_t\|_{T,1}.$$

We refer to [34] for more details. In addition, for $M \in \mathbb{R}_+^*$, $a > 0$, $b > 0$ and $r > 0$, we denote

$$X_T(M, a, b, r) = \left\{ \begin{array}{l} (\eta, Q) \in X_T : \|\eta\|_{T,2} \leq M, \|Q\|_{T,4} \leq M \\ \|\eta_t\|_{T,1} \leq r, \|Q_t\|_{T,1} \leq r, d + \varepsilon \eta \geq a \\ g(d + \varepsilon \eta) - \varepsilon^2 \frac{Q^2}{(d + \varepsilon \eta)^2} \geq b, \\ \eta(0, x) = \eta_0(x), Q(0, x) = Q_0(x) \end{array} \right\},$$

and $\Omega = [0, T] \times \mathbb{R}$. Take $(\eta_0, Q_0) \in \mathcal{T}$ satisfying Conditions (3.3.3) and (3.3.4). Let $V = (\rho, P) \in X_T(M, a, b, r)$ and consider a linearized version of (3.3.9)-(3.3.10) as follows

$$\begin{cases} \partial_t \eta + Q_x - \beta \varepsilon Q_{xxx} = 0, \\ \partial_t (1 - \alpha \varepsilon \partial_x^2) Q + \varepsilon \frac{2P}{d + \varepsilon \rho} Q_x + \left(g(d + \varepsilon \rho) - \varepsilon^2 \frac{P^2}{(d + \varepsilon \rho)^2} \right) \eta_x = 0. \end{cases} \quad (3.3.11)$$

$$(3.3.12)$$

The initial value problem (3.3.11)-(3.3.12) with initial conditions $\eta(t, x) = \eta_0(x)$, $Q(0, x) = Q_0(x)$ defines a mapping

$$\begin{aligned} \mathcal{S} : X_T &\longrightarrow X_T \\ (\rho, P) &\longmapsto (\eta, Q). \end{aligned}$$

We want to show that there exists a time $T > 0$ and constants M, a, b and r such that \mathcal{S} maps the closed ball $X_T(M, a, b, r)$ into itself and \mathcal{S} is a contraction mapping under the constraint that it acts on $X_T(M, a, b, r)$ in the norm $\|\cdot\|_{T,0}$. We begin with the high order estimates on η and Q . Applying ∂_x on (3.3.11), we derive

$$\partial_t \eta_x + Q_{xx} - \beta \varepsilon Q_{xxxx} = 0. \quad (3.3.13)$$

The same procedure on (3.3.12) gives

$$\begin{aligned} \partial_t (1 - \alpha \varepsilon \partial_x^2) Q_x + \varepsilon \frac{2P}{d + \varepsilon \rho} Q_{xx} + \varepsilon \left(\frac{2P}{d + \varepsilon \rho} \right)_x Q_x \\ + \left(g(d + \varepsilon \rho) - \varepsilon^2 \frac{P^2}{(d + \varepsilon \rho)^2} \right) \eta_{xx} + \left(g(d + \varepsilon \rho) - \varepsilon^2 \frac{P^2}{(d + \varepsilon \rho)^2} \right)_x \eta_x = 0. \end{aligned} \quad (3.3.14)$$

Applying again ∂_x on Equations (3.3.13) and (3.3.14) we get

$$\partial_t \eta_{xx} + Q_{xxx} - \beta \varepsilon Q_{xxxxx} = 0, \quad (3.3.15)$$

$$\begin{aligned} \partial_t (1 - \alpha \varepsilon \partial_x^2) Q_{xx} + \varepsilon \frac{2P}{d + \varepsilon \rho} Q_{xxx} + 2\varepsilon \left(\frac{2P}{d + \varepsilon \rho} \right)_x Q_{xx} + \varepsilon \left(\frac{2P}{d + \varepsilon \rho} \right)_{xx} Q_x \\ + \left(g(d + \varepsilon \rho) - \varepsilon^2 \frac{P^2}{(d + \varepsilon \rho)^2} \right) \eta_{xxx} + 2 \left(g(d + \varepsilon \rho) - \varepsilon^2 \frac{P^2}{(d + \varepsilon \rho)^2} \right)_x \eta_{xx} \\ + \left(g(d + \varepsilon \rho) - \varepsilon^2 \frac{P^2}{(d + \varepsilon \rho)^2} \right)_{xx} \eta_x = 0. \end{aligned} \quad (3.3.16)$$

In order to cancel the fifth-order derivative terms in (3.3.15), we multiply Equation (3.3.15) by $\left(g(d + \varepsilon \rho) - \varepsilon^2 \frac{P^2}{(d + \varepsilon \rho)^2} \right) \eta_{xx}$ and Equation (3.3.16) by $Q_{xx} - \beta \varepsilon Q_{xxxx}$ and integrate the resulting equations over \mathbb{R} . For simplicity, we denote

$$s(\rho, P) = g(d + \varepsilon \rho) - \varepsilon^2 \frac{P^2}{(d + \varepsilon \rho)^2}.$$

We then obtain after integration by parts and cancellations

$$\begin{aligned}
& \frac{1}{2} \int_{\mathbb{R}} \left[\left(g(d + \varepsilon\rho) - \varepsilon^2 \frac{P^2}{(d + \varepsilon\rho)^2} \right) \partial_t(\eta_{xx}^2) + \partial_t \left(Q_{xx}^2 + \varepsilon(\beta + \alpha)Q_{xxx}^2 + \varepsilon^2 \alpha\beta Q_{xxxx}^2 \right) \right] dx \\
&= - \int_{\mathbb{R}} s(\rho, P) Q_{xxx} \eta_{xx} dx - \varepsilon \int_{\mathbb{R}} \left(\frac{2P}{d + \varepsilon\rho} \right) Q_{xxx} \left(Q_{xx} - \varepsilon\beta Q_{xxxx} \right) dx \\
&\quad - 2\varepsilon \int_{\mathbb{R}} \left(\frac{2P}{d + \varepsilon\rho} \right)_x Q_{xx} \left(Q_{xx} - \varepsilon\beta Q_{xxxx} \right) dx \\
&\quad - \varepsilon \int_{\mathbb{R}} \left(\frac{2P}{d + \varepsilon\rho} \right)_{xx} Q_x \left(Q_{xx} - \varepsilon\beta Q_{xxxx} \right) dx \\
&\quad - \int_{\mathbb{R}} s(\rho, P) \eta_{xxx} Q_{xx} dx - 2 \int_{\mathbb{R}} \left(s(\rho, P) \right)_x \eta_{xx} \left(Q_{xx} - \varepsilon\beta Q_{xxxx} \right) dx \\
&\quad - \int_{\mathbb{R}} \left(s(\rho, P) \right)_{xx} \eta_x \left(Q_{xx} - \varepsilon\beta Q_{xxxx} \right) dx - \varepsilon\beta \int_{\mathbb{R}} \left(s(\rho, P) \right)_x \eta_{xx} Q_{xxxx} dx. \tag{3.3.17}
\end{aligned}$$

Note that in (3.3.17), the terms

$$\int_{\mathbb{R}} s(\rho, P) Q_{xxx} \eta_{xx} dx, \text{ and } \int_{\mathbb{R}} s(\rho, P) \eta_{xxx} Q_{xx} dx$$

are not of order ε . Nevertheless, a direct integration by parts furnishes

$$\begin{aligned}
& \int_{\mathbb{R}} s(\rho, P) Q_{xxx} \eta_{xx} dx + \int_{\mathbb{R}} s(\rho, P) \eta_{xxx} Q_{xx} dx \\
&= - \int_{\mathbb{R}} \left(s(\rho, P) \right)_x Q_{xx} \eta_{xx} dx \\
&= -\varepsilon \int_{\mathbb{R}} \left(g\rho - \varepsilon \frac{P^2}{(d + \varepsilon\rho)^2} \right)_x Q_{xx} \eta_{xx} dx, \tag{3.3.18}
\end{aligned}$$

since

$$\left(s(\rho, P) \right)_x = \varepsilon \left(g\rho - \varepsilon \frac{P^2}{(d + \varepsilon\rho)^2} \right)_x.$$

Using (3.3.18), the Cauchy-Schwarz estimate, the continuous embedding $H^1(\mathbb{R}) \hookrightarrow L^\infty(\mathbb{R})$ and the fact that $(\rho, P) \in X_T(M, a, b, r)$, we get

$$\begin{aligned}
& \frac{1}{2} \int_{\mathbb{R}} \left[\left(g(d + \varepsilon\rho) - \varepsilon^2 \frac{P^2}{(d + \varepsilon\rho)^2} \right) \partial_t(\eta_{xx}^2) + \partial_t \left(Q_{xx}^2 + \varepsilon(\beta + \alpha)Q_{xxx}^2 + \varepsilon^2 \alpha\beta Q_{xxxx}^2 \right) \right] dx \\
&\leq \varepsilon C_0 \|\eta_{xx}\|_0 \|Q_{xx}\|_0 + \varepsilon C_1 \left(\|Q_x\|_0^2 + \|Q_{xx}\|_0^2 + \varepsilon \|Q_{xxx}\|_0^2 + \varepsilon^2 \|Q_{xxxx}\|_0^2 \right) \\
&\quad + \varepsilon C_2 \|\eta\|_2 \left(\|Q_{xx}\|_0 + \varepsilon \|Q_{xxxx}\|_0 \right), \tag{3.3.19}
\end{aligned}$$

where the constants C_0, C_1 and C_2 depends only on M, a, r, β . We now treat the non-standard term of Estimate (3.3.19), namely

$$\begin{aligned}
& \int_{\mathbb{R}} \left(g(d + \varepsilon\rho) - \varepsilon^2 \frac{P^2}{(d + \varepsilon\rho)^2} \right) \partial_t(\eta_{xx}^2) dx = \partial_t \int_{\mathbb{R}} \left(g(d + \varepsilon\rho) - \varepsilon^2 \frac{P^2}{(d + \varepsilon\rho)^2} \right) (\eta_{xx}^2) dx \\
&\quad - \int_{\mathbb{R}} \partial_t \left(\varepsilon g\rho - \varepsilon^2 \frac{P^2}{(d + \varepsilon\rho)^2} \right) \eta_{xx}^2 dx. \tag{3.3.20}
\end{aligned}$$

Since $(\rho, P) \in X_T(M, a, b, r)$, we deduce that

$$\left| \int_{\mathbb{R}} \left(g(d + \varepsilon\rho) - \varepsilon^2 \frac{P^2}{(d + \varepsilon\rho)^2} \right)_t (\eta_{xx}^2) dx \right| \leq \varepsilon C_3 \|\eta_{xx}\|_0^2, \quad (3.3.21)$$

where the constant C_3 depends only on M , a and r . Integrating inequality (3.3.19) from 0 to t we obtain, using (3.3.20) and (3.3.21)

$$\begin{aligned} & \int_{\mathbb{R}} \left[s(\rho, P) \eta_{xx}^2 + Q_{xx}^2 + \varepsilon(\beta + \alpha) Q_{xxx}^2 + \varepsilon^2 \alpha \beta Q_{xxxx}^2 \right] dx \\ & \leq \int_{\mathbb{R}} \left[s(\rho_0, Q_0) \eta_{0xx}^2 + Q_{0xx}^2 + \varepsilon(\beta + \alpha) Q_{0xxx}^2 + \varepsilon^2 \alpha \beta Q_{0xxxx}^2 \right] dx \\ & + \varepsilon \left(C_3 \int_0^t \|\eta_{xx}(s)\|_0^2 ds + C_0 \int_0^t \|\eta_{xx}(s)\|_0 \|Q_{xx}(s)\|_0 ds \right. \\ & + C_1 \int_0^t (\|Q_{xx}(s)\|_0^2 + \varepsilon \|Q_{xxx}(s)\|_0^2 + \varepsilon^2 \|Q_{xxxx}(s)\|_0^2) ds \\ & \left. + C_2 \int_0^t \|\eta(s)\|_2 (\|Q_{xx}(s)\|_0 + \varepsilon \|Q_{xxx}(s)\|_0) ds \right) \end{aligned} \quad (3.3.22)$$

Note that similar estimates can be obtained on Systems (3.3.11)-(3.3.12) and (3.3.13)-(3.3.14). Using the fact that

$$g(d + \varepsilon\rho) - \varepsilon^2 \frac{P^2}{(d + \varepsilon\rho)^2} \geq b,$$

and choosing M such that

$$\begin{aligned} M^2 & \geq \frac{2}{b} \int_{\mathbb{R}} \left[s(\eta_0, Q_0) \eta_{0xx}^2 + Q_{0xx}^2 + \varepsilon(\beta + \alpha) Q_{0xxx}^2 + \varepsilon^2 \alpha \beta Q_{0xxxx}^2 \right] dx \\ & + \frac{2}{b} \int_{\mathbb{R}} \left[s(\eta_0, Q_0) \eta_{0x}^2 + Q_{0x}^2 + \varepsilon(\beta + \alpha) Q_{0xx}^2 + \varepsilon^2 \alpha \beta Q_{0xxx}^2 \right] dx \\ & + \frac{2}{b} \int_{\mathbb{R}} \left[s(\eta_0, Q_0) \eta_0^2 + Q_0^2 + \varepsilon(\beta + \alpha) Q_{0x}^2 + \varepsilon^2 \alpha \beta Q_{0xx}^2 \right] dx \end{aligned}$$

we deduce from (3.3.22) and Gronwall's inequality that one can find a time $T = O(\frac{1}{\varepsilon})$ depending only on M , a , b and r such that

$$\|\eta\|_{T,2} \leq M, \quad \|Q\|_{T,4} \leq M \quad \text{on } [0, T]. \quad (3.3.23)$$

It remains to prove that the solution (η, Q) belongs to the ball $X_T(M, a, b, r)$. By (3.3.11), (3.3.12), (3.3.23) and using the fact that

$$\|\rho\|_{T,2} \leq M, \quad \|P\|_{T,4} \leq M \quad \text{on } [0, T],$$

we get directly

$$\|\eta_t\|_{T,1} \leq \|Q_x\|_{T,1} + \beta \varepsilon \|Q_{xxx}\|_{T,1} \leq C_4,$$

$$\begin{aligned}
\|Q_t\|_{T,1} &= \|(1 - \alpha\varepsilon\partial_x^2)^{-1}\left(\varepsilon\frac{2P}{d+\varepsilon\rho}Q_x + \left(g(d+\varepsilon\rho) - \varepsilon^2\frac{P^2}{(d+\varepsilon\rho)^2}\right)\eta_x\right)\|_{T,1} \\
&\leq \|\varepsilon\frac{2P}{d+\varepsilon\rho}Q_x + \left(g(d+\varepsilon\rho) - \varepsilon^2\frac{P^2}{(d+\varepsilon\rho)^2}\right)\eta_x\|_{T,1} \\
&\leq C_5,
\end{aligned}$$

where C_4 and C_5 depends only on M . Then choosing r such that $r \geq \max(C_4, C_5)$, we get

$$\|\eta_t\|_{T,1} \leq r, \quad \|Q_t\|_{T,1} \leq r.$$

Here we recall that (η_0, Q_0) satisfy Conditions (3.3.3) and (3.3.4). Then choosing $a > 0$ such that

$$d + \varepsilon\eta_0(x) \geq 2a \text{ on } \mathbb{R},$$

and writing

$$\eta(t, x) = \eta_0(x) + \int_0^t \partial_s \eta(s, x) ds,$$

leads to

$$\begin{aligned}
d + \varepsilon\eta(t, x) &= d + \varepsilon\eta_0(x) + \varepsilon \int_0^t \partial_s \eta(s, x) ds \\
&\geq 2a - \varepsilon C(r)T \\
&\geq a \text{ on } \Omega,
\end{aligned}$$

where the constant $C(r)$ depends only on r and for $T = O(\frac{1}{\varepsilon})$ small enough. The same argument provides, choosing $b > 0$ such that

$$g(d + \varepsilon\eta_0) - \varepsilon^2 \frac{Q_0^2}{(d + \varepsilon\eta_0)^2} \geq 2b \text{ on } \mathbb{R},$$

$$\begin{aligned}
g(d + \varepsilon\eta) - \varepsilon^2 \frac{Q^2}{(d + \varepsilon\eta)^2} &= g(d + \varepsilon\eta_0) - \varepsilon^2 \frac{Q_0^2}{(d + \varepsilon\eta_0)^2} \\
&\quad + \varepsilon \int_0^t \partial_s \left(g\eta - \varepsilon^2 \frac{Q^2}{(d + \varepsilon\eta)^2} \right) ds \\
&\geq 2b - \varepsilon C(M, a, r)T \\
&\geq b \text{ on } \Omega,
\end{aligned}$$

where the constant $C(M, a, r)$ depends only on M , a and r and for $T = O(\frac{1}{\varepsilon})$ small enough. This proves that $(\eta, Q) \in X_T(M, a, b, r)$. Hence \mathcal{S} maps the closed ball $X_T(M, a, b, r)$ into itself. We then prove that \mathcal{S} is a contracting mapping in the ball $X_T(M, a, b, r)$ endowed with the metric Y_T where

$$Y_T = \left\{ (\eta, Q) \in \left(C([0, T]; L^2(\mathbb{R}))\right)^2 / \|(\eta, Q)\|_{Y_T}^2 = \|\eta\|_{T,0}^2 + \|Q\|_{T,0}^2 < +\infty \right\}.$$

Let $(\rho_1, P_1) \in X_T(M, a, b, r)$, $(\rho_2, P_2) \in X_T(M, a, b, r)$ and put $(\eta_1, Q_1) = \mathcal{S}(\rho_1, P_1)$, $(\eta_2, Q_2) = \mathcal{S}(\rho_2, P_2)$ the corresponding solutions to Equations (3.3.11)-(3.3.12) with the same initial conditions. The equations satisfied by $\lambda = \eta_1 - \eta_2$ and $R = Q_1 - Q_2$ read

$$\partial_t \lambda + R_x - \beta \varepsilon R_{xxx} = 0, \quad (3.3.24)$$

$$\begin{aligned} & \partial_t (1 - \alpha \varepsilon \partial_x^2) R + \varepsilon \left(\frac{2P_1}{d + \varepsilon \rho_1} - \frac{2P_2}{d + \varepsilon \rho_2} \right) (Q_2)_x + \varepsilon \frac{2P_1}{d + \varepsilon \rho_1} R_x \\ & + \varepsilon \left(g(\rho_1 - \rho_2) - \varepsilon \frac{P_1^2}{(d + \varepsilon \rho_1)^2} + \varepsilon \frac{P_2^2}{(d + \varepsilon \rho_2)^2} \right) (\eta_2)_x + \left(g(d + \varepsilon \rho_1) - \varepsilon^2 \frac{P_1^2}{(d + \varepsilon \rho_1)^2} \right) \lambda_x = 0. \end{aligned} \quad (3.3.25)$$

Since all the nonlinear terms in Equation (3.3.25) are of class C^1 with respect to their arguments, we deduce directly that there exists a constant $C(M, a, b, r)$ such that

$$||(\eta_1, Q_1) - (\eta_2, Q_2)||_{Y_T} \leq C(M, a, b, r) \varepsilon T ||(\rho_1, P_1) - (\rho_2, P_2)||_{Y_T},$$

proving the desired result for $T = O(\frac{1}{\varepsilon})$ small enough. Moreover, the ball $X_T(M, a, b, r)$, endowed with the metric of Y_T is closed. By the contraction mapping principle, there exists a unique solution (η, Q) to (3.3.5)-(3.3.8) defined on $[0, T]$ satisfying

$$\eta \in C([0, T]; L^2(\mathbb{R})) \cap L^\infty(0, T; H^2(\mathbb{R})),$$

$$Q \in C([0, T]; L^2(\mathbb{R})) \cap L^\infty(0, T; H^4(\mathbb{R})),$$

which ends the proof of Theorem 1. \square

3.4 Solitary waves solutions for Boussinesq systems

In this section, we prove the existence and uniqueness of solitary waves for Equations (3.2.1) (Beji-Nadaoka), Equations (3.2.3) (Madsen-Sørensen) and for Equations (3.2.2) (Nwogu) assuming that the bathymetry d is constant. Note that we are not able to handle the Nwogu-Abbott system (3.2.4). Nevertheless in Section 3.4.4, we propose some insights for this problem.

The results obtained here are summed up in the following theorem :

Theorem 2. *We recall that $c_0 = \sqrt{gd}$ and consider the three following set of equations.*

1) Beji-Nadaoka equations.

We define $\gamma = \alpha_B + 1/3$ and assume that one of the following alternative is satisfied :

i) $\gamma = 0$, $c > c_0$,

ii) $\alpha_B < 0$, $\gamma > 0$, $c > c_0$,

iii) $\alpha_B > 0$, $\gamma > 0$, $c \in (c_0, c_0 \frac{2 - \alpha_B}{\sqrt{\frac{\alpha_B}{\gamma}}})$.

Then Equations (3.2.1) admit a unique solitary wave of the form $(\eta_c(x - ct), u_c(x - ct))$. Furthermore, the relation between parameter c and the amplitude A of η_c is given by

$$c^4 \gamma \left[\frac{A^3}{6(d+A)^3} - \frac{A^2}{2(d+A)^2} \right] + c^2 c_0^2 \left[\gamma \log\left(\frac{A+d}{d}\right) - \gamma \frac{A}{d+A} + \frac{\alpha_B}{2} \frac{A^2}{d(d+A)} \right] - c_0^4 \frac{\alpha_B A^2}{2d^2} = 0. \quad (3.4.1)$$

Conversely, if $\gamma < 0$, $\alpha_B < 0$ and $c \geq 0$, then Equations (3.2.1) have no positive solutions of the previous form.

2) Madsen-Sørensen equations.

For all $c > c_0$, Equations (3.2.3) admit a unique solitary wave of the form $(\eta_c(x - ct), q_c(x - ct))$. In addition, the relation between parameter c and the amplitude A of η_c is given by

$$c^2 = c_0^2 \frac{\frac{A^2}{2} + \frac{A^3}{6d}}{dA - d^2 \log\left(\frac{d+A}{d}\right)}. \quad (3.4.2)$$

Conversely, if $c \leq c_0$, then Equations (3.2.3) have no positive solutions of the previous form.

3) Nwogu equations.

Assume that one of the following alternative is satisfied :

i) $\alpha \in (-\frac{1}{2}, -\frac{1}{9})$ and $c > c_0$,

ii) $\alpha \in (-\frac{1}{9}, 0)$ and $c > c_0 \sqrt{\frac{\frac{\beta^2}{\alpha^2}}{2 - \frac{\beta}{\alpha}}}$.

Then Equations (3.2.2) admit a unique solitary wave of the form $(\eta_c(x - ct), u_c(x - ct))$. The amplitude U of u_c and parameter c satisfy

$$\begin{aligned} \frac{1}{6} U^3 - \left(\frac{c}{2} + \frac{\beta c_0^2}{4c\alpha} \right) U^2 + c_0^2 \left(\frac{c}{3} + \frac{\beta}{2c\alpha} (\beta c_0^2 - \alpha c^2) \right) \frac{U}{c\alpha}, \\ - \frac{c_0^2 (\beta c_0^2 - \alpha c^2)}{c^2 \alpha^2} \left(\frac{c}{3} + \frac{\beta}{2c\alpha} (\beta c_0^2 - \alpha c^2) \right) \log\left(1 + \frac{c\alpha}{\beta c_0^2 - \alpha c^2} U\right) = 0. \end{aligned} \quad (3.4.3)$$

Conversely, if $c \leq c_0$, then Equations (3.2.2) have no positive solutions of the previous form.

4) Nwogu-Abbott equations.

For all $c \leq c_0$, Equations (3.2.4) have no positive solutions $(\eta_c(x - ct), q_c(x - ct))$. In addition, when $c > c_0$, we conjecture that there exists positive solution of Nwogu-Abbott Equations. In this direction, we present some numerical computations.

Finally, in cases 1), 2) and 3), the solitary waves decay exponentially at infinity in the sense of Theorem 3.

Remark 1. Considering the Nwogu system in the case $\alpha \in (-\frac{1}{9}, 0)$ ($\theta \in (-1 + \sqrt{7}/3, 0)$), and $c_0 < c \leq c_0 \sqrt{\frac{\beta^2}{\frac{\alpha^2}{2-\beta}}}$, we are not able to conclude concerning the existence and uniqueness of a solitary wave. See the end of Section 3.4.3 for more informations.

To start, we recall that a solitary wave is a global solution of the generic form $u(t, x) = u_c(x - ct)$ where c is the celerity of the wave and u_c is a profile independent of the time t satisfying the two conditions

$$\lim_{x \rightarrow \pm\infty} u_c(x) = 0, \quad u_c(x_0) > 0 \text{ for some } x_0 \in \mathbb{R}. \quad (3.4.4)$$

Plugging this relation into the previous Boussinesq equations leads to stationary equations. We present the details for each equations in the next sections. Note that, we also give the relation between the celerity and the amplitude of the solitary wave. To our knowledge, this relation has never been presented in literature for Boussinesq system and appears to be essential in view of performing effective numerical computations.

We recall now the classical theorem by H. Berestycki and P.-L.Lions (see [15]), which gives a necessary and sufficient condition for the existence and uniqueness of a positive solution to the stationary equation of the type $-u'' = g(u)$.

Theorem 3. *Let g be a locally Lipschitz continuous real function with $g(0) = 0$. Let $G(z) = \int_0^z g(s)ds$. Consider the problem*

$$-u'' = g(u), \quad u \in C^2(\mathbb{R}), \quad (3.4.5)$$

$$\lim_{x \rightarrow \pm\infty} u(x) = 0, \quad u(x_0) > 0 \text{ for some } x_0 \in \mathbb{R}.$$

There is a unique positive solution $u \in H^1(\mathbb{R}) \cap C^2(\mathbb{R})$ up to translations to problem (3.4.5) if and only if

$$\xi_0 = \inf\{\xi > 0, G(\xi) = 0\} \text{ exists, and satisfies } \xi_0 > 0, g(\xi_0) > 0. \quad (3.4.6)$$

In addition, if one assumes that

$$\lim_{s \rightarrow 0} \frac{g(s)}{s} \leq -m < 0,$$

then u, u', u'' decay exponentially at infinity, that is there exists $C, \delta > 0$, such that for $n = 0, 1, 2$,

$$|\partial_x^n u(x)| \leq C \exp(-\delta|x|), \quad x \in \mathbb{R}.$$

Remark 2. Under the assumptions of Theorem 3, the solution u of (3.4.5) can be obtained as the solution of the initial value problem

$$\begin{cases} -u'' = g(u), \\ u(0) = \xi_0, \quad u'(0) = 0. \end{cases}$$

Furthermore, this solution satisfies

- (i) $u(x) = u(-x)$, $x \in \mathbb{R}$,
- (ii) $u'(x) < 0$, $x \in \mathbb{R}^+$,
- (iii) $0 < u(x) \leq \xi_0$, $x \in \mathbb{R}$.

3.4.1 Solitary waves solutions for the Beji-Nadaoka equations

We recall the Beji-Nadaoka equations (3.2.1) with constant bathymetry. We assume that $\alpha_B \in \mathbb{R}$ and define $\gamma = \alpha_B + 1/3$

$$\begin{cases} \eta_t + [h\bar{u}]_x = 0 \\ \bar{u}_t + g\eta_x + \bar{u}\bar{u}_x - \gamma d^2\bar{u}_{txx} - \alpha_B gd^2\eta_{xxx} = 0. \end{cases} \quad (3.4.7)$$

$$(3.4.8)$$

We look for solitary waves under the form

$$\begin{cases} \eta(t, x) = \eta_c(x - ct), \\ \bar{u}(t, x) = u_c(x - ct), \end{cases}$$

where η_c, u_c are profile in $H^1(\mathbb{R})$. A direct computation shows that the system satisfied by η_c, u_c can be written, after one integration,

$$\begin{cases} \eta_c = \frac{du_c}{c - u_c}, \\ -cu_c + g\eta_c + \frac{u_c^2}{2} + c\gamma d^2 u_c'' - \alpha_B gd^2 \eta_c'' = 0. \end{cases} \quad (3.4.9)$$

$$(3.4.10)$$

Remark 3. From Equation (3.4.9), we obtain

$$u_c = c \frac{\eta_c}{d + \eta_c}, \quad (3.4.11)$$

since $d \geq 0$, we deduce that

$$u_c < c,$$

In Equation (3.4.10), it is obvious that parameter γ plays a crucial role and we discuss now the existence of a solution of System (3.4.9)-(3.4.10) considering successively the case $\gamma = 0$ and $\gamma \neq 0$.

Case 1 : $\gamma = 0$.

The Beji-Nadaoka system (3.4.9)-(3.4.10) reduces to

$$\begin{cases} u_c = \frac{c\eta_c}{d + \eta_c}, \\ -cu_c + g\eta_c + \frac{u_c^2}{2} + \frac{gd^2}{3}\eta_c'' = 0, \end{cases}$$

from which we deduce by substitution the following autonomous ODE on η_c

$$-\frac{gd^2}{3}\eta_c'' = -c^2 \frac{\eta_c}{d + \eta_c} + g\eta_c + \frac{c^2\eta_c^2}{2(d + \eta_c)^2},$$

which can be rewritten, after simplifications, as

$$-\eta_c'' = \frac{3}{gd^2} \left(\frac{c^2 d^2}{2(d + \eta_c)^2} - \frac{c^2}{2} + c_0^2 \frac{\eta_c}{d} \right). \quad (3.4.12)$$

Introducing the function g defined as

$$g(s) = \frac{3}{gd^2} \left(\frac{c^2 d^2}{2(d+s)^2} - \frac{c^2}{2} + c_0^2 \frac{s}{d} \right),$$

it is obvious that Equation (3.4.12) can be put under the form (3.4.5) of Theorem 3. A direct integration provides

$$G(s) := \int_0^s g(t) dt = \frac{3}{gd^2} \left(\frac{c^2 d}{2} - \frac{c^2 d^2}{2(d+s)} - \frac{c^2}{2}s + c_0^2 \frac{s^2}{2d} \right).$$

In order to apply Theorem 3, we give the behavior of functions g and G for $s \geq 0$.

Firstly, we remark that $g(0) = G(0) = 0$. Moreover it is easy to prove that

$$g(s) = 0 \iff (s = 0 \text{ or } s = s_1 \text{ or } s = s_2),$$

where

$$s_1 := d \frac{\left(\frac{c^2}{c_0^2} - 4\right) - \sqrt{8\frac{c^2}{c_0^2} + \frac{c^4}{c_0^4}}}{4}, \quad s_2 := d \frac{\left(\frac{c^2}{c_0^2} - 4\right) + \sqrt{8\frac{c^2}{c_0^2} + \frac{c^4}{c_0^4}}}{4}.$$

Clearly $s_1 < 0$ for all value of c . Hence we concentrate on s_2 . We can distinguish two cases :

- For $c \leq c_0$, $s_2 \leq 0$, then g is positive on \mathbb{R}_+^* . Theorem 3 ensures that Equation (3.4.12) has no solution under the expected form.
- For $c > c_0$, $s_2 > 0$ and g is negative on $(0, s_2)$ and positive on $(s_2, +\infty)$. From $G(0) = 0$, it is clear that $G(s_2) < 0$. In addition, since $\lim_{s \rightarrow +\infty} G(s) = +\infty$, G has a unique zero s_3 in $(s_2, +\infty)$ such as $g(s_3) > 0$. Applying Theorem 3, we deduce that Equation (3.4.12) admits a unique positive solution $\eta_c \in H^1(\mathbb{R})$. Introducing

$$u_c = \frac{c\eta_c}{d + \eta_c},$$

it is clear that (u_c, η_c) is the unique solution to (3.4.9)-(3.4.10). Moreover, denoting by A the amplitude of the solution η_c and recalling that necessarily $A = s_3$ (see Remark 2), which means that $G(A) = 0$, we deduce the relation satisfied by A and c :

$$c^2 = c_0^2 \frac{d + A}{d}.$$

Finally, we prove that solutions η_c and u_c have exponential decay at infinity, studying the following limit for $c > c_0$ (which corresponds to the solitary waves existence condition for these equations)

$$\frac{g(s)}{s} = \frac{3}{gd^2} \left(\frac{-2c^2 d - c^2 s}{2(d+s)^2} + \frac{c_0^2}{d} \right) \longrightarrow \frac{3}{gd^3} (c_0^2 - c^2) < 0, \text{ when } s \rightarrow 0.$$

From Theorem 3, we deduce that η_c decays exponentially at infinity and that $\eta_c(x) > 0$, $\forall x \in \mathbb{R}$. Furthermore, this result leads to the exponential decay of u_c , $\forall x \in \mathbb{R}$

$$\begin{aligned} |u_c(x)| &= \left| \frac{c\eta_c(x)}{d + \eta_c(x)} \right| \leq \left| \frac{c}{d} \eta_c(x) \right| \leq K_1 \exp(-\delta|x|), \\ |u'_c(x)| &= \left| \frac{cd\eta'_c(x)}{(d + \eta_c(x))^2} \right| \leq K_2 \exp(-\delta|x|), \\ |u''_c(x)| &= \left| \frac{cd\eta'_c(x)^2}{(d + \eta_c(x))^3} + \frac{cd|\eta''_c(x)|}{(d + \eta_c(x))^2} \right| \leq K_3 \exp(-\delta|x|), \end{aligned}$$

where K_1 , K_2 , K_3 are positive constants.

Case 2 : $\gamma \neq 0$.

In this case, Equation (3.4.9) provides that

$$\eta''_c = cd\left(\frac{u''_c}{(c - u_c)^2} + \frac{2u'^2_c}{(c - u_c)^3}\right),$$

which gives by Equation (3.4.10)

$$\begin{aligned} (c\gamma d^2(c - u_c)^2 - \alpha_B d^2 c c_0^2) u''_c - \frac{2cc_0^2 \alpha_B d^2}{(c - u_c)} u'^2_c - cu_c(c - u_c)^2 \\ + c_0^2 u_c(c - u_c) + \frac{u_c^2(c - u_c)^2}{2} = 0. \end{aligned} \quad (3.4.13)$$

Since Equation (3.4.13) is a quasilinear elliptic equation, we perform a change of variable to transform (3.4.13) into a semilinear one (see [30, 31]). More precisely, let us define $u_c = f(v_c)$ where $f : \mathbb{R}_+ \rightarrow \mathbb{R}$ will be determined later on. One has

$$u'_c = v'_c f'(v_c),$$

and

$$u''_c = v''_c f'(v_c) + v'^2_c f''(v_c).$$

Performing this change of functions into (3.4.13) leads to

$$\begin{aligned} (c\gamma d^2(c - u_c)^2 - \alpha_B d^2 c c_0^2) u''_c - \frac{2cc_0^2 \alpha_B d^2}{(c - u_c)} u'^2_c = (c\gamma d^2(c - u_c)^2 - \alpha_B d^2 c c_0^2) f'(v_c) v''_c \\ + \left((c\gamma d^2(c - f(v_c))^2 - \alpha_B d^2 c c_0^2) f''(v_c) - \frac{2cc_0^2 \alpha_B d^2}{(c - f(v_c))} f'(v_c)^2 \right) v'^2_c. \end{aligned}$$

We choose $f(s)$ satisfying the following ODE in order to eliminate the quasilinear terms in v'^2_c ,

$$((c - f(s))^2 - \frac{\alpha_B}{\gamma} c_0^2) f''(s) - \frac{2c_0^2 \alpha_B}{\gamma(c - f(s))} f'(s)^2 = 0. \quad (3.4.14)$$

Assuming that $f'(s) \neq 0$, then (3.4.14) can be rewritten into

$$\frac{f''(s)}{f'(s)} = \frac{2c_0^2 \alpha_B}{\gamma(c - f(s))((c - f(s))^2 - \frac{\alpha_B}{\gamma} c_0^2)} f'(s),$$

or equivalently

$$\frac{f''(s)}{f'(s)} = -\frac{2f'(s)}{(c-f(s))} + \frac{2(c-f(s))f'(s)}{((c-f(s))^2 - \frac{\alpha_B}{\gamma}c_0^2)}.$$

After integrations, we obtain successively, taking $f(0) = 0$,

$$f'(s) = \frac{(c-f(s))^2}{(c-f(s))^2 - c_0^2 \frac{\alpha_B}{\gamma}}, \quad (3.4.15)$$

$$s = f(s) - \frac{c_0^2 \alpha_B}{\gamma(c-f(s))} + \frac{c_0^2 \alpha_B}{c\gamma}. \quad (3.4.16)$$

We expect f to be a diffeomorphism on an interval of \mathbb{R}_+ containing 0. Let us compute

$$(f^{-1})'(t) = \frac{1}{f'(f^{-1}(t))} = 1 - \frac{c_0^2 \alpha_B}{\gamma(c-t)^2}.$$

We deduce that :

- if $\alpha_B \gamma > 0$ and $c^2 > c_0^2 \frac{\alpha_B}{\gamma}$, then $(f^{-1})'(t) > 0$ on $[0, c - c_0 \sqrt{\frac{\alpha_B}{\gamma}}]$, which implies that f is a diffeomorphism from $[0, c(1 - \frac{c_0}{c} \sqrt{\frac{\alpha_B}{\gamma}})^2]$ to $[0, c - c_0 \sqrt{\frac{\alpha_B}{\gamma}}]$,
- If $\alpha_B \gamma < 0$, then $(f^{-1})'(t) > 0$ on $[0, c)$ which implies that f is a diffeomorphism from $[0, +\infty)$ to $[0, c)$.

In the sequel, we assume that $c^2 > c_0^2 \frac{\alpha_B}{\gamma}$. Performing the change of variable $u_c = f(v_c)$ in Equation (3.4.13), we obtain the following ODE of the form (3.4.5) on the new variable v_c

$$-v_c'' = \frac{1}{c\gamma d^2} \left(-cf(v_c) + \frac{cc_0^2}{c-f(v_c)} - c_0^2 + \frac{f(v_c)^2}{2} \right). \quad (3.4.17)$$

We introduce the function g as

$$g(s) = \frac{1}{c\gamma d^2} \left(-cf(s) + \frac{cc_0^2}{c-f(s)} - c_0^2 + \frac{f(s)^2}{2} \right),$$

and compute its primitive G , using the change of variable $t = f(x)$ and the relation (3.4.15),

$$\begin{aligned} G(s) &= \int_0^s g(t) dt \\ &= \frac{1}{c\gamma d^2} \left(\frac{f(s)^3}{6} - \frac{c}{2}f(s)^2 - c_0^2 f(s) - c_0^2 \frac{\alpha_B}{2\gamma} f(s) - cc_0^2 \log\left(\frac{c-f(s)}{c}\right) \right. \\ &\quad \left. + \frac{c_0^2 \alpha_B}{2\gamma} \frac{c^2}{c-f(s)} + \frac{c_0^2 \alpha_B}{\gamma} \frac{c_0^2}{c-f(s)} - \frac{c_0^4 \alpha_B}{2\gamma} \frac{c}{(c-f(s))^2} - \frac{cc_0^2 \alpha_B}{2\gamma} - \frac{c_0^4 \alpha_B}{2\gamma c} \right). \end{aligned}$$

We want to show that the function G has a unique zero on $(0, c)$, for suitable values of c . For convenience, we define $t = f(s)$ and introduce h a function of t :

$$h(t) = g(s) = \frac{1}{c\gamma d^2} \left(-ct + \frac{cc_0^2}{c-t} - c_0^2 + \frac{t^2}{2} \right),$$

and we compute its primitive H

$$H(t) = G(s).$$

As f is a diffeomorphism, equation $g(s) = 0$ is equivalent to $h(t) = 0$, which allows us to concentrate on h . Computations lead to

$$h(t) = 0 \Leftrightarrow t = 0 \text{ or } -\frac{t^2}{2} + \frac{3c}{2}t + (c_0^2 - c^2) = 0.$$

It implies that h has 3 zeros in $\mathbb{R} \setminus \{c\}$, $\forall \alpha_B \in \mathbb{R} \setminus \{-\frac{1}{3}\}$,

$$t_0 = 0, \quad t_1 = c \frac{3 - \sqrt{1 + 8\frac{c_0^2}{c^2}}}{2}, \quad t_2 = c \frac{3 + \sqrt{1 + 8\frac{c_0^2}{c^2}}}{2}.$$

We first remark that for any $c \in \mathbb{R}^+$, $t_2 > c$. As we search zero satisfying $t < c$ (see remark 3), t_2 doesn't play any role in our analysis. Since our method depends on the properties of f , we have to separate the case $\alpha_B \gamma > 0$ from the case $\alpha_B \gamma < 0$.

- case 1 : $\alpha_B \gamma > 0$. We recall that in this case f is a diffeomorphism from $[0, c(1 - \frac{c_0}{c} \sqrt{\frac{\alpha_B}{\gamma}})^2)$ to $[0, c - c_0 \sqrt{\frac{\alpha_B}{\gamma}})$. A direct computations shows that

$$t_1 \in (0, c - c_0 \sqrt{\frac{\alpha_B}{\gamma}}) \iff c \in (c_0, c_0 \frac{2 - \frac{\alpha_B}{\gamma}}{\sqrt{\frac{\alpha_B}{\gamma}}})$$

As a consequence, if $c \notin (c_0, c_0 \frac{2 - \frac{\alpha_B}{\gamma}}{\sqrt{\frac{\alpha_B}{\gamma}}})$, $g(s) \geq 0$ for all $s \in [0, c(1 - \frac{c_0}{c} \sqrt{\frac{\alpha_B}{\gamma}})^2)$, from which we deduce that G is increasing. By Theorem 3, we deduce that Equation (3.4.13) does not admit any solution in this case.

Conversely, if $c \in (c_0, c_0 \frac{2 - \frac{\alpha_B}{\gamma}}{\sqrt{\frac{\alpha_B}{\gamma}}})$, $t_1 \in (0, c - c_0 \sqrt{\frac{\alpha_B}{\gamma}})$, then $f^{-1}(t_1) \in [0, c(1 - \frac{c_0}{c} \sqrt{\frac{\alpha_B}{\gamma}})^2)$. Thus if $\gamma > 0$ (resp. $\gamma < 0$), then G decreases (resp. increases) on $(0, f^{-1}(t_1)]$ and increases (resp. decreases) on $[f^{-1}(t_1), c(1 - \frac{c_0}{c} \sqrt{\frac{\alpha_B}{\gamma}})^2)$. Starting from $G(0) = 0$, one has $G(f^{-1}(t_1)) < 0$ (resp. $G(f^{-1}(t_1)) > 0$). Since

$$\lim_{s \rightarrow c(1 - \frac{c_0}{c} \sqrt{\frac{\alpha_B}{\gamma}})^2} G(s) = \lim_{t \rightarrow c - c_0 \sqrt{\frac{\alpha_B}{\gamma}}} H(t) = +\infty \text{ (resp. } -\infty\text{)},$$

we deduce, by the mean-value Theorem, that G admits a unique zero $s_m \in (f^{-1}(t_1), c(1 - \frac{c_0}{c} \sqrt{\frac{\alpha_B}{\gamma}})^2)$, proving that $g(s_m) > 0$ (resp. $g(s_m) < 0$). Applying Theorem 3, it is clear that Equation (3.4.13) admits a unique positive solution satisfying (3.4.4) only if $\gamma > 0$ and $\alpha_B > 0$ when $c \in (c_0, c_0 \frac{2 - \frac{\alpha_B}{\gamma}}{\sqrt{\frac{\alpha_B}{\gamma}}})$ and we conclude that Equations (3.4.9)-(3.4.10) admit a unique positive solution as in the case $\gamma = 0$.

- case 2 : $\alpha_B \gamma < 0$. In this case, since $\gamma = \alpha_B + \frac{1}{3}$, one has necessarily $\gamma > 0$ and $\alpha_B < 0$.

If $c \leq c_0$, then $t_1 \leq 0$ which implies that g is negative in $(0, +\infty)$ and G is increasing on $(0, +\infty)$ showing that Equation (3.4.17) has no solution in the expected form.

If $c > c_0$, t_1 is the only zero in $(0, c)$ of function h , then G decreases on $[0, f^{-1}(t_1)]$ and increases on $[f^{-1}(t_1), +\infty)$. Since $G(0) = 0$, one has $G(f^{-1}(t_1)) < 0$. Moreover, using the following limit $\lim_{s \rightarrow +\infty} G(s) = \lim_{t \rightarrow c} H(t) = +\infty$, and applying the mean-value Theorem, one proves that G has a unique zero $s_m \in (f^{-1}(t_1), +\infty)$ with $g(s_m) > 0$. We conclude that Equation (3.4.9)-(3.4.10) admit a unique positive solution.

We are now ready to give the relation between the amplitude A of η_c and the propagation velocity c . Indeed, by Theorem 3, using (3.4.11), we deduce that the quantity

$$f^{-1}\left(\frac{cA}{A+d}\right)$$

is a zero of the function G . It leads to the following relation

$$c^4 \left[\frac{A^3}{6(d+A)^3} - \frac{A^2}{2(d+A)^2} \right] + c^2 c_0^2 \left[\log\left(\frac{A+d}{d}\right) - \frac{A}{d+A} + \frac{\alpha_B}{2\gamma} \frac{A^2}{d(d+A)} \right] - c_0^4 \frac{\alpha_B A^2}{2\gamma d^2} = 0. \quad (3.4.18)$$

To conclude, we study the solutions have exponential decay at infinity. We recall that $c^2 > c_0^2 \frac{\alpha_B}{\gamma}$, $0 < v_c \leq s_m$, and that $s_m < c(1 - \frac{c_0}{c} \sqrt{\frac{\alpha_B}{\gamma}})^2$ if $\alpha_B \gamma > 0$. Since $t \rightarrow 0$ when $s \rightarrow 0$, we deduce

$$\begin{aligned} \frac{g(s)}{s} &= \frac{h(t)}{f^{-1}(t)} = \frac{1}{c\gamma d^2} \left(\frac{c_0^2 - c^2 - t^2/2}{-ct + c^2 - c_0^2 \frac{\alpha_B}{\gamma}} \right), \\ &\xrightarrow[s \rightarrow 0]{} \frac{1}{c\gamma d^2} \left(\frac{c_0^2 - c^2}{c^2 - c_0^2 \frac{\alpha_B}{\gamma}} \right) < 0. \end{aligned}$$

Applying Theorem 3, one can show that v_c decays exponentially at infinity. Coming back to $u_c = f(v_c)$, we observe, since f is increasing, that

$$0 < u_c(x) \leq f(s_m) < \min(c - c_0 \sqrt{\frac{\alpha_B}{\gamma}}, c),$$

$$|f'(v_c)| = \left| \frac{(c - f(v_c))^2}{(c - f(v_c))^2 - c_0^2 \frac{\alpha_B}{\gamma}} \right| \leq M_1,$$

where $M_1 \in \mathbb{R}_+^*$. In the same way, we can show that there exists $M_2 \in \mathbb{R}_+^*$ such that

$$|f''(s)| = \left| \frac{2c_0^2 \alpha_B}{\gamma((c-f(s))^2 - \frac{\alpha_B}{\gamma} c_0^2)(c-f(s))} f'(s)^2 \right| \leq M_2.$$

Applying the finite-increments Theorem on f , we deduce

$$|u_c(x)| = |f(v_c(x)) - f(0)| \leq M_1 |v_c(x)| \leq C_1 \exp(-\delta|x|),$$

with $C_1 \in \mathbb{R}_*^+$.

In addition,

$$|u'_c(x)| = |v'_c(x)f'(v_c(x))| \leq M_1|v'_c(x)| \leq C_2 \exp(-\delta|x|),$$

$$\begin{aligned} |u''_c(x)| &\leq |v''_c(x)f'(v_c(x))| + |v'_c(x)^2f''(v_c(x))| \\ &\leq M_1|v''_c(x)| + M_2|v'_c(x)|^2 \\ &\leq C_3 \exp(-\delta|x|), \end{aligned}$$

where $C_2, C_3 \in \mathbb{R}_*^+$. Recalling that

$$\eta_c = \frac{du_c}{c - u_c}, \quad u_c(x) \leq f(s_m) < c.$$

one has

$$\eta_c \leq \frac{d}{c - f(s_m)} u_c(x) \leq K_1 \exp(-\delta|x|).$$

In the same way,

$$|\eta'_c| \leq \frac{dc}{(c - f(s_m))^2} |u'_c(x)| \leq K_2 \exp(-\delta|x|),$$

$$|\eta''_c| \leq \frac{dc}{(c - f(s_m))^2} |u''_c(x)| + \frac{2dc}{(c - f(s_m))^3} |u'_c(x)|^2 \leq K_3 \exp(-\delta|x|),$$

where K_1, K_2, K_3 are positive constants which ends the proof of Theorem 2, case 1.

To illustrate the use of the relation (3.4.1), we give an example of a solitary wave solution to the Beji-Nadaoka equations on Figure 3.1. We have computed a solitary wave using a Runge-Kutta Strongly-Stability Preserving method with an initial amplitude equal to 0.2 for $\alpha_B = 1/15$. Computations lead to the following value : $c \approx 3.42$ and $u_c(0) \approx 0.570$.

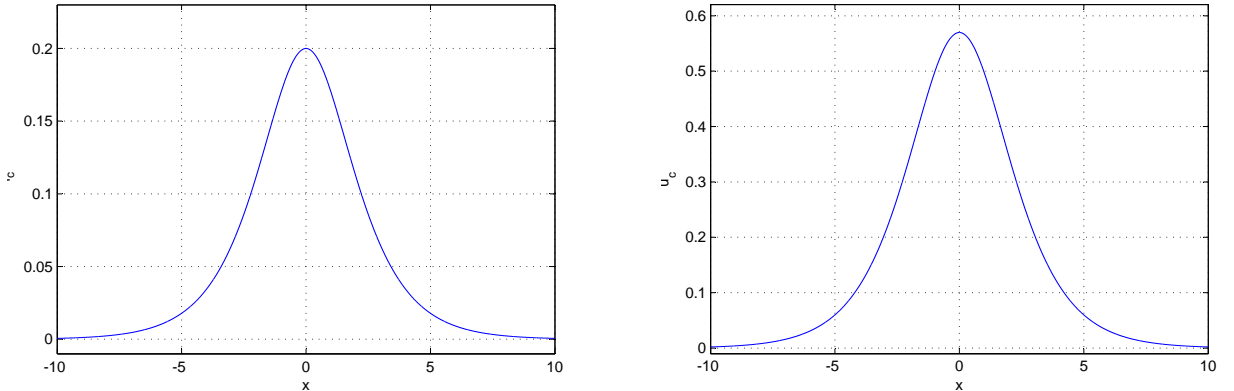


Figure 3.1 – Solitary waves for Beji-Nadaoka equations (η_c is on the left and u_c on the right), with $d = 1$, $\eta_c^0 = 0.2$ and $\alpha_B = 1/15$.

3.4.2 Solitary waves solutions for Madsen-Sørensen equations

We recall the Madsen-Sørensen equations, with a constant bathymetry d ,

$$\begin{cases} \eta_t + \bar{q}_x = 0, \\ \bar{q}_t + gh\eta_x + \left(\frac{\bar{q}^2}{h}\right)_x - Bd^2\bar{q}_{txx} - \beta gd^3\eta_{xxx} = 0, \end{cases} \quad \begin{aligned} (3.4.19) \\ (3.4.20) \end{aligned}$$

where $B = \beta + 1/3$, $\beta \in \mathbb{R}$. We look for solitary waves under the form

$$\begin{cases} \eta(t, x) = \eta_c(x - ct) \\ \bar{q}(t, x) = q_c(x - ct), \end{cases}$$

where the profiles η_c, q_c are in $H^1(\mathbb{R})$. Plugging these relations into System (3.4.19)-(3.4.20), we obtain, after one integration, the following set of equations

$$\begin{cases} q_c = c\eta_c, \\ -cq_c + c_0^2\eta_c + \frac{g}{2}\eta_c^2 + \left(\frac{q_c^2}{h}\right) + cBd^2q_c'' - \beta gd^3\eta_c'' = 0. \end{cases} \quad \begin{aligned} (3.4.21) \\ (3.4.22) \end{aligned}$$

Plugging (3.4.21) into (3.4.22), one obtains the following ODE satisfied by η_c

$$-c^2\eta_c + c_0^2\eta_c + \frac{g}{2}\eta_c^2 + c^2 \frac{\eta_c^2}{d + \eta_c} + d^2(c^2B - \beta c_0^2)\eta_c'' = 0,$$

which can be rewritten into

$$-\eta'' = \frac{1}{K} \left(-c^2\eta + c_0^2\eta + \frac{c_0^2}{2d}\eta^2 + c^2 \frac{\eta^2}{d + \eta} \right), \quad (3.4.23)$$

where $K = d^2(c^2B - \beta c_0^2)$ and assuming $c^2 \neq \frac{\beta}{B}c_0^2$.

Remark 4. Note that when $K = 0$, there are not non trivial solitary wave solutions of Madsen-Sørensen equations.

Following Theorem 3, we define the function g and its primitive G

$$g(s) = \frac{1}{K} \left(-c^2s + c_0^2s + \frac{c_0^2}{2d}s^2 + c^2 \frac{s^2}{d + s} \right),$$

$$G(s) := \int_0^s g(t) dt = \frac{1}{K} \left(-c^2ds + c_0^2 \frac{s^2}{2} + \frac{c_0^2}{6d}s^3 + c^2d^2 \log\left(\frac{d+s}{d}\right) \right),$$

and we investigate the behavior of G for all value of c .

For that purpose, we observe that the equation $g(s) = 0$ has three solutions

$$s_0 = 0, \quad s_1 = d \frac{-3 - \sqrt{1 + 8\frac{c^2}{c_0^2}}}{2}, \quad s_2 = d \frac{-3 + \sqrt{1 + 8\frac{c^2}{c_0^2}}}{2}.$$

Clearly, $s_1 < 0$ for all $c \in \mathbb{R}_+$. Consequently, we concentrate on s_2 . We distinguish two cases :

- For $c \leq c_0$, $s_2 \leq 0$ which implies that g doesn't vanish in \mathbb{R}_+^* . Then, G has no zeros in \mathbb{R}_+^* . We conclude by Theorem 3 that Equation (3.4.23) has no solution.

• For $c > c_0$, K is positive and $s_2 > 0$. Then g is negative on $(0, s_2)$ and positive on $(s_2, +\infty)$. Since $G(0) = 0$, we deduce that $G(s_2) < 0$. Moreover, it is easy to see that $\lim_{s \rightarrow +\infty} G(s) = +\infty$. By the mean-value Theorem, we prove that G has a unique zero s_m in $(s_2, +\infty)$ with $g(s_m) > 0$. By Theorem 3, Equation (3.4.23) admits a unique solution $\eta_c \in H^1(\mathbb{R})$. Finally, denoting $q_c = c\eta_c$, it is clear that (q_c, η_c) is the unique solution to (3.4.21)-(3.4.22). Furthermore, the relation between the velocity c and the maximal amplitude $A > 0$ of η_c is given by $G(A) = 0$, that is

$$c^2 = c_0^2 \frac{\frac{A^2}{2} + \frac{A^3}{6d}}{dA - d^2 \log(\frac{d+A}{d})}. \quad (3.4.24)$$

To conclude, we show that solutions η_c and q_c have exponential decay at infinity. Note that, since $q_c = c\eta_c$, it is sufficient to show this result for η_c . For that purpose, we study the following limit considering $c > c_0$,

$$\frac{g(s)}{s} = \frac{1}{K} \left(c_0^2 - c^2 + \frac{c_0^2}{2d}s + c^2 \frac{s}{d+s} \right) \xrightarrow{s \rightarrow 0} \frac{1}{K} (c_0^2 - c^2) < 0.$$

Applying the Theorem 3, η_c has exponential decay at infinity.

We end this section by giving a solitary wave solution to Madsen and Sørensen equations using (3.4.24) (see Figure 3.2). We have computed a solitary wave with an initial amplitude equal to 0.2 for $\beta = 1/15$ using a Runge-Kutta Strongly-Stability Preserving method. It leads to the following values : $c \approx 3.44$ and $q_c(0) \approx 0.688$.

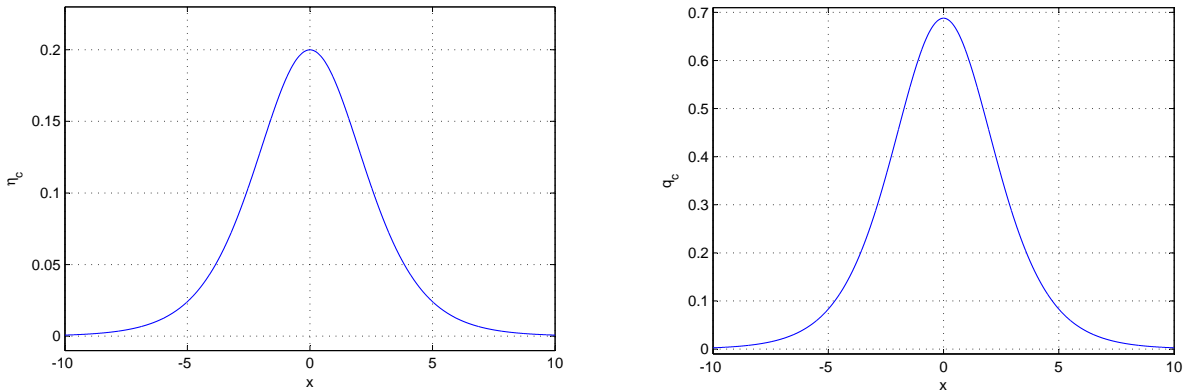


Figure 3.2 – Solitary waves for Madsen and Sørensen equations (η_c is on the left and q_c on the right), with $d = 1$, $\eta_c^0 = 0.2$ and $\beta = 1/15$.

3.4.3 Solitary waves solutions for Nwogu equations

We recall the Nwogu equations with constant bathymetry d . Take $\alpha \in (-\frac{1}{2}, 0)$, $\beta = \alpha + 1/3$ (so that $\beta \in (-\frac{1}{6}, \frac{1}{3})$) and consider

$$\begin{cases} \eta_t + [(\eta + d)u^\alpha]_x + \beta d^3 u_{xxx}^\alpha = 0, \\ u_t^\alpha + u^\alpha u_x^\alpha + g\eta_x + \alpha d^2 u_{txx}^\alpha = 0. \end{cases} \quad (3.4.25)$$

$$(3.4.26)$$

Remark 5. If $\beta = 0$, the system corresponds to the so-called Peregrine equations. It can also be obtained by taking $\alpha_B = 0$ in the Beji-Nadaoka equations (3.4.7)-(3.4.8). According to Section 3.4.1, there exists a unique solitary waves solution to the Peregrine equations.

We look for solitary waves under the form

$$\begin{cases} \eta(t, x) = \eta_c(x - ct) \\ u^\alpha(t, x) = u_c(x - ct), \end{cases}$$

where $\eta_c, u_c \in H^1(\mathbb{R})$. By plugging these quantities in Equations (3.4.25) and (3.4.26), we obtain after one integration

$$\begin{cases} -c\eta_c + [(\eta_c + d)u_c] + \beta d^3 u_c'' = 0, \\ -cu_c + \frac{u_c^2}{2} + g\eta_c - c\alpha d^2 u_c'' = 0, \end{cases} \quad (3.4.27)$$

$$(3.4.28)$$

from which we derive, by elimination, the following relation between η_c and u_c

$$\eta_c = d \frac{cu_c/3 - \beta u_c^2/2}{c_0^2 \beta - c^2 \alpha + cau_c}. \quad (3.4.29)$$

Since we are looking for positive and finite solutions which tend to zero at infinity, the function u_c has to take value in an interval of \mathbb{R}^+ containing 0. We want to find non-negative solutions η_c and u_c . In order to respect this condition, we treat successively the case $\beta > 0$ and $\beta < 0$:

- case $\beta < 0$

A quick study provides (note that u_c is assumed to be positive)

$$\frac{c}{3} - \frac{\beta}{2} u_c > 0 \Leftrightarrow u_c \geq 0.$$

In addition,

$$c_0^2 \beta - c^2 \alpha + cau_c \geq 0 \Leftrightarrow u_c \leq c - \frac{\beta}{\alpha} \frac{c_0^2}{c}.$$

We conclude that, when $\beta < 0$, $\eta_c \geq 0$ only when

$$0 \leq u_c \leq c - \frac{\beta}{\alpha} \frac{c_0^2}{c},$$

which leads to the following condition on parameters c , c_0 , α and β

$$c^2 > \frac{\beta}{\alpha} c_0^2.$$

- case $\beta > 0$

A quick study provides

$$\frac{c}{3} - \frac{\beta}{2} u_c > 0 \Leftrightarrow u_c < \frac{2c}{3\beta}.$$

In addition,

$$c_0^2 \beta - c^2 \alpha + c \alpha u_c \geq 0 \Leftrightarrow u_c \leq c - \frac{\beta}{\alpha} \frac{c_0^2}{c}.$$

It provides again that $c^2 > \frac{\beta}{\alpha} c_0^2$ but for this case, $\beta/\alpha < 0$. Then, this condition is always satisfied.

We conclude that, when $\beta > 0$, $\eta_c \geq 0$ only when u_c satisfies

$$0 \leq u_c < c - \frac{\beta}{\alpha} \frac{c_0^2}{c} \text{ and } 0 \leq u_c < \frac{2c}{3\beta},$$

and we assume in the sequel that $c^2 > \frac{\beta}{\alpha} c_0^2$.

In order to obtain the ODE satisfied by u_c , we multiply (3.4.27) by c and (3.4.28) by d , to obtain, by adding the resulting equations

$$-\frac{d^2}{3} u_c'' = \frac{(c_0^2 - c^2) \frac{u_c}{3} + \frac{cu_c^2}{2} - \frac{u_c^3}{6}}{\alpha(c_0^2 - c^2) + \frac{c_0^2}{3} + \alpha cu_c}.$$

As usual, taking into account the previous remarks, we introduce the function g on the interval $[0, \min \left(c - \frac{\beta}{\alpha} \frac{c_0^2}{c}, \frac{2c}{3\beta} \right))$

$$g(s) = \frac{(c_0^2 - c^2) \frac{s}{3} + \frac{cs^2}{2} - \frac{s^3}{6}}{\alpha(c_0^2 - c^2) + \frac{c_0^2}{3} + \alpha cs},$$

and its primitive

$$\begin{aligned} G(s) &:= \int_0^s g(x) dx, \\ &= \frac{1}{6} s^3 - \left(\frac{c}{2} + \frac{\beta c_0^2}{4\alpha} \right) s^2 + c_0^2 \left(\frac{c}{3} + \frac{\beta}{2\alpha} (\beta c_0^2 - \alpha c^2) \right) \frac{s}{\alpha}, \\ &\quad - \frac{c_0^2 (\beta c_0^2 - \alpha c^2)}{c^2 \alpha^2} \left(\frac{c}{3} + \frac{\beta}{2\alpha} (\beta c_0^2 - \alpha c^2) \right) \log \left(1 + \frac{\alpha c}{\beta c_0^2 - \alpha c^2} s \right). \end{aligned}$$

A quick study provides that the solutions to $g(s) = 0$ are

$$s_0 = 0, \quad s_1 = c \frac{3 - \sqrt{1 + 8K}}{2}, \quad s_2 = c \frac{3 + \sqrt{1 + 8K}}{2},$$

where $K = \frac{c_0^2}{c^2}$.

- For $c \leq c_0$, g doesn't vanish in $[0, \min \left(c - \frac{\beta}{\alpha} \frac{c_0^2}{c}, \frac{2c}{3\beta} \right))$ from which we deduce that so does G . Then Equations (3.4.27)-(3.4.28) have no solution.

-
- If the condition

$$c > \max \left(c_0, \sqrt{\frac{\frac{\beta^2}{\alpha^2}}{2 - \frac{\beta}{\alpha}}} c_0 \right)$$

is satisfied, then s_1 is the only zero of g in the interval $[0, c - \frac{\beta c_0^2}{\alpha c}]$. Since, in this case, $c - \frac{\beta c_0^2}{\alpha c} \leq \frac{2c}{3\beta}$, we deduce that

$$g(s) \leq 0, \text{ for } s \in [0, s_1],$$

$$g(s) > 0, \text{ for } s \in [s_1, c - \frac{\beta c_0^2}{\alpha c}),$$

and

$$G(s_1) < 0.$$

Recalling that $\alpha < 0$, it is clear that

$$\lim_{t \rightarrow c - \frac{\beta c_0^2}{\alpha c}} G(t) = +\infty,$$

and then the mean-value Theorem provides that G admits a unique zero $s_m \in [s_1, c - \frac{\beta c_0^2}{\alpha c}]$ satisfying $g(s_m) > 0$.

Again, Theorem 3 furnishes the existence of a unique solution u_c to Equation (3.4.29). It is then clear that u_c and η_c are the only solutions to the Nwogu equations (3.4.27)-(3.4.28) for all

$$c > \max \left(c_0, c_0 \sqrt{\frac{\frac{\beta^2}{\alpha^2}}{2 - \frac{\beta}{\alpha}}} \right). \quad (3.4.30)$$

Remark 6. If $\alpha \in (-\frac{1}{9}, 0)$, then

$$c_0 < c_0 \sqrt{\frac{\frac{\beta^2}{\alpha^2}}{2 - \frac{\beta}{\alpha}}}.$$

We deduce that for c such as

$$c_0 < c < c_0 \sqrt{\frac{\frac{\beta^2}{\alpha^2}}{2 - \frac{\beta}{\alpha}}},$$

$c - \frac{\beta c_0^2}{\alpha c} > \frac{2c}{3\beta}$, Recalling that we look for a function u_c satisfying for all $x \in \mathbb{R}$, $0 < u_c(x) < \frac{2c}{3\beta}$, g is defined on interval $[0, \frac{2c}{3\beta}]$. Consequently s_1 is the only zero of g on $[0, \frac{2c}{3\beta}]$. We deduce that the existence of a solution to Equation (3.4.29) depends on the sign of $G(\frac{2c}{3\beta})$. More precisely, if $G(\frac{2c}{3\beta}) > 0$, Equation (3.4.29) admits a unique solution whereas in the opposite case, there is no solution. Unfortunately, we are not able here to determine easily the sign of $G(\frac{2c}{3\beta})$ but as suggested by Figure 3.3, we conjecture that it is always positive which provides consequently the existence of u_c for all $c > c_0$ and $\alpha \in (-1/2, 0)$

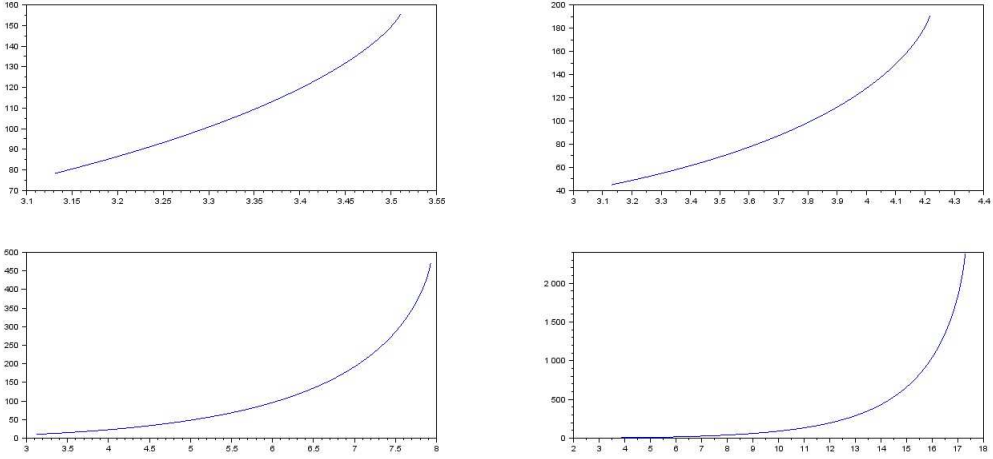


Figure 3.3 – The values of $G(\frac{2c}{3\beta})$ with respect to $c_0 < c < c_0 \sqrt{\frac{\beta^2}{\frac{\alpha^2}{2-\beta}}}$ and for $\beta = 0.2333$ (top left), $\beta = 0.2593$ (top right), $\beta = 0.2963$ (bottom left), $\beta = -0.3233$ (bottom right).

Coming back to the case (3.4.30), we write the relation between the velocity c and the amplitude U of u_c

$$\begin{aligned} \frac{1}{6}U^3 - \left(\frac{c}{2} + \frac{\beta c_0^2}{4ca}\right)U^2 + c_0^2 \left(\frac{c}{3} + \frac{\beta}{2ca}(\beta c_0^2 - \alpha c^2)\right) \frac{U}{ca}, \\ - \frac{c_0^2(\beta c_0^2 - \alpha c^2)}{c^2 \alpha^2} \left(\frac{c}{3} + \frac{\beta}{2ca}(\beta c_0^2 - \alpha c^2)\right) \log(1 + \frac{ca}{\beta c_0^2 - \alpha c^2} U) = 0. \end{aligned}$$

To conclude, we investigate the exponential decay of solutions.

$$\frac{g(t)}{t} = \frac{(c_0^2 - c^2)\frac{1}{3} + \frac{ct}{2} - \frac{t^2}{6}}{\alpha(c_0^2 - c^2) + \frac{c_0^2}{3} + \alpha ct} \xrightarrow[t \rightarrow 0]{} \frac{(c_0^2 - c^2)\frac{1}{3}}{\alpha(c_0^2 - c^2) + \frac{c_0^2}{3}} < 0,$$

proving that u_c is exponentially decaying at infinity. Moreover, direct computations show that

$$\begin{aligned} |\eta_c(x)| &= |d \frac{cu_c(x)/3 - \beta u_c(x)^2/2}{c_0^2 \beta - c^2 \alpha + ca u_c(x)}| \leq d \frac{c/3 + |\beta| s_m/2}{c_0^2 \beta - c^2 \alpha + ca s_m} |u_c(x)| \\ &\leq L_1 \exp(-\delta|x|), \end{aligned}$$

$$|\eta_c''(x)| \leq L_2 \exp(-\delta|x|),$$

$$|\eta_c'''(x)| \leq L_3 \exp(-\delta|x|),$$

where L_1, L_2, L_3 are positive.

We end this section by computing a solitary wave for Nwogu equations (see Figure 3.4). Again, using a Runge-Kutta Strongly-Stability Preserving method, we have computed a solitary wave with an initial amplitude equal to 0.2 for $\beta = -1/15$. Computations lead to $c \approx 3.42$ and $u_c(0) \approx 0.561$.

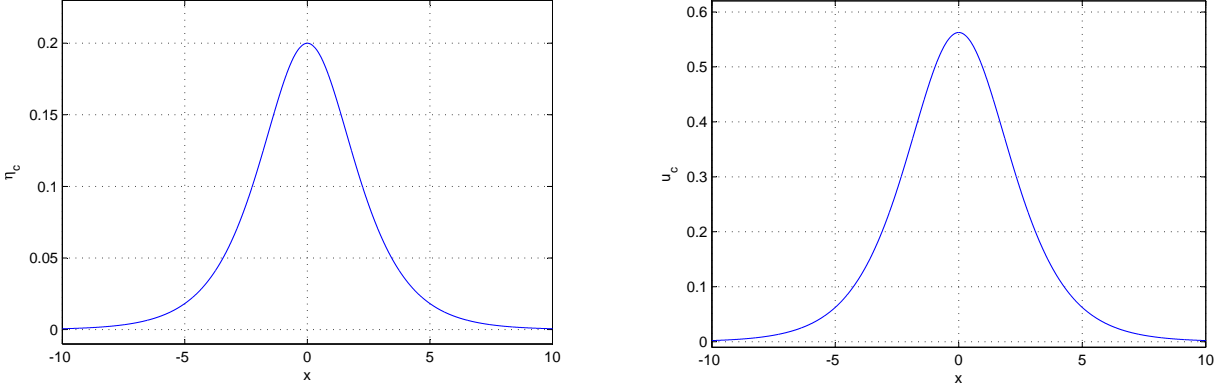


Figure 3.4 – Solitary wave for Nwogu equations (η_c is on the left and u_c on the right), with $d = 1$, $\eta_c^0 = 0.2$ and $\beta = -1/15$.

3.4.4 Discussion on solitary waves for Nwogu-Abbott equations

In this section, we propose a study of solitary waves for the Nwogu-Abbott equations. Note that we don't provide existence results.

We recall the Nwogu-Abbott equations with constant bathymetry d . Take $\alpha \in (-\frac{1}{2}, 0)$, $\beta = \alpha + 1/3$ (so that $\beta \in (-\frac{1}{6}, \frac{1}{3})$) and consider

$$\left\{ \begin{array}{l} \eta_t + q_x^\alpha + \beta d^2 q_{xxx}^\alpha = 0, \\ q_t^\alpha + \left(\frac{(q^\alpha)^2}{d + \eta} \right)_x + g(d + \eta)\eta_x + \alpha d^2 q_{txx}^\alpha = 0. \end{array} \right. \quad (3.4.31)$$

$$(3.4.32)$$

Remark 7. If $\beta = 0$, the system corresponds to the so-called Abbott equations. It can also be obtained by taking $\beta = 0$ in the Madsen-Sørensen Equations (3.4.19)-(3.4.20). According to Section 3.4.2, there exists a unique solitary wave solution to the Abbott equations for a celerity $c > c_0$. Then, we assume that $\beta \neq 0$.

We look for solitary waves under the form

$$\left\{ \begin{array}{l} \eta(t, x) = \eta_c(x - ct), \\ q^\alpha(t, x) = q_c(x - ct), \end{array} \right.$$

where $\eta_c, q_c \in H^1(\mathbb{R})$. By plugging these quantities in Equations (3.4.31) and (3.4.32), we obtain after integration

$$\left\{ \begin{array}{l} -c\eta_c + q_c + \beta d^2 q_c'' = 0, \\ -cq_c + \frac{q_c^2}{d + \eta_c} + g\frac{\eta_c^2}{2} + c_0^2 \eta_c - cad^2 q_c'' = 0. \end{array} \right. \quad (3.4.33)$$

$$(3.4.34)$$

Non-existence result

Using Equation (3.4.33) to express η_c in function of q and q'' , it is possible to eliminate η_c in Equation (3.4.34), leading to the following relation between $-q''$ and q

$$h(q, -q'') = 0,$$

where $h : \mathbb{R} \times \mathbb{R} \rightarrow \mathbb{R}$ is a continuously differentiable function defined as

$$h(x, y) = a_3y^3 + a_2(x)y^2 + a_1(x)y + a_0(x), \quad (3.4.35)$$

with

$$\begin{aligned} a_3 &= -\frac{\beta^3 c_0^2 d^5}{2c^3}, \\ a_2(x) &= \frac{3c_0^2 \beta^2 d^3}{2c^3}x + \frac{3c_0^2 \beta^2 d^4}{2c^2} - \alpha \beta d^4, \\ a_1(x) &= -\left(\frac{3c_0^2 \beta d}{2c^3}x^2 + \left(\frac{3c_0^2 \beta d^2}{c^2} - \beta d^2 - \alpha d^2\right)x + \left(\frac{c_0^2 \beta d^3}{c} - c \alpha d^3\right)\right), \\ a_0(x) &= \frac{c_0^2}{2c^3 d}x^3 + \frac{3c_0^2}{2c^2}x^2 + \left(\frac{c_0^2 d}{c} - cd\right)x. \end{aligned}$$

We apply the Implicit Function Theorem in the point $(0, 0)$. As a consequence if $c^2 \neq \frac{\beta}{\alpha}c_0^2$, one has $h_y(0, 0) \neq 0$. There exists an open set \mathcal{U} containing 0, another open set \mathcal{V} containing 0 and a unique continuously differentiable function $g : \mathcal{U} \rightarrow \mathcal{V}$ such that

$$\forall (x, y) \in \mathcal{U} \times \mathcal{V}, h(x, y) = 0 \Leftrightarrow y = g(x).$$

It transpires that when $q \in \mathcal{U}$ and $q'' \in \mathcal{V}$, the following relation

$$-q'' = g(q) \quad (3.4.36)$$

is satisfied.

As a consequence, we can refer to the Theorem 3. Note that we do not have explicit expression of g , the only information concerning $g(s)$ is that it is a root of the polynom $h(s, X)$ for all s in \mathcal{U} . If the function g has no zero in $\mathcal{U} \cap \mathbb{R}_*^+$, then its primitive is monotonous and there are not solitary waves with small amplitudes for Nwogu-Abbott equations. We remark that for all s in $\mathcal{U} \cap \mathbb{R}_*^+$, $g(s) = 0$ if and only if the polynom $h(s, X)$ admits zero as a root. But, the polynom may admit zero as a root only when coefficient $a_0(s)$ may be equal to zero. A quick study provides that the solutions to $a_0(s) = 0$ are

$$s_0 = 0, s_1 = \frac{cd}{2} \left(-3 - \sqrt{1 + 8 \frac{c^2}{c_0^2}} \right), s_2 = \frac{cd}{2} \left(-3 + \sqrt{1 + 8 \frac{c^2}{c_0^2}} \right).$$

For $c \leq c_0$, the equation $a_0(s) = 0$ has no solution in \mathbb{R}_*^+ , then $g(s)$ cannot be equal to zero for all s in $\mathcal{U} \cap \mathbb{R}_*^+$. As a consequence, Equations (3.4.33)-(3.4.34) don't admit solitary waves in this situation.

Approximate computations

In the previous subsection, we have proved that the Nwogu-Abbott equations don't admit solutions in the form $(\eta_c(x - ct), u_c(x - ct))$ with small amplitudes when $c \leq c_0$. But we can't conclude when $c > c_0$. Then, we conjecture that, in this situation, there exist positive solutions of Nwogu-Abbott equations. In order to perform some effective numerical computations of solitary waves, we start this subsection by presenting a method to approximate the amplitude A for a given propagation celerity $c > c_0$.

Eliminating q''_c in System (3.4.33)-(3.4.34), we obtain a relation satisfied by η_c and q_c

$$q_c = \frac{d + \eta_c}{2\beta} \left(\frac{c}{3} - \sqrt{\frac{c^2}{9} - 4 \frac{\beta}{d + \eta_c} \left(\frac{\beta c_0^2 \eta_c^2}{2d} + (\beta c_0^2 - \alpha c^2) \eta_c \right)} \right). \quad (3.4.37)$$

The relation (3.4.37) is only defined when the term in the square root is positive. As a consequence, we deduce that η_c has to satisfy

$$0 \leq \eta_c \leq s_{max},$$

where

$$s_{max} = \frac{d}{4\beta^2} \left(\frac{1}{9} + 4\beta(\alpha + \beta \frac{c_0^2}{c^2}) + \sqrt{\frac{8}{9}\beta^2 + \left(\frac{1}{9} + 4\beta(\alpha - \beta \frac{c_0^2}{c^2}) \right)} \right).$$

In the sequel, we note f_c the function depending on c and defined for all $s \in [0, s_{max}]$ as

$$f_c(s) = \frac{d + s}{2\beta} \left(\frac{c}{3} - \sqrt{\frac{c^2}{9} - 4 \frac{\beta}{d + s} \left(\frac{\beta c_0^2 s^2}{2d} + (\beta c_0^2 - \alpha c^2) s \right)} \right).$$

We are looking for non-negative solutions η_c and q_c of Equations (3.4.31)-(3.4.32). In order to respect this condition, we treat successively the case $\beta > 0$ and $\beta < 0$:

- case $\beta > 0$

A brief study provides that

$$f_c(s) \geq 0 \Leftrightarrow s \geq 2d \left(\frac{\alpha c^2}{\beta c_0^2} - 1 \right).$$

As $\alpha \in (-1, 0)$ and $\beta = \alpha + \frac{1}{3}$, $\frac{\beta}{\alpha} < 1$, it transpires that $2d \left(\frac{\alpha c^2}{\beta c_0^2} - 1 \right) < 0$. We conclude that, in this situation, q_c is positive when η_c is in $[0, s_m]$.

- case $\beta < 0$

A brief study provides that

$$f_c(s) \geq 0 \Leftrightarrow s \leq 2d \left(\frac{\alpha c^2}{\beta c_0^2} - 1 \right).$$

Note that, assuming $c > c_0$, $2d \left(\frac{\alpha c^2}{\beta c_0^2} - 1 \right)$ is always positive when β is negative.

We conclude that q_c is positive when η_c is in $[0, 2d \left(\frac{\alpha c^2}{\beta c_0^2} - 1 \right)]$.

This study provides a maximal value of amplitude for a given celerity. In the sequel, we propose a method to approach the value of A .

Firstly, multiplying Equation (3.4.33) by q'_c and integrating with respect to $\xi = x - ct$ between $-\infty$ and 0 (we assume that the solitary wave reaches its maximum at $\xi = 0$)

$$-c \int_{-\infty}^0 \eta_c(\xi) q'_c(\xi) d\xi + \int_{\infty}^0 q_c(\xi) q'_c(\xi) d\xi + \beta d^2 \int_{\infty}^0 q'_c(\xi) q''_c(\xi) d\xi = 0. \quad (3.4.38)$$

As q_c and q'_c tend to zero when $\xi \rightarrow +\infty$ and $q'_c(0) = 0$, it is possible to simplify Equation (3.4.38)

$$-c \int_{-\infty}^0 \eta_c(\xi) q'_c(\xi) d\xi + q_c(0)^2 = 0, \quad (3.4.39)$$

Integrating by part the integral of Equation (3.4.39) gives

$$-c\eta_c(0)q_c(0) + c \int_{-\infty}^0 q_c(\xi) \eta'_c(\xi) d\xi + q_c(0)^2 = 0. \quad (3.4.40)$$

If A denotes the amplitude of the solitary wave, we deduce that $\eta_c(0) = A$ and $q_c(0) = f_c(A)$. Introducing a new variable $v = \eta_c(\xi)$, Equation (3.4.40) becomes

$$-cA f_c(A) + c \int_0^A f_c(v) dv + f_c(A)^2 = 0. \quad (3.4.41)$$

We end by using a Newton algorithm on the function (we use a quadrature method to compute the integral)

$$x \rightarrow -cx f_c(x) + c \int_0^x f_c(v) dv + f_c(x)^2,$$

in order to compute the value of A . To conclude, we substitute q_c by $f(\eta_c)$ in Equation (3.4.33) to solve numerically equations (3.4.33)-(3.4.34) with a Runge-Kutta Strongly-Stability Preserving scheme applied on the resulting equation, with the initial condition

$$\begin{pmatrix} \eta_c(0) \\ \eta'_c(0) \end{pmatrix} = \begin{pmatrix} A \\ 0 \end{pmatrix}.$$

We end this section by computing an approximate solitary wave for Nwogu-Abbott equations (see Figure 3.5). We have computed a solitary wave with an initial amplitude equal to 0.2 for $\beta = -1/15$, using the method described in this subsection. Then $c \approx 3.44$ and $q_c(0) \approx 0.678$.

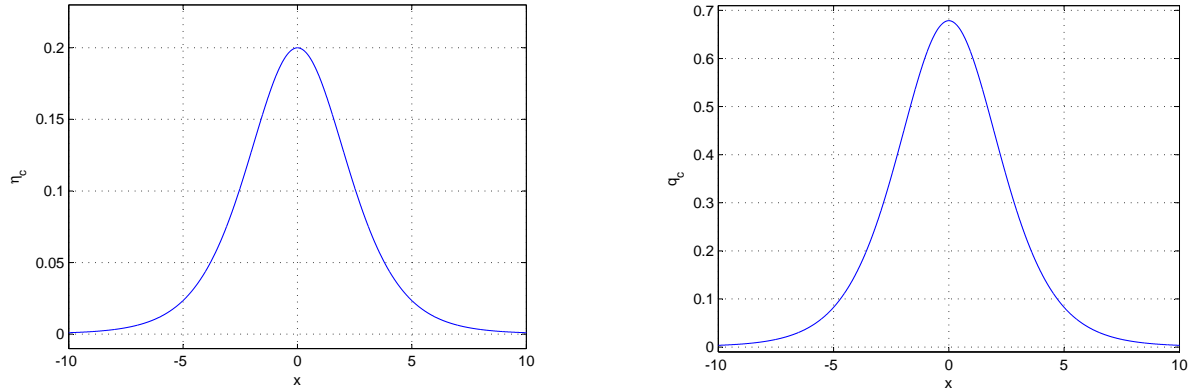


Figure 3.5 – Approximate solitary wave for Nwogu-Abbott equations (η_c is on the left and q_c on the right), with $d = 1$, $\eta_c^0 = 0.2$ and $\beta = -1/15$.

Chapter 4

On the nonlinear behavior of Boussinesq type models : wave amplitude-velocity vs wave amplitude-flux forms

Contents

4.1	Introduction	86
4.2	Weakly nonlinear Boussinesq type models	87
4.2.1	Models of Peregrine and Abbott	88
4.2.2	Beji-Nadaoka and BNA models	89
4.2.3	Madsen-Sørensen and MSP models	90
4.2.4	Nwogu and NA models	91
4.2.5	Summary	92
4.3	Theoretical analysis of the models	93
4.3.1	Properties of Airy model	93
4.3.2	Dispersion properties	96
4.3.3	Shoaling properties	100
4.4	Numerical experiments	106
4.4.1	Numerical discretization and implementation	106
4.4.2	Initial validation	107
4.4.3	Physical experiments	110
4.5	Conclusions	117

4.1 Introduction

The modeling of wave transformation in the near shore region requires a physically correct description of both dispersive and nonlinear effects. The use of asymptotic depth averaged Boussinesq Type models for this task is quite common [23]. These models have to be used with much care. Quite often, weakly-nonlinear variants of these models, such as those proposed in [1, 11, 57, 60, 63], are used outside of their range of applicability, e.g. when reaching breaking conditions. In these cases fully-nonlinear models should be used instead [42]. Moreover, to actually include the energy dissipation effects associated to wave breaking, either ad-hoc viscosity terms are included, or a coupling with the shallow water equations is introduced [71, 70, 23, 46]. Despite of the fact that they are theoretically well-adapted only for small amplitude waves, in practice these models provide accurate results also when they are used outside of their domain of validity [65, 23, 46]. The key to this success is actually the use of a properly designed wave breaking model, which includes a breaking detection criterion and a dissipation mechanism. The challenge for a correct capturing of these fronts is the understanding of the genuinely nonlinear physics underlying breaking, as well as the behavior of the underlying dispersive wave propagation model, and in particular the wave shoaling when approaching the nonlinear regime. Accounting for genuinely nonlinear effects is thus a research topic of high priority [23]. While the linear properties of the models can be thoroughly studied analytically [36], in the nonlinear case some properties, such as e.g. the shoaling behavior, must be studied numerically.

There exist several types of weakly nonlinear Boussinesq type models. These all provide different approximations of the Euler equations. The design properties of these models are often the linear dispersion relation and shoaling coefficient which are expected to be as close as possible to those of the linear wave theory for the range of wavenumbers relevant for the applications sought. Given a linear dispersion relation and linear shoaling coefficient, it is known that two nonlinear sets of Partial Differential Equations (PDEs) can be formulated, both degenerating to the same linearized system. Denoting by a the wave amplitude, d_0 the mean water level, and λ the wavelength, these two models are alternate forms within the same asymptotics in terms of the nonlinearity $\varepsilon = a/d_0$ and dispersion $\sigma = d_0/\lambda$ parameters. The main difference lies in the nature of the higher order derivatives, which can either be applied to the velocity u , or to the flux $q = hu$, h denoting the total depth. These formulations are referred here to as *amplitude-velocity*, and *amplitude-volume flux* forms. Examples of such couples and details of derivations are given in Chapter 2.

To gain better understanding in the properties of weakly nonlinear Boussinesq type models, this chapter presents a thorough analytical and numerical characterization of their nonlinear behavior. For a given couple linear dispersion relation-linear shoaling parameter, we start by recalling two nonlinear sets of PDEs : the first one in amplitude-velocity form, the other one in amplitude-volume flux form. The theory is applied to four linear relations corresponding to the models of Peregrine [63] and to the enhanced models of Beji-Nadaoka [11], Madsen-Sørensen [57] and Nwogu [60]. For each of these models, we give the corresponding alternate formulation. The

main result of the chapter can be summarized as follows : while in the linearized case four types of behaviors are observed, corresponding to the given four linear relations, when approaching the nonlinear regime, only two types of behavior are observed, which are practically independent on the linear dispersion relations and shoaling parameters, and depend only on whether the model is formulated in amplitude-velocity or amplitude-volume flux form. This observation is confirmed by both theoretical arguments and numerical results.

The present study gives important insight in the behavior of Boussinesq type models, especially in view of the applications of breaking detection criteria. In particular, our result shows that these criteria must take into account not only the type of breaking expected in the flow but also the underlying form of the propagation model. For simplicity, we only consider here models well adapted to the near shore range (reduced wave numbers $\sigma \leq 0.5$), however very similar arguments can be used to study deep water variants [56].

The structure of the chapter is the following. In Section 4.2, we recall the weakly nonlinear Boussinesq equations derived in Chapter 2 and we discuss the construction of models in amplitude-velocity and amplitude-flux forms for different particular cases. Section 4.3 presents the theoretical analysis of the systems of PDEs and in particular the analysis of the propagation of higher order harmonics, which gives an indication of the non-linear behavior of the models. Finally, numerical tests in both linear and nonlinear regimes are discussed in Section 4.4.

4.2 Weakly nonlinear Boussinesq type models

In this section, We review a certain number of weakly nonlinear Boussinesq type models. We recall that these models are obtained as depth averaged asymptotic approximations of the incompressible Euler equations. In particular, if a denotes a reference wave amplitude, d_0 a reference water depth, and λ a typical wavelength, we consider the nonlinearity parameter ε and the dispersion parameter σ defined by

$$\varepsilon = \frac{a}{d_0}, \quad \sigma = \frac{d_0}{\lambda}.$$

Weakly dispersive Boussinesq type models are obtained under the small amplitude hypothesis $\varepsilon = \mathcal{O}(\sigma^2)$, as asymptotic approximations of the order $\mathcal{O}(\varepsilon\sigma^2, \sigma^4)$. We refer to Chapter 2 for details concerning the basic derivation of the models. In this section, our objective is to recall some of the models most commonly encountered in literature and to discuss the construction of amplitude-velocity and amplitude-flux forms having the same linearized behavior.

In the following, we will use the notation $d(x)$ for the variable mean/still water level, η for the surface elevation and $h = d + \eta$ for the depth (cf. figure 4.1).

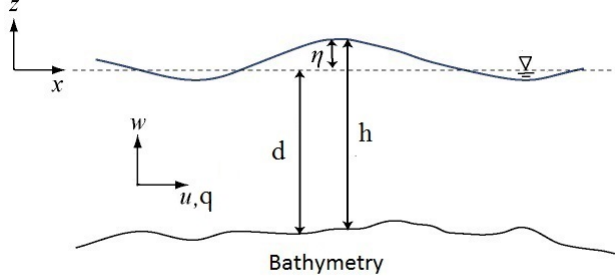


Figure 4.1 – Sketch of the free surface flow problem, main parameters description.

4.2.1 Models of Peregrine and Abbott

The most common Boussinesq type model is the one introduced by Peregrine in [63]

$$\begin{cases} \eta_t + [(d + \eta)u]_x = 0, \\ u_t + uu_x + g\eta_x - \left(\frac{d}{2}[du]_{xxt} - \frac{d^2}{6}u_{xxt} \right) = 0. \end{cases} \quad (4.2.1)$$

Here u denotes the depth-averaged velocity. One can rewrite the Peregrine equations in terms of the conservative variables (h, q) , where $q = hu$ denotes the volume flux. Introducing the Non-Linear Shallow Water (NLSW) flux by

$$F^{SW} = \frac{q^2}{h} + g\frac{h^2}{2}, \quad (4.2.2)$$

we obtain the following set of equations

$$\begin{cases} h_t + q_x = 0, \\ q_t + F_x^{SW} - ghd_x - hP_t(u) = 0. \end{cases} \quad (4.2.3)$$

System (4.2.3) allows to underline the structure of the Peregrine model, which is obtained by adding to the NLSW equations a term given by the product of the depth with the time derivative of an elliptic linear differential operator. This elliptic operator, denoted by $P(\cdot)$ in (4.2.3), is defined by

$$P(\cdot) = \frac{d}{2}[(\cdot)d]_{xx} - \frac{d^2}{6}(\cdot)_{xx}. \quad (4.2.4)$$

An asymptotically equivalent system can be obtained by neglecting terms of order $\varepsilon\sigma^2$, leading to the Abbott system [1]

$$\begin{cases} h_t + q_x = 0, \\ Q_t(q) + F_x^{SW} - ghd_x = 0. \end{cases} \quad (4.2.5)$$

In the linearized case, the models of Peregrine and of Abbott are equivalent and share the same linear dispersive and linear shoaling characteristics. In the nonlinear case, the two systems are

both approximations of the Euler equations of order $\mathcal{O}(\varepsilon\sigma^2, \sigma^4)$, however they do differ as the dispersive terms are expressed in terms of the derivatives of u in the Peregrine one and in terms of the derivatives of q in (4.2.5). In the latter, we see once more the appearance of the time derivative of a linear elliptic operator, denoted by $Q(\cdot)$ and defined by

$$Q(\cdot) = (\cdot) - d \left(\frac{d}{2} (\cdot)_{xx} - \frac{d^2}{6} \left[\frac{(\cdot)}{d} \right]_{xx} \right). \quad (4.2.6)$$

Compared to (4.2.3), System (4.2.5) has a more compact and seemingly conservative structure, as it does not involve any additional non-conservative product w.r.t the NLSW equations.

The limited accuracy of Systems (4.2.1) and (4.2.5), e.g. in terms of linear dispersion relations, has pushed the development of the so-called enhanced models. These are improved approximations which, while still remaining of order $\mathcal{O}(\varepsilon\sigma^2, \sigma^4)$ w.r.t the Euler equations, provide substantially improved approximations of the linearized dispersion relations and shoaling coefficients of the original three dimensional equations. These models are considered in the following sections.

4.2.2 Beji-Nadaoka and BNA models

An improved system can be obtained starting from the non-dimensional system of Peregrine adding negligible terms of order σ^4 and $\varepsilon\sigma^2$ (see Section 2.6.1 for details). It leads to the enhanced system proposed by Beji and Nadaoka [11] (model BN), which reads

$$\begin{cases} \eta_t + q_x = 0, \\ u_t + uu_x + g\eta_x - (1 + \alpha_B)P_t(u) - g\alpha_B P(\eta_x) = 0, \end{cases} \quad (4.2.7)$$

where $P(\cdot)$ is the elliptic operator given in (4.2.4). The model of Beji and Nadaoka can be also written in terms of the conservative variables (h, q) as

$$\begin{cases} h_t + q_x = 0, \\ q_t + F_x^{SW} - ghd_x - (1 + \alpha_B)hP_t(u) - gh\alpha_B P(\eta_x) = 0. \end{cases} \quad (4.2.8)$$

The additional free parameter α_B allows to improve the dispersion relation of the system w.r.t. the one of Peregrine's model. System (4.2.8) is written in amplitude-velocity form, as the dispersive terms involve derivatives of the velocity and not of the flux q . We can derive an asymptotically equivalent system in amplitude-flux form proceeding exactly as we have done for the Peregrine equations in non-dimensional form (details are in Chapter 2). The final result is the *Beji-Nadaoka-Abbott* model (BNA) reading

$$\begin{cases} h_t + q_x = 0, \\ \check{Q}_t(q) + F_x^{SW} - ghd_x - gd\alpha_B P(\eta_x) = 0, \end{cases} \quad (4.2.9)$$

where the operator $\check{Q}(\cdot)$ is very close to $Q(\cdot)$ given in (4.2.6) and differs by the presence of the tuning parameter α_B

$$\check{Q}(\cdot) = (\cdot) - (1 + \alpha_B)d\left(\frac{d}{2}(\cdot)_{xx} - \frac{d^2}{6}\left[\frac{(\cdot)}{d}\right]_{xx}\right). \quad (4.2.10)$$

While for $\alpha_B = 0$ System (4.2.8) reduces to the model of Peregrine, model (4.2.9) reduces in this limit to the equations of Abbott. When $\alpha_B \neq 0$ the BNA model has a less compact form, compared to (4.2.5), due to the presence of the additional term $-g\alpha_B dP(\eta_x)$.

4.2.3 Madsen-Sørensen and MSP models

The enhanced model proposed by Madsen and Sørensen in [57] is obtained with a procedure very similar to the one discussed in the previous paragraph adding neglectable terms of order σ^4 and $\varepsilon\sigma^2$ and in the mild slope hypothesis by neglecting terms containing d_x^2 and d_{xx} (see Section 2.6.2). The resulting equations read

$$\begin{cases} h_t + q_x = 0, \\ \hat{q}_t(q) + F_x^{SW} - ghd_x - g\beta d\hat{P}(\eta_x) = 0, \end{cases} \quad (4.2.11)$$

where $\hat{P}(\cdot)$ and $\hat{q}(\cdot)$ are defined by

$$\hat{P}(\cdot) = d^2(\cdot)_{xx} + 2dd_x(\cdot)_x, \quad (4.2.12)$$

and

$$\hat{q}(\cdot) = (\cdot) - \left(\frac{1}{3} + \beta\right)d^2(\cdot)_{xx} - \frac{d}{3}d_x(\cdot)_x. \quad (4.2.13)$$

System 4.2.11 reduces exactly to the one of Abbott for the choice of $\beta = 0$ and for a constant bathymetry, but it has a more complex structure due to the term $g\beta d\hat{P}(\eta_x)$. The free parameter β , however, allows to substantially improve the linear dispersion and shoaling properties w.r.t. (4.2.5). The model is clearly in amplitude-flux form and an asymptotically equivalent system in wave amplitude velocity form can be obtained by manipulations very similar to those done for the other models (see Chapter 2). The final form of the model in the mild slope hypothesis is

$$\begin{cases} h_t + q_x = 0, \\ q_t + F_x^{SW} - ghd_x + h\bar{P}_t(u) - \beta gh\hat{P}(\eta_x) = 0, \end{cases} \quad (4.2.14)$$

where

$$\bar{P}(\cdot) = -\left(\frac{1}{3} + \beta\right)d^2(\cdot)_{xx} - (1 + 2\beta)dd_x(\cdot)_x. \quad (4.2.15)$$

In the following we will refer to this model as to the *Madsen-Sørensen-Peregrine* system (MSP).

Note that simple manipulations show that, if one considers constant bathymetry, the BN and the MSP systems as well as the BNA and the MS systems collapse onto one another provided that $\beta = \alpha_B/3$. All these models indeed share the same linear dispersion relation. For non-constant bathymetries, these models define two families of linear shoaling parameters, as we will see in Section 4.3.2.

4.2.4 Nwogu and NA models

The study of enhanced Boussinesq equations would not be complete without taking into account the extended model of Nwogu [60] obtained by enhancing the system of Peregrine by replacing the depth averaged velocity by the velocity at an arbitrary elevation z_α . For simplicity, in the following developments, we still denote by u the quantity $u(t, x, z = z_\alpha)$, but it should be clear that the physical meaning of this quantity is different from the depth averaged horizontal speed present in all the previous models. Setting $z_\alpha = \theta d$, for some $\theta \in (-1, 0)$, the model of Nwogu can be written as [60]

$$\begin{cases} \eta_t + \left[q + dP^b(u) \right]_x = 0, \\ u_t + uu_x + g\eta_x + P_t^a(u) = 0. \end{cases} \quad (4.2.16)$$

This model has a more complex structure, with additional operators appearing in both equations. In particular, the operators $P^a(\cdot)$ and $P^b(\cdot)$ are linear elliptic operators with similar structure to $P(\cdot)$ (cf. Equation (4.2.4)), but with different coefficients

$$P^a(\cdot) = a_1 \frac{d^2}{6} (\cdot)_{xx} - a_2 \frac{d}{2} [(\cdot)d]_{xx}, \quad (4.2.17)$$

$$P^b(\cdot) = b_1 \frac{d^2}{6} (\cdot)_{xx} - b_2 \frac{d}{2} [(\cdot)d]_{xx}. \quad (4.2.18)$$

The values of such coefficients are expressed as function of the tuning parameter θ and read

$$a_1 = 3\theta^2; \quad a_2 = -2\theta; \quad b_1 = 3\theta^2 - 1; \quad b_2 = -2\theta - 1.$$

Remark 8. Note that

$$A_1 = \frac{a_1}{6}; \quad A_2 = -\frac{a_2}{2}; \quad B_1 = \frac{b_1}{6}; \quad B_2 = -\frac{b_2}{2},$$

where A_1, A_2, B_1, B_2 are notations introduced in Section 2.6.3 of Chapter 2.

The equations of Peregrine are recovered for the choice $a_1 = a_2 = 1, b_1 = b_2 = 0$. Note that it is not possible to retrieve these values for any $\theta \in (-1, 0)$. With simple manipulations, we can recast model (4.2.16) in terms of time evolution of the flux q as

$$\begin{cases} h_t + \left[hu + dP^b(u) \right]_x = 0, \\ [hu]_t + F_x^{SW} - ghd_x + hP_t^a(u) + u \left[dP^b(u) \right]_x = 0. \end{cases} \quad (4.2.19)$$

Last equations show that, among the amplitude-velocity enhanced models, the model of Nwogu is the one with the most complex structure when written in terms of (η, q) .

Again, we can derive an asymptotically equivalent system in amplitude-flux form which degenerates to the same linearized equations as the model of Nwogu.

$$\begin{cases} h_t + Q_x^b(q) = 0, \\ Q_t^a(q) + F_x^{SW} - ghd_x = 0, \end{cases} \quad (4.2.20)$$

where the operators $Q^a(\cdot)$ and $Q^b(\cdot)$ are defined by

$$Q^a(\cdot) = (\cdot) + d \left(a_1 \frac{d^2}{6} \left[\frac{(\cdot)}{d} \right]_{xx} - a_2 \frac{d}{2} (\cdot)_{xx} \right), \quad (4.2.21)$$

$$Q^b(\cdot) = (\cdot) + d \left(b_1 \frac{d^2}{6} \left[\frac{(\cdot)}{d} \right]_{xx} - b_2 \frac{d}{2} (\cdot)_{xx} \right). \quad (4.2.22)$$

The system obtained has a similar compact structure as Equations (4.2.5), but it has the exact same linear characteristics of the equations of Nwogu. In this case, for $a_1 = a_2 = 1$, $b_1 = b_2 = 0$ we recover the model of Abbott. In the following we refer to these equations as the *Nwogu-Abbott* model (NA). Note that, even though we will still refer to these equations as being in amplitude-flux form, strictly speaking the quantity q in (4.2.20) is not a total horizontal flux, its value physically corresponding to the depth times the velocity at $z = \theta d$.

4.2.5 Summary

In this section we have considered the most popular Boussinesq type models of the literature. We have shown that for each model, or for a given pair of linear dispersion relation-linear shoaling coefficient, we can derive asymptotically equivalent amplitude-velocity and amplitude-flux forms. Some examples of these couples can be already found in [36]. We have given a thorough list of these couples.

We summarize here the models which will be studied in the rest of the chapter listing by couples those which have the same linearized system

- Models of Peregrine (4.2.3) (amplitude-velocity) and of Abbott (4.2.5) (amplitude-flux) ;
- Model of Beji and Nadaoka (4.2.8) (amplitude-velocity) and BNA model (4.2.9) (amplitude-flux) ;
- Model of Madsen-Sørensen (4.2.11) (amplitude-flux) and MSP model (4.2.14) (amplitude-velocity) ;
- Model of Nwogu (4.2.16) (amplitude-velocity) and NA model (4.2.20) (amplitude-flux) .

The objective of the following sections is to study the properties of these systems. First, we will consider the aspect of wave propagation, in both linear and nonlinear cases. Then we will provide an analytical and numerical study of the linear and nonlinear shoaling characteristics of these models.

4.3 Theoretical analysis of the models

This section is devoted to the analysis of the theoretical properties of the models. In the linear case, the eight systems of PDEs presented in Section 4.2 reduce by construction to four families of linearized models. For given constant bathymetries, the models of Beji-Nadaoka and of Madsen-Sørensen also degenerate to the same system of PDEs. In this case, we will briefly recall the linear dispersion analysis and then discuss the behavior of second order harmonics. The analysis of the higher order harmonics shows that the nonlinear form of the system has a dramatic effect on the amplitudes of the harmonics, which basically depends on whether the system is written in amplitude-velocity or amplitude-flux form.

For non-constant bathymetries, a linear ODE can be derived to compute the shoaling coefficient in the linearized case. We will recall this procedure and compare the shoaling coefficients for the different models considered here. Note that the nonlinear shoaling properties are investigated numerically in Section 4.4.

4.3.1 Properties of Airy model

It is common to compare the linear dispersion characteristics of the Boussinesq equations with those of the linear wave theory of Airy. This section is devoted to the computations of quantities for the linear Airy wave theory, which are generally used.

Considering a monochromatic unidirectional wave with frequency ω and wavenumber k , we recall the definition of three dispersion characteristics.

Definition 1 (Phase velocity). The phase velocity C is the velocity of a point on the free surface of a periodic wave propagating with a constant shape for a constant bottom. Mathematically, it is defined as

$$C = \frac{\omega}{k}, \quad (4.3.1)$$

Definition 2 (Group velocity). The group velocity C_g is the velocity of the propagation of energy in a wave train. Mathematically, it is defined as

$$C_g = \frac{\partial \omega}{\partial k}. \quad (4.3.2)$$

Using the phase velocity definition, we get

$$C_g = C + k \frac{\partial C}{\partial k}.$$

Definition 3 (Linear shoaling gradient). The shoaling gradient coefficient α_s relates the change in wave amplitude to the change in bathymetry. Mathematically, it can be expressed using the following relation

$$\frac{A_x}{A} = -\alpha_s \frac{d_x}{d}, \quad (4.3.3)$$

where A is the initial wave amplitude and d the bathymetry.

We start by finding the expressions of phase velocity and shoaling gradient for the Airy theory.

Before going further, we recall how to obtain the Airy system. We start from the Euler equations with kinematic boundary conditions (see Chapter 2 for details),

$$u_t + uu_x + wu_z + \frac{p_x}{\rho} = 0, \quad (4.3.4)$$

$$w_t + uw_x + ww_z + \frac{p_z}{\rho} + g = 0, \quad (4.3.5)$$

$$u_x + w_z = 0, \quad (4.3.6)$$

$$u_z - w_x = 0, \quad (4.3.7)$$

$$w = \eta_t + u\eta_x, \quad z = \eta, \quad (4.3.8)$$

$$p = 0, \quad z = \eta, \quad (4.3.9)$$

$$w = -d_x u, \quad z = -d. \quad (4.3.10)$$

As we deal with an incompressible and irrotational flow, the velocity vector comes from a potential Φ . We are going to reformulate Euler system in function of this potential. Equation (4.3.4) and (4.3.5) become

$$\Phi_{xt} + \Phi_x \Phi_{xx} + \Phi_z \Phi_{xz} + \frac{p_x}{\rho} = 0, \quad (4.3.11)$$

$$\Phi_{zt} + \Phi_x \Phi_{zx} + \Phi_z \Phi_{zz} + \frac{p_z}{\rho} + g = 0. \quad (4.3.12)$$

Integrating the first equation with respect to the variable x and the second one with respect to z , we obtain

$$\Phi_t + \frac{1}{2}(\Phi_x^2 + \Phi_z^2) + \frac{p}{\rho} + gz = \mathcal{D}(t), \quad (4.3.13)$$

where \mathcal{D} is a function that depends only on the time t . If we replace Φ with $\Phi - \int_0^t \mathcal{D}(s)ds$, equation (4.3.13) can be written under the following form

$$\Phi_t + \frac{1}{2}(\Phi_x^2 + \Phi_z^2) + \frac{p}{\rho} + gz = 0. \quad (4.3.14)$$

Then, we evaluate equation (4.3.14) at $z = \eta$ to obtain a new formulation of Euler equation,

$$\Phi_t + \frac{1}{2}(\Phi_x^2 + \Phi_z^2) + g\eta = 0, \quad z = \eta(t, x), \quad (4.3.15)$$

$$\Phi_z = \eta_t + \Phi_x \eta_x, \quad z = \eta(t, x), \quad (4.3.16)$$

$$\Phi_{xx} + \Phi_{zz} = 0, \quad -d(x) \leq z \leq \eta(t, x), \quad (4.3.17)$$

$$\Phi_z = -d_x \Phi_x, \quad z = -d(x). \quad (4.3.18)$$

Remark 9. Equation (4.3.14) is the Bernoulli formulation. Remark that these equations can be used to obtain the water-waves equations (see [49] for details).

These equations are used to compute the reference for phase velocity and linear shoaling gradient to calibrate Boussinesq equations linear characteristics. Firstly, we linearize the Euler system (4.3.15)-(4.3.18) around the rest state

$$\Phi_t + g\eta = 0, \quad z = 0, \quad (4.3.19)$$

$$\Phi_z = \eta_t, \quad z = 0, \quad (4.3.20)$$

$$\Phi_{xx} + \Phi_{zz} = 0, \quad -d \leq z \leq 0, \quad (4.3.21)$$

$$\Phi_z = -d_x \Phi_x, \quad z = -d. \quad (4.3.22)$$

In the following, system (4.3.19)-(4.3.22) will be called the Airy system.

Phase velocity of the Airy equations

To compute the phase velocity, we follow the method detailed in [36, 57]. Note that the phase velocity is defined for a constant bottom, hence we assume that $d \equiv d_0$.

We start by eliminating η in System (4.3.19)-(4.3.22) by applying ∂_t on Equation (4.3.19) and substituting η_t into Equation (4.3.20),

$$\Phi_{tt} + g\Phi_z = 0, \quad z = 0, \quad (4.3.23)$$

$$\Phi_{xx} + \Phi_{zz} = 0, \quad -d \leq z \leq 0, \quad (4.3.24)$$

$$\Phi_z = 0, \quad z = -d. \quad (4.3.25)$$

We look for a solution under the following particular form

$$\Phi(t, x, z) = B(z) \exp\left(j(\omega t - kx)\right), \quad (4.3.26)$$

where B is the amplitude, ω the frequency, k the wavenumber and $j^2 = -1$. Substituting expression of Φ in Equation (4.3.24), we obtain an ordinary differential equation satisfied by B with respect to z

$$B_{zz} - k^2 B = 0. \quad (4.3.27)$$

The solutions of (4.3.27) are

$$B(z) = \alpha \cosh(k(z - d)) + \beta \sinh(k(z - d)).$$

Using condition (4.3.25), we deduce that

$$\Phi(t, z, x) = \alpha \cosh(k(z - d)) \exp\left(j(\omega t - kx)\right), \quad (4.3.28)$$

where α is a real constant which doesn't play any role in the rest of the study. To conclude, we substitute (4.3.26) in Equation (4.3.23) to derive

$$-\omega^2 \Phi(t, x, 0) + g\alpha k \sinh(kd) \exp\left(j(\omega t - kx)\right) = 0, \quad (4.3.29)$$

from which we obtain the expression of the phase velocity for the linear wave theory

$$C_{Stokes}^2 = \frac{\omega^2}{k^2} = g \frac{\tanh(kd)}{k} = gd \frac{\tanh(kd)}{kd}. \quad (4.3.30)$$

Shoaling gradient of Airy equations

In order to find the expression of the shoaling coefficient of Airy equations, we follow the computations presented by Madsen and Sørensen [57]. We use the energy flux conservation principle considering a varying bottom d

$$\frac{\partial}{\partial x} (A^2 C_g) = 0, \quad (4.3.31)$$

where A is the wave amplitude and C_g is the group velocity defined previously

$$C_g = \frac{1}{2}(1 + G)C_{Stokes},$$

with $G = \frac{2kd}{\sinh(kd)}$ and C_{Stokes} is the phase velocity given by Equation (4.3.30) for a constant bottom. Equation (4.3.31) gives

$$\frac{A_x}{A} = -\frac{1}{2} \left(\frac{G_x}{1 + G} + \frac{[C_{Stokes}]_x}{C_{Stokes}} \right). \quad (4.3.32)$$

In addition, using (4.3.1), it is possible to obtain the following relation considering a constant frequency ω

$$\frac{[C_{Stokes}]_x}{C_{Stokes}} = -\frac{k_x}{k}. \quad (4.3.33)$$

Furthermore, we can express k_x/k in function of d_x/d by using (4.3.30) and assuming that ω and g are constants. Substituting the expressions of $\frac{[C_{Stokes}]_x}{C_{Stokes}}$ and $\frac{k_x}{k}$ in Equation (4.3.32), we obtain

$$\frac{A_x}{A} = -\alpha_s^{Stokes} \frac{d_x}{d}, \quad (4.3.34)$$

with

$$\alpha_s^{Stokes} = \frac{\left(1 + 0.5(1 - \cosh(2kd))G\right)G}{(1 + G)^2}.$$

Expressions (4.3.39) and (4.3.34) are used as a reference to give a hierarchy between linear characteristics of Boussinesq models.

4.3.2 Dispersion properties

The dispersion properties can be investigated by means of a Fourier analysis on a horizontal bottom. Although the derivation of the equations has been based on the assumption that $\sigma^2 \ll 1$ and $\varepsilon = \mathcal{O}(\sigma^2)$, here we assume that $\varepsilon \ll 1$ and take any arbitrary σ^2 . The procedure follows closely the one used by Madsen and Schaffer in [56]. Considering a non-dimensional form of the models, we look for a solution under the form

$$\tilde{\eta} = a_1 \cos(\xi) + \varepsilon a_2 \cos(2\xi), \quad \tilde{u} = u_1 \cos(\xi) + \varepsilon u_2 \cos(2\xi), \quad (4.3.35)$$

where $\xi = \tilde{\omega}\tilde{t} - \tilde{k}\tilde{x}$, $\tilde{\omega}$ being the non-dimensional angular frequency and \tilde{k} the corresponding non-dimensional wavenumber

$$\tilde{\omega} = \frac{L}{\sqrt{gd_0}}\omega, \quad \tilde{k} = Lk.$$

We give some details for the derivation for Peregrine's model, the analysis of the other models is similar with small variations discussed in a final remark.

First-order solution. The linear dispersion properties of the models emerges looking at the first-order solutions. Substituting (4.3.35) in System (4.2.1) for non dimensional variables, for instance, and collecting terms of $\mathcal{O}(1)$ leads to the system

$$\begin{cases} -\tilde{\omega}a_1 + \tilde{k}\tilde{d}u_1 = 0, \\ -\tilde{\omega}u_1 + \tilde{k}a_1 + \sigma^2\tilde{\omega}\frac{\tilde{k}^2\tilde{d}^2}{3}u_1 = 0, \end{cases} \quad (4.3.36)$$

which can be easily solved, giving

$$\begin{cases} u_1 = \frac{\tilde{\omega}}{\tilde{k}\tilde{d}}a_1, \\ \frac{\tilde{\omega}^2}{\tilde{k}^2\tilde{d}} = \frac{1}{1 + \frac{\phi^2}{3}}, \end{cases} \quad (4.3.37)$$

with $\tilde{\phi} = \sigma\tilde{k}\tilde{d}$. The second equation of (4.3.37) represents the non-dimensional phase velocity \tilde{C} of the Peregrine model which, expressed in terms of dimensional variables becomes

$$C^2 = \frac{\omega^2}{k^2} = \frac{gd}{1 + \frac{\phi^2}{3}}, \quad (4.3.38)$$

with $\phi = \sigma kd$. It represents the rate at which the phase of the wave propagates in space (so the velocity at which every frequency of the wave propagates); in this sense it is the linear dispersion relation for the Peregrine model. The reference to which this value must be compared is the linear dispersion relation (4.3.30), that is

$$C_{Stokes}^2 = gd \frac{\tanh(\phi)}{\phi}. \quad (4.3.39)$$

Note that an expansion of the right-hand-side of the last two equation for small value of k shows that (4.3.38) matches (4.3.39) only up to order 2. Figure 4.2 summarizes the linear dispersion characteristics of the models considered here. The figure reports the ratio C/C_{Stokes} for all the models considered (another method to compute the phase velocity is detailed in Subsection 4.3.3). As anticipated, the eight systems of PDEs introduced reduce in the linearized case and for constant bathymetry to only three families of linear dispersion relations, which explains the presence of only four curves in the figure, including the exact solution.

The linear dispersion relations depend on the choice of the values of the tuning parameters α_B , β and θ . For all the models one can match the Padé approximation of the dispersion relations of the Stokes wave theory. This can be quickly shown to lead to the following relations between the parameters of the different enhanced models [53]

$$\beta = \alpha_B/3; \quad \theta = \sqrt{\frac{1 - 2\alpha_B}{3}} - 1. \quad (4.3.40)$$

The comparison can thus be done by using α_B as the only tuning parameter. As shown on Figure 4.2, the Beji-Nadaoka and Madsen-Sørensen curves are superimposed and correspond to the classical choice of $\alpha_B = 0.2$ [11, 57]. Setting $\alpha_B = 0.17$, yields the optimum value for the model of Nwogu [60].

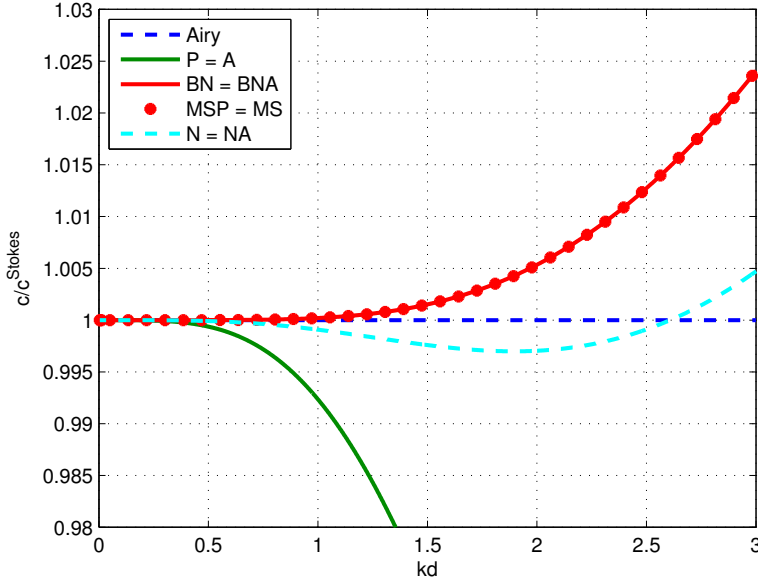


Figure 4.2 – Phase velocity ratio for all the models : P stands for Peregrine (eq. (4.2.3)), A for Abbott (eq. (4.2.5)), BN and BNA for Beji-Nadaoka and Beji-Nadaoka-Abbott (eq.s (4.2.8) and (4.2.9) resp.), MS and MSP for Madsen-Sørensen and Madsen-Sørensen-Peregrine (eq.s (4.2.11) and (4.2.14) resp.), and N and NA for Nwogu and Nwogu-Abbott (eq.s (4.2.19) and (4.2.20) resp.).

Second-order solution. Putting again (4.3.35) into the system (4.2.1) with non-dimensional variable and collecting terms of order $\mathcal{O}(\varepsilon)$, one obtains

$$\begin{cases} -2\tilde{\omega}a_2 + 2\tilde{k}\tilde{d}u_2 + \tilde{k}a_1u_1 = 0, \\ -2\tilde{\omega}u_2 + 2\tilde{k}a_2 + \frac{\tilde{k}}{2}u_1^2 - \frac{8}{3}\sigma^2\tilde{k}^2\tilde{\omega}u_2 = 0. \end{cases} \quad (4.3.41)$$

Using the first equation of System (4.3.37), one can write

$$\begin{pmatrix} \tilde{m}_{11} & \tilde{m}_{12} \\ \tilde{m}_{21} & \tilde{m}_{22} \end{pmatrix} \begin{pmatrix} a_2 \\ u_2 \end{pmatrix} = \frac{a_1^2}{\tilde{d}} \begin{pmatrix} \tilde{F}_1 \\ \tilde{F}_2 \end{pmatrix}, \quad (4.3.42)$$

where

$$\begin{aligned} \tilde{m}_{11} &= 2\tilde{\omega}, \quad \tilde{m}_{12} = -2\tilde{k}\tilde{d}, \quad \tilde{m}_{21} = -2\tilde{k}, \quad \tilde{m}_{22} = 2\tilde{\omega}(1 + 4/3\tilde{\phi}), \\ \tilde{F}_1 &= \tilde{\omega}, \quad \tilde{F}_2 = \frac{\tilde{\omega}^2}{2\tilde{d}\tilde{k}}. \end{aligned}$$

By solving the previous linear system, using the dispersion relation to simplify $\tilde{\omega}$ and passing to dimensional variables leads to the expression

$$a_2 = \frac{3}{4} \frac{a_1^2}{d} \frac{1}{\phi^2} \left(1 + \frac{8}{9}\phi^2 \right), \quad (4.3.43)$$

where $\phi = kd$. This value can be compared to the one found for the Stokes theory [56]

$$a_2^{Stokes} = \frac{1}{4} \left(\frac{a_1^2}{d} \right) \phi \coth(\phi)(3 \coth^2(\phi) - 1). \quad (4.3.44)$$

Remark 10. In adapting this procedure to the several Boussinesq type models of Section 4.2, a particular attention must be paid for the A, MS and NA systems. For these models, the relevant ansatz is $\tilde{q} = q_1 \cos(\xi) + \varepsilon q_2 \cos(2\xi)$. Subsequently, one has

$$\varepsilon \frac{\tilde{q}^2}{\tilde{d} + \varepsilon \tilde{\eta}} = \varepsilon \frac{\tilde{q}^2}{\tilde{d}} + \mathcal{O}(\varepsilon^2),$$

from which we deduce that

$$\varepsilon \left(\frac{\tilde{q}^2}{\tilde{d} + \varepsilon \tilde{\eta}} \right)_{\tilde{x}} = \varepsilon 2\tilde{k} \frac{q_1^2}{\tilde{d}} \sin(\xi) \cos(\xi) + \mathcal{O}(\varepsilon^2).$$

The analysis of the first and second harmonics can then be performed assembling the proper order linear systems.

The results obtained for the different models are compared on Figure 4.3 in terms of the ratio a_2/a_2^{Stokes} . The first obvious remark is that the second harmonic, taking into account the nonlinear behavior of the PDEs, reveals six different families of models. This is expected since, as already remarked, for flat bathymetry the MS and BNA models and the MSP and BN coincide.

The most striking result, however, is that only two different trends are observed depending uniquely on whether the model is in amplitude-velocity or amplitude-flux form. In particular, all the models in amplitude-flux form underestimate the nonlinear effects since the error monotonically increasing as the reduced wavenumber increases. On the contrary, all the models in amplitude-velocity form give a non-monotone trend, with an initial overestimation of the amplitude, and a peak close to $kd = 1$ for the enhanced models. Also, the error obtained with this class of models is smaller, the ratio being closer to one.

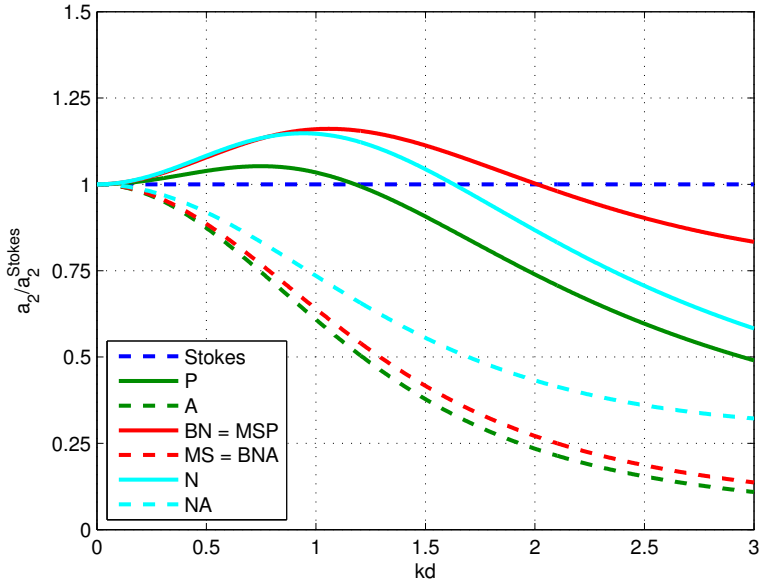


Figure 4.3 – Ratio of the second harmonic a_2/a_2^{Stokes} for the models considered. Continuous line : amplitude-velocity models. Dashed lines : amplitude-velocity models. Refer to figure 4.2 for the legend.

4.3.3 Shoaling properties

We have presented linear and nonlinear dispersion characteristics for different Boussinesq models with constant bottom. Despite enhanced Boussinesq models (Beji-Nadaoka, Beji-Nadaoka-Abbott, Madsen-Sørensen, Madsen-Sørensen-Peregrine, Nwogu or Nwogu-Abbott equations) have the same linear dispersion characteristics, differences are found when bottom varies. To calibrate these differences, we follow the study of linear shoaling presented by Madsen and Sørensen [57] or Dingemans [36]. We assume that the bathymetry varies slowly, which implies that $d = d(\delta x)$ with $\delta \ll 1$. Furthermore, for this study, we consider solutions u and η of the form

$$u(t, x) = U(\delta x) \exp \left(j(-\omega t + \frac{1}{\delta} S(\delta x)) \right), \quad \eta(t, x) = A(\delta x) \exp \left(j(-\omega t + \frac{1}{\delta} S(\delta x)) \right). \quad (4.3.45)$$

where $S = \int k(x)dx$ and $j^2 = -1$.

We recall that the linear shoaling coefficient relates the rate of change in wave amplitude to the rate of change in depth. Then we search for a function $\alpha_s = s(d, k)$, such as

$$\frac{A_x}{A} = -\alpha_s \frac{d_x}{d}. \quad (4.3.46)$$

Plugging Expressions (4.3.45) into different models leads to particular ODEs. When we keep all terms in order of δ^0 , we retrieve the phase velocity expression. Those of order δ^1 provide an analytical expression for the shoaling gradient coefficient α_s .

In order to simplify the future computations, we need the following expressions

$$\begin{aligned}
u_x &= jku + \delta \frac{U_x}{U} u, \quad (du)_x = jkdu + \delta \left(\frac{U_x}{U} + \frac{d_x}{d} \right) du, \\
u_{xx} &= -k^2 u + j\delta k \left(2 \frac{U_x}{U} + \frac{k_x}{k} \right) u + \mathcal{O}(\delta^2), \\
(du)_{xx} &= -k^2 du + j\delta k \left(2 \frac{U_x}{U} + 2 \frac{d_x}{d} + \frac{k_x}{k} \right) du + \mathcal{O}(\delta^2), \\
u_{xxx} &= -jk^3 u - \delta k^2 \left(3 \frac{U_x}{U} + 3 \frac{k_x}{k} \right) u + \mathcal{O}(\delta^2), \\
(du)_{xxx} &= -jk^3 du - \delta k^2 \left(3 \frac{U_x}{U} + 3 \frac{d_x}{d} + 3 \frac{k_x}{k} \right) du + \mathcal{O}(\delta^2), \\
u_{xxxx} &= k^4 u - j\delta k^3 \left(4 \frac{U_x}{U} + 6 \frac{k_x}{k} \right) u + \mathcal{O}(\delta^2), \\
(du)_{xxxx} &= k^4 du - j\delta k^3 \left(4 \frac{U_x}{U} + 4 \frac{d_x}{d} + 6 \frac{k_x}{k} \right) du + \mathcal{O}(\delta^2).
\end{aligned} \tag{4.3.47}$$

Before going further, let us remember that linearized models formulated in (η, u) and in (η, q) are the same.

Beji-Nadaoka equations

In this section, we recall the expression of the phase velocity of Beji-Nadaoka equations and we give the linear shoaling coefficient of this system.

Let us start by recalling the linear part of Beji-Nadaoka system

$$\eta_t + (du)_x = 0, \tag{4.3.48}$$

$$u_t + g\eta_x + (1 + \alpha_B) \left(\frac{d^2}{6} u_{txx} - \frac{d}{2} (du)_{txx} \right) + \alpha_B g \left(\frac{d^2}{6} \eta_{xxx} - \frac{d}{2} (d\eta_x)_{xx} \right) = 0. \tag{4.3.49}$$

The terms in η can be eliminated easily applying operator ∂_x to Equation (4.3.48) and ∂_t to Equation (4.3.49).

$$u_{tt} - g(du)_{xx} + (1 + \alpha_B) \left(\frac{d^2}{6} u_{txx} - \frac{d}{2} (du)_{txx} \right) - \alpha_B g \left(\frac{d^2}{6} (du)_{xxx} - \frac{d}{2} (d(du)_x)_{xxx} \right) = 0. \tag{4.3.50}$$

We substitute the expression of u , given by Equation (4.3.45), and we use (4.3.47) to obtain a relation between ω , k , d and U . We omit it due to its very complex expression.

Considering all terms of order $\mathcal{O}(1)$, we find the Beji-Nadaoka linear dispersion which leads to

$$C^2 = gd \frac{1 + \frac{\alpha_B}{3} k^2 d^2}{1 + (\frac{\alpha_B}{3} + \frac{1}{3}) k^2 d^2}. \tag{4.3.51}$$

Note that for $\alpha_B = 0$, we obtain the phase velocity (4.3.38) provided by the Peregrine equations given in Section 4.3.2.

When we keep all terms of order δ , we obtain a relation in the following form

$$\alpha_1 \frac{U_x}{U} + \alpha_2 \frac{d_x}{d} + \alpha_3 \frac{k_x}{k} = 0, \quad (4.3.52)$$

with

$$\begin{aligned} \alpha_1 &= 2 + 4\alpha_B \frac{k^2 d^2}{3} + 2\alpha_B(1 + \alpha_B) \frac{k^4 d^4}{9}, \\ \alpha_2 &= 2 - (1 - 6\alpha_B) \frac{k^2 d^2}{3} + 4\alpha_B(1 + \alpha_B) \frac{k^4 d^4}{9}, \\ \alpha_3 &= 1 + \alpha_B \frac{k^2 d^2}{3}. \end{aligned} \quad (4.3.53)$$

In order to express k_x/k in terms of d_x/d , we differentiate (4.3.51) considering ω as a constant. It leads to the following relation

$$\frac{k_x}{k} = -\alpha_4 \frac{d_x}{d}, \quad (4.3.54)$$

where

$$\alpha_4 = \frac{1}{2} \frac{1 + (2\alpha_B - 1) \frac{k^2 d^2}{3} + \alpha_B(\alpha_B + 1) \frac{k^4 d^4}{9}}{1 + 2\alpha_B \frac{k^2 d^2}{3} + \alpha_B(\alpha_B + 1) \frac{k^4 d^4}{9}}. \quad (4.3.55)$$

Substituting this relation in Equation (4.3.52), we express U_x/U in function of d_x/d ,

$$\frac{U_x}{U} = -\alpha_5 \frac{d_x}{d}, \quad (4.3.56)$$

where

$$\alpha_5 = \frac{\alpha_2 - \alpha_3 \alpha_4}{\alpha_1}.$$

To conclude, substituting (4.3.45) in Equation (4.3.48), we derive

$$-j\omega A + jkdU + \delta \left(\frac{U_x}{U} + \frac{d_x}{d} \right) dU = 0. \quad (4.3.57)$$

It transpires that

$$A = \frac{kd}{\omega} U. \quad (4.3.58)$$

Applying ∂_x to Equation (4.3.58), we get

$$\frac{A_x}{A} = \frac{U_x}{U} + \frac{k_x}{k} + \frac{d_x}{d}. \quad (4.3.59)$$

Substituting (4.3.56)-(4.3.54) in Equation (4.3.59), we obtain the linear shoaling coefficient of the Beji-Nadaoka equations satisfying

$$\frac{A_x}{A} = -\alpha_s \frac{d_x}{d}, \quad (4.3.60)$$

with $\alpha_s = (1 - \alpha_5 - \alpha_4)$.

Madsen-Sørensen equations

In this section, we recall the phase velocity of Madsen-Sørensen equations and we give the linear shoaling coefficient furnished by this system.

Let us start by recalling the linear version of the Madsen-Sørensen system

$$\eta_t + q_x = 0, \quad (4.3.61)$$

$$q_t + gd\eta_x - (B + \frac{1}{3})d^2q_{txx} - \frac{d}{3}d_xq_{tx} - Bgd^3\eta_{xxx} - 2Bgd^2d_x\eta_{xx} = 0. \quad (4.3.62)$$

In the previous system, we eliminate q by a derivative procedure and we look for η under the form (4.3.45). Collecting the terms of order $\mathcal{O}(1)$, we obtain the phase velocity

$$C^2 = gd \frac{1 + Bk^2d^2}{1 + (B + \frac{1}{3})k^2d^2}. \quad (4.3.63)$$

Note that it is the same expression than the one emanating from the Beji-Nadaoka equations with the particular choice of $B = \alpha_B/3$.

Collecting now the terms of order δ , we obtain the following relation

$$\alpha_1 \frac{A_x}{A} + \alpha_2 \frac{d_x}{d} + \alpha_3 \frac{k_x}{k} = 0, \quad (4.3.64)$$

where

$$\begin{aligned} \alpha_1 &= 2 + 4Bk^2d^2 + 2B(B + \frac{1}{3})k^4d^4, \\ \alpha_2 &= 1 + (4B - \frac{2}{3})k^2d^2 + B(3B + \frac{2}{3})k^4d^4, \\ \alpha_3 &= 1 + 6Bk^2d^2 + 5B(B + \frac{1}{3})k^4d^4. \end{aligned} \quad (4.3.65)$$

Again, it is possible to express k_x/k in function of d_x/d differentiating Equation (4.3.63) assuming ω is constant

$$\frac{k_x}{k} = -\alpha_4 \frac{d_x}{d},$$

with

$$\alpha_4 = \frac{1}{2} \frac{1 + (2B - \frac{1}{3})k^2d^2 + B(B + \frac{1}{3})k^4d^4}{1 + 2Bk^2d^2 + B(B + \frac{1}{3})k^4d^4}. \quad (4.3.66)$$

We substitute (4.3.66) in Equation (4.3.64) to obtain

$$\frac{A_x}{A} = -\alpha_s \frac{d_x}{d},$$

where α_s is the shoaling coefficient given by

$$\alpha_s = \frac{\alpha_2 - \alpha_3\alpha_4}{\alpha_1}. \quad (4.3.67)$$

Nwogu equations

We start from the linearized Nwogu equations

$$\eta_t + (du)_x + \left[\frac{b_1}{6} d^3 u_{xx} - \frac{b_2}{2} d^2 (du)_{xx} \right]_x = 0, \quad (4.3.68)$$

$$u_t + g\eta_x + \frac{a_1}{6} d^2 u_{txx} - \frac{a_2}{2} d (du)_{txx} = 0. \quad (4.3.69)$$

We eliminate η from the system applying ∂_t to Equation (4.3.69) and ∂_x to (4.3.68). We take u under the particular form (4.3.45) and we substitute it in the resulting equation using (4.3.47). In order to simplify the notations, we denote $\alpha = \frac{b_1}{6} - \frac{b_2}{2}$ and $\beta = \frac{b_1}{6} - \frac{b_2}{2}$. Remark that $\alpha = \beta + 1/3$.

Again, terms of order of $\mathcal{O}(1)$ give the phase velocity

$$C^2 = gd \frac{1 - \beta k^2 d^2}{1 - \alpha k^2 d^2}. \quad (4.3.70)$$

It is the same expression than the ones emanating from Beji-Nadaoka and Madsen-Sørensen equations with $\beta = -\alpha_B/3$.

Terms of order of δ furnish the following relation

$$\alpha_1 \frac{U_x}{U} + \alpha_2 \frac{d_x}{d} + \alpha_3 \frac{k_x}{k} = 0, \quad (4.3.71)$$

with

$$\begin{aligned} \alpha_1 &= 2 - 4\beta k^2 d^2 + 2\alpha\beta k^4 d^4, \\ \alpha_2 &= 2 - 2k^2 d^2 (A_2 + 3B_1 + 4B_2) + 2k^4 d^4 \left(A_1(3B_1 + 4B_2) + A_2(2B_1 + 3B_2) \right), \\ \alpha_3 &= 1 - 6\beta k^2 d^2 + 5\alpha\beta k^4 d^4. \end{aligned} \quad (4.3.72)$$

Applying ∂_x to Equation (4.3.70), we obtain

$$\frac{k_x}{k} = -\alpha_4 \frac{d_x}{d}, \quad (4.3.73)$$

with

$$\alpha_4 = \frac{1}{2} \frac{1 + (\alpha - 3\beta)k^2 d^2 + \alpha\beta k^4 d^4}{1 - 2\beta k^2 d^2 + \alpha\beta k^4 d^4}. \quad (4.3.74)$$

Substituting (4.3.73) in Equation (4.3.71), we express U_x/U in terms of d_x/d

$$\frac{U_x}{U} = -\alpha_5 \frac{d_x}{d},$$

where

$$\alpha_5 = \frac{\alpha_2 - \alpha_3 \alpha_4}{\alpha_1}.$$

In order to find the shoaling gradient, it is necessary to express the wave amplitude A in function of d , k and U . For this purpose, we take η under the form of (4.3.45) and we substitute in Equation (4.3.68), neglecting terms of order δ to get

$$A = \frac{kdU}{\omega} - \beta k^3 d^3 \frac{U}{\omega}. \quad (4.3.75)$$

We deduce that

$$\frac{A_x}{A} = (1 - \beta) \frac{U_x}{U} + (1 - 3\beta) \frac{d_x}{d} + (1 - 3\beta) \frac{k_x}{k}. \quad (4.3.76)$$

The linear shoaling gradient of Nwogu equations α_s is therefore given by

$$\frac{A_x}{A} = -\alpha_s \frac{d_x}{d},$$

where

$$\alpha_s = \left(1 - 3\beta - (1 - \beta)\alpha_5 - (1 - 3\beta)\alpha_4 \right) \frac{d_x}{d}. \quad (4.3.77)$$

Comparisons between Boussinesq models

Firstly, we underline that for a given variation (usually linear) of the bathymetry, the local wavenumber $k(x)$ must also be obtained by solving an ODE of the type

$$\frac{k_x}{k} = -\gamma \frac{d_x}{d}, \quad (4.3.78)$$

where $d(x)$ is given by the physical configuration. The expression for γ can be found in the previous subsections ((4.3.55) for the Beji-Nadaoka model, (4.3.66) for the Madsen-Sørensen model and (4.3.74) for the Nwogu model). The values of the shoaling parameter can thus be represented in two different ways. The one which is the most classically reported takes the form $s_0 = s(d(x), k_0)$ and represents its variation w.r.t. $k_0 d$, where k_0 is the wavenumber of the incoming wave. This leads to the classical result reported on the left on Figure 4.4 for the models considered here⁽¹⁾. However, the variation shown in the picture is not the actual one obtained in practice. To obtain this variation, one has to consider that k varies with respect to x and thus must integrate (4.3.78) to obtain the values $k(x)$. Then, it is possible to integrate (4.3.46) in order to compute the actual wave amplitudes. The shoaling coefficient can then still be plotted against $k_0 d$, by computing for a given x the corresponding values of $k_0 d(x)$ and the local value of

$$\alpha_s = s(d(x), k(x)) = -\frac{A_x(x)d(x)}{(A(x)d_x(x))}.$$

These computations are reported on the right of Figure 4.4 and are similar to the one reported without any explanation in [57]. Note that the correct amplitudes are obtained only when one considers the variation of the wavenumber in the integration of (4.3.46).

¹The optimal values of the free parameters given in Section 4.3.2 are used for the plot.

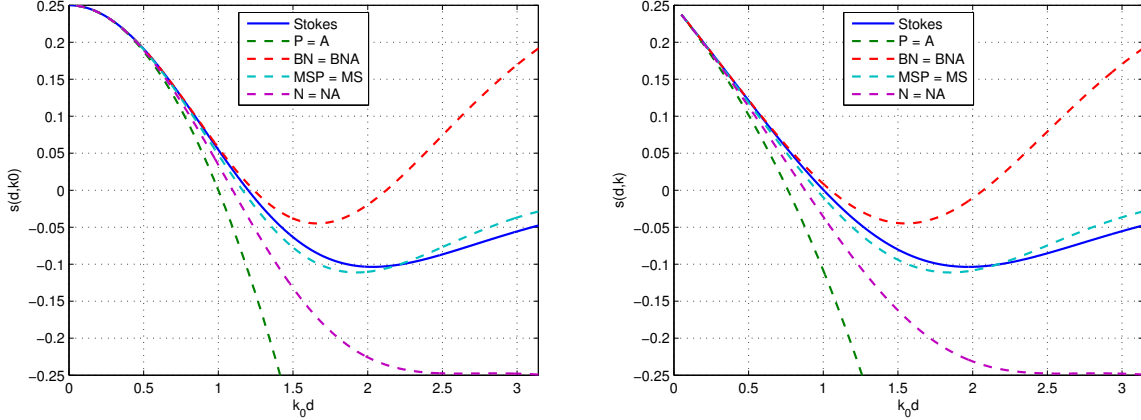


Figure 4.4 – Linear shoaling: representation of the linear shoaling coefficient α_s of the several Boussinesq type models defined by (4.3.46). On the left is sketched $\alpha_s = s(d(x), k_0)$, thus computing the values of α_s using the initial wavenumber of the signal k_0 . On the right, instead, the variation of k along the domain is considered in the computation of the shoaling coefficient, thus: $\alpha_s = s(s(x), k(x))$.

For completeness, we discuss the behavior of the shoaling coefficient α_s for each model considered in this chapter. Figure 4.4 shows classical results : the Peregrine (and Abbott) model provides a large error already for small wavenumbers with considerable low values of α_s ; the model of Nwogu gives a better approximation yet still underestimating the wave amplitude already for moderate wavenumbers; the model of Madsen and Sørensen gives the best approximation among the models considered here; the model of Beji and Nadaoka overestimates the wave amplitudes, with errors similar to those of the model of Nwogu.

4.4 Numerical experiments

4.4.1 Numerical discretization and implementation

The aim of the numerical tests is to further study the nonlinear properties of the models. In particular, we want to exhibit the shoaling characteristics in regions close to breaking conditions. To achieve this goal, one should require the numerics to be well-validated and the results to be as much as possible independent on the numerical methods. For this reason, we have proceeded as follows. Two different numerical discretizations have been used for each test, which has been performed on several meshes to guarantee as much as possible scheme and grid independence. In particular, we have used both a finite difference scheme and a finite element one. The finite difference scheme is based on the approach proposed by Wei and Kirby, which discretizes the shallow water terms of the equations using a fourth-order finite difference formula, while the dispersive terms are treated with a second order accuracy scheme [74]. The second method used is instead a \mathbb{P}_1 continuous finite element discretization based on a standard Galerkin finite element solution of the elliptic sub-problems which define the auxiliary variables $P(\cdot)$, $Q(\cdot)$, $\check{Q}(\cdot)$, $q(\cdot)$, etc, plus a standard Galerkin projection for the first order time dependent PDEs of the several models taken into account: (4.2.3), (4.2.5), (4.2.8), (4.2.9), (4.2.11), (4.2.14), (4.2.19),

(4.2.20). This procedure, introduced in [73] to discretize the model of Nwogu, has been also recently used in [64] to solve the Madsen-Sørensen equations. Moreover, it appears to have an accuracy close to a fourth order finite difference scheme both analytically and numerically and to that of the scheme of [74]. In all the tests made in this chapter, the two different space discretizations have led to virtually indistinguishable results. In the following, we will not show this comparison, but only report the main findings.

In the sequel, we present and discuss two type of tests : initial verification benchmarks, in which the results are compared to analytical solutions for both flat and variable bathymetry; physical experiments, in which we have investigated the behavior of the models in conditions close to wave breaking.

4.4.2 Initial validation

We discuss here two verification tests : the propagation of a solitary wave over a flat bathymetry and a linear shoaling test. These tests allow to verify our implementation of the models. Additionally, the linear shoaling experiments bring to the fore that, in the linear regime, all the numerical models actually do recover the behavior predicted by the linear shoaling analysis.

Soliton propagation

In this section, we consider the approximation of exact solitary wave solutions of the models presented. Quite often in literature, approximate solitary waves are used. Our purpose here is to be able to quantitatively certify our implementation. For this reason, we have chosen to use semi-analytical solutions. Details on the computation of these solutions as well as physical and mathematical conditions for their existence are given in Chapter 3. The resulting solitary waves shapes are reported in Figure 4.5 for a wave of amplitude $A/d_0 = 0.2$. Surprisingly, two families of solitary waves seem to emerge, models in amplitude-velocity form giving steeper and more peaky profile.

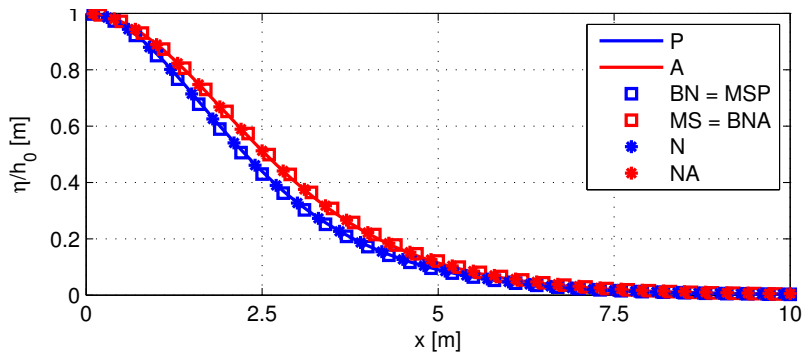


Figure 4.5 – Semi-analytical exact solitary waves for the Boussinesq models of the chapter.

To verify our implementation of the models, we have performed a grid convergence analysis on the solitary wave of Figure 4.5, characterized by an amplitude $A/d_0 = 0.2$, with $d_0 = 1 [m]$. The numerical results have been compared to the analytical (initial) profile after the wave has

travelled for a length of 100 [m]. The meshes used for the test contain 1000, 2000, 4000 and 8000 equally spaced cells. In Figure 4.6, we have plotted the L^2 -norm of the error for each model, using the same amplitude. The slopes obtained for the error exhibit a convergence with third order of accuracy for all the models except for the Nwogu-Abbott model (4.2.20).

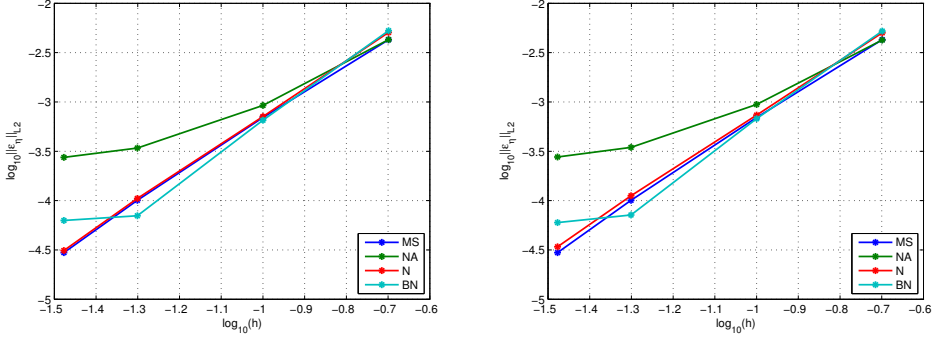


Figure 4.6 – Grid convergence results for the Galerkin finite element (left) and Wei and Kirby finite difference (right) scheme.

The accuracies of the other models are similar to the ones obtained with the same schemes applied to the Madsen-Sørensen equations in [64] confirming a proper implementation.

The lack of convergence observed for the Nwogu-Abbott equations is at first quite surprising since the solution looks excellent at a simple visual inspection as shown on the left picture of Figure 4.7. A closer inspection reveals that actually a relatively large error at the foot of the solitary wave is produced by the technique used to approach a solitary wave for NA equations (see Section 3.4.4), especially when one compares to the accurate and smooth profiles obtained for the other models. Note that computations of exact solitary wave of the Nwogu-Abbott model is currently still an unsolved issue.

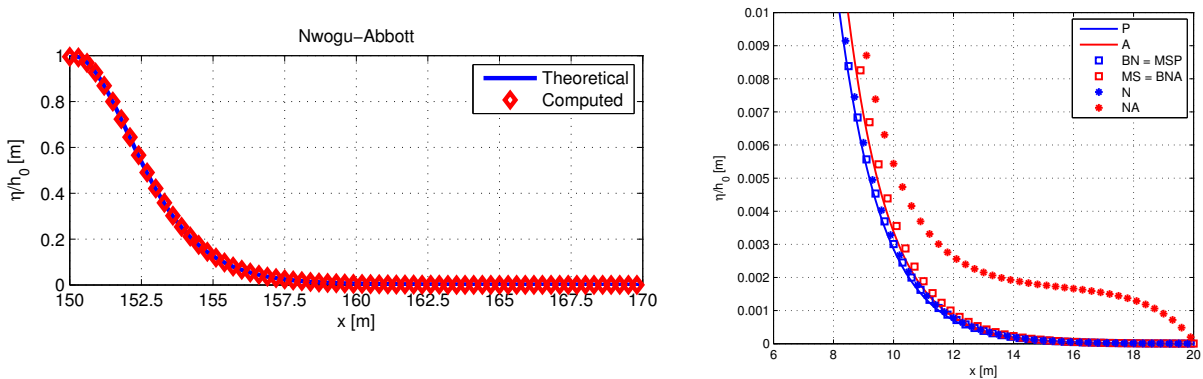


Figure 4.7 – Solitary wave propagation. Left : comparison between numerical and analytical solution for the NA model. Right : error at the foot of the semi-analytical wave for the NA model

Linear shoaling test

To further verify our implementation, we have performed the shoaling test proposed by Madsen and Sørensen in [57]. A periodic signal of amplitude $a = 0.05$ m and period $T = 4$ s propagates over an initial constant water depth of $h_0 = 13$ m. The periodic signal has been generated using a source method discussed in [64, 74]. The source of the periodic wave has been set at $x_0 = 100$ m of the domain $[0, 850]$ m. The bottom is flat for the first 50 m from the position of the periodic wave generator, it has a constant up-slope of 1 : 50 from $x = 150$ m to $x = 800$ m and it then returns flat until the end of the domain. In this way, the local values of the parameter $\varepsilon = a_0/h$, which represents the effects of nonlinearity, vary between the values 0.0038 and 0.25, attesting that we are working in the linear regime and the nonlinear effects can be actually neglected. Two wide absorbing sponge layers of 60 m long have been used at the two boundaries of the domain restricting the region of study of the shoaling to interval $[0, 790]$, but avoiding undesirable reflections due to the upper bottom shape discontinuity. The finest mesh used has a uniform grid size of $\Delta_x = 0.333$.

For this test case, a theoretical envelope of the signal amplitude can be obtained from the linear shoaling analysis by integrating (4.3.46). This curve is used as a reference to compare and validate the numerical results. For this particular case, the theoretical envelopes of the models are sketched on the left picture on Figure 4.8, while the right picture shows the typical wave profiles obtained⁽²⁾.

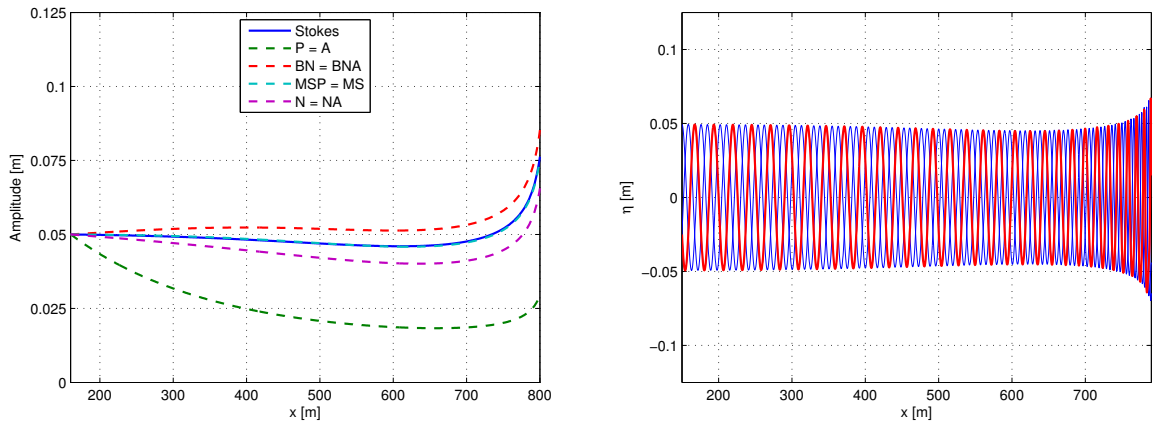


Figure 4.8 – Linear shoaling. Left : theoretical envelope of the maximum wave amplitude. Right: line plots of the surface elevation computed using the MS model.

The comparison of the envelopes obtained by our numerical computations with the theoretical ones is summarized on Figure 4.9. We can observe that the theoretical results are very well-reproduced by all the models and that, as expected, the Madsen-Sørensen and Madsen-Sørensen-Peregrine models produce almost superimposed results, as well as the Beji-Nadaoka

²Result of the Madsen-Sørensen model.

and Beji-Nadaoka-Abbott models, and the Nwogu and Nwogu-Abbott ones. Very close to the end of the slope, nonlinear effects begin, and we can clearly see a difference appearing between the linear theory and the numerical solution of the nonlinear equations.

The curves corresponding to the Peregrine and Abbott models are not presented in Figure 4.9 due to the fact that for such low amplitude waves we were unable to obtain a stable periodic signal by the internal wave generator strategy, at least not in the form described in [64] and implemented here.

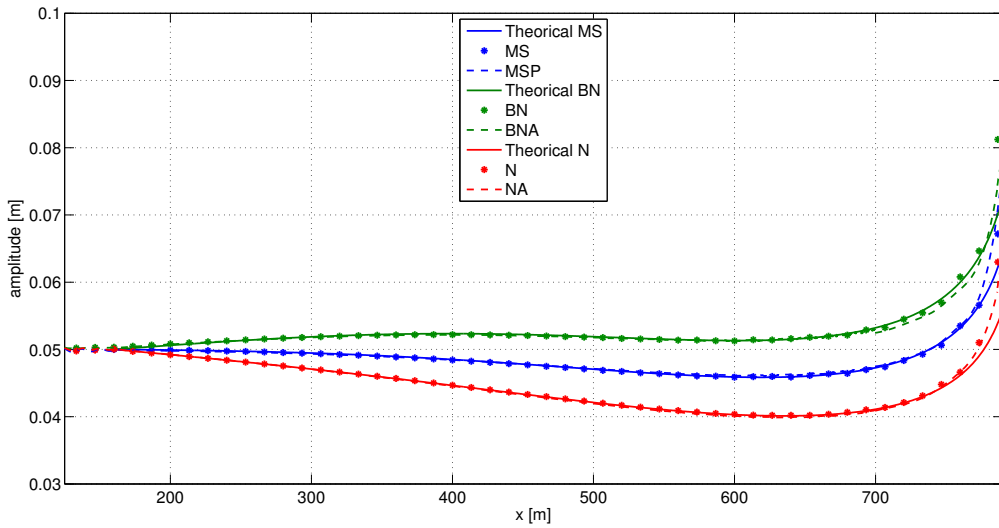


Figure 4.9 – Linear shoaling: maximum elevation

4.4.3 Physical experiments

This section is devoted to the nonlinear properties of the models. We consider two kind of experiments. The first one is the nonlinear shoaling tests performed in [42]. The second involves the propagation of monochromatic waves over a submerged bar in two configurations : a non-breaking situation and a breaking one. Note that for the second configuration, no breaking model is included. However, the results allow to study and compare the shape of the wave obtained with the different models in a more complex flow.

Nonlinear shoaling test

This test case allows to study the wave shoaling characteristics of the different models considered here in conditions close to wave breaking. It has been initially proposed by Grilli et al. in [42] and consists in propagating a solitary wave of amplitude $A/d_0 = 0.2$ m on a water depth $d_0 = 0.44$ m. The shoaling takes place onto a constant slope of 1 : 35 (see Figure 4.10). Note that, in this experiment, the local values of the nonlinearity parameter are roughly $\varepsilon = a_0/h \in [0.2; 2.2]$,

which means that we are reaching the nonlinear regime.

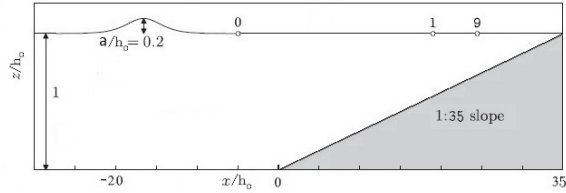


Figure 4.10 – Shoaling of a solitary wave; computational configuration and gauges position.

The numerical results obtained with the models of the chapter are compared to the data of the laboratory experiments given in [42]. The data available consist in the values of the free-surface elevations measured in 10 gauges situated at stations from 0 to 9 (see Figure 4.10), where the gauge 0 is positioned just before the toe of the slope and the gauge 9 is located close to the wave breaking point. We refer to [42] for the precise description of the setup.

In our test, the gauge 0 is used to calibrate the phase of the solutions. Note that the semi-analytical solitary waves depend on the form of the model. The resulting shoaling wave profiles are compared to the experiments in Figures 4.11 and 4.12, while the spatial evolution of the peak height is compared to the experiments in Figure 4.13.

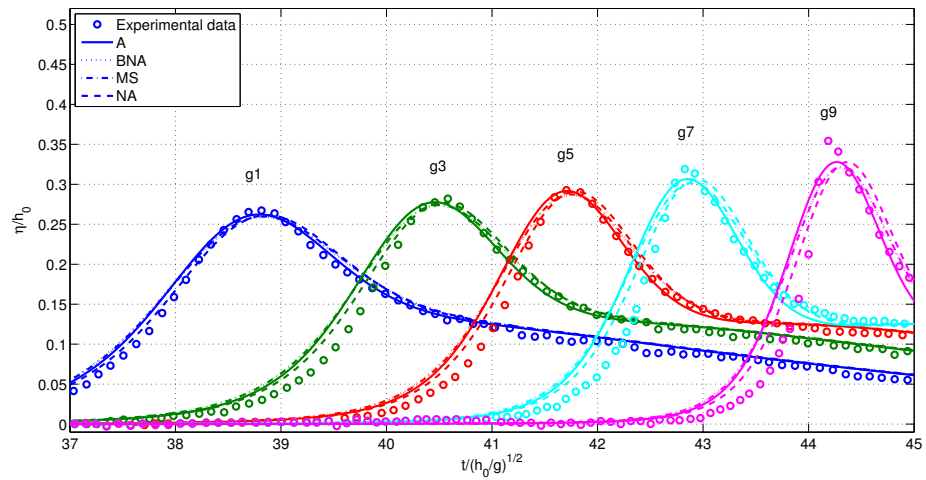


Figure 4.11 – Nonlinear shoaling. Comparison between computed wave heights at gauges 1, 3, 5, 7 and 9 and data of [42] ; models in amplitude-flux form.

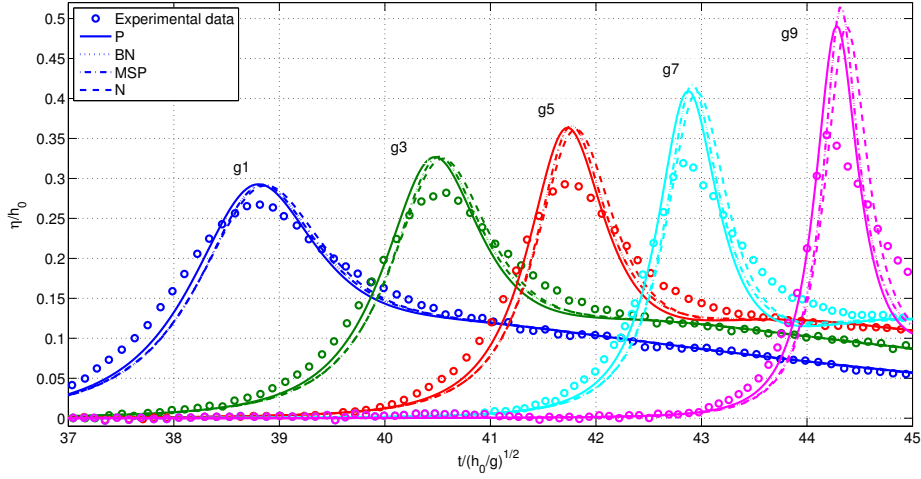


Figure 4.12 – Nonlinear shoaling. Comparison between computed wave heights at gauges 1, 3, 5, 7 and 9 and data of [42] ; models in amplitude-velocity form.

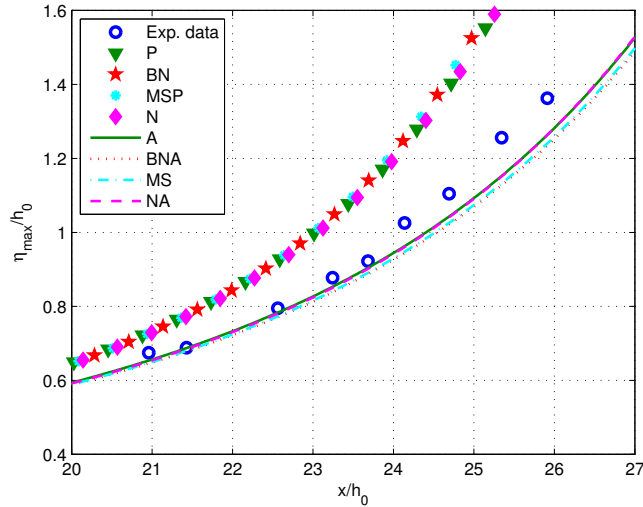


Figure 4.13 – Nonlinear shoaling. Comparison between computed wave peak evolution and data from [42].

The results exhibit two distinct behaviors. All the models in amplitude-velocity form provide waves with considerably higher peaks and fronts with larger slope compared to the data, while all the models in amplitude-flux form give shorter waves with smaller slopes. Note that this behavior is independent of the quality of the linearized system.

This result is extremely important if one wants to use these models in conjunction with a breaking detection plus dissipation mechanism. Indeed, whether based on the slope of the front, on wave curvature, or on wave height, two distinct parametrizations of the detection criterion are necessary for these two family of models. In particular, looking at gauge 9, which is roughly where wave breaking should be detectable, we can see that while amplitude-velocity models

have front slopes and wave heights larger than those of the data, velocity-flux models give lower amplitudes and, more importantly, much smaller front slopes. For criteria based on the shape of the profiles, such as those discussed e.g. in [70, 46], this means that for a given parametrization of the constants involved in the breaking criterion, amplitude-velocity models might give an early breaking, while amplitude-flux models will most likely give a late breaking, or no breaking at all. We remark once more that this result is independent of the quality of the model in terms of linear phase accuracy, the models of Peregrine and Abbott giving results considerably close to their enhanced versions.

Periodic wave propagation over a submerged bar

The last experiment is devoted to the study of the behavior of the models in a more complex situation. We consider the classical tests of monochromatic waves propagating on a submerged bar, for which extensive experimental data are available [10]. The geometry of the experiment is sketched on Figure 4.14. Monochromatic waves are generated and propagate on a depth of $d_0 = 0.4$ m before reaching the submerged bar. The periodic wave shoals over the 1:20 front slope, developing higher harmonics which are then released from the carrier frequency on the 1:10 slope of the lee side of the obstacle. We consider two configurations. Case (a) : wave amplitude $A/d_0 = 0.025$ and period $T = 2.02$ s. Case (b) : wave amplitude $A/d_0 = 0.0675$ and period $T = 2.525$ s. The first case is often used to validate dispersive wave propagation models. In the second case, considerably nonlinear conditions are obtained toward the end of the slope, where breaking is known to occur.

The periodic wave is generated by means of a periodic wave generator located at $x = 10$ m in the domain $[0, 35]$ m and two sponge layers with 3 m of thickness are used at the two boundaries in order to absorb any wave reaching the boundaries. In both cases, the finest grid used has a size of $\Delta_x = 0.04$ m. The numerical results are compared with the data of Beji and Battjes given in [10]. In particular, the first gauge is always used to calibrate the phase of the signal with the experiments, while the other probes are used to compare and validate the models. For further details on the tests and for the exact location of the gauges the interested reader can consult [10, 36, 46].

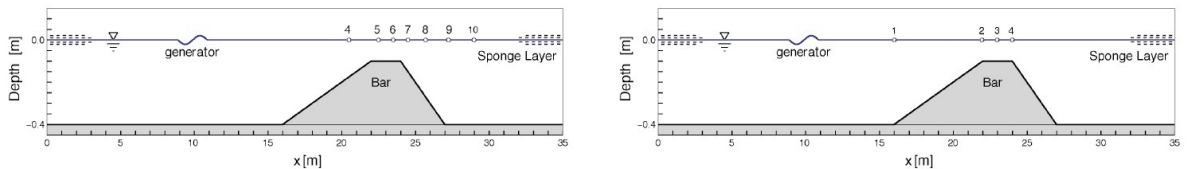


Figure 4.14 – Periodic wave propagation over a submerged bar: sketch of the computational configuration and of the gauges position; case (a) on the left, case (b) on the right.

Case (a). In this case, the wave signal has been phase calibrated w.r.t. the experimental data at gauge 4. The result is presented on Figure 4.15. In Figures 4.16, 4.17, 4.18 and 4.19, we show

the comparison between computed and experimental signals. In all the figures, the continuous lines are used for models in amplitude-flux form, and dashed lines for models in amplitude-velocity form. For brevity, we only consider gauge 5, located on the plateau, and gauge 7, which is placed after the obstacle.

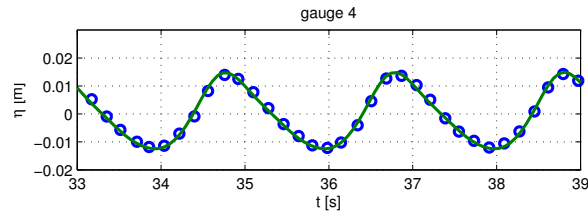


Figure 4.15 – Propagation over a submerged bar, case (a); data in gauge 4 are used for the signal synchronization.

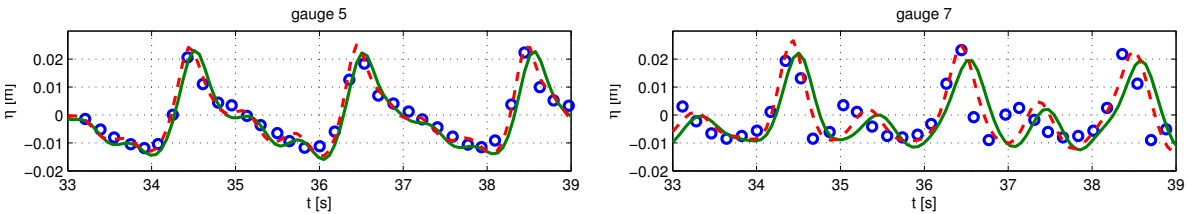


Figure 4.16 – Propagation over a submerged bar, case (a); data in gauge 5 (left) and gauge 7 (right): experimental data [10] (○), A model (—), P model (---).

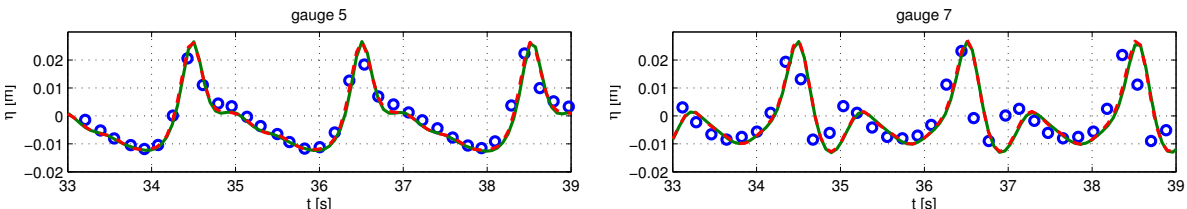


Figure 4.17 – Propagation over a submerged bar, case (a); data in gauge 5 (left) and gauge 7 (right): experimental data [10] (○), BNA model (—), BN model (---).

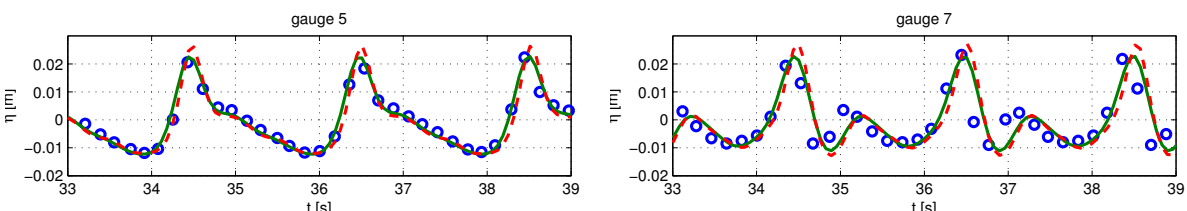


Figure 4.18 – Propagation over a submerged bar, case (a); data in gauge 5 (left) and gauge 7 (right): experimental data [10] (○), MS model (—), MSP model (---).

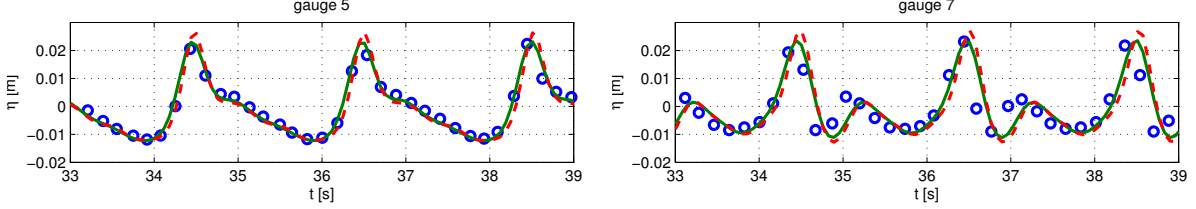


Figure 4.19 – Propagation over a submerged bar, case (a); data in gauge 5 (left) and gauge 7 (right): experimental data [10] (○), NA model (—), N model (---).

The following remarks can be made. On the plateau, after shoaling has occurred, models in amplitude-velocity form give waves which have slightly higher peaks and steeper slopes, however the differences are small (roughly 5% or below). The main remark that can be perhaps made is that the models of Peregrine and Abbott seem to have a larger phase advance in gauge 7 when compared to the other models. This is confirmed by the data reported for completeness in Figure 4.20, where the models of Peregrine and Abbott are compared with the Nwogu enhanced variant, giving results very similar to those of the other models. The picture shows clearly that, for this case, to have a good approximation of the linear dispersion relations is more important than the form of the models.

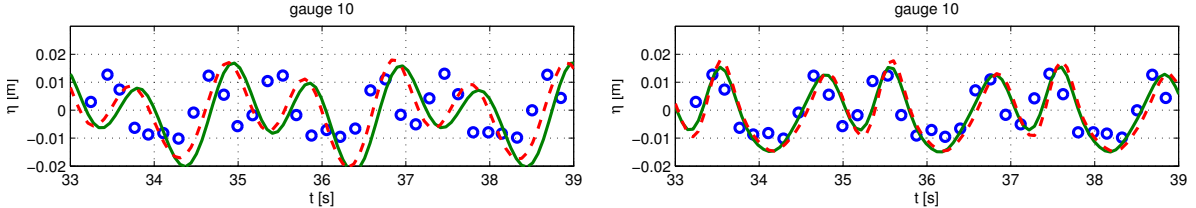


Figure 4.20 – Propagation over a submerged bar, case (a); data in gauge 10 for the models of Peregrine and Abbott (left), and for the enhanced variants of Nwogu and Nwogu-Abbott (right). Experimental data [10] (○). Left figure : A model (—), P model (---). Right figure : NA model (—), N model (---).

Case (b). In this case, wave breaking is expected to occur around gauge 2, at the end of the slope. As already remarked, no breaking criteria are included in our models so that the nonlinear behavior of the Boussinesq models is observed. For this case, the numerical results are phase calibrated w.r.t. experimental data measured at gauge 1, as shown in Figure 4.21.

We then compare the computed wave heights with the data in gauge 2, at the end of the slope, and gauge 4, at the end of the plateau. The results are reported on Figures 4.22, 4.23, 4.24 and 4.25. As before, continuous lines are used for models in amplitude-flux form and dashed lines for models in amplitude-velocity form.

The conclusions are the following : one can observe that already in gauge 2, there is a substantial difference in the height of the peaks. Indeed, models using the amplitude-velocity formulation gives some peaks with taller wave heights with a ratio of more than 20% and consequently, steeper wave fronts. This difference is even more visible in gauge 4, where the difference goes up to more than 35%. Models in amplitude-flux form clearly give gentler slopes

and shorter waves. As for the nonlinear shoaling test presented before, the results are practically independent on the linear characteristics of the systems and depend only on the formulation, that is amplitude-velocity versus amplitude-flux form.

Once more, if one considers wave breaking detection, we see that a same criterion cannot be applied simultaneously to models of the two families, at least not with the same parametrization.

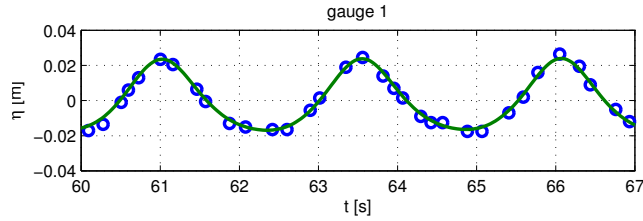


Figure 4.21 – Propagation over a submerged bar, case (b); data in gauge 1 are used for the signal synchronization.

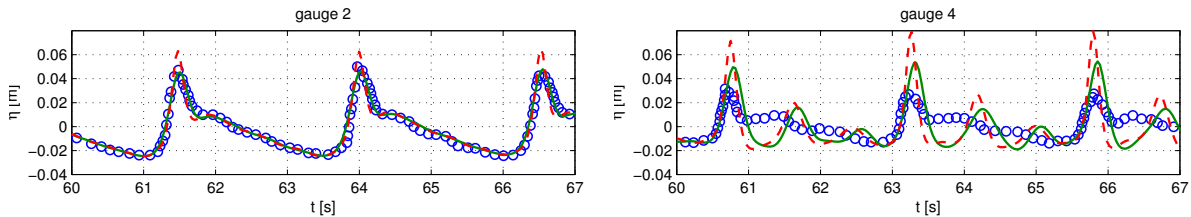


Figure 4.22 – Propagation over a submerged bar, case (b); data in gauge 2 (left) and gauge 4 (right): experimental data [10] (○), A model (—), P model (---).

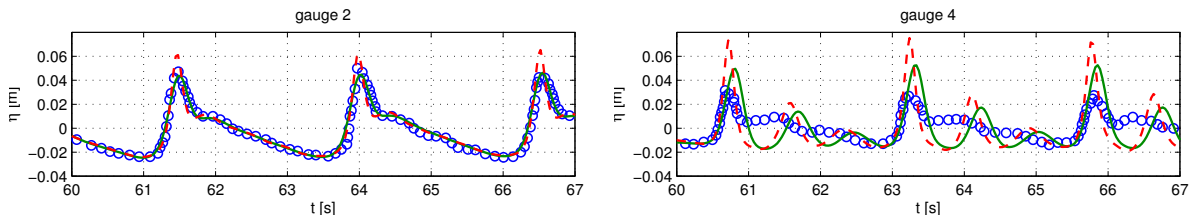


Figure 4.23 – Propagation over a submerged bar, case (b); data in gauge 2 (left) and gauge 4 (right): experimental data [10] (○), BNA model (—), BN model (---).

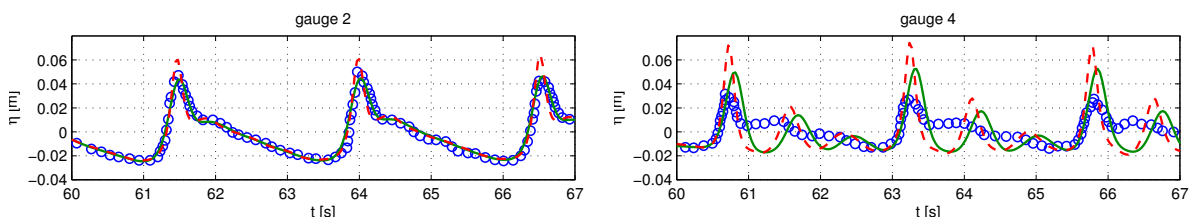


Figure 4.24 – Propagation over a submerged bar, case (b); data in gauge 2 (left) and gauge 4 (right): experimental data [10] (○), MS model (—), MSP model (---).

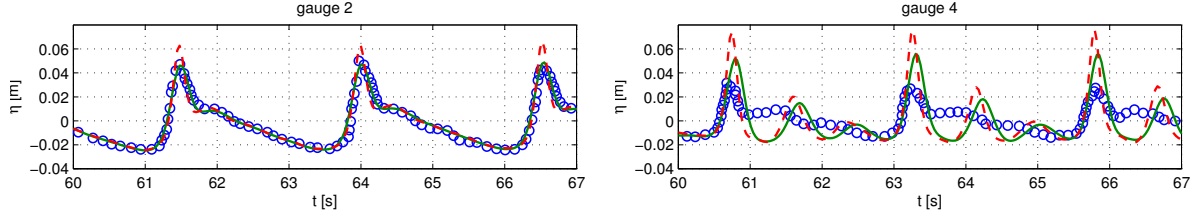


Figure 4.25 – Propagation over a submerged bar, case (b); data in gauge 2 (left) and gauge 4 (right): experimental data [10] (\circ), NA model (—), N model (---).

4.5 Conclusions

In this chapter, we have considered the impact of the formulation of weakly nonlinear Boussinesq models on their behavior in situations in which nonlinearity is not neglectable. We have recalled how, within the same asymptotic truncation, a given linearized form, hence a given dispersion relation and shoaling coefficient, allow to derive two sets of PDEs : one, referred to as amplitude-velocity form, in which dispersive terms contain differential operators applied to the velocity; the other, referred to as amplitude-flux form, in which these operators are applied to the flux.

The analytical and numerical study of these models has shown that : as soon as nonlinear effects start being relevant, the main factor influencing the behavior of the model lies in its formulation, that is amplitude-velocity versus amplitude-flux form, enhanced models giving the same results as the Peregrine or the Abbott equations. This fact has been demonstrated analytically by the study of the propagation of higher harmonics, following [56], and numerically with tests involving shoaling in genuinely nonlinear regimes. While in the linear case we have as many models as the number of linear dispersion relations and linear shoaling coefficients, in the nonlinear case, only two types of behaviors are observed.

This work has important consequences on the way in which wave breaking conditions are applied to these models, as well as on the way in which wave breaking dissipation is included. Clearly, breaking criteria should not be the same for the two family of models, and perhaps even the amount of dissipation in breaking regions necessary in the two cases should be different.

Chapter 5

Discrete asymptotic equations for long wave propagation

Contents

5.1	Introduction	120
5.2	Context and notations	120
5.3	Galerkin discretization of the Peregrine equations	122
5.4	A new setting to derive discrete asymptotic models	124
5.4.1	Semi-discretization of the 2D-Euler equations in non-dimensional form	124
5.4.2	Asymptotic expansions on the velocity U and the pressure P	127
5.4.3	Depth-averaged equations	130
5.5	Study of the linear dispersion characteristics.	133
5.5.1	Linear characteristics of the new numerical model.	133
5.5.2	Linear characteristics of the classical Peregrine model.	138
5.5.3	Analysis of the computations	139
5.6	Numerical experiments	142
5.6.1	Soliton propagation	142
5.6.2	Linear dispersion and linear shoaling test	143
5.7	Conclusions and perspectives	145

5.1 Introduction

Wave transformation in near shore zone is well-described by the incompressible Euler equations. Due to their three-dimensional character, these equations are often too costly if one wants to perform numerical experiments, and often replaced by asymptotic depth-averaged models known as Boussinesq equations. A major characteristic of these models is their ability to describe the dispersive behavior of wave propagation. Generally, the linear and nonlinear dispersion characteristics of the waves represented by Boussinesq models can be improved by including high order contributions in the double asymptotic expansion in terms of the ratios wave height over wave length (dispersion) and wave height over depth (nonlinearity) [51]. Other techniques to improve the linear dispersion characteristics involve the inclusion of extra dispersive differential terms, derived either from a linear wave equation [11, 55], or by replacing depth-averaged values by point values at a properly chosen depth [60]. When numerically simulating the propagation of long waves, the physics represented by these continuous systems of Partial Differential Equations (PDE) is further filtered by the numerical scheme, and in particular by the form of the truncation error. For most of Boussinesq models, the task of designing an accurate numerical discretization is a nontrivial one, due to the presence of dispersion terms. Several approaches exist in literature, each with its own advantages and drawbacks. For details, the interested reader may refer to [17, 21, 38, 45, 59, 64], to the review [23], and references there in. One of the questions not addressed in almost all the relevant literature is the one of the interaction between models and schemes truncation : these are related to the neglected asymptotic terms in one case, and to the truncation error in the other. The objective of this chapter is to study the interaction scheme-PDE and to propose a framework to obtain new schemes with improved characteristics w.r.t. existing approaches. For this purpose, we reverse the model derivation procedure. More precisely, we propose to discretize partially the incompressible Euler equations in the horizontal direction using a finite element method, and then perform a formal asymptotic analysis similar to the one used to derive continuous Boussinesq equations. For that purpose, we choose the simplest Boussinesq system : The Peregrine equations. This new paradigm leads to a very promising scheme with improved dispersion properties.

The chapter is organized as follows. In Section 5.2 we introduce some important notation. The finite element discretization of a well known Boussinesq system (Peregrine one), and most of the algebraic operators involved in our analysis are presented in Section 5.3. The Section 5.4 is devoted to the derivation of the new numerical scheme. The theoretical analysis of these discrete asymptotic models is presented in Section 5.5. Finally, Section 5.6 presents a numerical evaluation of the performances of the schemes confirming our theoretical results.

5.2 Context and notations

For simplicity, we only deal with 2-D and 1-D problems. Denote by (x, z) respectively the horizontal and the vertical spatial dimension. Denote by $d(x)$ the depth at still water and $\eta(t, x)$ the surface elevation from its rest position. The total depth is then $h(t, x) = d(x) + \eta(t, x)$ (see

Figure 5.1).

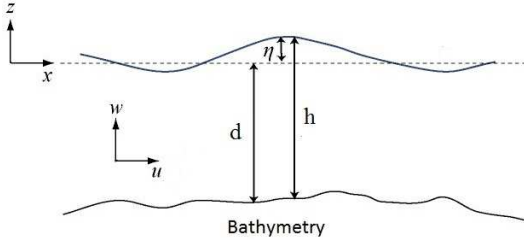


Figure 5.1 – Sketch of the free surface flow problem, main parameters description.

Let a be a typical wave amplitude, d_0 a reference water depth and λ a typical wavelength. In view of performing an asymptotic analysis, we introduce the nonlinearity parameter ε and the dispersion parameter σ defined by

$$\varepsilon = \frac{a}{d_0}, \quad \sigma = \frac{d_0}{\lambda}.$$

Under the Boussinesq hypothesis $\varepsilon = \mathcal{O}(\sigma^2)$, Peregrine first derived (see [63] or Section 2.5.1), from the Euler equations, the following standard system of Boussinesq's type

$$\begin{aligned} \eta_t + (h\bar{u})_x &= 0, \\ \bar{u}_t + \bar{u}\bar{u}_x + g\eta_x + \left(\frac{d^2}{6}\bar{u}_{txx} - \frac{d}{2}(d\bar{u})_{txx}\right) &= 0. \end{aligned} \tag{5.2.1}$$

The model describes the evolution of the depth-averaged velocity \bar{u} and the surface elevation η within an accuracy of $\mathcal{O}(\varepsilon\sigma^2, \sigma^4)$ w.r.t. the Euler equations. The set of Equations (5.2.1) is now well-understood from the computational point of view and a classical numerical scheme can be obtained by using the finite element method in the following setting. On an interval $[r, s]$, we introduce a set of nodes

$$r = x_0 < x_1 < \dots < x_N = s,$$

where we take a constant space step $\Delta_x = x_{i+1} - x_i, \forall i \in \{0, \dots, N-1\}$. For simplicity, we deal with periodic boundary conditions with the convention $x_{-1} = x_N$ and $x_{N+1} = x_0$.

We denote by E , \bar{U} , D and H the vectors of the nodal values of η , \bar{u} , d and h . Similarly to what has been done in [73, 72] (cf. also [64] and references therein), we apply the \mathbb{P}_1 Galerkin method to approximate the variational form of (5.2.1). In particular, we denote by $\{\varphi_i\}_{0 \leq i \leq N}$ the standard piecewise linear continuous Lagrange basis, and introduce the discrete velocity, wave height and depth polynomials as follows

$$\bar{u}_\Delta(t, x) = \sum_{i=0}^N \bar{u}_i(t)\varphi_i(x), \quad \eta_\Delta(t, x) = \sum_{i=0}^N \eta_i(t)\varphi_i(x), \quad d_\Delta(x) = \sum_{i=0}^N d_i\varphi_i(x). \tag{5.2.2}$$

In addition, for given columns vectors $A = (a_i)_{0 \leq i \leq N}$ and $B = (b_i)_{0 \leq i \leq N}$, we introduce the operator \diamond used to propose a matrix compact formulation of the numerical schemes. It is defined as :

$$\begin{aligned} \mathbb{R}^N \times \mathbb{R}^N &\rightarrow \mathbb{R}^N \\ (A, B) &\rightarrow A \diamond B := (a_i b_i)_{0 \leq i \leq N} \end{aligned}$$

In the sequel, A^2 simplifies $A \diamond A$. As an example, the vector $(h_i(\mathcal{N}\bar{U})_i)_{i \in \{0, \dots, N\}}$ can be rewritten as $H \diamond (\mathcal{N}\bar{U})$, where \mathcal{N} is the first order derivative matrix. In the next section, we apply the Galerkin method to equations (5.2.1) in order to give a scheme which will be used as a reference one in the sequel and to familiarize the reader with the notations.

5.3 Galerkin discretization of the Peregrine equations

We start by deriving a spatially discretized version of (5.2.1) using the Galerkin finite element scheme. Since we deal with varying bathymetry, we first rewrite (5.2.1) by expanding the derivatives terms

$$\eta_t + ((d + \eta)\bar{u})_x = 0, \quad (5.3.1)$$

$$\bar{u}_t + \bar{u}\bar{u}_x + g\eta_x - \frac{d^2}{3}\bar{u}_{txx} - dd_x\bar{u}_{tx} - \frac{dd_{xx}}{2}\bar{u}_t = 0. \quad (5.3.2)$$

According to the Galerkin method (see [37]) using \mathbb{P}_1 function, we multiply (5.3.1) by the Galerkin basis φ_i and we integrate the resulting equation between x_{i-1} and x_{i+1} , for $i \in \{0, \dots, N\}$, with the convention $x_{-1} = x_N$ and $x_{N+1} = x_0$ coming from the choice of the periodic boundary conditions to obtain

$$\frac{d}{dt} \int_{x_{i-1}}^{x_{i+1}} \eta_\Delta(t, x)\varphi_i(x)dx - \int_{x_{i-1}}^{x_{i+1}} (d_\Delta(x) + \eta_\Delta(t, x))\bar{u}_\Delta(t, x)\varphi'_i(x)dx = 0. \quad (5.3.3)$$

In the \mathbb{P}_1 case, evaluating all the integrals exactly w.r.t. the linear spatial variation of d_Δ , η_Δ , and \bar{u}_Δ , we derive from (5.3.3), using the decomposition (5.2.2) and evaluating all the integrals involving φ_i , for all $i \in \{0, \dots, N\}$

$$\begin{aligned} &\frac{\Delta_x}{6} \frac{\partial}{\partial t} (\eta_{i+1} + 4\eta_i + \eta_{i-1}) \\ &+ \frac{1}{3} \left(2 \frac{h_{i+1}\bar{u}_{i+1} - h_{i-1}\bar{u}_{i-1}}{2} + h_i \frac{\bar{u}_{i+1} - \bar{u}_{i-1}}{2} + \bar{u}_i \frac{h_{i+1} - h_{i-1}}{2} \right) = 0. \end{aligned} \quad (5.3.4)$$

Applying the same procedure to Equation (5.3.2), one has, performing integration by parts, for all $i \in \{0, \dots, N\}$,

$$\begin{aligned} &\int_{x_{i-1}}^{x_{i+1}} \frac{d}{dt} \bar{u}_\Delta(t, x)\varphi_i(x)dx - \int_{x_{i-1}}^{x_{i+1}} \left(\frac{\bar{u}_\Delta^2(t, x)}{2} + g\eta_\Delta(t, x) \right) \varphi'_i(x)dx \\ &+ \int_{x_{i-1}}^{x_{i+1}} \left(-\varphi_i(x)dd'_\Delta(\bar{u}_\Delta)_{tx} + \frac{(d_\Delta^2(x)\varphi_i(x))_x}{3}(\bar{u}_\Delta(t, x))_{tx} + \frac{(\varphi_i(x)d_\Delta(x)(\bar{u}_\Delta(t, x))_t)_x}{2}d'_\Delta \right) dx \\ &= 0. \end{aligned} \quad (5.3.5)$$

Plugging relations (5.2.2) in (5.3.5), one derives after the computation of the different integrals, for all $i \in \{0, \dots, N\}$

$$\begin{aligned} & \frac{\Delta_x}{6} \frac{d}{dt} (\bar{u}_{i+1} + 4\bar{u}_i + \bar{u}_{i-1}) + \frac{1}{3} \left(\frac{\bar{u}_{i+1}^2 - \bar{u}_{i-1}^2}{2} + \bar{u}_i \frac{\bar{u}_{i+1} - \bar{u}_{i-1}}{2} \right) + g \frac{\eta_{i+1} - \eta_{i-1}}{2} \\ & - \frac{1}{6\Delta_x} \frac{d}{dt} \left(2d_i \bar{u}_i (d_{i+1} - 2d_i + d_{i-1}) + (d_{i+1}^2 \bar{u}_{i+1} - 2d_i^2 \bar{u}_i + d_{i-1}^2 \bar{u}_{i-1}) \right. \\ & \left. + d_i (d_{i+1} \bar{u}_{i+1} - 2d_i \bar{u}_i + d_{i-1} \bar{u}_{i-1}) - \bar{u}_i (d_{i+1}^2 - 2d_i^2 + d_{i-1}^2) \right) = 0. \end{aligned} \quad (5.3.6)$$

In order to rewrite the discrete equations (5.3.6) in a simpler and more compact form, we define the mass matrix \mathcal{M} , the first order derivative matrix \mathcal{N} and the second order derivative matrix \mathcal{Q} (which represents the laplacian operator) with periodic boundary conditions as follows

$$\begin{aligned} \mathcal{M} &= \frac{1}{6} \begin{pmatrix} 4 & 1 & 0 & \cdots & 0 & 1 \\ 1 & \ddots & \ddots & \ddots & & 0 \\ 0 & \ddots & \ddots & \ddots & \ddots & \vdots \\ \vdots & \ddots & \ddots & \ddots & \ddots & 0 \\ 0 & \ddots & \ddots & \ddots & 1 & \\ 1 & 0 & \cdots & 0 & 1 & 4 \end{pmatrix}, \quad \mathcal{N} = \frac{1}{2\Delta_x} \begin{pmatrix} 0 & 1 & 0 & \cdots & 0 & -1 \\ -1 & \ddots & \ddots & \ddots & & 0 \\ 0 & \ddots & \ddots & \ddots & \ddots & \vdots \\ \vdots & \ddots & \ddots & \ddots & \ddots & 0 \\ 0 & & \ddots & \ddots & \ddots & 1 \\ 1 & 0 & \cdots & 0 & -1 & 0 \end{pmatrix}, \\ \mathcal{Q} &= \frac{1}{\Delta_x^2} \begin{pmatrix} -2 & 1 & 0 & \cdots & 0 & 1 \\ 1 & \ddots & \ddots & \ddots & & 0 \\ 0 & \ddots & \ddots & \ddots & \ddots & \vdots \\ \vdots & \ddots & \ddots & \ddots & \ddots & 0 \\ 0 & & \ddots & \ddots & \ddots & 1 \\ 1 & 0 & \cdots & 0 & 1 & -2 \end{pmatrix}. \end{aligned}$$

In addition, we introduce the following column vectors

$$\bar{U} = (\bar{u}_i)_{0 \leq i \leq N}, \quad E = (\eta_i)_{0 \leq i \leq N}, \quad D = (d_i)_{0 \leq i \leq N}, \quad H = D + E.$$

Equation (5.3.4) can thus be written as

$$\frac{d}{dt} \mathcal{M}E + \frac{1}{3} \left(2\mathcal{N}(h_i \bar{u}_i)_{i \in \{0, \dots, N\}} + (h_i(\mathcal{N}\bar{U})_i)_{i \in \{0, \dots, N\}} + (\bar{u}_i(\mathcal{N}H)_i)_{i \in \{0, \dots, N\}} \right) = 0.$$

Using the operator \diamond introduced previously, the discrete equations (5.3.4)-(5.3.6) can be compactly written as

$$\mathcal{M} \frac{d}{dt} E + \frac{1}{3} (2\mathcal{N}(H \diamond \bar{U}) + H \diamond (\mathcal{N}\bar{U}) + \bar{U} \diamond (\mathcal{N}H)) = 0, \quad (5.3.7)$$

$$\frac{d}{dt} \mathcal{M}\bar{U} + \frac{1}{3} (\mathcal{N}(\bar{U}^2) + \bar{U} \diamond (\mathcal{N}\bar{U})) + g\mathcal{N}E - \frac{1}{6}\{D; \bar{U}_t\} = 0, \quad (5.3.8)$$

where we have introduced

$$\{D; \bar{U}_t\} = Q(D^2 \diamond \bar{U}_t) + D \diamond (Q(D \diamond \bar{U}_t)) + 2(D \diamond \bar{U}_t) \diamond (QD) - \bar{U}_t \diamond (QD^2). \quad (5.3.9)$$

Equations (5.3.7)-(5.3.8) will be taken in the sequel as the classical scheme for the Peregrine equations and be used in Sections 5.5 and 5.6 to make some comparison with the new scheme introduced in the next section.

5.4 A new setting to derive discrete asymptotic models

We recall that the aim of this chapter is to propose a systematic method to obtain new numerical models describing free surface flows. It is based on the following idea : reverse the model derivation procedure and *first discretize partially the Incompressible Euler equations and then derive fully discrete asymptotic equations by performing an asymptotic analysis*. In this Section, we illustrate the potential of this idea, applying this method to the couple Euler-Peregrine equations. We apply the Galerkin method to the variable x and then we perform the asymptotic analysis of Peregrine's type to the resulting equations. Of course, when one deals with non-linear equations, this procedure does not commute with the classical one. This strategy is similar to the one proposed for compressible multiphase flows in [2].

5.4.1 Semi-discretization of the 2D-Euler equations in non-dimensional form

We start from the 2D-Euler equations written in terms of velocity (u, w) , pressure p , constant density ρ and vertical gravity acceleration g :

$$u_t + uu_x + wu_z + \frac{p_x}{\rho} = 0, \quad (5.4.1)$$

$$w_t + uw_x + ww_z + \frac{p_z}{\rho} + g = 0, \quad (5.4.2)$$

$$u_x + w_z = 0, \quad (5.4.3)$$

$$u_z - w_x = 0, \quad (5.4.4)$$

where the last equation represents the irrotationality condition. For simplicity we discuss in this chapter the two-dimensional case, but the derivation in the 3D case is quite similar and will be reported elsewhere. We consider periodic boundary conditions in the x direction, while on the free surface and sea-bed level we use the classical conditions :

- at the free surface $z = \eta$

$$w = \eta_t + u\eta_x, \quad p = 0, \quad (5.4.5)$$

- on the seafloor $z = -d$

$$w = -ud_x. \quad (5.4.6)$$

Let d_0 be the averaged depth, a a typical wave amplitude, and λ a typical wavelength. The following usual non-dimensional variables are introduced

$$\tilde{x} = \frac{x}{\lambda}, \quad \tilde{z} = \frac{z}{d_0}, \quad \tilde{t} = \frac{\sqrt{gd_0}}{\lambda} t, \quad \tilde{\eta} = \frac{\eta}{a}, \quad \tilde{u} = \frac{d_0}{a\sqrt{gd_0}} u, \quad \tilde{w} = \frac{\lambda}{a} \frac{1}{\sqrt{gd_0}} w, \quad \tilde{p} = \frac{p}{gd_0\rho}, \quad \Delta_{\tilde{x}} = \frac{\Delta_x}{\lambda}, \quad \tilde{d} = \frac{d}{d_0}.$$

Using the notation introduced above, the Euler equations and the irrotationality condition can be recast in a non-dimensional form as

$$\varepsilon \tilde{u}_{\tilde{t}} + \varepsilon^2 \tilde{u} \tilde{u}_{\tilde{x}} + \varepsilon^2 \tilde{w} \tilde{u}_{\tilde{z}} + \tilde{p}_{\tilde{x}} = 0, \quad (5.4.7)$$

$$\varepsilon \sigma^2 \tilde{w}_{\tilde{t}} + \varepsilon^2 \sigma^2 \tilde{u} \tilde{w}_{\tilde{x}} + \varepsilon^2 \sigma^2 \tilde{w} \tilde{w}_{\tilde{z}} + \tilde{p}_{\tilde{z}} + 1 = 0, \quad (5.4.8)$$

$$\tilde{u}_{\tilde{x}} + \tilde{w}_{\tilde{z}} = 0, \quad (5.4.9)$$

$$\tilde{u}_{\tilde{z}} - \sigma^2 \tilde{w}_{\tilde{x}} = 0 \quad (\text{so } \tilde{u}_{\tilde{z}} = \mathcal{O}(\sigma^2)). \quad (5.4.10)$$

The boundary conditions become :

- at the free surface $\tilde{z} = \varepsilon \tilde{\eta}$

$$\tilde{w} = \tilde{\eta}_{\tilde{t}} + \varepsilon \tilde{u} \tilde{\eta}_{\tilde{x}}, \quad \tilde{p} = 0, \quad (5.4.11)$$

- at the bed $\tilde{z} = -\tilde{d}$

$$\tilde{w} = -\tilde{u} \tilde{d}_{\tilde{x}}. \quad (5.4.12)$$

Our goal is to obtain a Boussinesq's type approximation of the Euler system (5.4.7)-(5.4.12), under the assumptions $\varepsilon \ll 1$, $\sigma \ll 1$, and in the specific weakly nonlinear regime $\varepsilon = \mathcal{O}(\sigma^2)$, meaning that there exists constant $C > 0$ such that $\varepsilon \leq C\sigma^2$. We now apply a Galerkin method on the variable x keeping t and z unchanged. *It is assumed that $\Delta_{\tilde{x}} = \mathcal{O}(\sigma)$ (it transpires that $\Delta_x = \mathcal{O}(d_0)$).* In the sequel, for simplicity, we drop the " ~ " and we introduce for all $i \in \{0, \dots, N\}$,

$$u_i(t, z) = u(t, x_i, z), \quad w_i(t, z) = w(t, x_i, z), \quad \eta_i(t) = \eta(t, x_i), \quad p_i(t, z) = p(t, x_i, z).$$

In addition, the discrete horizontal velocity, wave height, depth, vertical velocity and pressure polynomials are written in the Galerkin basis as follows

$$\begin{aligned} u_{\Delta}(t, x, z) &= \sum_{i=0}^N u_i(t, z) \varphi_i(x), \quad w_{\Delta}(t, x, z) = \sum_{i=0}^N w_i(t, z) \varphi_i(x), \quad \eta_{\Delta}(t, x) = \sum_{i=0}^N \eta_i(t) \varphi_i(x), \\ p_{\Delta}(t, x, z) &= \sum_{i=0}^N p_i(t, z) \varphi_i(x), \quad d_{\Delta}(x) = \sum_{i=0}^N d_i \varphi_i(x). \end{aligned} \quad (5.4.13)$$

We recall that we focus on periodic boundary condition that is we introduce $x_{-1} = x_N$ and $x_{N+1} = x_0$. Note that the adaptation of our method with general boundary conditions is a full working that is going to be studied in future (the existence of solutions for Boussinesq

equations is not trivial even for Dirichlet conditions [3]). The finite element discrete equations corresponding to (5.4.7)-(5.4.8)-(5.4.9)-(5.4.10) can be written as, for all $i \in \{0, \dots, N\}$

$$\varepsilon \frac{\Delta_x}{6} \frac{d}{dt} (u_{i+1} + 4u_i + u_{i-1}) + \frac{\varepsilon^2}{3} \left(\frac{u_{i+1}^2 - u_{i-1}^2}{2} + u_i \frac{u_{i+1} - u_{i-1}}{2} \right) + \frac{p_{i+1} - p_{i-1}}{2} = \mathcal{O}(\varepsilon^2 \sigma^2), \quad (5.4.14)$$

$$\varepsilon \sigma^2 \frac{\Delta_x}{6} \frac{d}{dt} (w_{i+1} + 4w_i + w_{i-1}) + \frac{\Delta_x}{6} \frac{d}{dz} (p_{i+1} + 4p_i + p_{i-1}) + \Delta_x = \mathcal{O}(\varepsilon^2 \sigma^2), \quad (5.4.15)$$

$$\frac{u_{i+1} - u_{i-1}}{2} + \frac{\Delta_x}{6} \frac{d}{dz} (w_{i+1} + 4w_i + w_{i-1}) = 0, \quad (5.4.16)$$

$$\frac{\Delta_x}{6} \frac{d}{dz} (u_{i+1} + 4u_i + u_{i-1}) - \sigma^2 \frac{w_{i+1} - w_{i-1}}{2} = 0. \quad (5.4.17)$$

For the boundary conditions, we propose to integrate (5.4.11) along the curve $z = \varepsilon\eta$ and equation (5.4.12) along the curve $z = -d$. For that purpose, we choose to introduce

$$\begin{aligned} \hat{w}_\Delta &= \sum_{i=0}^N w_i(t, \varepsilon\eta(t, x_i)) \varphi_i(x), & \check{w}_\Delta &= \sum_{i=0}^N w_i(t, -d(x_i)) \varphi_i(x), \\ \hat{u}_\Delta &= \sum_{i=0}^N u_i(t, \varepsilon\eta(t, x_i)) \varphi_i(x), & \check{u}_\Delta &= \sum_{i=0}^N u_i(t, -d(x_i)) \varphi_i(x). \end{aligned} \quad (5.4.18)$$

The boundary conditions (5.4.11)-(5.4.12) then write

- at the free surface

$$\begin{aligned} \frac{\Delta_x}{6} \left(\hat{w}_{i+1}(t) + 4\hat{w}_i(t) + \hat{w}_{i-1}(t) \right) &= \frac{\Delta_x}{6} \frac{d}{dt} \left(\eta_{i+1}(t) + 4\eta_i(t) + \eta_{i-1}(t) \right) \\ &+ \frac{1}{3} \left(\frac{\varepsilon\eta_{i+1}(t)\hat{u}_{i+1}(t) - \varepsilon\eta_{i-1}(t)\hat{u}_{i-1}(t)}{2} \right. \\ &\left. - \varepsilon\eta_i(t) \frac{\hat{u}_{i+1}(t) - \hat{u}_{i-1}(t)}{2} + 2\hat{u}_i(t) \frac{\varepsilon\eta_{i+1}(t) - \varepsilon\eta_{i-1}(t)}{2} \right), \end{aligned} \quad (5.4.19)$$

$$\frac{\Delta_x}{6} \left(p_{i+1}(t, \varepsilon\eta_{i+1}) + 4p_i(t, \varepsilon\eta_i) + p_{i-1}(t, \varepsilon\eta_{i-1}) \right) = 0, \quad (5.4.20)$$

- at the bed

$$\begin{aligned} \frac{\Delta_x}{6} \left(\check{w}_{i+1}(t) + 4\check{w}_i(t) + \check{w}_{i-1}(t) \right) &= \\ -\frac{1}{3} \left(\frac{d_{i+1}\check{u}_{i+1}(t) - d_{i-1}\check{u}_{i-1}(t)}{2} - d_i \frac{\check{u}_{i+1}(t) - \check{u}_{i-1}(t)}{2} + 2\check{u}_i(t) \frac{d_{i+1} - d_{i-1}}{2} \right). \end{aligned} \quad (5.4.21)$$

Introducing the following column vector

$$W = (w_i)_{0 \leq i \leq N}, \quad U = (u_i)_{0 \leq i \leq N}, \quad E = (\eta_i)_{0 \leq i \leq N}, \quad P = (p_i)_{0 \leq i \leq N}, \quad D = (d_i)_{0 \leq i \leq N}, \quad \mathcal{I} = \begin{pmatrix} 1 \\ \vdots \\ 1 \end{pmatrix}$$

$$\hat{W} = \left(w_i(\varepsilon\eta_i) \right)_{0 \leq i \leq N}, \quad \hat{U} = \left(u_i(\varepsilon\eta_i) \right)_{0 \leq i \leq N}, \quad \check{W} = \left(w_i(-d_i) \right)_{0 \leq i \leq N}, \quad \check{U} = \left(u_i(-d_i) \right)_{0 \leq i \leq N},$$

we can rewrite Equations (5.4.14)-(5.4.21) into the following matrix-form :

$$\varepsilon \frac{d}{dt} \mathcal{M}U + \frac{\varepsilon^2}{3} (\mathcal{N}(U^2) + U \diamond (\mathcal{N}U)) + \mathcal{N}P = \mathcal{O}(\varepsilon^2\sigma^2), \quad (5.4.22)$$

$$\varepsilon\sigma^2 \frac{d}{dt} \mathcal{M}W + \frac{d}{dz} \mathcal{M}P + \mathcal{I} = \mathcal{O}(\varepsilon^2\sigma^2), \quad (5.4.23)$$

$$\mathcal{N}U + \mathcal{M} \frac{d}{dz} W = 0, \quad (5.4.24)$$

$$\mathcal{M} \frac{d}{dz} U - \sigma^2 \mathcal{N}W = 0. \quad (5.4.25)$$

The boundary conditions become

- at the free surface

$$\mathcal{M}\hat{W} = \frac{d}{dt} \mathcal{M}E + \frac{\varepsilon}{3} \left(\mathcal{N}(E \diamond \hat{U}) - E \diamond (\mathcal{N}\hat{U}) + 2\hat{U} \diamond (\mathcal{N}E) \right), \quad \mathcal{M}\hat{P} = 0, \quad (5.4.26)$$

- at the bottom

$$\mathcal{M}\check{W} = -\frac{1}{3} \left(\mathcal{N}(D \diamond \check{U}) - D \diamond (\mathcal{N}\check{U}) + 2\check{U} \diamond (\mathcal{N}D) \right). \quad (5.4.27)$$

System (5.4.22)-(5.4.27) represents the first step in our analysis. The next two sections are dedicated to the transformation of this system into an asymptotic set of equations.

5.4.2 Asymptotic expansions on the velocity U and the pressure P

In this section, we derive an asymptotic expansion in terms of σ for the semi-discrete horizontal velocity $U = U(t, z)$ following the procedure presented by Peregrine in [63]. More precisely, we prove the following proposition.

Proposition 4 (Discrete asymptotic consistency). *The pressure P and the velocity U satisfy expansions of the form*

$$P = \varepsilon E - z\mathcal{I} + \varepsilon\sigma^2 \left(\frac{z^2}{2} \mathcal{K}\bar{U} + z[D; \bar{U}] \right) + \mathcal{O}(\varepsilon^2\sigma^2, \varepsilon\sigma^4),$$

$$U = \bar{U} + \sigma^2 \left(\frac{D^2}{6} \diamond (\mathcal{K}^2\bar{U}) - \frac{z^2}{2} \mathcal{K}^2\bar{U} - z\mathcal{K}[D; \bar{U}] - \frac{D}{2} \diamond (\mathcal{K}[D; \bar{U}]) \right) + \mathcal{O}(\varepsilon\sigma^2, \sigma^4),$$

where the averaged velocity $\bar{U} = \bar{U}(t)$ is defined in (5.4.37).

Proof. Since \mathcal{M} is invertible, we obtain from the integration of (5.4.25) between 0 and an arbitrary depth z ,

$$U(t, z) = U^0(t) + \mathcal{O}(\sigma^2), \quad (5.4.28)$$

where $U^0(t)$ is a matrix vector depending only on t and corresponds to the value of U at $z = 0$. Substituting Relation (5.4.28) in Equation (5.4.24) and setting $\mathcal{K} = \mathcal{M}^{-1}\mathcal{N}$, we derive

$$\frac{d}{dz}W = -\mathcal{K}U^0 + \mathcal{O}(\sigma^2). \quad (5.4.29)$$

Integrating each line $i \in \{0, \dots, N\}$ of Equation (5.4.29) with respect to z between $-d_i$ and an arbitrary depth z ($-d_i < z < \epsilon\eta_i$), using the boundary condition (5.4.27) and the estimates (5.4.28) on U , we obtain

$$W = -(z\mathcal{I} + D) \diamond (\mathcal{K}U^0) - \frac{1}{3} \left(\mathcal{K}(D \diamond U^0) - \mathcal{M}^{-1}(D \diamond (\mathcal{N}U^0)) + 2\mathcal{M}^{-1}(U^0 \diamond (\mathcal{N}D)) \right) + \mathcal{O}(\sigma^2). \quad (5.4.30)$$

In view of (5.4.30), it is natural to introduce the following bracket

$$[A; B] = A \diamond (\mathcal{K}B) + \frac{1}{3} \left(\mathcal{K}(A \diamond B) - \mathcal{M}^{-1}(A \diamond (\mathcal{N}B)) + 2\mathcal{M}^{-1}(B \diamond (\mathcal{N}A)) \right). \quad (5.4.31)$$

Considering this notation, Equation (5.4.30) becomes

$$W = - \left(z(\mathcal{K}U^0) + [D; U^0] \right) + \mathcal{O}(\sigma^2). \quad (5.4.32)$$

Plugging (5.4.32) in (5.4.25) and integrating the resulting equation between 0 and z , one derives the following expansion on U

$$U = U^0 - \sigma^2 \left(\frac{z^2}{2} \mathcal{K}^2 U^0 + z[D; U^0] \right) + \mathcal{O}(\sigma^4). \quad (5.4.33)$$

Looking for a similar expansion on the pressure array P , we substitute Equation (5.4.32) in Equation (5.4.23). Using the fact that $\mathcal{M}\mathcal{I} = \mathcal{I}$, we obtain

$$\frac{d}{dz}P = -\mathcal{I} - \epsilon\sigma^2 \frac{d}{dt} \left(z\mathcal{K}U^0 + [D; U^0] \right) + \mathcal{O}(\epsilon^2\sigma^2, \epsilon\sigma^4). \quad (5.4.34)$$

Furthermore, integrating each line $i \in \{0, \dots, N\}$ of Equation (5.4.34) with respect to z from an arbitrary depth to the free surface $\epsilon\eta_i$, we can write

$$P = \epsilon E - z\mathcal{I} + \epsilon\sigma^2 \left(\frac{z^2}{2} \mathcal{K}U^0 + z[D; U^0] \right) + \mathcal{O}(\epsilon^2\sigma^2, \epsilon\sigma^4). \quad (5.4.35)$$

Substituting Equations (5.4.35) and (5.4.33) in (5.4.22), we obtain an equation for the zero-th order velocity U^0 , equivalent to Equation 2.28 in [72], which reads :

$$\frac{d}{dt}\mathcal{M}U^0 + \frac{\epsilon}{3} (\mathcal{N}(U^0 \diamond U^0) + U^0 \diamond (\mathcal{N}U^0)) + \mathcal{N}E = \mathcal{O}(\epsilon\sigma^2, \sigma^4). \quad (5.4.36)$$

Note that the choice of the constant of integration in (5.4.28) is not unique. However it transpires that the choice of U^0 (which is the value of the horizontal velocity U at $z = 0$) is not optimal as observed in [72]. This is why, in the sequel, we are going to get rid of it by introducing the averaged velocity matrix $\bar{U} = (\bar{u}_i)_{0 \leq i \leq N}$ where

$$\bar{u}_i(t) = \frac{1}{d_i + \varepsilon\eta_i} \int_{-d_i}^{\varepsilon\eta_i} u_i(t, z) dz, \quad (5.4.37)$$

and by looking for an equation satisfied by \bar{U} . In this direction, we first derive the relation between U^0 and \bar{U} . Equation (5.4.33) provides, for all $i \in \{0, \dots, N\}$,

$$u_i = u_i^0 - \sigma^2 \left(\frac{z^2}{2} (\mathcal{K}^2 U^0)_i + z (\mathcal{K}[D; U^0])_i \right) + \mathcal{O}(\sigma^4),$$

and by integration between $-d_i$ and $\varepsilon\eta_i$, we immediately get, using Taylor expansion,

$$\begin{aligned} \bar{u}_i &= u_i^0 - \frac{\sigma^2}{\varepsilon\eta_i + d_i} \left(\int_{-d_i}^{\varepsilon\eta_i} \frac{z^2}{2} dz (\mathcal{K}^2 U^0)_i + \int_{-d_i}^{\varepsilon\eta_i} zdz (\mathcal{K}[D; U^0])_i \right) + \mathcal{O}(\sigma^4), \\ &= u_i^0 - \frac{\sigma^2}{(d_i + \varepsilon\eta_i)} \left(\frac{d_i^3}{6} (\mathcal{K}^2 U^0)_i - \frac{d_i^2}{2} (\mathcal{K}[D; U^0])_i \right) + \mathcal{O}(\varepsilon\sigma^2, \sigma^4), \\ &= u_i^0 - \sigma^2 \left(\frac{d_i^2}{6} (\mathcal{K}^2 U^0)_i - \frac{d_i}{2} (\mathcal{K}[D; U^0])_i \right) + \mathcal{O}(\varepsilon\sigma^2, \sigma^4). \end{aligned}$$

This furnishes the desired relation

$$\bar{U} = U^0 - \sigma^2 \left(\frac{D^2}{6} \diamond (\mathcal{K}^2 U^0) - \frac{D}{2} \diamond (\mathcal{K}[D; U^0]) \right) + \mathcal{O}(\varepsilon\sigma^2, \sigma^4), \quad (5.4.38)$$

or equivalently

$$U^0 = \bar{U} + \sigma^2 \left(\frac{D^2}{6} \diamond (\mathcal{K}^2 \bar{U}) - \frac{D}{2} \diamond (\mathcal{K}[D; \bar{U}]) \right) + \mathcal{O}(\varepsilon\sigma^2, \sigma^4). \quad (5.4.39)$$

Then it transpires that $U^0 = \bar{U} + \mathcal{O}(\sigma^2)$. Substituting in (5.4.39), we derive

$$U^0 = \bar{U} + \sigma^2 \left(\frac{D^2}{6} \diamond (\mathcal{K}^2 \bar{U}) - \frac{D}{2} \diamond (\mathcal{K}[D; \bar{U}]) \right) + \mathcal{O}(\varepsilon\sigma^2, \sigma^4). \quad (5.4.40)$$

Finally, plugging (5.4.40) into (5.4.33), one obtains the expansion of U as a function of the depth averaged velocity \bar{U} which is similar to Expansion (2.3.14) derived in Section 2.3

$$U = \bar{U} + \sigma^2 \left(\frac{D^2}{6} \diamond (\mathcal{K}^2 \bar{U}) - \frac{z^2}{2} \mathcal{K}^2 \bar{U} - z \mathcal{K}[D; \bar{U}] - \frac{D}{2} \diamond (\mathcal{K}[D; \bar{U}]) \right) + \mathcal{O}(\varepsilon\sigma^2, \sigma^4). \quad (5.4.41)$$

We substitute Equation (5.4.41) in (5.4.35)

$$P = \varepsilon E - z \mathcal{I} + \varepsilon\sigma^2 \left(\frac{z^2}{2} \mathcal{K} \bar{U} + z [D; \bar{U}] \right) + \mathcal{O}(\varepsilon^2\sigma^2, \varepsilon\sigma^4), \quad (5.4.42)$$

which ends the proof of Proposition 4. \square

5.4.3 Depth-averaged equations

The aim of this section is to provide the final new discrete numerical model.

Proposition 5 (Discrete asymptotic equation of Peregrine). *The surface elevation vector E and the depth-averaged velocity vector \bar{U} satisfy, neglecting terms of order σ^4*

$$\begin{aligned} \frac{d}{dt} \mathcal{M}E + \mathcal{M}[H; \bar{U}] + \mathcal{M}B &= 0, \\ \frac{d}{dt} \mathcal{M}\bar{U} + \frac{1}{3} (\mathcal{N}(\bar{U}^2) + \bar{U} \diamond (\mathcal{N}\bar{U})) + g\mathcal{N}E + \mathcal{M} \frac{d}{dt} \left(\frac{D^2}{6} \diamond (\mathcal{K}^2 \bar{U}) - \frac{D}{2} \diamond (\mathcal{K}[D; \bar{U}]) \right) &= 0, \end{aligned}$$

where B is a vector introduced in the sequel.

Proof. In order to derive the equation on \bar{U} (known as the momentum equation in the literature), we substitute (5.4.40) in (5.4.36) to obtain :

$$\frac{d}{dt} \mathcal{M}\bar{U} + \frac{\varepsilon}{3} (\mathcal{N}(\bar{U}^2) + \bar{U} \diamond (\mathcal{N}\bar{U})) + \mathcal{N}E + \sigma^2 \mathcal{M} \frac{d}{dt} \left(\frac{D^2}{6} \diamond (\mathcal{K}^2 \bar{U}) - \frac{D}{2} \diamond \mathcal{K}[D; \bar{U}] \right) = \mathcal{O}(\varepsilon\sigma^2, \sigma^4).$$

In addition, to derive an equation on E (that is the continuity equation), we combine (5.4.26) and (5.4.27) to get

$$\begin{aligned} \hat{W} - \check{W} &= \frac{d}{dt} E + \varepsilon \frac{\mathcal{M}^{-1}}{3} (\mathcal{N}(E \diamond \hat{U}) - E \diamond (\mathcal{N}\hat{U}) + 2\hat{U} \diamond (\mathcal{N}E)) \\ &\quad + \frac{\mathcal{M}^{-1}}{3} (\mathcal{N}(D \diamond \check{U}) - D \diamond (\mathcal{N}\check{U}) + 2\check{U} \diamond (\mathcal{N}D)). \end{aligned} \tag{5.4.43}$$

We integrate each lines of (5.4.43) between $-d_i$ and $\varepsilon\eta_i$, for all $i \in \{0, \dots, N\}$, to obtain

$$\int_{-d_i}^{\varepsilon\eta_i} (\mathcal{K}U)_i dz + \hat{W}_i - \check{W}_i = 0,$$

which can be recast as

$$E_t + [H; \bar{U}] + B = 0, \tag{5.4.44}$$

where

$$\begin{aligned} B &= \left(\int_{-d_i}^{\varepsilon\eta_i} (\mathcal{K}U)_i dz \right)_{0 \leq i \leq N} - [H; \bar{U}] + \frac{\varepsilon}{3} (\mathcal{K}(E \diamond \hat{U}) - \mathcal{M}^{-1}(E \diamond (\mathcal{N}\hat{U})) + 2\mathcal{M}^{-1}(\hat{U} \diamond (\mathcal{N}E))) \\ &\quad - \frac{1}{3} (\mathcal{K}(-D \diamond \check{U}) - \mathcal{M}^{-1}(-D \diamond (\mathcal{N}\check{U})) + 2\mathcal{M}^{-1}(\check{U} \diamond (\mathcal{N}(-D))). \end{aligned} \tag{5.4.45}$$

We can remark that the expression B is no more than a discretized version of the so-called Leibniz' Rule⁽¹⁾. In order to be more precise, we compute explicitly B by taking successively

¹We recall the Leibniz' Rule : Given $f(x, z)$, $a(x)$ and $b(x)$, where f and $\frac{\partial f}{\partial x}$ are continuous in x and z , and a and b are differentiable functions of x ,

$$\frac{\partial}{\partial x} \left(\int_{a(x)}^{b(x)} f(x, z) dz \right) = \int_{a(x)}^{b(x)} \frac{\partial}{\partial x} f(x, z) dz + f(x, b(x))b'(x) - f(x, a(x))a'(x).$$

$z = \varepsilon\eta_i$ and $z = -d_i$ in (5.4.41) to obtain the values of \hat{U} and \check{U} :

$$\begin{aligned}\hat{U} &= \bar{U} + \sigma^2 \left(\frac{D^2}{6} \diamond (\mathcal{K}^2 \bar{U}) - \frac{\varepsilon^2 E^2}{2} \mathcal{K}^2 \bar{U} - \varepsilon E \diamond \mathcal{K}[D; \bar{U}] - \frac{D}{2} \diamond (\mathcal{K}[D; \bar{U}]) \right) + \mathcal{O}(\varepsilon\sigma^2, \sigma^4), \\ \check{U} &= \bar{U} + \sigma^2 \left(-\frac{D^2}{3} \diamond (\mathcal{K}^2 \bar{U}) + \frac{D}{2} \diamond (\mathcal{K}[D; \bar{U}]) \right) + \mathcal{O}(\varepsilon\sigma^2, \sigma^4).\end{aligned}\tag{5.4.46}$$

By substituting Equations (5.4.41) and (5.4.46) into Equation (5.4.45), this provides the complete expression of B

$$\begin{aligned}B &= \sigma^2 \left(\frac{1}{6} D \diamond (\mathcal{K}(D^2 \diamond (\mathcal{K}^2 \bar{U}))) - \frac{1}{6} D^3 \diamond (\mathcal{K}^3 \bar{U}) - \frac{1}{9} \mathcal{K}(D^3 \diamond (\mathcal{K}^2 \bar{U})) \right. \\ &\quad + \frac{1}{9} \mathcal{M}^{-1} D \diamond (\mathcal{N}(D^2 \diamond (\mathcal{K}^2 \bar{U}))) + \frac{1}{2} D^2 \diamond (\mathcal{K}^2[D; \bar{U}]) - \frac{1}{2} D \diamond (\mathcal{K}(D \diamond (\mathcal{K}[D; \bar{U}]))) \\ &\quad + \frac{1}{6} \mathcal{K}(D^2 \diamond (\mathcal{K}[D; \bar{U}])) - \frac{1}{6} \mathcal{M}^{-1} D \diamond (\mathcal{N}D \diamond (\mathcal{K}[D; \bar{U}])) \\ &\quad \left. - \frac{2}{9} \mathcal{M}^{-1} (\mathcal{N}D) \diamond (D^2 \diamond (\mathcal{K}^2 \bar{U})) + \frac{1}{3} \mathcal{M}^{-1} ((\mathcal{N}D) \diamond (D \diamond (\mathcal{K}[D; \bar{U}]))) \right) + \mathcal{O}(\varepsilon\sigma^2, \sigma^4).\end{aligned}$$

Finally, multiplying (5.4.44) by \mathcal{M} , we obtain the new discrete equations in non-dimensional form, reading

$$\frac{d}{dt} \mathcal{M}E + \mathcal{M}[H; \bar{U}] + \mathcal{M}B = 0.\tag{5.4.47}$$

$$\frac{d}{dt} \mathcal{M}\bar{U} + \frac{\varepsilon}{3} (\mathcal{N}(\bar{U}^2) + \bar{U} \diamond (\mathcal{N}\bar{U})) + \mathcal{N}E + \sigma^2 \mathcal{M} \frac{d}{dt} \left(\frac{D^2}{6} \diamond (\mathcal{K}^2 \bar{U}) - \frac{D}{2} \diamond \mathcal{K}[D; \bar{U}] \right) = \mathcal{O}(\varepsilon\sigma^2, \sigma^4)\tag{5.4.48}$$

□

To go further, we now investigate the behavior of the vector B . It appears that B has the same accuracy of order $\mathcal{O}(\varepsilon\sigma^2, \sigma^4)$ as that of the equations and then can be neglected in the sequel. For that purpose, we establish the following proposition.

Proposition 6 (Discrete Leibniz rule and consistency with Peregrine's model). *For any bathymetry d , the additional term B in Equation (5.4.47) satisfies*

$$B = \mathcal{O}(\varepsilon\sigma^2, \sigma^4).$$

As a consequence, the numerical scheme (5.4.47)-(5.4.48) becomes

$$\frac{d}{dt} \mathcal{M}E + \mathcal{M}[H; \bar{U}] = \mathcal{O}(\varepsilon\sigma^2, \sigma^4),\tag{5.4.49}$$

$$\frac{d}{dt} \mathcal{M}\bar{U} + \frac{1}{3} (\mathcal{N}(\bar{U}^2) + \bar{U} \diamond (\mathcal{N}\bar{U})) + \mathcal{N}E - \sigma^2 \frac{d}{dt} \left(\frac{d_0^2}{3} (\mathcal{N}\mathcal{K}\bar{U}) \right) = \mathcal{O}(\varepsilon\sigma^2, \sigma^4),\tag{5.4.50}$$

and is consistent with the Peregrine Equations (5.2.1).

Proof. For a better understanding, we first assume that the bathymetry $d = d_0$ is constant. In this setting, one has $D = d_0\mathcal{I}$ and the operator $D\diamond$ is no more than the multiplication by the real d_0 , that is, for example, $D\diamond U = d_0U$. From Equation (5.4.45), B is equal to

$$B = 0 + \mathcal{O}(\varepsilon\sigma^2, \sigma^4).$$

More generally, assume now that the bathymetry d is not constant. For any regular function u and its discrete version $(u_i)_{0 \leq i \leq N}$, a Taylor expansion provides

$$u_{i+1} = u_i + \Delta_x u_x(x_i) + \frac{\Delta_x^2}{2} u_{xx}(x_i) + \frac{\Delta_x^3}{6} u_{xxx}(x_i) + \dots, \quad (5.4.51)$$

and

$$u_{i-1} = u_i - \Delta_x u_x(x_i) + \frac{\Delta_x^2}{2} u_{xx}(x_i) - \frac{\Delta_x^3}{6} u_{xxx}(x_i) + \dots \quad (5.4.52)$$

Combining (5.4.51) and (5.4.52), we can prove that, for all $i \in \{0, \dots, N\}$

$$\begin{aligned} (\mathcal{N}U)_i &= u_x(x_i) + \frac{\Delta_x^2}{6} u_{xxx}(x_i) + \mathcal{O}(\Delta_x^4), \\ (\mathcal{M}^{-1}U)_i &= u(x_i) - \frac{\Delta_x^2}{6} u_{xx}(x_i) + \mathcal{O}(\Delta_x^4), \quad (\mathcal{K}U)_i = u_x(x_i) + \mathcal{O}(\Delta_x^4). \end{aligned}$$

Plugging these expansions in Equations (5.4.47) and (5.4.48), we obtain

$$\begin{aligned} \eta_t + (h\bar{u})_x - \frac{\Delta_x^2}{6} \left(\eta_{txx} + (h\bar{u})_{xxx} + h_{xx}\bar{u}_x + \sigma^2 \left(\frac{d^2 d_{xx}\bar{u}_{xxx}}{6} + \frac{7}{6} dd_x d_{xx}\bar{u}_{xx} \right. \right. \\ \left. \left. + \left(\frac{3}{2} dd_{xx}^2 d_x^2 d_{xx} + \frac{5}{6} dd_x d_{xxx} \right) \bar{u}_x + dd_{xx} d_{xxx} \bar{u} \right) \right) + \mathcal{O}(\Delta_x^4) = \mathcal{O}(\varepsilon\sigma^2, \sigma^4), \end{aligned}$$

$$\begin{aligned} \bar{u}_t + \bar{u}\bar{u}_x + \eta_x + \sigma^2 \left(\frac{d^2}{6} \bar{u}_{txx} - \frac{d}{2} (d\bar{u})_{txx} \right) + \frac{\Delta_x^2}{6} \left(\left(\bar{u}_t + \bar{u}\bar{u}_x + \eta_x + \sigma^2 \frac{d^2}{6} \bar{u}_{txx} \right. \right. \\ \left. \left. - \sigma^2 \frac{d}{2} (d\bar{u})_{txx} \right)_{xx} - \bar{u}_x \bar{u}_{xx} + \sigma^2 \frac{d}{2} (d_{xx}\bar{u}_x)_x \right) + \mathcal{O}(\Delta_x^4) = \mathcal{O}(\varepsilon\sigma^2, \sigma^4), \end{aligned}$$

proving that our numerical scheme is consistent with the continuous Peregrine equations (5.2.1). In addition, B is equal to

$$\begin{aligned} B = -\sigma^2 \frac{\Delta_x^2}{6} \left(\frac{d^2 d_{xx}\bar{u}_{xxx}}{6} + \frac{7}{6} dd_x d_{xx}\bar{u}_{xx} + \left(\frac{3}{2} dd_{xx}^2 d_x^2 d_{xx} + \frac{5}{6} dd_x d_{xxx} \right) \bar{u}_x \right. \\ \left. + dd_{xx} d_{xxx} \bar{u} + \mathcal{O}(\Delta_x^2) \right) + \mathcal{O}(\varepsilon\sigma^2, \sigma^4), \end{aligned}$$

from which it transpires that B contains only terms of order $\Delta_x^2\sigma^2$, $\varepsilon\sigma^2$ or σ^4 (actually, B is consistent with Leibniz' Rule). Recalling that $\Delta_{\tilde{x}} = \mathcal{O}(\sigma)$, one has

$$B = \sigma^2 \mathcal{O}(\Delta_{\tilde{x}}^2) + \mathcal{O}(\varepsilon\sigma^2, \sigma^4) = \mathcal{O}(\varepsilon\sigma^2, \sigma^4),$$

which ends the proof of Proposition 6. \square

To end this section, we return to the physical variables and neglect the contribution of B in (5.4.47)-(5.4.48) to obtain a new discrete approximation consistent with the Peregrine equations (5.2.1)

$$\frac{d}{dt} \mathcal{M}E + \mathcal{M}[H; \bar{U}] = 0, \quad (5.4.53)$$

$$\frac{d}{dt} \mathcal{M}\bar{U} + \frac{1}{3} (\mathcal{N}(\bar{U}^2) + \bar{U} \diamond (\mathcal{N}\bar{U})) + g\mathcal{N}E + \mathcal{M} \frac{d}{dt} \left(\frac{D^2}{6} \diamond (\mathcal{K}^2\bar{U}) - \frac{D}{2} \diamond (\mathcal{K}[D; \bar{U}]) \right) = 0. \quad (5.4.54)$$

We see that, while involving similar algebraic operations, the new discretization is different from the classical one, even for the simple situation of the Peregrine equations. Firstly, there are some differences in the nonlinear terms in the continuity (wave height) equation. Actually, the discretization of this terms in the classical scheme is symmetric. It treats the nonlinear derivatives terms “ $h\bar{u}_x$ ” and “ $h_x\bar{u}$ ” with the same approach while the new scheme discretize differently these terms. In addition, the main differences are found in the treatment of the third order derivatives terms which correspond to the dispersive terms of Peregrine equations. When the classical scheme involve the operator $\{\cdot, \cdot\}$, the new scheme has a discrete structure close to the continuous one using the operator $[\cdot; \cdot]$. Then, it is natural to think that we will see differences in the linear dispersion characteristics of the two discretizations. In next section, we will study the exact linear dispersion and linear shoaling gradient provided by the two numerical scheme.

5.5 Study of the linear dispersion characteristics.

The aim of this section is to give some insights to measure the accuracy of the new method developped in the previous sections. For that purpose, we exhibit the dispersion relation as well as the shoaling coefficients of the linearized version of the scheme (5.4.53)-(5.4.54). This study is widely inspired by the one presented in Section 4.3.3 and firstly proposed by Dingemans in [36] in the context of slowly-varying water depth, that is we assume that $d = d(\delta x)$ with $\delta \ll 1$. For the sake of completeness, we also compare our computations with the ones performed on the linearized version of the classical scheme (5.3.7)-(5.3.8).

5.5.1 Linear characteristics of the new numerical model.

We first introduce the linearized version of the scheme (5.4.53)-(5.4.54) around the rest state :

$$\frac{d}{dt} \mathcal{M}E + \mathcal{M}[D; \bar{U}] = 0, \quad (5.5.1)$$

$$\frac{d}{dt} \mathcal{M}\bar{U} + g\mathcal{N}E + \mathcal{M} \frac{d}{dt} \left(\frac{D^2}{6} \diamond (\mathcal{K}^2\bar{U}) - \frac{D}{2} \diamond (\mathcal{K}[D; \bar{U}]) \right) = 0. \quad (5.5.2)$$

As usual, when one deals with linear equations, a lot of computations can be performed explicitly. Indeed, differentiating (5.5.2) with respect to t , multiplying (5.5.1) by \mathcal{N} and substituting the

resulting equations, one obtains a decouple equation on the vector \bar{U} :

$$\mathcal{M}\bar{U}_{tt} - g\mathcal{N}[D; \bar{U}] + \mathcal{M}\left(\frac{D^2}{6} \diamond (\mathcal{K}^2\bar{U}) - \frac{D}{2} \diamond (\mathcal{K}[D; \bar{U}])\right)_{tt} = 0. \quad (5.5.3)$$

In order to exhibit the dispersion relation associated with (5.5.1)-(5.5.2), we then look for a *plane-wave* solution under the form

$$\bar{U} = \left(\bar{u}_i\right)_{0 \leq i \leq N}$$

where

$$\bar{u}_i = \bar{u}(t, x_i) \text{ with } \bar{u}(t, x) = \mathbf{U}(\delta x) \exp\left(-j\omega t + \frac{j}{\delta} K(\delta x)\right), \quad j^2 = -1. \quad (5.5.4)$$

Owning the solution \bar{U} , it is pertinent to introduce the wave number

$$k(\delta x) = \frac{\partial}{\partial x} \left(\frac{1}{\delta} K(\delta x) \right),$$

and for all $i \in \{0, \dots, N\}$, $k_i = k(\delta x_i)$. Then, we determine conditions on k and \mathbf{U} so that \bar{U} is a solution to the linear system (5.5.3). A Taylor expansion around the point $x = x_i$ provides directly

$$\bar{u}_{i+1} = \left(1 + \delta(j\frac{\Delta_x^2}{2}k'(\delta x_i) + \Delta_x \frac{\mathbf{U}'(\delta x_i)}{\mathbf{U}_i})\right) \bar{u}_i e^{jk_i \Delta_x} + \mathcal{O}(\delta^2), \quad (5.5.5)$$

$$\bar{u}_{i-1} = \left(1 + \delta(j\frac{\Delta_x^2}{2}k'(\delta x_i) - \Delta_x \frac{\mathbf{U}'(\delta x_i)}{\mathbf{U}_i})\right) \bar{u}_i e^{-jk_i \Delta_x} + \mathcal{O}(\delta^2). \quad (5.5.6)$$

In view of (5.5.3), we deduce that, $\forall i \in \{1, \dots, n\}$

$$\begin{aligned} (\mathcal{N}\bar{U})_i &= \left(jk_i \sin_c(k_i \Delta_x) - \delta \frac{k_i^2 \Delta_x^2}{2} \sin_c(k_i \Delta_x) \frac{k'(\delta x_i)}{k_i} \right. \\ &\quad \left. + \delta \cos(k_i \Delta_x) \frac{\mathbf{U}'(\delta x_i)}{\mathbf{U}_i}\right) \bar{u}_i + \mathcal{O}(\delta^2). \end{aligned} \quad (5.5.7)$$

$$\begin{aligned} (\mathcal{M}\bar{U})_i &= \left(\frac{1}{3}(2 + \cos(k_i \Delta_x)) + j\delta \frac{k_i \Delta_x^2}{6} (\cos(k_i \Delta_x) \frac{k'(\delta x_i)}{k_i} + \right. \\ &\quad \left. 2 \sin_c(k_i \Delta_x) \frac{\mathbf{U}'(\delta x_i)}{\mathbf{U}_i})\right) \bar{u}_i + \mathcal{O}(\delta^2). \end{aligned} \quad (5.5.8)$$

Note that it is not possible to plug directly (5.5.7)-(5.5.8) into (5.5.3), due to the presence of the vector $(\mathcal{M}^{-1}\bar{U})$ in the bracket $[D; \bar{U}]$. Indeed, it is necessary to express each term $(\mathcal{M}^{-1}\bar{U})$ with respect to \bar{u}_i . To overcome this difficulty, the idea is to introduce the following new variables

$$\begin{aligned} V &= \mathcal{M}^{-1}\mathcal{N}(D \diamond \bar{U}), \quad X = \mathcal{M}^{-1}\mathcal{N}\bar{U}, \quad Z = \mathcal{M}^{-1}(D \diamond (\mathcal{N}\bar{U})), \\ W &= \mathcal{M}^{-1}(\bar{U} \diamond (\mathcal{N}D)), \quad Y = \mathcal{M}^{-1}\mathcal{N}X, \\ T &= \left(D \diamond X + \frac{1}{3}(V - Z + 2W)\right), \quad S = \mathcal{M}^{-1}\mathcal{N}T, \end{aligned}$$

and to perform asymptotic expansions of order δ^2 on these variables. Using these new vectors, one can rewrite Equation (5.5.3) into

$$\mathcal{M}\bar{U}_{tt} - g\mathcal{N}T + \mathcal{M}\left(\frac{D^2}{6}\diamond Y_{tt} - \frac{D}{2}\diamond S_{tt}\right) = 0. \quad (5.5.9)$$

Note first that the vectors V, X, Z, W, Y and T depend only on \bar{U} . It is then natural to introduce the following functions

$$\begin{aligned} \mathbf{v} &= \mathbf{V}(\delta x) \exp\left(-j\omega t + \frac{j}{\delta}K(\delta x)\right), \mathbf{x} = \mathbf{X}(\delta x) \exp\left(-j\omega t + \frac{j}{\delta}K(\delta x)\right), \\ \mathbf{z} &= \mathbf{Z}(\delta x) \exp\left(-j\omega t + \frac{j}{\delta}K(\delta x)\right), \mathbf{w} = \mathbf{W}(\delta x) \exp\left(-j\omega t + \frac{j}{\delta}K(\delta x)\right), \\ \mathbf{y} &= \mathbf{Y}(\delta x) \exp\left(-j\omega t + \frac{j}{\delta}K(\delta x)\right), \mathbf{t} = \mathbf{T}(\delta x) \exp\left(-j\omega t + \frac{j}{\delta}K(\delta x)\right), \\ \mathbf{s} &= \mathbf{S}(\delta x) \exp\left(-j\omega t + \frac{j}{\delta}K(\delta x)\right), \end{aligned}$$

where $\mathbf{V}(\delta x), \mathbf{X}(\delta x), \mathbf{Z}(\delta x), \mathbf{W}(\delta x), \mathbf{Y}(\delta x), \mathbf{T}(\delta x)$ and $\mathbf{S}(\delta x)$ denote the amplitude of respectively $\mathbf{v}, \mathbf{x}, \mathbf{z}, \mathbf{w}, \mathbf{y}, \mathbf{t}$ and \mathbf{s} . Using Equations (5.5.7) and (5.5.8), one can rewrite (5.5.9) for all $i \in \{0, \dots, n\}$

$$\begin{aligned} &- \omega^2 \left(\frac{1}{3}(2 + \cos(k_i \Delta_x)) + j\delta \frac{k_i \Delta_x^2}{6} (\cos(k_i \Delta_x) \frac{k'(\delta x_i)}{k_i} + 2 \sin_c(k_i \Delta_x) \frac{\mathbf{U}'(\delta x_i)}{\bar{u}_i}) \right) \bar{u}_i \\ &- g \left(jk_i \sin_c(k_i \Delta_x) - \delta \frac{k_i^2 \Delta_x^2}{2} \sin_c(k_i \Delta_x) \frac{k'(\delta x_i)}{k_i} + \delta \cos(k_i \Delta_x) \frac{\mathbf{T}'(\delta x_i)}{\mathbf{T}(\delta x_i)} \right) \mathbf{T}(\delta x_i) \\ &- \frac{\omega^2}{6} \left(\frac{1}{3}(2 + \cos(k_i \Delta_x)) + j\delta \frac{k_i \Delta_x^2}{6} (\cos(k_i \Delta_x) \frac{k'(\delta x_i)}{k_i} + 2 \sin_c(k_i \Delta_x) \frac{(d^2(\delta x_i) \mathbf{Y}(\delta x_i))'}{d_i^2 \mathbf{Y}(\delta x_i)}) \right) d_i^2 \mathbf{Y}(\delta x_i) \\ &+ \frac{(\omega^2)}{2} \left(\frac{1}{3}(2 + \cos(k_i \Delta_x)) + j\delta \frac{k_i \Delta_x^2}{6} (\cos(k_i \Delta_x) \frac{k'(\delta x_i)}{k_i} + 2 \sin_c(k_i \Delta_x) \frac{(d_i(\delta x_i) \mathbf{S}(\delta x_i))'}{d \mathbf{S}(\delta x_i)}) \right) d_i \mathbf{S}(\delta x_i) = 0. \end{aligned}$$

It remains to estimate the first order derivatives $\mathbf{U}'(\delta x_i), \mathbf{T}'(\delta x_i), \mathbf{Y}'(\delta x_i)$ and $\mathbf{S}'(\delta x_i)$. First observe that $\mathcal{M}X = \mathcal{N}\bar{U}$ which provides, using (5.5.7)-(5.5.8),

$$\begin{aligned} &\left(\frac{1}{3}(2 + \cos(k_i \Delta_x)) + j\delta \frac{k_i \Delta_x^2}{6} \left(\cos(k_i \Delta_x) \frac{k'(\delta x_i)}{k_i} + 2 \sin_c(k_i \Delta_x) \frac{\mathbf{X}'(\delta x_i)}{\mathbf{X}(\delta x_i)} \right) \right) \mathbf{X}(\delta x_i) \\ &= \left(jk_i \sin_c(k_i \Delta_x) - \delta \frac{k_i^2 \Delta_x^2}{2} \sin_c(k_i \Delta_x) \frac{k'(\delta x_i)}{k_i} + \delta \cos(k_i \Delta_x) \frac{\mathbf{U}'(\delta x_i)}{\mathbf{U}(\delta x_i)} \right) \mathbf{U}(\delta x_i) + \mathcal{O}(\delta^2). \end{aligned} \quad (5.5.10)$$

Collecting the terms of order δ^0 in the last expression, one gets

$$\mathbf{X}(\delta x_i) = jk_i \frac{\sin_c(k_i \Delta_x)}{\frac{1}{3}(2 + \cos(k_i \Delta_x))} \mathbf{U}(\delta x_i) + \mathcal{O}(\delta). \quad (5.5.11)$$

Assuming that Equation (5.5.11) is valid for the continuous variable x , one derives, by first applying the neperian logarithm and then by differentiating the resulting relation, that

$$\frac{\mathbf{X}'(\delta x_i)}{\mathbf{X}(\delta x_i)} = \frac{\mathbf{U}'(\delta x_i)}{\mathbf{U}(\delta x_i)} + \left(\frac{\cos(k_i \Delta_x)}{\sin_c(k_i \Delta_x)} + \frac{k_i^2 \Delta_x^2}{3} \frac{\sin_c(k_i \Delta_x)}{\frac{1}{3}(2 + \cos(k_i \Delta_x))} \right) \frac{k'(\delta x_i)}{k_i} + \mathcal{O}(\delta). \quad (5.5.12)$$

Plugging (5.5.12) in Equation (5.5.10), one obtains

$$\begin{aligned} \mathbf{X}(\delta x_i) &= j k_i \frac{\sin_c(k_i \Delta_x)}{\frac{1}{3}(2 + \cos(k_i \Delta_x))} \mathbf{U}(\delta x_i) \\ &+ \delta \left(\left(\frac{\cos(k_i \Delta_x)}{\frac{1}{3}(2 + \cos(k_i \Delta_x))} + \frac{k_i^2 \Delta_x^2}{3} \frac{\sin_c(k_i \Delta_x)^2}{(\frac{1}{3}(2 + \cos(k_i \Delta_x)))^2} \right) \frac{\mathbf{U}'(\delta x_i)}{\mathbf{U}(\delta x_i)} \right. \\ &+ \left. \left(\frac{k_i^2 \Delta_x^2}{3} \frac{\sin_c(k_i \Delta_x)(\cos(k_i \Delta_x) - 1)}{(\frac{1}{3}(2 + \cos(k_i \Delta_x)))^2} + \frac{k_i^4 \Delta_x^4}{9} \frac{\sin_c(k_i \Delta_x)^3}{(\frac{1}{3}(2 + \cos(k_i \Delta_x)))^3} \right) \frac{k'(\delta x_i)}{k_i} \right) \mathbf{U}(\delta x_i) \\ &+ \mathcal{O}(\delta^2). \end{aligned} \quad (5.5.13)$$

Following the same procedure, we express the variables \mathbf{Z} and \mathbf{W} in terms of \mathbf{U} as follows

$$\begin{aligned} \mathbf{Z}(\beta x_i) &= j k_i d_i \frac{\sin_c(k_i \Delta_x)}{\frac{1}{3}(2 + \cos(k_i \Delta_x))} \mathbf{U}(\beta x_i) + \beta d_i \left[\beta d_i \left(\frac{k_i^2 \Delta_x^2}{3} \frac{\sin_c(k_i \Delta_x)^2}{[\frac{1}{3}(2 + \cos(k_i \Delta_x))]^2} \right) \frac{d'(\beta x_i)}{d_i} \right. \\ &+ \left(\frac{\cos(k_i \Delta_x)}{\frac{1}{3}(2 + \cos(k_i \Delta_x))} + \frac{k_i^2 \Delta_x^2}{3} \frac{\sin_c(k_i \Delta_x)^2}{[\frac{1}{3}(2 + \cos(k_i \Delta_x))]^2} \right) \frac{\mathbf{U}'(\beta x_i)}{\mathbf{U}(\beta x_i)} \\ &+ \beta d_i \left(\frac{k_i^2 \Delta_x^2}{3} \frac{\sin_c(k_i \Delta_x)(\cos(k_i \Delta_x) - 1)}{[\frac{1}{3}(2 + \cos(k_i \Delta_x))]^2} \right. \\ &\left. \left. + \frac{k_i^4 \Delta_x^4}{9} \frac{\sin_c(k_i \Delta_x)^3}{[\frac{1}{3}(2 + \cos(k_i \Delta_x))]^3} \right) \frac{k'(\beta x_i)}{k_i} \right] \mathbf{U}(\beta x_i) + \mathcal{O}(\beta^2), \end{aligned} \quad (5.5.14)$$

$$\mathbf{W}(\beta x_i) = \frac{\beta d_i}{\frac{1}{3}(2 + \cos(k_i \Delta_x))} \frac{d'(\beta x_i)}{d_i} \mathbf{U}(\beta x_i). \quad (5.5.15)$$

Coming back to (5.5.9), one obtains the expression of ω , using the expressions of the amplitudes of U , T , Y and S and collecting in the resulting equation the term of order δ^0 , for all $i \in \{0, \dots, N\}$,

$$\frac{\omega^2}{g d_i k_i^2} = \frac{\sin_c(k_i \Delta_x)^2}{(\frac{1}{3}(2 + \cos(k_i \Delta_x)))^2 + \frac{k_i^2 d_i^2}{3} \sin_c(k_i \Delta_x)^2}. \quad (5.5.16)$$

Furthermore, collecting the term of order δ , one gets a relation between \mathbf{U} , k , and the bathymetry d :

$$\alpha_{1,i}^{(1)} \frac{\mathbf{U}'(\delta x_i)}{\mathbf{U}_i} + \alpha_{2,i}^{(1)} \frac{d'(\delta x_i)}{d_i} + \alpha_{3,i}^{(1)} \frac{k'(\delta x_i)}{k_i} = 0. \quad (5.5.17)$$

Equation (5.5.17) describes the effect of linear shoaling since the numbers $\alpha_{1,i}^{(1)}$, $\alpha_{2,i}^{(1)}$ and $\alpha_{3,i}^{(1)}$ are known as the linear shoaling coefficients. Using (5.5.16), one can compute these three coefficients (we omit the details for simplicity), for all $i \in \{0, \dots, N\}$,

$$\alpha_{1,i}^{(1)} = 2 \cos(k_i \Delta_x) \frac{(\frac{1}{3}(2 + \cos(k_i \Delta_x)))}{\sin_c(k_i \Delta_x)} + 2 \frac{k_i^2 \Delta_x^2}{3} \sin_c(k_i \Delta_x)$$

$$\alpha_{2,i}^{(1)} = 2 \frac{1 + 2 \cos(k_i \Delta_x)}{3} \frac{\left(\frac{1}{3}(2 + \cos(k_i \Delta_x))\right)}{\sin_c(k_i \Delta_x)} - \frac{1 + 2 \cos(k_i \Delta_x)}{3} \frac{\sin_c(k_i \Delta_x)}{\left(\frac{1}{3}(2 + \cos(k_i \Delta_x))\right)} \frac{k_i^2 d_i^2}{3}$$

$$\alpha_{3,i}^{(1)} = \frac{\cos(k_i \Delta_x)^2}{\sin_c(k_i \Delta_x)^2} \left(\frac{1}{3}(2 + \cos(k_i \Delta_x)) \right) + 2 \frac{k_i^2 \Delta_x^2}{3} (\cos(k_i \Delta_x) - 1) + \frac{k_i^4 \Delta_x^4}{9} \frac{\sin_c(k_i \Delta_x)^2}{\left(\frac{1}{3}(2 + \cos(k_i \Delta_x))\right)}$$

$$+ \frac{k_i^2 d_i^2}{3} \left(\frac{\cos(k_i \Delta_x)^2}{2 \sin_c(k_i \Delta_x)} \left(\frac{\left(\frac{1}{3}(2 + \cos(k_i \Delta_x))\right)^2}{\sin_c(k_i \Delta_x)} - 1 \right) + 2 \frac{k_i^4 \Delta_x^4}{9} \frac{\sin_c(k_i \Delta_x)^2 (1 - \cos(k_i \Delta_x))}{\left(\frac{1}{3}(2 + \cos(k_i \Delta_x))\right)^2} \right).$$

Differentiating formally the dispersion relation (5.5.16) and assuming that ω is constant, we deduce that k_i has to satisfy the following condition

$$\frac{k'(\delta x_i)}{k_i} = -\alpha_4^{(1)} \frac{d'(\delta x_i)}{d_i}, \quad (5.5.18)$$

where, for all $i \in \{0, \dots, N\}$,

$$\alpha_{4,i}^{(1)} = \frac{1}{2} \frac{1 - \frac{k_i^2 d_i^2}{3} \frac{\sin_c(k_i \Delta_x)^2}{\left(\frac{1}{3}(2 + \cos(k_i \Delta_x))\right)^2}}{\frac{\cos(k_i \Delta_x)}{\sin_c(k_i \Delta_x)} + \frac{k_i^2 \Delta_x^2}{3} \frac{\sin_c(k_i \Delta_x)}{\left(\frac{1}{3}(2 + \cos(k_i \Delta_x))\right)}}.$$

This relation is used to compute formally k_i for $i \in \{0, \dots, N\}$ and for a given bathymetry and therefore to obtain the coefficients $\alpha_{1,i}^{(1)}$, $\alpha_{2,i}^{(1)}$ and $\alpha_{3,i}^{(1)}$. Finally, following [36], we obtain an expression of the amplitude velocity \mathbf{U}_i , for all $i \in \{0, \dots, N\}$

$$\frac{\mathbf{U}'_i}{\mathbf{U}_i} = -\alpha_{s,i}^{(1)} \frac{d'_i}{d_i}, \quad (5.5.19)$$

where

$$\alpha_{s,i}^{(1)} = \frac{\alpha_{2,i}^{(1)} - \alpha_{3,i}^{(1)} \alpha_{4,i}^{(1)}}{\alpha_{1,i}^{(1)}}. \quad (5.5.20)$$

In order to find the theoretical amplitude of the surface elevation \mathbf{A} , we assume that $E = (\eta_i)_{0 \leq i \leq N}$, where

$$\eta_i = \mathbf{A}(\delta x_i) \exp \left(-j\omega t + \frac{j}{\delta} K(\delta x_i) \right). \quad (5.5.21)$$

Substituting in Equation (5.5.1), we obtain an expression of \mathbf{A}_i in function of \mathbf{U}_i for all $i \in \{0, \dots, N\}$

$$\mathbf{A}_i = \frac{d_i}{\sqrt{g d_i}} \sqrt{1 + \frac{k_i^2 d_i^2}{3} \frac{\sin_c(k_i \Delta_x)}{\frac{1}{3}(2 + \cos(k_i \Delta_x))}} \mathbf{U}_i. \quad (5.5.22)$$

Considering a periodic solution of linear Peregrine equations, Equations (5.5.19) and (5.5.22) give an approximate value of amplitudes \mathbf{A} and \mathbf{U} furnished by the new numerical scheme for a given bathymetry d . In the sequel we compare these results to the continuous results of Peregrine model in view of presenting the influence of numerical schemes on periodic solutions.

5.5.2 Linear characteristics of the classical Peregrine model.

We consider now the linear classical numerical model presented in Section 3.

$$\mathcal{M} \frac{d}{dt} E + \frac{1}{3} (2\mathcal{N}(D \diamond \bar{U}) + D \diamond (\mathcal{N}\bar{U}) + \bar{U} \diamond (\mathcal{N}D)) = 0, \quad (5.5.23)$$

$$\frac{d}{dt} \mathcal{M}\bar{U} + g\mathcal{N}E - \frac{1}{6}\{D; \bar{U}_t\} = 0. \quad (5.5.24)$$

We reproduce the same procedure as in section 5.5.1. The terms of order of δ^0 gives the linear dispersion relation, for all $i = 0, \dots, N$,

$$\frac{\omega^2}{gd_i k_i^2} = \frac{\sin_c(k_i \Delta_x)^2}{\frac{1}{3}(2 + \cos(k_i \Delta_x)) \left(\frac{1}{3}(2 + \cos(k_i \Delta_x)) + \frac{1 - \cos(k_i \Delta_x)}{\frac{k_i^2 \Delta_x^2}{2}} \frac{k_i^2 d_i^2}{3} \right)}, \quad (5.5.25)$$

whereas the terms of order of δ provides the linear shoaling coefficients as follows

$$\begin{aligned} \alpha_{1,i}^{(2)} &= 2 \left(\frac{1}{3}(2 + \cos(k_i \Delta_x)) \right) \sin_c(k_i \Delta_x) \cos(k_i \Delta_x) + \\ &\quad 2 \frac{k_i^2 d_i^2}{3} \left(\sin_c(k_i \Delta_x) \cos(k_i \Delta_x) \frac{1 - \cos(k_i \Delta_x)}{\frac{k_i^2 \Delta_x^2}{2}} - \sin_c(k_i \Delta_x)^3 \right) \\ &\quad + \frac{k_i^2 \Delta_x^2}{3} \left(2 \sin_c(k_i \Delta_x)^3 + \frac{k_i^2 d_i^2}{3} \frac{\sin_c(k_i \Delta_x)^3}{\frac{1}{3}(2 + \cos(k_i \Delta_x))} \frac{1 - \cos(k_i \Delta_x)}{\frac{k_i^2 \Delta_x^2}{2}} \right), \\ \alpha_{2,i}^{(2)} &= \left(\frac{1}{3}(2 + \cos(k_i \Delta_x)) \right) \sin_c(k_i \Delta_x) \frac{5 \cos(k_i \Delta_x) + 1}{3} \\ &\quad + \frac{k_i^2 d_i^2}{3} \left(\frac{1 - \cos(k_i \Delta_x)}{\frac{k_i^2 \Delta_x^2}{2}} \sin_c(k_i \Delta_x) \frac{5 \cos(k_i \Delta_x) + 1}{3} - 3 \sin_c(k_i \Delta_x) \right) \\ &\quad + \frac{k_i^2 \Delta_x^2}{3} \left(\sin_c(k_i \Delta_x)^3 + \frac{k_i^2 d_i^2}{3} \frac{\sin_c(k_i \Delta_x)^3}{(\frac{1}{3}(2 + \cos(k_i \Delta_x)))} \frac{1 - \cos(k_i \Delta_x)}{\frac{k_i^2 \Delta_x^2}{2}} \right), \\ \alpha_{3,i}^{(2)} &= \left(\frac{1}{3}(2 + \cos(k_i \Delta_x)) \right) \cos(k_i \Delta_x)^2 + \frac{k_i^2 d_i^2}{3} \left(\frac{1 - \cos(k_i \Delta_x)}{\frac{k_i^2 \Delta_x^2}{2}} \cos(k_i \Delta_x)^2 \right. \\ &\quad \left. - \sin_c(k_i \Delta_x)^2 \cos(k_i \Delta_x) \right) + \frac{k_i^2 \Delta_x^2}{6} \left(4 \sin_c(k_i \Delta_x)^2 \cos(k_i \Delta_x) - 3 \sin_c(k_i \Delta_x)^2 \right. \\ &\quad \left. - k_i^2 d_i^2 \frac{1 - \cos(k_i \Delta_x)}{\frac{k_i^2 \Delta_x^2}{2}} \frac{\sin_c(k_i \Delta_x)^2}{\frac{1}{3}(2 + \cos(k_i \Delta_x))} \right) + \frac{k_i^4 d_i^4}{9} \left(\frac{\sin_c(k_i \Delta_x)^4}{\frac{1}{3}(2 + \cos(k_i \Delta_x))} \right. \\ &\quad \left. + \frac{k_i^2 d_i^2}{3} \frac{\sin_c(k_i \Delta_x)^4}{(\frac{1}{3}(2 + \cos(k_i \Delta_x)))^2} \frac{1 - \cos(k_i \Delta_x)}{\frac{k_i^2 \Delta_x^2}{2}} \right). \end{aligned}$$

Differentiating Equation (5.5.25), assuming that ω is constant, we obtain the relation that must satisfies each k_i for all $i \in \{0, \dots, N\}$

$$\frac{k'_i}{k_i} = -\alpha_{4,i}^{(2)} \frac{d'_i}{d_i}, \quad (5.5.26)$$

where

$$\alpha_{4,i}^{(2)} = \frac{1}{2C} \left(\frac{\frac{1}{3}(2 + \cos(k_i \Delta_x))}{\cos(k_i \Delta_x)} - \frac{k_i^2 d_i^2}{3} \frac{1 - \cos(k_i \Delta_x)}{\cos(k_i \Delta_x) \frac{k_i^2 \Delta_x^2}{2}} \right),$$

and

$$C = \frac{\frac{1}{3}(2 + \cos(k_i \Delta_x))}{\sin_c(k_i \Delta_x)} + \frac{k_i^2 d_i^2}{3} \left(\frac{1 - \cos(k_i \Delta_x)}{\sin_c(k_i \Delta_x) \frac{k_i^2 \Delta_x^2}{2}} - \frac{\sin_c(k_i \Delta_x)}{\cos(k_i \Delta_x)} \right) \\ + \frac{k_i^2 \Delta_x^2}{3 \cos(k_i \Delta_x)} \left(\sin_c(k_i \Delta_x) + \frac{k_i^2 d_i^2}{6} \frac{\sin_c(k_i \Delta_x)(1 - \cos(k_i \Delta_x))}{\frac{1}{3}(2 + \cos(k_i \Delta_x)) \frac{k_i^2 \Delta_x^2}{2}} \right).$$

Again, we obtain the relation between the amplitude U_i of the surface elevation and the bathymetry which can be written as, for all $i \in \{0, \dots, N\}$,

$$\frac{\mathbf{U}'_i}{\mathbf{U}_i} = -\alpha_{s,i}^{(2)} \frac{d'_i}{d_i}, \quad (5.5.27)$$

where

$$\alpha_{s,i}^{(2)} = \frac{\alpha_{2,i}^{(2)} - \alpha_{3,i}^{(2)} \alpha_{4,i}^{(2)}}{\alpha_{1,i}^{(2)}}.$$

Finally, for this numerical scheme, Amplitude and velocity satisfy

$$\mathbf{A}_i = \frac{d_i}{\sqrt{g d_i}} \sqrt{1 + \frac{(1 - \cos(k_i \Delta_x))}{\frac{k_i^2 \Delta_x^2}{2}} \frac{1}{\frac{1}{3}(2 + \cos(k_i \Delta_x))} \frac{k_i^2 d_i^2}{3}} \mathbf{U}_i. \quad (5.5.28)$$

Considering a periodic solution of linear Peregrine equations, Equations (5.5.27) and (5.5.28) give an approximate value of amplitudes \mathbf{A} and \mathbf{U} furnished by the classical numerical scheme for a given bathymetry d . In the next section, we compare the discrete linear dispersion characteristics presented above to the continuous one presented in Chapter 4.

5.5.3 Analysis of the computations

In this section, we study the linear dispersion relations derived in Section 5.5.1 and 5.5.2. More precisely, we draw the phase velocity and the amplitude of the wave with respect to the dispersion parameter σ in shoaling conditions for each scheme and we compare the results with the ones predicted by the linear theory associated to the Peregrine equations (5.2.1).

Phase velocity

The phase velocity is usually given by the relation $C = \omega/k$. As observed in literature, we can consider k and d as constant functions ($k = k_0$, and $d = d_0$ see [72] for more details). Then, the phase velocity of our new numerical scheme (5.5.1)-(5.5.2) is given by (5.5.16) while that derived for the classical scheme (5.3.7)-(5.3.8) is given by (5.5.25). Our aim is to plot the two curves (5.5.16)-(5.5.25) and make a comparison with the one predicted by the linear theory computed in Chapter 4 :

$$C_P^2 = \frac{gd}{1 + \frac{k^2 d^2}{3}}. \quad (5.5.29)$$

We first fix the wavelength λ and we put $\Delta_x = \frac{\lambda}{N_\lambda}$ where N_λ is the number of discretization points by wavelength. A direct computation gives $k\Delta_x = 2\pi/N_\lambda$. We recall that $\sigma = \frac{d}{\lambda}$, showing that $kd = 2\pi\sigma$. In Figure 5.2, we draw the relative errors between (5.5.2) and (5.5.25) and the phase velocity predicted by the linear theory. The error er is defined, for each scheme, by

$$\text{er} = 100 \left(\frac{C - C_P}{C_P} \right).$$

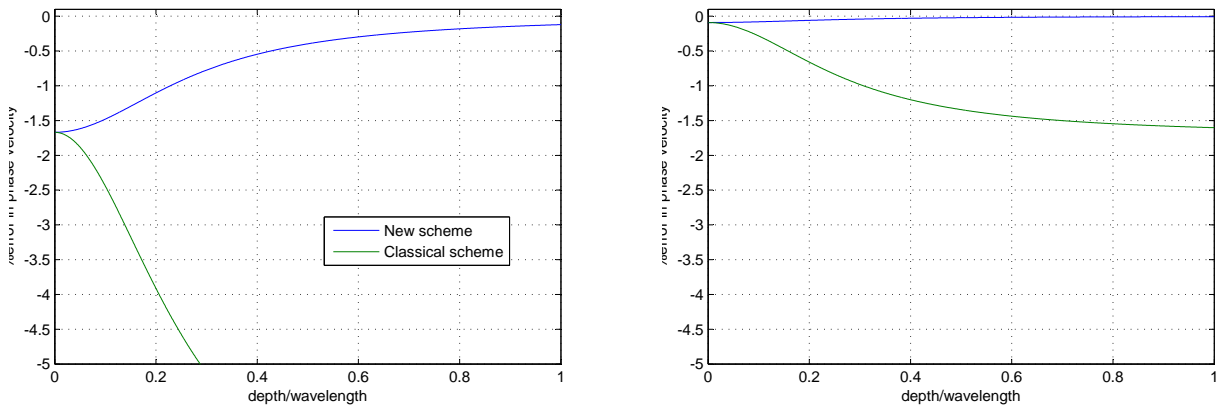


Figure 5.2 – Comparison of the phase velocity ($N_\lambda = 5$ on the left, $N_\lambda = 10$ on the right) of the classical and the new numerical scheme with the one given by the linear theory w.r.t σ .

In Figure 5.2, one can observe that for $N_\lambda = 5$, the error coming from the new scheme is acceptable (less than 1.6%) whereas the one of the classical scheme is greater than 5% for depths bigger than 0.3. For $N_\lambda = 10$, although the error of the classical scheme is better than in the previous case (less than 2%), the one of the new scheme is much better and stays very close to 0. We conclude here that our new numerical scheme seems to reproduce much better the linear dispersive effects.

Linear shoaling test

We first recall the expression of the shoaling coefficients given by the linear theory associated with the Peregrine equations (5.2.1). Details are given in Section 4.3.3 taking $\alpha_B = 0$.

$$\alpha_1 = 2, \alpha_2 = 2 - \frac{k^2 d^2}{3}, \alpha_3 = 1, \alpha_4 = \frac{1}{2} \left(1 - \frac{k^2 d^2}{3} \right),$$

and the expression of the surface elevation amplitude

$$A = \sqrt{1 + \frac{k^2 d^2}{3}} \frac{d}{\sqrt{gd}} U. \quad (5.5.30)$$

Our aim is to compare, for a given situation, the evolution of the amplitude of the waves with respect to the space variable x given by the two relations (5.5.22) and (5.5.28) and the one derived from the linear theory. To this end, we perform the following test proposed by Madsen and Sørensen in [57]. We consider a periodic wave with an initial amplitude $a = 0.05$ and a wavelength $\lambda = 15$ starting from the position $x = 100$. It propagates over an initial constant water depth $d_0 = 13$. The bottom is flat until $x = 150$ and it has a constant up-slope of $\frac{1}{50}$ from $x = 150$ to $x = 790$. We compute the evolution of the wave amplitude with respect to x . For that, we propose the following procedure. Firstly, we integrate formally the relation between k and d ((5.5.18) for the new scheme), given by the differential equation

$$\frac{k'}{k} = -\alpha_4 \frac{d'}{d}.$$

We use a Strongly Stability-Preserving Runge-Kutta method (SSP-RK) to compute the solution k , using $k_0 = \frac{2\pi}{\lambda}$ as initial condition. Then, we substitute this function k in the expression of α_s , and we compute the amplitude of the velocity U by integrating the relation

$$\frac{\mathbf{U}'}{\mathbf{U}} = -\alpha_s \frac{d'}{d}.$$

Again, we use a SSP-RK method and $\mathbf{U}(100) = a \frac{\sqrt{gd_0}}{d_0}$ as initial condition. Then, we deduce the theoretical amplitude of the wave elevation using Equations (5.5.22) (for the new scheme) and (5.5.28) (for the classical one). Fixing the value of Δ_x , it is possible to compute formally the surface elevation amplitude for each scheme. The results are presented in Figure 5.3.

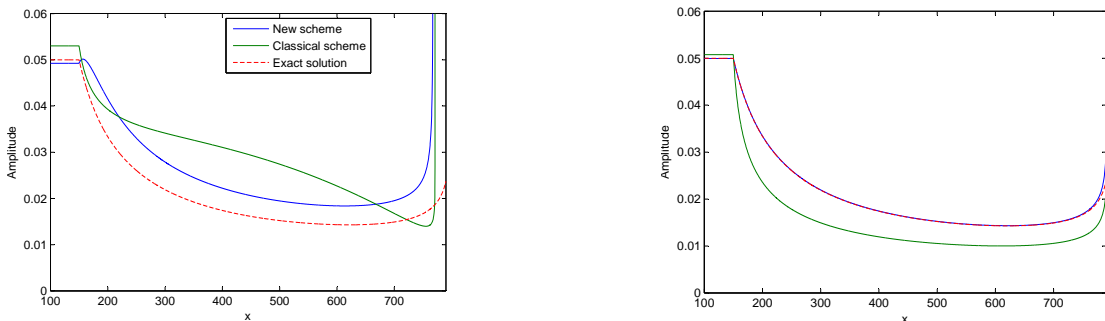


Figure 5.3 – Evolution of the wave amplitude for the two numerical schemes and for Peregrine equations. Left : $\Delta_x = 3$ ($N_\lambda = 5$). Right : $\Delta_x = 1.5$ ($N_\lambda = 10$).

We observe that when Δ_x is small, the curves of the two schemes match the theoretical one, meaning that both schemes converge. However, when Δ_x becomes larger, one can see that the curve computed with the new scheme stays close to the theoretical one while the one computed with the classical scheme furnishes a bad behavior of the amplitude of the wave.

5.6 Numerical experiments

This section is devoted to the investigation of the behavior of the two schemes (5.4.53)-(5.4.54) and (5.3.7)-(5.3.8). To this end, we present different test cases : the propagation of solitary waves over a flat bathymetry, the propagation of a periodic wave on a flat bottom and on a constant slope. These test cases bring to the fore major differences between the two numerical models and confirms the preliminary results of Section 5.5. The choice of these test cases are motivated by the fact that it is possible to find analytical solution. But there exist test which highlight other characteristics. The interest reader can refer to [4], [48], [54] or [69].

5.6.1 Soliton propagation

We first consider the propagation of an exact solitary wave solution to the Peregrine equations, with an amplitude equal to 0.2, over a flat bathymetry $d_0 = 1$. Details on the computation of this solution for Peregrine equations as well as mathematical conditions for the existence are given in secton 3.4.1. The space interval is equal to $[0, 200]$. In order to check our implementations, we have performed a grid convergence analysis. Numerical results have been compared with the initial profile (which is the profile of the exact solution). The meshes used contain respectively 1000, 2000, 4000 and 8000 points. In Figure 5.4, we have plotted the L^2 -norm of the error for each scheme. The scheme (5.4.53)-(5.4.54) provides an error 3 or 5 times less important than that corresponding to (5.3.7)-(5.3.8). We deduce that with the same initial finite elements method, the new procedure decreases the error.

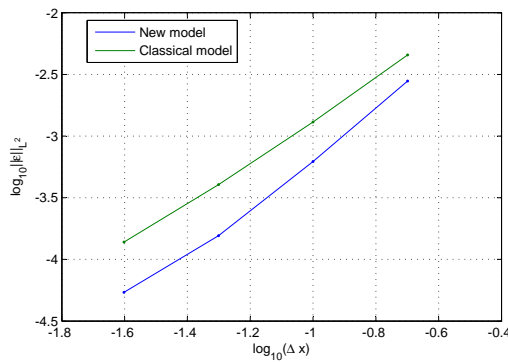


Figure 5.4 – Grid convergence results for a solitary wave propagating over a constant slope for the two numerical schemes.

5.6.2 Linear dispersion and linear shoaling test

In this section, we want to investigate the linear characteristics of the two numerical schemes. The idea is to confirm the study presented in Section 5.5.

Firstly, we remark that there exist exact periodic traveling wave for the linear Peregrine equations with constant bathymetry. These solutions can be written under the form:

$$\eta(t, x) = A \cos(k_0 x - \omega t), \bar{u}(t, x) = \frac{A}{d_0} \frac{\omega}{k_0} \cos(k_0 x - \omega t), \quad (5.6.1)$$

where $k_0 = 2\pi/\lambda$, A is the amplitude of η , and

$$\frac{\omega^2}{k_0^2} = \frac{gd_0}{1 + \frac{k_0^2 d_0^2}{3}}.$$

Linear dispersion test

The first test case consists in the propagation of an exact periodic traveling wave solution to the linear Peregrine equations, with an amplitude equal to 0.05 [m] over a flat bathymetry $d_0 = 13$ [m] and a wavelength $\lambda = 15$ [m] (then $\sigma = 0.87$). The space interval is equal to $[0, 150]$. We have performed computations for the two schemes with meshes containing 50 points (5 points per wavelength, and $\Delta_x = 3$), using periodic boundary conditions.

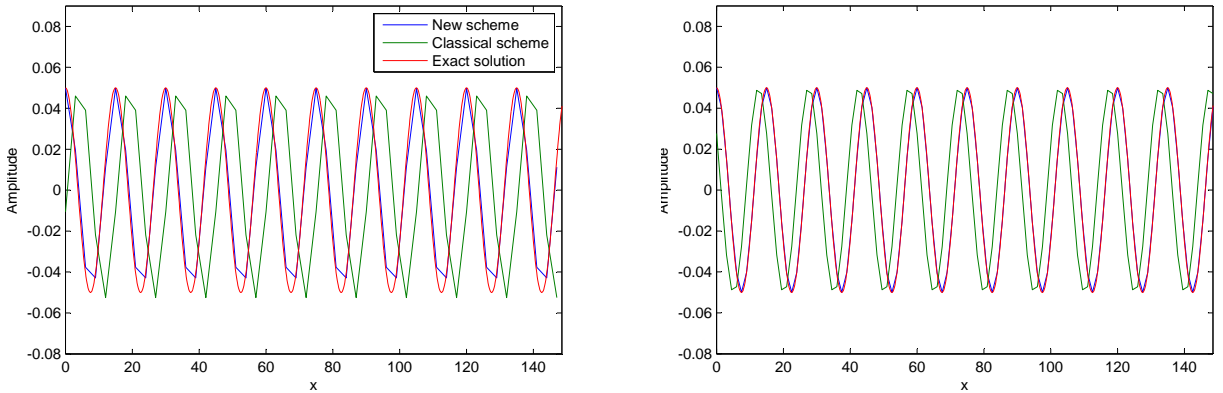


Figure 5.5 – Evolution of a traveling periodic wave for the two numerical schemes: Left : $\Delta_x = 3$ ($N_\lambda = 5$). Right : $\Delta_x = 1.5$ ($N_\lambda = 10$).

In figure 5.5, we have plotted the results of the two schemes and the exact solution. One can observe a difference in the phase behavior of the two schemes. The solution computed with the new scheme (5.5.1)-(5.5.2) matches very well the reference curve, while the scheme (5.5.23)-(5.5.24) is shifted. Furthermore, for $N_\lambda = 5$, the green curve exhibits some small amplitude defects. But for $N_\lambda = 10$, one can observe that the classical scheme provides better results without reaching the precision of the other scheme. It confirms the results presented in Figure 5.2. Finally, to compare the accuracy of the two models in these conditions, we have performed

a grid convergence analysis. In Figure 5.6, we have plotted the error in the L^2 -norm for each scheme, corresponding to successively 100, 300, 500 and 1000 points.

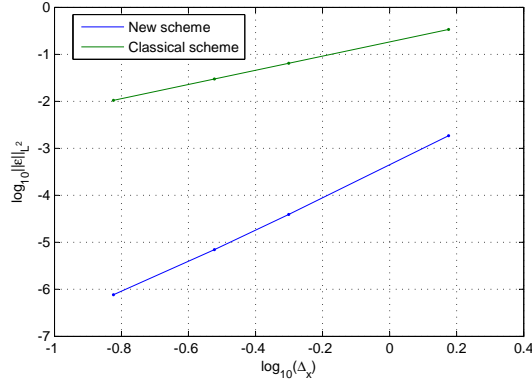


Figure 5.6 – Grid convergence results for a periodic traveling wave propagating over a constant slope for the two numerical schemes.

The slope obtained for the scheme (5.4.53)-(5.4.54) shows a convergence of order 3.4 while that corresponding to (5.3.7)-(5.3.8) is equal to 1.5. Furthermore, it is clear that the new model gives better results with 100 points than the classical scheme with 1000 points. We can deduce from this analysis that the new numerical scheme better reproduces linear dispersion effects.

Linear shoaling test

To further verify the results of Section 5.5, we have performed the test case described in this section. Let us recall the procedure. A periodic wave of amplitude $A = 0.05$ [m] and wavelength $\lambda = 15$ [m] propagates over an initial constant bottom $d_0 = 13$ [m]. The periodic wave has been generated using a relaxation zone method [16]. The bottom is flat for the first 150 m, it has a constant slope of 1/50 from $x = 150$ [m] to $x = 800$ [m]. A wide absorbing sponge layers of 60 [m] long have been used at $x = 790$ [m]. The wave propagates during a time of 500 s, in order to stabilize the solution. Note that, to our knowledge, it is not possible to give an analytical solution in this configuration. We then decide to compute a reference solution using a very refined mesh of 10000 points ($\Delta_x = 0.085$) and the scheme (5.5.23)-(5.5.24). This solution is used as a standard in the sequel to make the comparisons. The conclusion doesn't changed if one computes the reference solution with the scheme (5.5.1)-(5.5.2).

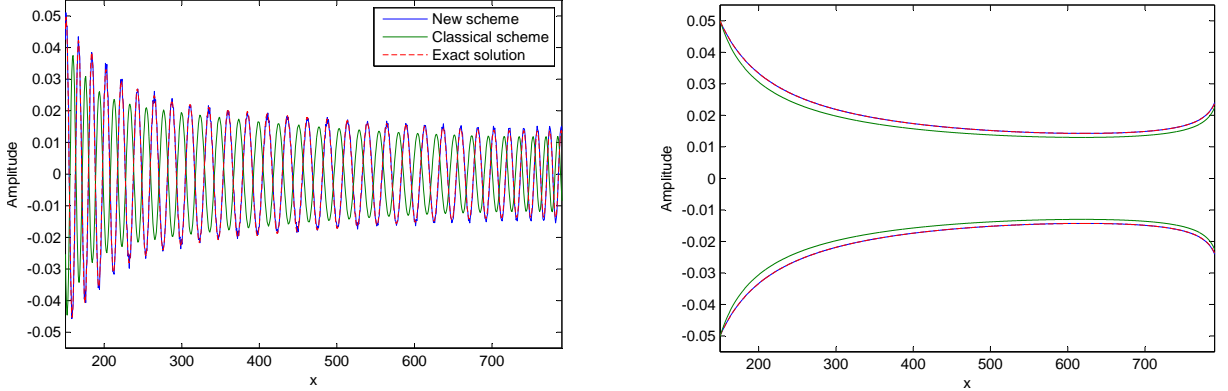


Figure 5.7 – Left: Shoaling wave profiles of Peregrine schemes ($\Delta_x = 0.85$). Right: Theoretical envelope of the two numerical schemes ($\Delta_x = 0.85$).

In Figure 5.7, we have plotted the linear shoaling wave profile using a mesh containing 1000 ($\Delta_x = 0.85$) points for the two numerical schemes as well as the reference solution, and the theoretical envelope given by the analysis of Section 5.5.3. Clearly, one can observe a major difference in the behavior of the two schemes. The solution emanating from the linear new scheme (5.5.1)-(5.5.2) matches very well the reference curve, showing that the convergence as already occurs with a few numbers of points while it is obviously not the case for the linear classical scheme (5.5.23)-(5.5.24). Indeed, the green curve exhibit some amplitude and phase defects. This test case confirms results given in Section 5.5, presented on Figure 5.7 on the right.

5.7 Conclusions and perspectives

We have presented a new systematic method to obtain discrete numerical model in the study of incompressible free surface flows. In order to evaluate the power of this method, we have considered the case of the so-called Peregrine equations and performed the computations in this academic situation. We have compared our new numerical scheme with the one obtained by performing directly a Galerkin method on the Peregrine equations. Finally, by the use of several numerical experiments, we have shown the efficiency of our new scheme to reproduce the linear effects although it is similar to the classical one in a nonlinear regime. Moreover, we claim that the method does not give a unique model. The choice of the initial scheme applied on Euler equations is an extra degree of freedom.

In the next chapter, we apply this new procedure to derive numerical schemes for the Extended Boussinesq's models of Nwogu (see Section 2.6.3 for the derivation of the continuous system) as well as for the Green-Naghdi equations (see Section 2.7 for the derivation).

Chapter 6

Discrete asymptotic equations for Nwogu model

Contents

6.1	Introduction	148
6.2	Setting and Notation	149
6.3	A new setting for deriving discrete Green-Naghdi and Nwogu equations	151
6.3.1	Extension of the procedure to obtain the Green-Naghdi equations.	151
6.3.2	Discrete Nwogu equations	155
6.3.3	Study of the linear dispersion characteristics.	157
6.4	Numerical experiments	160
6.4.1	Soliton propagation.	160
6.4.2	Periodic wave propagation	161
6.4.3	Periodic wave propagation over a shelf.	162
6.5	Conclusion and future works	164

6.1 Introduction

Wave transformation in near shore zone is well-described by the incompressible Euler equations. Due to their strong complexity in three dimensions, it is natural to replace it by asymptotic equations in order to perform some effective numerical computations. The use of Boussinesq depth-averaged velocity type models for this task is quite common. These models have the advantage to take into account the dispersive and nonlinear effects which appear to be crucial when one wants to modelize physical situations. Recently, many authors have extended the Boussinesq equations to include more dispersion effects [11, 57]. As a consequence, the resulting models present dispersion characteristics closer than those emanating from the linear wave theory. Most of these works ride on the same idea : the inclusion of extra dispersive differential terms which are neglectable in the asymptotic analysis. Another idea was introduce by O. Nwogu in 1994 and consists in the replacement of depth-averaged velocity by another one evaluated at a properly chosen depth [60]. Actually, this model is relevant when one wants to use it outside of its range of validity [60, 72, 36].

For most of Boussinesq models, the task of designing an accurate numerical discretization is a non trivial one, due to the presence of dispersion terms. Several approaches exist in literature, each with its own advantages and drawbacks. For details, the interested reader may refer to [17, 21, 38, 45, 59, 64]. Furthermore, this numeric treatment doesn't take into account the interaction between asymptotic models and schemes truncation. To investigate this important issue, a new procedure has been introduced in [13] (see Chapter 5) : firstly we discretize partially the incompressible Euler equations in the horizontal direction using a finite element method and then we perform a formal asymptotic analysis similar to the ones used to derive continuous Boussinesq equations, depending on the asymptotic regime one wants to investigate.

It has been developed for the Peregrine asymptotic regime and has furnished promising results, improving the linear characteristics of the scheme in comparison to the classical one obtained by writting directly a \mathbb{P}_1 Galerkin method on the Peregrine equations. One limitation of that work comes from the nature of Peregrine equations. It has been proved that its dispersion characteristics appear not adapted for practical applications (see Chapter 4 or [72]). This is why, in this chapter, we extend this method to the Nwogu equations. Actually, we propose to modify directly the numerical scheme consistent with the Peregrine equations obtained in Chapter 5 in order to get another one which will approximate the Nwogu equations. It is believed that the resulting numerical scheme will have improved linear characteristics as it was true for the Peregrine equations.

The chapter is organized as follows. In Section 6.2 we recall some important notations, most of the algebraic operators involved in our analysis and we introduce a classical scheme used to solve the Nwogu equations. In Section 6.3, we extend the new paradigm to the Green-Naghdi model and the Nwogu one. This section is concluded with a theoretical study of linear characteristics of the discrete Nwogu equations. Finally, Section 6.4 presents a numerical evaluation of the performances of the schemes emanating from the Nwogu system.

6.2 Setting and Notation

Before going further, let us recall some notations. For simplicity, in this chapter, we only deal with 2-D and 1-D problems. We denote by (x, z) respectively the horizontal and the vertical spatial dimension, by $d(x)$ the depth at still water and by $\eta(t, x)$ the surface elevation from its rest position. The total depth is then $h(t, x) = d(x) + \eta(t, x)$ (see Figure 5.1).

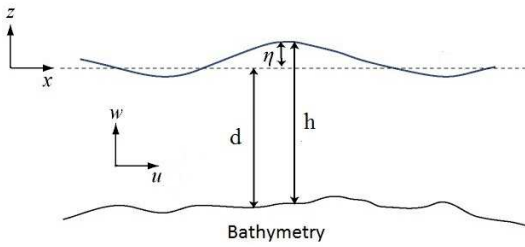


Figure 6.1 – Sketch of the free surface flow problem, main parameters description.

Let a be a typical wave amplitude, d_0 a reference water depth and λ a typical wavelength. In view of performing an asymptotic analysis, we introduce the nonlinearity parameter ε and the dispersion parameter σ defined by

$$\varepsilon = \frac{a}{d_0}, \quad \sigma = \frac{d_0}{\lambda}.$$

Under the Boussinesq hypothesis $\varepsilon = \mathcal{O}(\sigma^2)$, Peregrine (see [63]) first derived, from the Euler equations, the following standard system of Boussinesq's type

$$\begin{aligned} \eta_t + (h\bar{u})_x &= 0, \\ \bar{u}_t + \bar{u}\bar{u}_x + g\eta_x + \left(\frac{d^2}{6}\bar{u}_{txx} - \frac{d}{2}(d\bar{u})_{txx}\right) &= 0. \end{aligned} \tag{6.2.1}$$

The model describes the evolution of the depth-averaged velocity \bar{u} and the surface elevation η within an accuracy of $\mathcal{O}(\varepsilon\sigma^2, \sigma^4)$ w.r.t. the Euler equations. It has been proved that this system is only an accurate approximation to Stokes first order wave theory only for very small values of σ ([36]). Many works have concentrated on extending the validities of the linear dispersion relation to larger values of σ [11, 55]. It is in this context that O. Nwogu proposed a new system of equation describing the evolution of the velocity evaluated at an arbitrary depth u^α and the surface elevation η . This idea permits to introduce a degree of freedom to improve the linear dispersion of the system (see [60]). We recall the resulting equations

$$\begin{aligned} \eta_t + (hu^\alpha)_x + [B_1d^3u_{xx}^\alpha + B_2d^2(du^\alpha)_{xx}]_x &= 0, \\ u_t^\alpha + u^\alpha u_x^\alpha + g\eta_x + d^2A_1u_{txx}^\alpha - A_2d(du^\alpha)_{txx} &= 0, \end{aligned} \tag{6.2.2}$$

where

$$A_1 = \frac{\theta^2}{2}, \quad A_2 = \theta, \quad B_1 = \frac{\theta^2}{2} - \frac{1}{6}, \quad B_2 = \theta + \frac{1}{2},$$

with $\theta \in (0, 1)$.

The set of Equations (6.2.2) is now well-understood from the computational point of view. A classical numerical scheme can be obtained by applying the finite element method on a reformulated Nwogu system (6.2.3) in order to deal with the third order derivatives terms. For that purpose, we introduce a new intermediate variable v leading to the following three equations system

$$\begin{aligned} \eta_t + (hu^\alpha)_x + v_x &= 0, \\ v &= B_1 d^3 u_{xx}^\alpha + B_2 d^2 (du^\alpha)_{xx}, \\ u_t^\alpha + u^\alpha u_x^\alpha + g\eta_x + d^2 (A_1 u_{txx}^\alpha - A_2 d(du^\alpha)_{txx}) &= 0. \end{aligned} \tag{6.2.3}$$

The finite element method is used in the following setting (see also Section 5.2). On an interval $[r, s]$, we introduce a set of nodes

$$r = x_0 < x_1 < \dots < x_N = s,$$

where, for simplicity, we take a constant space step $\Delta_x = x_{j+1} - x_j, \forall j \in \{0, \dots, N\}$. We denote by E , U^α , V , D and H the vectors of the nodal values of η , u^α , v , d and h . Similarly to what has been done in [13], we apply the \mathbb{P}_1 Galerkin method to approximate the variational form of (6.2.3). In particular, we denote by $\{\varphi_j\}_{0 \leq j \leq N}$ the standard piecewise linear continuous Lagrange basis with periodic boundary conditions, and introduce the discrete velocity u_Δ^α , wave height η_Δ , variable v_Δ and depth polynomials d_Δ as follows

$$\begin{aligned} u_\Delta^\alpha(t, x) &= \sum_{j=0}^N u_j^\alpha(t) \varphi_j(x), \quad \eta_\Delta(t, x) = \sum_{j=0}^N \eta_j(t) \varphi_j(x), \\ v_\Delta(t, x) &= \sum_{j=0}^N v_j(t) \varphi_j(x), \quad d_\Delta(x) = \sum_{j=0}^N d_j \varphi_j(x). \end{aligned}$$

The Galerkin approximation of (6.2.3), under the hypothesis of exact integration w.r.t. all the discrete polynomials involved, can be written in a compact matrix form

$$\frac{d}{dt} \mathcal{M}E + \frac{1}{3} \left(2\mathcal{N}(H \diamond U^\alpha) + H \diamond (\mathcal{N}U^\alpha) + U^\alpha \diamond (\mathcal{N}H) \right) + \mathcal{N}V = 0, \tag{6.2.4}$$

$$\mathcal{M}V = \mathcal{M}\{D, U^\alpha\}_1, \tag{6.2.5}$$

$$\frac{d}{dt} \mathcal{M}U^\alpha + \frac{1}{3} \left(\mathcal{N}((U^\alpha)^2) + U^\alpha \diamond (\mathcal{N}U^\alpha) \right) + g\mathcal{N}E + \frac{d}{dt} \{D, U^\alpha\}_2 = 0, \tag{6.2.6}$$

where

$$\begin{aligned} \{D, U^\alpha\}_1 &= B_1 D^3 \diamond (\mathcal{Q}U^\alpha) + \frac{B_2}{6} \left(\mathcal{Q}(D^3 \diamond U^\alpha) + D \diamond (\mathcal{Q}(D^2 \diamond U^\alpha)) + D^2 \diamond (\mathcal{Q}(D \diamond U^\alpha)) \right. \\ &\quad \left. + 3D^3 \diamond (\mathcal{Q}(U^\alpha)) - U^\alpha \diamond (\mathcal{Q}(D^3)) - D \diamond (U^\alpha \diamond (\mathcal{Q}(D^2))) + 5D^2 \diamond (U^\alpha \diamond (\mathcal{Q}D)) \right), \end{aligned}$$

and

$$\begin{aligned} \{D, U^\alpha\}_2 = & A_1 D^2 \diamond (\mathcal{Q} U^\alpha) + \frac{A_2}{3} \left(\mathcal{Q}(D^2 \diamond U^\alpha) + D \diamond (\mathcal{Q}(D \diamond U^\alpha)) \right. \\ & \left. + D^2 \diamond (\mathcal{Q} U^\alpha) - U^\alpha \diamond (\mathcal{Q}(D^2)) + 2D \diamond (U^\alpha \diamond (\mathcal{Q} D)) \right). \end{aligned}$$

Remark that \mathcal{M} , \mathcal{N} and \mathcal{Q} are the usual mass, derivation and stiffness matrices arising in the Galerkin discretization, introduced in Chapter 5. Moreover, for given columns vectors $A = (a_i)_{0 \leq i \leq N}$ and $B = (b_i)_{0 \leq i \leq N}$, we have introduced the operator \diamond :

$$\begin{aligned} \mathbb{R}^N \times \mathbb{R}^N & \rightarrow \mathbb{R}^N \\ (A, B) & \rightarrow A \diamond B := (a_i b_i)_{0 \leq i \leq N} \end{aligned}$$

In the sequel, A^2 simplifies $A \diamond A$. Substituting Equation (6.2.5) in (6.2.4) to eliminate V in the system, we obtain the discrete equations which are going to be referred to the “classical scheme” in the rest of this chapter :

$$\frac{d}{dt} \mathcal{M} E + \mathcal{M}[H; U^\alpha] + \mathcal{N}\{D, U^\alpha\}_1 = 0, \quad (6.2.7)$$

$$\frac{d}{dt} \mathcal{M} U^\alpha + \frac{1}{3} \left(\mathcal{N}((U^\alpha)^2) + U^\alpha \diamond (\mathcal{N} U^\alpha) \right) + g \mathcal{N} E + \frac{d}{dt} \{D, U^\alpha\}_2 = 0. \quad (6.2.8)$$

6.3 A new setting for deriving discrete Green-Naghdi and Nwogu equations

In Chapter 5, we have introduced a new paradigm leading to a numerical scheme which reproduces better the linear effects of continuous Peregrine equations than the one obtained performing a standard method. Then, it is natural to extend this method to other asymptotic models which reproduce better the theoretical linear dispersion such as Nwogu equations. This is the target of Section 6.3.2. In addition, a short change in the Peregrine analysis leads to Green-Naghdi equations. The following section is dedicated to the obtention of a new numerical scheme consistent with this fully non-linear system.

6.3.1 Extension of the procedure to obtain the Green-Naghdi equations.

In this section, we explain how to derive a new numerical scheme for the Green-Naghdi equations using the procedure developed for the Peregrine equations in [13]. We start by recalling the Green-Naghdi system presented in Section 2.7

$$\eta_t + (h\bar{u})_x = 0, \quad (6.3.1)$$

$$\bar{u}_t + \bar{u}\bar{u}_x + g\eta_x - \frac{1}{h} \left[\left(\frac{h^3}{3} - \frac{h^2 d}{2} \right) \mathbf{P} + \frac{h^2}{2} \mathbf{Q} \right]_x + d_x \left((h-d) \mathbf{P} + \mathbf{Q} \right) = 0, \quad (6.3.2)$$

where

$$\mathbf{P} = \bar{u}_{tx} + \bar{u}\bar{u}_{xx} - \bar{u}_x^2 \text{ and } \mathbf{Q} = (d\bar{u})_{tx} + \bar{u}(d\bar{u})_{xx} - \bar{u}_x(d\bar{u})_x,$$

and

$$\bar{u}(t, x) = \int_{-d}^{\eta} u(t, x, z) dz.$$

We recall notations and the 2D-Euler equations written in terms of velocity (u, w) , pressure p , constant density ρ and vertical gravity acceleration g already introduced in Chapter 5

$$u_t + uu_x + wu_z + \frac{p_x}{\rho} = 0, \quad (6.3.3)$$

$$w_t + uw_x + ww_z + \frac{p_z}{\rho} + g = 0, \quad (6.3.4)$$

$$u_x + w_z = 0, \quad (6.3.5)$$

$$u_z - w_x = 0, \quad (6.3.6)$$

where the last equation represents the irrotationality condition. On the free surface and sea-bed level we use the classical boundary conditions :

- at the free surface $z = \eta$

$$w = \eta_t + u\eta_x, p = 0, \quad (6.3.7)$$

- on the seafloor $z = -d$

$$w = -ud_x. \quad (6.3.8)$$

The following usual non-dimensional variables are introduced in order to perform an asymptotic analysis

$$\tilde{x} = \frac{x}{\lambda}, \tilde{z} = \frac{z}{d_0}, \tilde{t} = \frac{\sqrt{gd_0}}{\lambda} t, \tilde{\eta} = \frac{\eta}{a}, \tilde{u} = \frac{d_0}{a\sqrt{gd_0}} u, \tilde{w} = \frac{\lambda}{a} \frac{1}{\sqrt{gd_0}} w, \tilde{p} = \frac{p}{gd_0\rho}, \Delta_{\tilde{x}} = \frac{\Delta_x}{\lambda}, \tilde{d} = \frac{d}{d_0}.$$

Using the notations introduced above, the Euler equations and the irrotationality condition can be recast in a non-dimensional form as

$$\varepsilon \tilde{u}_{\tilde{t}} + \varepsilon^2 \tilde{u} \tilde{u}_{\tilde{x}} + \varepsilon^2 \tilde{w} \tilde{u}_{\tilde{z}} + \tilde{p}_{\tilde{x}} = 0, \quad (6.3.9)$$

$$\varepsilon \sigma^2 \tilde{w}_{\tilde{t}} + \varepsilon^2 \sigma^2 \tilde{u} \tilde{w}_{\tilde{x}} + \varepsilon^2 \sigma^2 \tilde{w} \tilde{w}_{\tilde{z}} + \tilde{p}_{\tilde{z}} + 1 = 0, \quad (6.3.10)$$

$$\tilde{u}_{\tilde{x}} + \tilde{w}_{\tilde{z}} = 0, \quad (6.3.11)$$

$$\tilde{u}_{\tilde{z}} - \sigma^2 \tilde{w}_{\tilde{x}} = 0. \quad (6.3.12)$$

The boundary conditions become :

- at the free surface $\tilde{z} = \varepsilon \tilde{\eta}$

$$\tilde{w} = \tilde{\eta}_{\tilde{t}} + \varepsilon \tilde{u} \tilde{\eta}_{\tilde{x}}, \tilde{p} = 0, \quad (6.3.13)$$

- at the bed $\tilde{z} = -\tilde{d}$

$$\tilde{w} = -\tilde{u} \tilde{d}_{\tilde{x}}, \quad (6.3.14)$$

where ε and σ are respectively the nonlinearity and the dispersion parameters defined as

$$\varepsilon = \frac{a}{d_0}, \quad \sigma = \frac{d_0}{\lambda}.$$

Then, we apply a Galerkin method on the variable x keeping t and z unchanged. In the sequel we drop the " ~ " and we introduce for all $i \in \{0, \dots, N\}$, $u_i(t, z) = u(t, x_i, z)$, $w_i(t, z) = w(t, x_i, z)$, $\eta_i(t, z) = \eta(t, x_i, z)$, $p_i(t, z) = p(t, x_i, z)$. In addition, the discrete horizontal velocity u_Δ , wave height η_Δ , depth d_Δ , vertical velocity w_Δ and pressure p_Δ polynomials are written in the Galerkin basis as follows

$$\begin{aligned} u_\Delta(t, x, z) &= \sum_{i=0}^N u_i(t, z) \varphi_i(x), \quad w_\Delta(t, x, z) = \sum_{i=0}^N w_i(t, z) \varphi_i(x), \quad \eta_\Delta(t, x) = \sum_{i=0}^N \eta_i(t) \varphi_i(x), \\ p_\Delta(t, x, z) &= \sum_{i=0}^N p_i(t, z) \varphi_i(x), \quad d_\Delta(x) = \sum_{i=0}^N d_i \varphi_i(x). \end{aligned} \tag{6.3.15}$$

We focus on periodic boundary conditions that is we introduce $x_{-1} = x_N$ and $x_{N+1} = x_0$. For the boundary conditions, we propose to integrate Equation (6.3.13) along the curve $z = \varepsilon\eta$ and Equation (6.3.14) along the curve $z = -d$. For that purpose, we choose to introduce

$$\begin{aligned} \hat{w}_\Delta &= \sum_{i=0}^N w_i(t, \varepsilon\eta(t, x_i)) \varphi_i(x), \quad \check{w}_\Delta = \sum_{i=0}^N w_i(t, -d(x_i)) \varphi_i(x), \\ \hat{u}_\Delta &= \sum_{i=0}^N u_i(t, \varepsilon\eta(t, x_i)) \varphi_i(x), \quad \check{u}_\Delta = \sum_{i=0}^N u_i(t, -d(x_i)) \varphi_i(x). \end{aligned} \tag{6.3.16}$$

Introducing the following column vectors

$$W = (w_i)_{0 \leq i \leq N}, \quad U = (u_i)_{0 \leq i \leq N}, \quad E = (\eta_i)_{0 \leq i \leq N}, \quad P = (p_i)_{0 \leq i \leq N}, \quad D = (d_i)_{0 \leq i \leq N}, \quad \mathcal{I} = \begin{pmatrix} 1 \\ \vdots \\ 1 \end{pmatrix}$$

$$\hat{W} = \left(w_i(\varepsilon\eta_i) \right)_{0 \leq i \leq N}, \quad \hat{U} = \left(u_i(\varepsilon\eta_i) \right)_{0 \leq i \leq N}, \quad \check{W} = \left(w_i(-d_i) \right)_{0 \leq i \leq N}, \quad \check{U} = \left(u_i(-d_i) \right)_{0 \leq i \leq N},$$

we can rewrite the discretization of Equations (6.3.9)-(6.3.14) into the following matrix-form (see Chapter 5 for details)

$$\varepsilon \frac{d}{dt} \mathcal{M}U + \varepsilon^2 \mathcal{M}\mathbf{b}_1(U, U) + \varepsilon^2 \sigma^2 \mathcal{M}\mathbf{b}_2(W, U_z) + \mathcal{N}P = 0, \tag{6.3.17}$$

$$\varepsilon \sigma^2 \frac{d}{dt} \mathcal{M}W + \varepsilon^2 \sigma^2 \mathcal{M}\mathbf{b}_1(U, W) + \varepsilon^2 \sigma^2 \mathcal{M}\mathbf{b}_2(W, W_z) + \frac{d}{dz} \mathcal{M}P + \mathcal{I} = 0, \tag{6.3.18}$$

$$\mathcal{N}U + \mathcal{M} \frac{d}{dz} W = 0, \tag{6.3.19}$$

$$\mathcal{M} \frac{d}{dz} U - \sigma^2 \mathcal{N} W = 0. \quad (6.3.20)$$

The boundary conditions become

- at the free surface

$$\mathcal{M} \hat{W} = \frac{d}{dt} \mathcal{M} E + \varepsilon \mathcal{M} \mathbf{b}_1(\hat{U}, E), \quad \mathcal{M} \hat{P} = 0, \quad (6.3.21)$$

- at the bottom

$$\mathcal{M} \check{W} = -\mathcal{M} \mathbf{b}_1(\check{U}, D), \quad (6.3.22)$$

where \mathbf{b}_1 and \mathbf{b}_2 are bilinear operators defined for two given column vector A and B as

$$\mathbf{b}_1(A, B) = \frac{1}{3} \left(\mathcal{K}(A \diamond B) - \mathcal{M}^{-1}(A \diamond (\mathcal{N}B)) + 2\mathcal{M}^{-1}(B \diamond (\mathcal{N}A)) \right), \quad (6.3.23)$$

$$\mathbf{b}_2(A, B) = \frac{1}{2} \left(A \diamond B + \mathcal{M}^{-1}(A \diamond (\mathcal{M}B)) + \mathcal{M}^{-1}(B \diamond (\mathcal{M}A) - \mathcal{M}^{-1}(A \diamond B)) \right). \quad (6.3.24)$$

Remark that vectors $\mathbf{b}_1(U, W)$ and $\mathbf{b}_2(W, U_z)$ are respectively the discretizations of the non linear terms “ uw_x ” and “ wu_z ” obtained for exact computations of the Galerkin integrals.

System (6.3.17)-(6.3.22) represents the first step in the analysis. In order to obtain discrete Green-Naghdi equations, we adapt the procedure detailed in Chapter 5 to the derivation of Green-Naghdi presented in Section 2.7. For that purpose, we perform the asymptotic analysis considering the particular asymptotic regime : $\varepsilon = \mathcal{O}(1)$, $\sigma \ll 1$. Furthermore, it is assumed that $\Delta_{\tilde{x}} = \mathcal{O}(\sigma)$ (it transpires that $\Delta_x = \mathcal{O}(d_0)$), where Δ_x is the spatial step of the discretization. As a consequence, it is possible to express the discrete horizontal velocity vector U and the discrete vertical velocity W in function of the discrete depth-averaged velocity vector $\bar{U} = (\bar{u}(t, x_i))_{0 \leq i \leq N}$ neglecting only terms of order σ^4 for U and σ^2 for W .

$$U = \bar{U} - \sigma^2 \left(\left(\frac{z^2}{2} - \left(\frac{H^2}{6} - \frac{(H-D) \diamond D}{2} \right) \right) \diamond (\mathcal{K}^2 \bar{U}) + \left(z - \left(\frac{H}{2} - D \right) \right) \diamond (\mathcal{K}[D; \bar{U}]) \right) + \mathcal{O}(\sigma^4), \quad (6.3.25)$$

$$W = - (z \mathcal{K} \bar{U} + [D; \bar{U}]) + \mathcal{O}(\sigma^2), \quad (6.3.26)$$

where $H = D + \varepsilon E$ and the operator bracket $[\cdot; \cdot]$ is defined as

$$[A; B] = A \diamond B + \mathbf{b}_1(B, A). \quad (6.3.27)$$

In addition, the pressure P can be expressed as

$$P = \varepsilon E - z \mathcal{I} + \varepsilon \sigma^2 \left(\frac{z^2 - (\varepsilon E)^2}{2} \mathcal{P} + (z - \varepsilon E) \mathcal{Q} \right) + \mathcal{O}(\sigma^4), \quad (6.3.28)$$

with

$$\mathcal{P} = \mathcal{K} \bar{U}_t + \varepsilon \mathbf{b}_1(\bar{U}, \mathcal{K} \bar{U}) - \varepsilon \mathbf{b}_2(\mathcal{K} \bar{U}, \mathcal{K} \bar{U}),$$

and

$$\mathcal{Q} = [D; \bar{U}_t] + \varepsilon \mathbf{b}_1(\bar{U}, [D; \bar{U}]) - \varepsilon \mathbf{b}_2([D; \bar{U}], \mathcal{K} \bar{U}).$$

Then, we substitute (6.3.25) and (6.3.28) in Euler equations, keeping in mind the very important hypothesis : $\Delta_x = \mathcal{O}(\sigma)$ which is useful to simplify some expression of order $\sigma^2 \Delta_x^2$. It leads to the following system

$$E_t + [H; \bar{U}] = 0, \quad (6.3.29)$$

$$(\mathcal{I}_N + \mathbf{T}(H, D)) \bar{U}_t + \mathbf{b}_1(\bar{U}, \bar{U}) + g\mathcal{K}E + \mathbf{R}_1(H, \bar{U}, D) + \mathbf{R}_2(H, \bar{U}, D) = 0, \quad (6.3.30)$$

where \mathcal{I}_N is the identity matrix of $\mathcal{M}_N(\mathbb{R})$ and where the linear operator \mathbf{T} is defined, for a given column vector X , as

$$\begin{aligned} \mathbf{T}(H, D)X &= \left(\frac{H^2}{6} - \frac{(H-D) \diamond D}{2} \right) \diamond (\mathcal{K}^2 X) + \left(\frac{H}{2} - D \right) \diamond (\mathcal{K}[D; X]) \\ &\quad - \frac{1}{2} \mathcal{K} \left((H-D)^2 \diamond (\mathcal{K}X) \right) - \mathcal{K} \left((H-D) \diamond [D; X] \right). \end{aligned} \quad (6.3.31)$$

Furthermore, \mathbf{R}_1 and \mathbf{R}_2 are nonlinear operators defined as

$$\begin{aligned} \mathbf{R}_1(H, \bar{U}, D) &= \mathbf{b}_1 \left(\bar{U}, \left(\frac{H^2}{6} - \frac{(H-D) \diamond D}{2} \right) \diamond (\mathcal{K}^2 \bar{U}) + \left(\frac{H}{2} - D \right) \diamond (\mathcal{K}[D; \bar{U}]) \right) \\ &\quad + \mathbf{b}_1 \left(\left(\frac{H^2}{6} - \frac{(H-D) \diamond D}{2} \right) \diamond (\mathcal{K}^2 \bar{U}) + \left(\frac{H}{2} - D \right) \diamond (\mathcal{K}[D; \bar{U}]), \bar{U} \right), \end{aligned} \quad (6.3.32)$$

$$\begin{aligned} \mathbf{R}_2(H, \bar{U}, D) &= \mathbf{b}_2([D; \bar{U}], \mathcal{K}[D; \bar{U}]) - \frac{1}{2} \mathcal{K}((H-D) \diamond \mathcal{P}) - \mathcal{K}((H-D) \diamond \mathcal{Q}) \\ &\quad - [H; \bar{U}] \diamond \left(\left(\frac{H}{3} - \frac{D}{2} \right) \diamond (\mathcal{K}^2 \bar{U}) + \frac{1}{2} \mathcal{K}[D; \bar{U}] \right). \end{aligned} \quad (6.3.33)$$

Details of this derivation and numerical investigations will be presented in a future work, but we can already remark that the linearized numerical scheme of Green-Naghdi around the rest state is exactly the same than the Peregrine one :

$$\frac{d}{dt} E + [D; \bar{U}] = 0, \quad (6.3.34)$$

$$\frac{d}{dt} \bar{U} + g\mathcal{K}E + \frac{d}{dt} \left(\frac{D^2}{6} \diamond (\mathcal{K}^2 \bar{U}) - \frac{D}{2} \diamond (\mathcal{K}[D; \bar{U}]) \right) = 0, \quad (6.3.35)$$

It transpires that the linear dispersion characteristics of this numerical scheme presented in Chapter 5 for the Peregrine equations are similar to the Green-Naghdi one.

6.3.2 Discrete Nwogu equations

The aim of this section is to derive a new numerical scheme consistent with the Nwogu equations by performing an asymptotic analysis on the non-dimensional discrete Euler system (6.3.17)-(6.3.22). The starting point of this work is the Peregrine system introduced in Chapter 5. More precisely, we start from the non-dimensional system :

$$\frac{d}{dt} \mathcal{M}E + \mathcal{M}[H; \bar{U}] = \mathcal{O}(\varepsilon\sigma^2, \sigma^4), \quad (6.3.36)$$

$$\frac{d}{dt} \mathcal{M}\bar{U} + \varepsilon \mathbf{b}_1(\bar{U}, \bar{U}) + \mathcal{N}E + \sigma^2 \mathcal{M} \frac{d}{dt} \left(\frac{D^2}{6} \diamond (\mathcal{K}^2 \bar{U}) - \frac{D}{2} \diamond (\mathcal{K}[D; \bar{U}]) \right) = \mathcal{O}(\varepsilon\sigma^2, \sigma^4). \quad (6.3.37)$$

We recall the expansions of the discrete horizontal velocity U in function of the discrete depth-averaged horizontal velocity \bar{U} neglecting the terms of order σ^4 and $\varepsilon\sigma^2$

$$U = \bar{U} + \sigma^2 \left(\frac{D^2}{6} \diamond (\mathcal{K}^2 \bar{U}) - \frac{z^2}{2} \mathcal{K}^2 \bar{U} - z \mathcal{K}[D; \bar{U}] - \frac{D}{2} \diamond (\mathcal{K}[D; \bar{U}]) \right) + \mathcal{O}(\varepsilon\sigma^2, \sigma^4), \quad (6.3.38)$$

where the operator bracket is defined in Equation (6.3.27).

From Equation (6.3.38), we derive an asymptotic expansion in terms of σ and ε for the particular discrete horizontal velocity U^α in function of the discrete horizontal depth-averaged velocity $\bar{U} = \bar{U}(t, z)$ evaluating expansion (6.3.38) on an arbitrary depth z_α

$$U^\alpha = \bar{U} + \sigma^2 \left(\left(\frac{D^2}{6} - \frac{z_\alpha^2}{2} \right) \diamond (\mathcal{K}^2 \bar{U}) - \left(z_\alpha + \frac{D}{2} \right) \diamond (\mathcal{K}[D; \bar{U}]) \right) + \mathcal{O}(\varepsilon\sigma^2, \sigma^4). \quad (6.3.39)$$

In order to find the discrete equations satisfied by E and U^α , we reverse the relation (6.3.39) neglecting terms of order $\varepsilon\sigma^2$ and σ^4

$$\bar{U} = U^\alpha + \sigma^2 \left(\left(\frac{z_\alpha^2}{2} - \frac{D^2}{6} \right) \diamond (\mathcal{K}^2 U^\alpha) + \left(z_\alpha + \frac{D}{2} \right) \diamond (\mathcal{K}[D; U^\alpha]) \right) + \mathcal{O}(\varepsilon\sigma^2, \sigma^4). \quad (6.3.40)$$

Then, we substitute (6.3.40) in the non-dimensional discrete Peregrine system (6.3.36)-(6.3.37) to obtain

$$\frac{d}{dt} \mathcal{M}E + \mathcal{M}[H; U^\alpha] + \sigma^2 \mathcal{M} \left[D; \left(\frac{z_\alpha^2}{2} - \frac{D^2}{6} \right) \diamond (\mathcal{K}^2 U^\alpha) + \left(z_\alpha + \frac{D}{2} \right) \diamond (\mathcal{K}[D; U^\alpha]) \right] = \mathcal{O}(\varepsilon\sigma^2, \sigma^4), \quad (6.3.41)$$

$$\frac{d}{dt} \mathcal{M}U^\alpha + \varepsilon \mathcal{M}\mathbf{b}_1(U^\alpha, U^\alpha) + \mathcal{N}E + \sigma^2 \mathcal{M} \frac{d}{dt} \left(\frac{z_\alpha^2}{2} \diamond (\mathcal{K}^2 U^\alpha) + z_\alpha \diamond (\mathcal{K}[D; U^\alpha]) \right) = \mathcal{O}(\varepsilon\sigma^2, \sigma^4). \quad (6.3.42)$$

To conclude, we return to the physical variables and neglect the terms of order $\varepsilon\sigma^2$ and σ^4 to obtain a new discrete approximation of the Nwogu equations

$$\frac{d}{dt} \mathcal{M}E + \mathcal{M}[H; U^\alpha] + \mathcal{M} \left[D; \left(\frac{z_\alpha^2}{2} - \frac{D^2}{6} \right) \diamond (\mathcal{K}^2 U^\alpha) + \left(z_\alpha + \frac{D}{2} \right) \diamond (\mathcal{K}[D; U^\alpha]) \right] = 0, \quad (6.3.43)$$

$$\frac{d}{dt} \mathcal{M}U^\alpha + \mathcal{M}\mathbf{b}_1(U^\alpha, U^\alpha) + g\mathcal{N}E + \mathcal{M} \frac{d}{dt} \left(\frac{z_\alpha^2}{2} \diamond (\mathcal{K}^2 U^\alpha) + z_\alpha \diamond (\mathcal{K}[D; U^\alpha]) \right) = 0. \quad (6.3.44)$$

Setting the arbitrary depth for all $i \in \{0, \dots, N\}$, $(z_\alpha)_i = \theta d_i$, where $\theta \in (-1, 0)$, the system is rewritten as,

$$\frac{d}{dt} \mathcal{M}E + \mathcal{M}[H; U^\alpha] + B_1 \mathcal{M} \left[D; D^2 \diamond (\mathcal{K}^2 U^\alpha) \right] + B_2 \mathcal{M} \left[D; D \diamond (\mathcal{K}[D; U^\alpha]) \right] = 0, \quad (6.3.45)$$

$$\frac{d}{dt} \mathcal{M}U^\alpha + \mathcal{M}\mathbf{b}_1(U^\alpha, U^\alpha) + g\mathcal{N}E + \mathcal{M}\frac{d}{dt} \left(A_1 D^2 \diamond (\mathcal{K}^2 U^\alpha) + A_2 D \diamond (\mathcal{K}[D; U^\alpha]) \right) = 0, \quad (6.3.46)$$

where

$$A_1 = \frac{\theta^2}{2}, \quad A_2 = \theta, \quad B_1 = \frac{\theta^2}{2} - \frac{1}{6}, \quad B_2 = \theta + \frac{1}{2},$$

and $\theta \in (0, 1)$.

We see that, while involving similar algebraic operations, the new discretization of Nwogu system (6.3.45)-(6.3.46) is different from the classical ones (6.2.7)-(6.2.8). As for Peregrine model, the major differences are in the treatment of the dispersive terms. Differences in the momentum equation, which involves the bracket operator $[\cdot; \cdot]$ for the new scheme and the operator $\{\cdot, \cdot\}_2$ for the classical one, are similar than ones observed for the Peregrine equations in Chapter 5. In addition, the third order derivatives terms of the continuity equation of the Nwogu system are treated differently by the two methods. The new scheme uses combinations of the bracket operator $[\cdot; \cdot]$ and the matrix \mathcal{K} , while the classical one uses the operator $\{\cdot, \cdot\}_1$ which involves only the second order derivative matrix \mathcal{Q} . Because of these differences, the dispersion characteristics of the two schemes will be different. Then, it is natural to investigate the theoretical behavior of these characteristics. This is the target of the next subsection.

6.3.3 Study of the linear dispersion characteristics.

The aim of this section is to investigate the phase velocity properties of the new numerical scheme (6.3.45)-(6.3.46). This study is widely inspired by the one proposed by Dingemans in [36] for the continuous situation.

We first introduce the linearized version of the scheme (6.3.45)-(6.3.46) around the rest state with a flat bottom. Note that for $D = d_0\mathcal{I}$, the bracket operator becomes

$$[D; U^\alpha] = d_0 \mathcal{K} U^\alpha.$$

Then, the linearized version of System (6.3.45)-(6.3.46) can be written under the following form

$$\frac{d}{dt} E + d_0 \mathcal{K} U^\alpha + \beta d_0^3 \mathcal{K}^3 U^\alpha = 0, \quad (6.3.47)$$

$$\frac{d}{dt} U^\alpha + g\mathcal{K} E + \alpha d_0^2 \frac{d}{dt} \mathcal{K}^2 U^\alpha = 0, \quad (6.3.48)$$

where $\beta = B_1 + B_2$ and $\alpha = A_1 + A_2$. Remark that β and α are linked by the relation $\beta = \alpha + 1/3$. As usual, when one deals with linear equations, a lot of computations can be performed explicitly. Indeed, differentiating (6.3.48) with respect to t , multiplying (6.3.47) by \mathcal{N} and substituting the resulting equations, one obtains a decoupled equation on the vector U^α

$$U_{tt}^\alpha - g d_0 \mathcal{K}^2 U^\alpha - \beta g d_0^3 \mathcal{K}^4 U^\alpha + \alpha d_0^2 \mathcal{K}^2 U_{tt}^\alpha = 0. \quad (6.3.49)$$

In order to exhibit the dispersion relation associated with (6.3.49), we then look for a plane-wave solution under the form $U^\alpha = (u_i^\alpha)_{0 \leq i \leq N}$, where, for all $i \in \{0, \dots, N\}$

$$u_i^\alpha = \mathbf{U} \exp(-j\omega t + jkx_i), \quad j^2 = -1, \quad (6.3.50)$$

where \mathbf{U} is the amplitude of the traveling wave, k is the wavenumber define as $k = 2\pi/\lambda$ and ω is the frequency of the wave. The goal is to determine the sufficient conditions on k and ω so that U^α is a solution to the linear equation (6.3.49). An expansion around the point $x = x_i$ provides directly

$$u_{i+1}^\alpha = u_i^\alpha e^{jk\Delta_x}, \quad (6.3.51)$$

$$u_{i-1}^\alpha = u_i^\alpha e^{-jk\Delta_x}. \quad (6.3.52)$$

Furthermore, direct computations give

$$\mathcal{N}U^\alpha = jksinc(k\Delta_x)U^\alpha. \quad (6.3.53)$$

$$\mathcal{M}U^\alpha = \frac{1}{3}(2 + \cos(k\Delta_x))U^\alpha. \quad (6.3.54)$$

As a consequence,

$$\mathcal{M}^{-1}U^\alpha = \frac{1}{\frac{1}{3}(2 + \cos(k\Delta_x))}U^\alpha. \quad (6.3.55)$$

Plugging (6.3.53), (6.3.54) and (6.3.55) into Equation (6.3.49), we get

$$\begin{aligned} -\omega^2 U^\alpha + gd_0 \left[\frac{ksinc(k\Delta_x)}{\frac{1}{3}(2 + \cos(k\Delta_x))} \right]^2 U^\alpha - \left[\frac{ksinc(k\Delta_x)}{\frac{1}{3}(2 + \cos(k\Delta_x))} \right]^4 \beta gd_0^3 U^\alpha \\ - \omega^2 \left[\frac{ksinc(k\Delta_x)}{\frac{1}{3}(2 + \cos(k\Delta_x))} \right]^2 \alpha d_0^2 U^\alpha = 0. \end{aligned} \quad (6.3.56)$$

Then, we obtain the expression of the exact phase velocity, defined as $C = \omega/k$, provided by the numerical scheme (6.3.45)-(6.3.46)

$$C_{new}^2 = \frac{\omega^2}{k^2} = gd_0 \left[\frac{sinc(k\Delta_x)}{\frac{1}{3}(2 + \cos(k\Delta_x))} \right]^2 \frac{\left(\frac{1}{3}(2 + \cos(k\Delta_x)) \right)^2 + sinc(k\Delta_x)^2 \beta k^2 d_0^2}{\left(\frac{1}{3}(2 + \cos(k\Delta_x)) \right)^2 + sinc(k\Delta_x)^2 \alpha k^2 d_0^2}. \quad (6.3.57)$$

Analysis of the computations.

This section is devoted to the comparison of the two phase velocities furnished by the two numerical schemes (6.3.45)-(6.3.46) and (6.2.7)-(6.2.8) presented previously. If we reproduce the computations of Section 6.3.3 on the linearized version of the classical numerical scheme (6.2.7)-(6.2.8), we obtain

$$\frac{d}{dt} \mathcal{M}E + \mathcal{M}[D; U^\alpha] + \mathcal{N}\{D, U^\alpha\}_1 = 0, \quad (6.3.58)$$

$$\frac{d}{dt} \mathcal{M}U^\alpha + g\mathcal{N}E + \frac{d}{dt}\{D, U^\alpha\}_2 = 0, \quad (6.3.59)$$

from which we deduce the expression of the phase velocity furnished by the classical scheme

$$C_{old}^2 = gd_0 \left[\frac{\text{sinc}(k\Delta_x)}{\frac{1}{3}(2 + \cos(k\Delta_x))} \right] \frac{\text{sinc}(k\Delta_x) + \frac{1-\cos(k\Delta_x)}{\Delta_x^2/2} \beta k^2 d_0^2}{\frac{1}{3}(2 + \cos(k\Delta_x)) + \frac{1-\cos(k\Delta_x)}{\Delta_x^2/2} \alpha k^2 d_0^2}. \quad (6.3.60)$$

Our aim is to plot the two curves given by Equations (6.3.57) and (6.3.60) and compare with the one predicted by the linear theory (see details in Chapter 4):

$$C_N^2 = gd_0 \frac{1 - \beta k^2 d^2}{1 - \alpha k^2 d^2}. \quad (6.3.61)$$

In our study, we choose the optimal value $\alpha = -0.39$ given by O. Nwogu in [60].

We first fix the wavelength λ and we put $\Delta_x = \lambda/N_\lambda$ where N_λ is the number of discretization points by wavelength and we recall that $kd_0 = 2\pi\sigma$.

In Figure 6.2, we draw the relative errors between the phase provided by the two numerical schemes and the phase velocity predicted by the linear theory. The relative error er is defined, for each scheme, by

$$\text{er} = 100 \left(\frac{C - C_P}{C_P} \right).$$

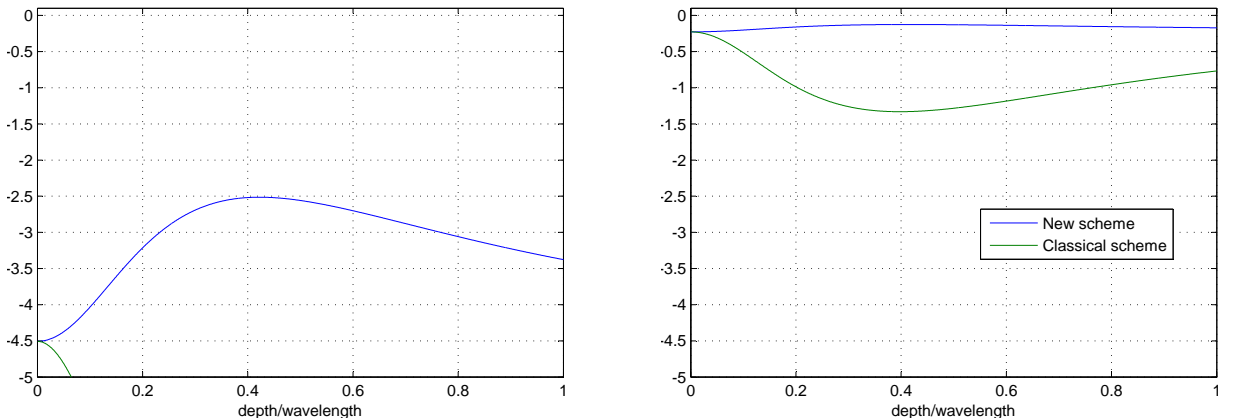


Figure 6.2 – Comparison of the phase velocity ($N_\lambda = 4$ on the left, $N_\lambda = 8$ on the right) of the classical and the new numerical scheme with the one given by the linear theory w.r.t σ .

In Figure 6.2, one can observe that for $N_\lambda = 4$, the error coming from the new scheme is acceptable (less than 5%) whereas the one of the classical scheme is greater than 5% for depths bigger than 0.07. For $N_\lambda = 8$, although the error of the classical scheme is better than in the previous case (less than 1.5%), the one of the new scheme is much better and stays very close to 0. We conclude here, as in the case of the Peregrine equations (see Chapter 5), that our new numerical scheme seems to reproduce much better the linear dispersive effects. These results are going to be numerically confirmed in the next section.

6.4 Numerical experiments

This section is devoted to the investigation of the behavior of the two schemes (6.3.43)-(6.3.44) and (6.2.7)-(6.2.8). To this end, we present different test cases : the propagation of solitary waves over a constant bathymetry to confirm our implementation, the propagation of a periodic wave with the linearized schemes on a constant bottom to highlight the conservation of dispersion characteristics. We conclude this section by the propagation of a periodic wave over a submerged bar which couples both linear dispersion and shoaling gradient characteristics. We just note that a Runge-Kutta Strongly-Stability Preserving method of order 3 is used as discretization in time.

6.4.1 Soliton propagation.

We first consider the propagation of an exact solitary wave solution to the Nwogu equations (details on the computation of this solution as well as mathematical conditions for the existence are given in [12] or in Section 3.4.3). The space interval is equal to $[0, 200]$. In order to check our implementations, we have performed a grid convergence analysis on the solitary wave characterized by an amplitude $A = 0.2$, over a flat bathymetry $d_0 = 1$. The numerical results have been compared to the analytical (initial) profile after the wave has travelled for a length of 100. The meshes used contain respectively 500, 1000, 2000 and 4000 points. In Figure 6.3, we have plotted the L^2 -norm of the error for each scheme.

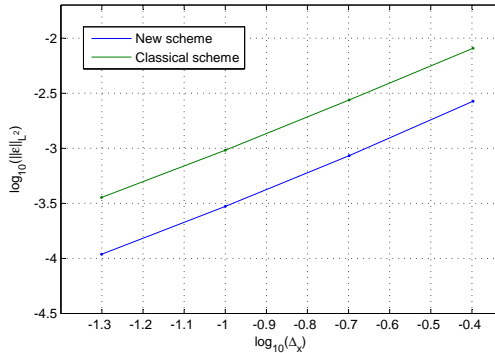


Figure 6.3 – Grid convergence results for a periodic traveling wave propagating over a flat bottom for the two numerical schemes.

The slopes obtained for the error show a convergence with third order of accuracy for both schemes confirming our implementation. In addition, the scheme (6.3.43)-(6.3.44) provide an error 3 times less important than that corresponding to (6.2.7)-(6.2.8). We deduce that with the same initial finite elements method, the new procedure decreases the error but doesn't change the order of convergence.

6.4.2 Periodic wave propagation

In this section, we want to investigate the linear characteristics of the two linear numerical schemes obtained from (6.3.45)-(6.3.46) and (6.2.7)-(6.2.8). The idea is to confirm numerically the study presented in Section 6.3.3.

Firstly, we remark that there exist exact periodic traveling wave for the linear Nwogu equations with constant bathymetry. These solutions can be written under the form

$$\eta(t, x) = A \cos(k_0 x - \omega t), \bar{u}(t, x) = \frac{A}{d_0(1 - \beta k^2 d_0^2)} \frac{\omega}{k_0} \cos(k_0 x - \omega t), \quad (6.4.1)$$

where $k_0 = 2\pi/\lambda$, A is the amplitude of η , and

$$\frac{\omega^2}{k_0^2} = g d_0 \frac{1 - \beta k_0^2 d_0^2}{1 - \alpha k_0^2 d_0^2}.$$

The test case consists in the propagation of a periodic traveling wave solution with an amplitude equal to 0.05 over a flat bathymetry $d_0 = 13$ and a wavelength $\lambda = 15$ (then $\sigma = 0.87$). The space interval is equal to $[0, 150]$. The numerical results have been compared to the analytical (initial) profile after the analytical periodic wave has travelled for a length of 150. We have performed computations for the two schemes with meshes containing 50 points (5 points per wavelength and $\Delta_x = 3$) and 100 points (10 points per wavelength and $\Delta_x = 1.5$), using periodic boundary conditions.

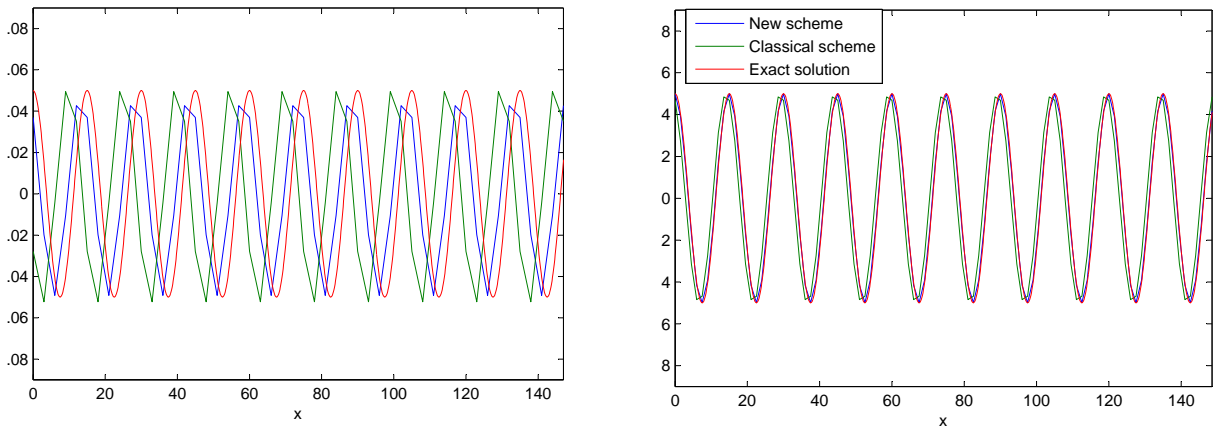


Figure 6.4 – Evolution of a solitary wave for the two numerical schemes: Left : $\Delta_x = 3$ ($N_\lambda = 5$). Right : $\Delta_x = 1.5$ ($N_\lambda = 10$).

In Figure 6.4, we have plotted the results of the two linear schemes (6.3.47)-(6.3.48), (6.3.58)-(6.3.59) and the exact analytical solution. One can observe a difference in the phase behavior of the two schemes which confirms the study presented in Section 6.3.3. Indeed, the new numerical scheme reproduce better the propagation velocity of the periodic wave for a low number of points. In addition, convergence seems to be faster for the new numerical scheme than for

the classical one. To confirm this feeling, we have performed a grid convergence analysis with meshes containing respectively 50, 100, 150, 300 and 500 points. In Figure 6.5, we have plotted the L^2 -norm of the error for each scheme.

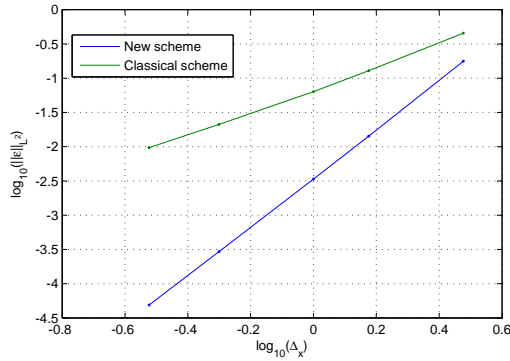


Figure 6.5 – Grid convergence results for a periodic traveling wave propagating over a flat bottom for the two numerical schemes.

The slopes obtained show a convergence with 3.5 order of accuracy for the new scheme and 1.7 order for the classical one. We deduce that the new scheme approximate better the dispersive behavior of the Nwogu equations.

6.4.3 Periodic wave propagation over a shelf.

This section is devoted to the study of the behavior of the two schemes (including nonlinear terms) in a more complex situation connecting the phase velocity and the shoaling gradient characteristics. It consists in the propagation of a periodic signal of amplitude $A = 0.01$ and period $T = 2$, generated with a relaxation zone, over a flat bathymetry $d_0 = 0.4$ before reaching a bar, whose profile is described in Figure 6.6. Two relaxation zones with thickness equal to 3 are used at the two boundaries of the domain in order to absorb any wave reaching the boundaries [16]. For the classical and the new schemes, we compute the solution using a spatial step $\Delta_x = 0.08$ (note that the hypothesis $\Delta_x \leq d_0$ is satisfied) with a time step equal to $\Delta_t = 0.03$. In particular, the comparison is made up on the time histories of the free surface profile recorded by gauges placed at spatial coordinates (see Figure 6.6).

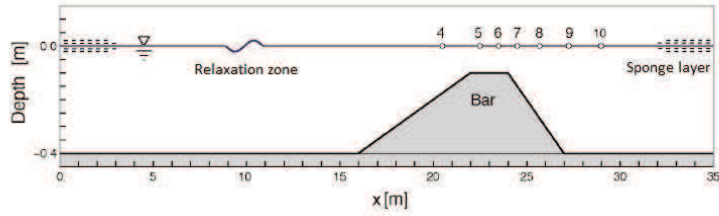


Figure 6.6 – Periodic wave propagation over a submerged bar.

We present in Figure 6.7 the global shape of the periodic wave which propagates during 50 seconds in order to stabilize the solutions. Note that, to our knowledge, it is not possible to give an analytical solution in this configuration. We then decide to compute a reference solution using a very refined mesh with $\Delta_x = 0.04$ and the classical scheme (6.2.7)-(6.2.8). This solution is used as a standard in the sequel to make the comparisons. The conclusion doesn't changed if one computes the reference solution with the new scheme (6.3.45)-(6.3.46).

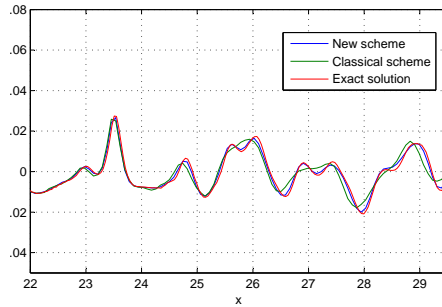


Figure 6.7 – Results of the periodic wave propagation over a submerged bar for each scheme.

One can observe differences in the behavior of the two schemes. The solution emanating from the new scheme (6.3.45)-(6.3.46) matches very well the reference curve, while the curve emanating from the classical one (6.2.7)-(6.2.8) exhibit some phase, amplitude and shape defects when x grows. In Figure 6.8, we have plotted the comparison between solutions computed with the two numerical schemes at gauges 5, 7, 9 and 10, which are positioned just after the shoaling region.

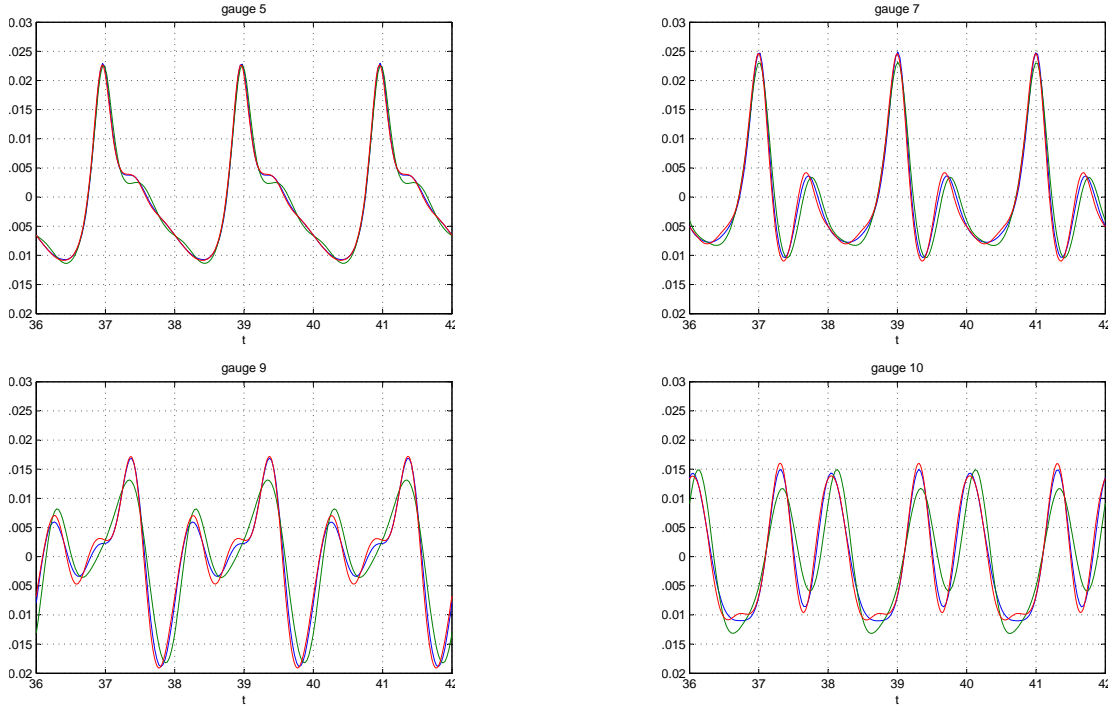


Figure 6.8 – Propagation over a submerged bar in gauge 5, 7, 9 and 10.

One can observe that the solution emanating from the new scheme is closer to the reference solution and produce a better shape than the solution computed with the classical scheme. In particular, at gauge 10, the classical scheme produces solution with phase defects and amplitude relative error of order of around 20%, while the solution emanating from the new scheme gives better phase and amplitude results.

6.5 Conclusion and future works

We have adapted the new method presented in Chapter 5 to obtain discrete numerical models consistent with the Nwogu and the Green-Naghdi equations. In order to evaluate the accuracy of this method on this particular Boussinesq model which includes dispersive terms with three order derivatives in space, we have compared our new numerical scheme with the one obtained by performing directly a Galerkin method on the Nwogu equations. Finally, by the use of several numerical experiments, we have shown the efficiency of our new scheme to reproduce the linear effects although it is similar to the classical one in a nonlinear regime.

The application of this procedure to asymptotic models in order to modelize a wave propagation is a new idea. A lot of works are still in progress. We recall one of the perspectives presented in Section 1.6 of the introduction. Firstly, we claim that the method does not give a unique model. The choice of the initial scheme applied on Euler equations is an extra degree of freedom (note that the discretizations of the kinematic boundary conditions are central because of their role in the definition of the operator bracket $[; ;]$). One of the important future work will involve the

adaptation of discrete asymptotic analysis to particular numerical schemes developed in order to solve the Euler equations.

An other idea consists in reversing the role of x and z . One could choose to perform a discretization in z and adapt the method to the resulting discrete equations. This idea is very close to the one which leads to the multilayers models. We hope we will better understand the connection between these models and the asymptotic ones.

In future works, we want also to study variations in stability and convergence results emanating from numerical schemes obtained with this procedure. It would permit to calibrate improvements of the method and of the choice of the initial numerical scheme in a more general framework.

In addition it will be necessary to investigate the effects of the procedure on the boundary conditions. Actually in this thesis we only dealt with periodic boundary conditions, using relaxation zones when it was necessary. But this is a very restrictive context and we have to know how to adapt this procedure on Dirichlet or Neumann boundary conditions.

To conclude, numerical tests in 2 dimensions will be very important. Actually, most of theoretical study (consistency results or dispersion analysis) presented in Chapter 5 and 6 can not be adapted in the 2 dimensional case.

Bibliography

- [1] M.B. ABBOTT, H.M. PETERSEN AND O. SKOVGAARD, Computations of short waves in shallow water. *Coast.Eng.*, (1978).
- [2] R. ABGRALL AND R. SAUREL, Discrete equations for physical and numerical compressible multiphase mixtures, *Journal of Computational Physics*, 186 (2003), pp. 361-396.
- [3] K. ADAMY, Existence of solutions for a Boussinesq system on the half line and on a finite interval. *Discrete Contin. Dyn. Syst.*, 29 (2011), pp. 25-49.
- [4] A. ALI ET. AL., Mechanical balance laws for Boussinesq models of surface water waves. *J. Nonlinear Sci.*, 22 (2012), pp. 371-398.
- [5] S. ALINHAC ET P. GÉRARD, Opérateurs pseudo-différentiels et théorème de Nash-Moser. *Editions du CNRS*, (1991).
- [6] B. ALVAREZ-SAMANIEGO AND D. LANNES, Large time existence for 3D water-waves and asymptotics, *Inventiones Math.*, 171 (2008), 485-541.
- [7] W. EL ASMAR AND O. NWOGU, Finite volume solution of Boussinesq-type equations on an unstructured grid, *J. McKee Smith (ed.), Proc. of the 30 th Int. Conf. on Coastal Engineering, San Diego, CA*, (2006).
- [8] P. Bacigaluppi, M. Ricchiuto and P. Bonneton: A 1D Stabilized Finite Element Model for Non-hydrostatic Wave Breaking and Run-up. *Finite Volumes for Complex Applications VII-Elliptic, Parabolic and Hyperbolic Problems*, Springer Proceedings in Mathematics & Statistics, (2014) vol. 78, pp. 779–790, isbn 978-3-319-05590-9
- [9] E.S. BAO, R.M. CHEN AND Q. LIU, Existence and symmetry of ground states to the Boussinesq abcd systems, *Arch. Rational Mech. Anal.*, 216 (2015), 569-591.
- [10] S. Beji and J.A. Battjes: Numerical simulations of nonlinear-wave propagation over a bar. *Coast.Eng.*, (1994) vol 23,
- [11] S. BEJI AND K. NADAOKA, A formal derivation and numerical modeling of the improved Boussinesq equations for varying depth, *Ocean Engineering*, 23 (1996), pp. 691-704.
- [12] S. Bellec and M. Colin : On the existence of solitary waves for Boussinesq type equations and a new conservative model. *Advances in Differential Equations*, 21 (2016), 945-976.

-
- [13] S. Bellec, M. Colin and M. Ricchiuto : Discrete asymptotic equations for long wave propagation. Preprint.
- [14] T. B. BENJAMIN, J. L. BONA AND J. J. MAHONY, Model equations for long waves in nonlinear dispersive systems. *Philosophical Transactions of the Royal Society A* , **272** (1972), 47-78.
- [15] H. BERESTYCKI, P.L. LIONS, Nonlinear scalar field equations I. *Arch. Rat. Mech. Anal.* , **82** (1983), 313-346.
- [16] H.B. BINGHAM AND Y. AGNON, A fourier-Boussinesq method for nonlinear water waves. *Eur. J. Mech. B/Fluids* 24 (2005), pp. 255-274.
- [17] M. BJØRKAVÅG AND H. KALISCH, Wave breaking in Boussinesq models for undular bores. *Phys. Lett.*, 275 (2011), pp. 1570-1578
- [18] J. L. BONA, M. CHEN AND J-C. SAUT, Boussinesq equations and other systems for small-amplitude long waves in nonlinear dispersive media: I. Derivation and the linear theory, *J. Nonlinear Sc.*, **12** (2002), 283-318.
- [19] J. L. BONA, M. CHEN AND J-C. SAUT, Boussinesq equations and other systems for small-amplitude long waves in nonlinear dispersive media: II. The nonlinear theory, *Nonlinearity*, **17** (2004), 925-952.
- [20] J. L. BONA, T. COLIN AND D. LANNES, Long-wave approximations for Water Waves, *Arch. rational Mech. Anal.*, **178**, (2005), 373-410.
- [21] P. BONNETON AND F. CHAZEL AND D. LANNES AND F. MARCHE AND M. TISSIER, A splitting approach for the fully nonlinear and weakly dispersive Green-Naghdi model. *Journal of Computational Physics*, 230 (2011), pp. 1479-1498.
- [22] J.V. BOUSSINESQ, Théorie de l'intumescence liquide appelée onde solitaire ou de translation se propageant dans un canal rectangulaire. *C.R. Acad. Sci. Paris Sér.*, A-B 72 (1871), pp. 755-759.
- [23] M. Brocchini: A reasoned overview on Boussinesq-type models: the interplay between physics, mathematics and numerics. *Proc. Royal Soc. A*, 2014
- [24] C. BURTEA, New long time existence results for a class of Boussinesq-type systems, *arXiv:1509.07797v2 [math.AP]*, 17 Nov 2015.
- [25] F. CHAZEL, D. LANNES AND F. MARCHE, Numerical simulation of strongly nonlinear and dispersive waves using a Green-Naghdi model, *J. Sci. Comput.*, **48** (2011), 105-116.
- [26] M. CHEN, N. NGUYEN AND S. SUN, Solitary Wave Solutions to Boussinesq Systems with Large Surface Tension, *Discrete Contin. Dyn. Syst. S*, **26** (2009), 1153-1184.

-
- [27] M. CHEN, N. NGUYEN AND S. SUN, Existence of Traveling wave Solutions to Boussinesq Systems, *Differential Integral Equations*, **24** (2011), 895-908.
- [28] R. CIENFUEGOS AND E. BARTHELEMY AND P. BONNETON, A fourth order compact finite volume scheme for fully nonlinear and weakly dispersive Boussinesq type equations. Part II: Boundary conditions and validation. *Int. J. Numer. Meth. Fluids*, (2006), vol 53.
- [29] D. CLAMOND AND D. DUTYKH, Fast accurate computation of the fully nonlinear solitary surface gravity wave, *Computers & Fluids*, **84** (2013), 35-38.
- [30] M. COLIN, Stability of stationary waves for a quasilinear Schrödinger equation in space dimension 2, *Adv. Differential Equations*, **8** (2003), 1-28.
- [31] M. COLIN, L. JEANJEAN, Solutions for a quasilinear Schrödinger equation: a dual approach, *Nonlinear Analysis*, **56** (2004), 213-226.
- [32] W. CRAIG, An existence theory for water-waves and the Boussinesq and the Kortweg-de Vries scaling limits, *Commun. Partial Differ. Equations*, **10** (2004), 787-1003.
- [33] F. DA LIO AND B. SIRAKOV, Symmetry results for viscosity solutions of fully nonlinear uniformly elliptic equations, *J. Eur. Math. Soc.*, **9** (2007), 317-330.
- [34] A. DE BOUARD, N. HAYASHI AND J. C. SAUT, Global existence of small solutions to a relativistic nonlinear Schrödinger equation, *Commun. Math. Phys.*, **189** (1997), 73–105.
- [35] A.I. DELIS, M. KAZOLEA, I.K. NIKOLOS AND C.E. SYNOLAKIS, An unstructured finite volume numerical scheme for extended 2d boussinesq-type equations, *Coastal Engineering*, **69** (2012), 42-46.
- [36] M.W. DINGEMANS, Water wave propagation over uneven bottoms. Advanced Series Ocean Eng., (1997), World Scientific
- [37] A. ERN AND J.-C. GUERMOND, Theory and practice of finite elements, Applied Mathematical Sciences Vol. 159, Springer (2004)
- [38] C. ESKILSSON AND S.J. SHERWIN, Spectral/HP discontinuous Galerkin methods for modelling 2D Boussinsq equations *Journal of Computational Physics*, 212 (2006), pp. 566-589.
- [39] A. FILIPPINI, S. BELLEC, M. COLIN AND M. RICCHIUTO, On the nonlinear behaviour of Boussinesq type models : amplitude-velocity vs amplitude-flux forms. *Coastal Engineering*, 99 (2014), pp. 109-123.
- [40] A.G. FILIPPINI AND M. RICCHIUTO, Upwind Residual discretization of enhanced Boussinesq equations for wave propagation over complex bathymetries *To appear in J. Comp. Phys.*, (2014).

-
- [41] D.R. FUHRMAN AND H.B BINGHAM, Numerical solution of fully nonlinear and highly dispersive Boussinesq equations in two horizontal dimensions, *Int. J. Numer. Meth. Fluids*, **44** (2004), 231-255.
 - [42] S.T. GRILLI, R. SUBRAMANYA, I.A. SVENDSEN AND J. VEERAMONY, Shoaling of solitary waves on plane beaches. *J.Waterw.Port.C.-ASCE*, (1994), vol. 120
 - [43] D. IONESCU-KRUSE, A New Two-Component System Modelling Shallow-Water Waves, *Quarterly of applied Mathematics*, (2013).
 - [44] M. KAZOLEA, Mathematical and computational modeling for the generation and propagation of waves in marine and coastal environments. PhD, Technical University of Crete, (2013).
 - [45] M. KAZOLEA, A.I. DELIS, I.K. NIKOLOS AND C.E. SYNOLAKIS, An unstructured finite volume numerical scheme for extended 2D Boussinesq-type equations. *Coastal Engineering*, **69** (2012), pp. 42-66.
 - [46] M. KAZOLEA, A.I. DELIS AND C. SYNOLAKIS, Numerical treatment of wave breaking on unstructured finite volume approximations for extended Boussinesq type equations. *J.Comput.Phys.*,(2014)
 - [47] J.T. KIRBY AND G. WEI, Time-dependent numerical code for extended Boussinesq equations, *ASCE Journal of Waterway, Port, Coastal and Ocean Engineering*, **120** (1995), 251-261.
 - [48] Z. KHORSAND ET. AL., On the shoaling of solitary waves in the KdV equation. *Proc. 34th Conf. Coastal Engrng.*, Seoul (2004).
 - [49] D. LANNES, The water waves problem *American Mathematical Society*, (2013).
 - [50] D. LANNES, Well-Posedness of the Water Waves Equations, *J. AM Math. Soc.*, **18** (2005), 605-654.
 - [51] D. LANNES AND P. BONNETON, Derivation of asymptotic two-dimensional time-dependent equations for surface water wave propagation, *Physics of fluids*, **21** (2009).
 - [52] D. LANNES AND F. MARCHE, A new class of fully nonlinear and weakly dispersive Green-Naghdi models for efficient 2D simulations, *Journal of Computational Physics*, **282** (2015), 238-268.
 - [53] C. LEE, Y.S. CHO AND S.B. YOON, A note on linear dispersion and shoaling properties in extended Boussinesq equations. *Ocean Eng.*,(2003), vol.30, pp.1849-1867
 - [54] M.S. LONGUET-HIGGINS ET. AL., Radiation stresses in water waves; a physical discussion with applications. *Deep-sea Research*, **11** (1964), pp. 529-562.

-
- [55] A. MADSEN, R.MURRAY AND O.R. SORENSEN, A new form of the Boussinesq equations with improved linear dispersion characteristics, *Coastal engineering*, **15** (1991), 371-388.
- [56] P. A. MADSEN AND H. A. SCHAFFER, Higher-Order Boussinesq-Type Equations for Surface Gravity Waves: Derivation and Analysis. *Phil. Trans. R. Soc. Lond. A*, (1998), vol. 356.
- [57] P.A.MADSEN AND O.R.SORENSEN, A new form of the Boussinesq equations with improved dispersion characteristics. Part 2: a slowing varying bathymetry. *Coast.Eng.*, (1992), vol.18, pp.183-204
- [58] B. MÉSOGNON, Limites singulières en faible amplitude pour l'équation des vagues. Physique mathématiques. Université Pierre et Marie Curie-Paris VI, 2015.
- [59] D.E. MITSOTAKIS, Boussinesq systems in two space dimensions over a variable bottom for the generation and propagation of tsunami waves. *Mat. Comp. Simul.*, 80 (2009), pp. 860-873.
- [60] O. NWOGU, Alternative form of Boussinesq equations for nearshore wave propagation, *ASCE Journal of Waterway, Port, Coastal and Ocean Engineering*, (1993), 618-638.
- [61] J. ORSZAGHOVA, A.G.L. BORTHWICK AND P.H. TAYLOR, From the paddle to the beach - A Boussinesq shallow water numerical wave tank based on Madsen and Sørensen's equations. *J.Comput.Phys.*, (2012), vol. 231, pp. 328–344
- [62] L.V. OVSJANNIKOV, Cauchy problem in a scale of Banach spaces and its application to the shallow water theory justification, *Appl. Meth. Funct. Anal. Probl. Mech.*, **503** (1976), 426-437.
- [63] D.H. PEREGRINE, Long waves on a beach, *J. Fluid Mech.*, **27** (1967), 815-827.
- [64] M. RICCHIUTO AND A.G. FILIPPINI, Residual discretization of enhanced Boussinesq equations for wave propagation over complex bathymetries. *J.Comput.Phys.*, (2014), pp. 306–341
- [65] V. Roeber and K.F. Cheung: Boussinesq-type model for energetic breaking waves in fringing reef environments. *Coast.Eng.*, (2012), vol. 70, pp. 1–20
- [66] M. TISSIER, P. BONNETON, F. MARCHE, F.CHAZEL AND D. LANNES, A new approach to handle wave breaking in fully non-linear Boussinesq models, *Coastal Engineering*, **67** (2012), 54-66.
- [67] J.-C. SAUT AND LI XU, The Cauchy problem on large time for surface waves Boussinesq systems, *J. Math. Pures et Appl.*, **97** (2012), 635-662.
- [68] J.-C. SAUT, C. WANG AND LI XU, The Cauchy problem on large time for surface waves Boussinesq systems II, *arXiv:1511.08824v1 [math.AP]*, 27 Nov 2015.

-
- [69] I.A. SVENDSEN ET. AL., On the deformation of periodic long waves over a gently sloping bottom. *J. Fluid Mech.*, 87 (1978), pp. 433-448.
 - [70] M. TISSIER, P. BONNETON, F. MARCHE, F. CHAZEL AND D. LANNES, A new approach to handle wave breaking in fully nonlinear Boussinesq models, *Coast.Eng.*, (2012), vol. 67
 - [71] M. TONELLI AND M. PETTI, Simulation of wave breaking over complex bathymetries by a Boussinesq model. *J.Hydraulic Res.*, (2011), vol.49
 - [72] M.K. WALKLEY, A Numerical Method for Extended Boussinesq Shallow-Water Wave Equations, *PhD University of Leeds*, (1999).
 - [73] M.A. WALKLEY AND M. BERZINS, A finite element method for the two-dimensional extended Boussinesq equations. *Int.J.Numer.Meth Fluids*, (2002), vol. 39
 - [74] G. WEI AND J.T. KIRBY, A time-dependent numerical code for extended Boussinesq equations. *J.Waterw.Port.C.-ASCE*, (1995), vol 120, pp. 251–261

